Cellular and Molecular Properties of the Neuroprotective *Wld*^{S} Gene

Thomas Malcolm Wishart

A thesis submitted for the degree of PhD in Neuroscience at the University of Edinburgh

2005

DECLARATION

I declare that the work described in this thesis and its composition are entirely my own unless otherwise stated.

Thomas Malcolm Wishart

ACKNOWLEDGMENTS

I have been very lucky. I was lucky to get such an interesting topic of research, lucky that Richard Ribchester saw fit to give me the chance to do all that I have done, that he had the confidence in my abilities to allow me a relatively free rein to do what I wanted to do. I am lucky to have worked in an environment where everyone is so nice and helpful. I would like to think that I have made a lot of friends during my time here and that has made this the most enjoyable experience I have had so far, and I would like to thank Richard for the opportunity, for giving me the benefit of his apparently boundless knowledge and experience, and being more than just the boss.

I would like to thank the Faculty of Medicine for my scholarship and everyone who has helped me throughout the course of the last three years but to name everyone individually would probably put me over the word limit and they already know who they are.

Specifically, I would like to thank David Wyllie, Mike Cousin, Adrian Thomson, Paul Skehel, Susan Middleton, RTPCR Steve (McDonald) and Darren Downing for more than their technical assistance. Thank you Big G (Jordan) and Wong for nothing in particular.

I would also like to thank Dr Phil (Chen) for putting up with me for the last three years, which I can imagine is an achievement worthy of some sort of award. Derek Thomson for being the font of all knowledge, the Big T (Gillingwater) for leading by example and getting me my first proper wage at the age of 26. Jane Haley I would like to thank you for being a good friend as well as baby sitting me on a daily basis.

Finally, I would like to thank my Mum and Dad for their encouragement, Yaiya and Di for their help, and tell Emily, that I appreciate you putting up with me all this time, and listening to me talk endlessly about things of no real interest to you, but it is you that make me to want to be better than I am.

ABSTRACT

The aim of this thesis is to advance our understanding of the mechanisms controlling nerve degeneration, by examining the molecular interactions of the *Wld*^{S} gene and its chimeric protein product. Wallerian degeneration is normally complete within twenty-four to forty-eight hours of axotomy, but in the mouse mutant C57Bl/Wld^S the process is delayed by up to three weeks. The *Wld*^{S} mutation comprises an 85Kb tandem triplication of genomic region containing the complete sequence for *Rbp7* (retinoid binding protein 7), *Nmnat1* (nicotinamide mononucleotide adenyltransferase) and the N-70 amino acids of *Ube4b* (a ubiquitin ligase). At the boundaries of this in frame tandem triplication, a chimeric "fusion" gene is formed comprising the N-70 *Ube4b* linked to *Nmnat*. The protein product localises to nuclei. Transgenic expression of the chimeric gene has previously been shown to be sufficient to reproduce the *Wld*^{S} nerve-degeneration phenotype in both mice and rats.

The main objectives in my research were; 1. To develop a rapid and effective method for determining the copy number of *Wld*^{S} alleles in mutant and transgenic *Wld*^{S} mouse lines. 2. To map the regional distribution and sub cellular localisation of the *Wld*^{S} chimeric protein product within the nervous system. 3. To test the hypothesis that the expression of the constituent components of the *Wld*^{S} chimeric gene is sufficient to alter mRNA levels of other genes that may themselves be downstream effectors of the *Wld*^{S} neuroprotective phenotype.

1. A rapid and cost effective method for genotyping was developed using quantitative real time PCR on genomic DNA from the spontaneous *Wld*^{S} mutant mouse and transgenic lines. This method allows the determination of *Wld*^{S} copy number (specifically a region of the N70-*Ube4b* portion of the *Wld*^{S} gene) for genotyping and calculating insertion number in transgenic lines.

2. A highly specific antibody generated against the Wld-18 peptide confirms that the *Wld*^{S} protein product is localised to neuronal nuclei. Mapping of the *Wld*^{S} protein

product in the CNS showed that the neuronal distribution is not uniform either in the spontaneous mutant or the transgenic models. The intranuclear distribution varied between and within cell types; some neurones showed intense, particulate staining, others showed fine speckling, while others had large nuclear inclusions that varied in shape. Cerebellar granule cells in the *Wld*^{S} mouse have a consistent expression pattern, with about 90% of cells containing at least one large nuclear inclusion of Wld^S protein. The expression of Wld^S - containing inclusions in these cells increased with postnatal age *in vivo* and also *in vitro* in primary cultures and cell lines. The inclusions persist, evidently without detriment to the animals as they mature. Co-immunostaining and/or co-transfection studies in the HEK293 cell lines suggested that the Wld^s protein co-localises with certain transcription factors including HDAC5; and members of the SMRT family; and a member of the ubiquitin proteasome system, VCP.

3. Microarray analysis and quantitative real time PCR of *Wld*^{S} compared with wild-type C57Bl6 mouse cerebellar mRNA indicated differences in expression levels for at least 11 genes outside the *Wld*^{S} locus. Some of these genes were down-regulated, but others were up-regulated. The greatest differences were strong down-regulation of *Pttg1* and strong up-regulation of a homologue of *Edr1*. Transfection of human (HEK293) cells with a *Wld*^{s}-eGFP construct mimicked changes shown in Wld^s mouse mRNA levels. The sub-cellular distribution of Wld^S protein is dependent on both the Nmnat-1 and Ube4b regions of the protein and both are required to target Wld^S protein to discrete intranuclear foci. The induced changes in *Pttg1* mRNA levels, but not the *Edr1*-like transcript, were partly mimicked by transfecting HEK293 cells with the *Nmnat*-1 component of the chimeric gene, or by exogenous administration of NAD at a concentration of 1mM. This effect was blocked by sirtenol, an inhibitor of the nuclear transcription factor Sirt1. Transfection with the N70-*Ube4b* component of the *Wld*^{S} gene partly mimicked up-regulation of the *Edr1*-like transcript but had no effect on expression levels of *Pttg*-1 mRNA. *Wld*^{s}-positive cerebellar granule cells show a protective phenotype, but *Pttg1*-KO peripheral nerves do not.

Together, these studies suggest that the *Wld*^{S} gene product functions as a bidirectional regulator of gene expression, driving up and down the transcription of several specific genes via more than one intra-nuclear signalling pathway. The summed effects of these variations in mRNA levels may be required for full expression of the *Wld*^{S} neuroprotective phenotype. Identification of the genes and proteins ultimately responsible may open up new possibilities for understanding and treatment of the consequences of injury to the nervous system, whether induced by trauma or by neurodegenerative disease.

TABLE OF CONTENTS

CHAPTER TWO:

ABBREVIATIONS

Δ	Change in
µg	Microgram
µm	Micrometer
µM	Micromolar
3'	3 prime
5'	5 prime
ACSF	Artificial cerebrospinal fluid
BAC	Bacterial artificial chromosome
Ccl21	Chemoking ligating factor 21
cDNA	Copy DNA
CGC	Cerebellar granule cell
CNS	Central nervous system
CNTF	Ciliary neurotrophic factor
C_T	Cycle threshold
Dap3	Death associated protein 3
DNA	Deoxyribose nucleic acid
dNTPs	Deoxynucleoside 5'triphosphates (d-A/G/C/T-TPs)
DRG	Dorsal root ganglion
dsDNA	Double stranded DNA
Edr1	Erythroid differentiation regulator 1
eGFP	Enhanced green fluorescent protein
EST	Expressed sequence tag
Fabp7	Fatty acid binding protein 7
GFP	Green fluorescent protein
HDAC	Histone deacetylases
HEK	Human embryonic kidney
Kb	Kilobases
Mbp-C	Myosin binding protein C
mg	Milligram
mM	Millimolar
mRNA	Messenger RNA
N-CoR	Nuclear corepressor
NGF	Nerve growth factor
nM	Nanomolar
Nmnat1/D4Cole1e	Nicotinamide mononucleotide adenyltransferase
P	Postnatal (i.e. P6 = postnatal day 6)
PCR	Polymerase chain reaction
PFGE	Pulse field gel electrophoresis
PML	Promyelotic leukaemia proteins
PNS	Peripheral nervous system
Pttg1	Pituitary transforming gene 1
PTX	Picrotoxin
Q-PCR	Quantitative PCR
RACE	Rapid amplification of cDNA ends
Rbp7	Retinoid binding protein 7

rDNA	Ribosomal DNA
RFLP	Restriction fragment length polymorphism
RFP	Red fluorescent protein
RNA	Ribonucleic acid
RT-PCR	Reverse transcriptase or Real time PCR
RXR	Retinoic acid receptors
SCG	Superior cervical ganglion
SHARP	SMRT/HDAC associated repressor protein
SMN	Spinal muscular atrophy protein
SMRT	Silencing mediator for retinoic acid and thyroid hormone receptors
snRNA	Small nucleolar RNA
ssDNA	Single stranded DNA
Ssr	Signal sequence receptor
TNFAIP3_IP protein	Tumor necrosis factor α interacting protein 3 interacting
TTX	Tetrodotoxin
Ube4b/Ufd2	Ubiquitination factor E4b
UNG	Uracil-N-glycosylase
UPS	Ubiquitin proteasome system
VCP	Valosine containing protein (p97/Cdc48)
Wld^S	Wallerian degeneration slow

Chapter 1:
Introduction

1.0. Introduction

"There are only two ways of coming to know a machine: one is that the master who made it should show us its artifice; the other is to dismantle it and examine its most minute parts separately and as a combined unit...." (Descartes, 1664).

The nervous system could be viewed in accordance with Descartes' mechanistic viewpoint, as a machine. An intricate machine, but still a machine. In order that we may understand how it works we must arguably dismantle and examine its component parts and their interactions. Simplistically, the nervous system comprises central (CNS) and peripheral (PNS) components (as they are currently labelled, the classification is obviously man made, not an inherent property of an integrated mechanism). These components may then be simplified further to a grouping of different cell types. The cells can be subclassified further as a collection of organelles and supporting material, made up of all the macromolecules now customarily associated with them.

The advent of molecular biology allows us to decompile processes within these cells and their organelles even further. In many respects, the field of modern molecular biology was spawned from the field of Mendelian genetics. Mendel carried out experiments that required extraordinary patience, and without which (and taking into account the work of others at the time including Köreuter and Gärtner), it is impossible to guess where the field of modern molecular biology would now stand. Mendel observed that phenotypic traits are determined by factors passed from parents to progeny, and that these factors are unchanged as they are inherited from generation to generation. Mendel's first (segregation) and second laws (independent assortment) explain to us his observed patterns of inheritance (Mendel, 1865). What Mendel did not know at this time, was that the factors he was describing are genes.

Molecular biology advanced at a prodigious rate following the publication of a seminal paper by Hershey and Chase (1952). Up to that point it was thought that protein was the genetic material of the cell, despite an earlier demonstration that DNA, not protein was responsible for the genetic transformation of rough bacteria to smooth. The scientific community remained unconvinced of the findings by Avery, McLeod and McCarty (1944) until Hershey and Chase firmly established DNA as the prime candidate containing the genetic information within organisms. This finding was followed quickly by elucidation of the structure of DNA by Watson and Crick in 1953. In the next major breakthrough of 1955, Arthur Kornberg demonstrated DNA replication *in vitro*. He found that he could do this using DNA fragments, dNTP's (nucleotides) and *E. coli* cell lysate. Eventually he purified a single enzyme and was able to achieve DNA replication *in vitro* with only DNA fragments, dNTP's, Mg^{++} ions and the Kornberg enzyme, now called DNA polymerase I (Kornberg 1959). In 1958, Meselson & Stahl demonstrated that DNA replication is semi-conservative by labelling (bacterial) parental DNA with ^{15}N and allowing the labelled strains to undergo a round of growth and therefore a round of DNA replication (Meselson & Stahl, 1958). The central dogma of molecular biology was first suggested by Crick in 1958. *"The central dogma of molecular biology deals with the detailed residue-by-residue transfer of sequential information, such information cannot be transferred from protein to either protein or nucleic acid"* (Crick 1958). Thus, once information is encoded as protein (DNA to RNA to protein) it cannot be returned to nucleic acid. There are currently no known exceptions to the central dogma, correctly stated. Once again Crick was ahead of his time and questioned how this flow of information ever began. In 1968 he suggested (what would later be termed the RNA world hypothesis in a 1986 article by Harvard molecular biologist Walter Gilbert), *"that RNA must have been the first genetic molecule, further suggesting that RNA, besides acting as a template, might also act as an enzyme and, in so doing, catalyze its own self-replication"*. The fact that some RNA may also be able to act as enzymes was not actually shown until the 1980s by Thomas R. Cech. By the 1970, the genetic code and the processes of transcription and translation had been elucidated and reverse transcriptase has been discovered (Temin & Mizutani 1970).

"You, your joys and your sorrows, your memories and your ambitions, your sense of personal identity and free will, are in fact no more than the behaviour of a vast assembly of nerve cells..." (Crick 1994). The ability to deconstruct the nervous system down to the molecular level has now allowed us to observe the consequences of various injuries and diseases that affect it. For example, molecular techniques have been critically important for studying the role of the aberrant accumulation of protein in neurones associated with Alzheimer's dementia, ischaemic death of cells following stroke and cell damage following head injury. Employing molecular biology techniques to further uncover general mechanisms of cell death and cell survival in the nervous system will therefore be of vital importance in order to develop suitable therapeutic strategies for a wide range of neurodegenerative disorders.

In this thesis I have used molecular biological techniques to further our understanding of how a spontaneous mutation (*Wld*^{s}) retards the consequences of one form of traumatic injury: a specific form of axonal degradation known as Wallerian degeneration.

1.1.0. What is Wallerian degeneration?

Wallerian degeneration is a process that results from injury and/or diseases that affect axons. It can be defined as the degeneration of the distal segment of a nerve fibre/axon that has been severed/separated from its cell body (Figure 1.1). The process of Wallerian degeneration was most famously described in 1850 by Augustus Waller. Waller carried out experiments on frog hypoglossal and glossopharyngeal nerves to investigate the effects of nerve lesions. Post lesion, he noted a loss of muscle contraction, and described the axon as appearing "discontinuous, fragmented and granulated" (see Stoll *et al.* 2002 & Gillingwater 2001). Wallerian degeneration has been well studied and is an elegant and reliable model system, which can be used to study the patho-physiology of traumatic injury as well as diseases of the nervous system (Raff et al., 2002; Coleman & Perry, 2002).

Although Waller did his pioneering work on amphibians, the main biological resources for studying this phenomenon in more recent times have been rodents. Generally, injured axons degenerate within three days of a nerve lesion in rats and mice (Coleman & Ribchester, 2004), by a sequence of events that are very similar across most species. However, there are exceptions to this in time scale. For example, in giant squid, crayfish and fish, isolated axons may be preserved for months rather than days.

One of the earliest morphological changes seen with Wallerian degeneration is the breakdown of the axonal cytoskeleton (Crawford *et al.* 1995). It has now been shown through electron microscopy that major early changes (within one to three days) following nerve transection include fragmentation of the endoplasmic reticulum, and disintegration of neurofilaments and microtubules (Glass & Griffin, 1991). Another distinctive degenerative marker is the swelling and lysis of mitochondria. Following this, breakdown and removal of the myelin sheath is initiated by phagocytosing macrophages (for review see Gillingwater & Ribchester, 2001). Macrophages and Schwann cells were shown to be important in Wallerian degeneration because myelin contains molecules that inhibit axonal growth and retard regeneration, whereas macrophages aid in the removal of these molecules, so the removal of myelin is conventionally thought to be a desirable end result of Wallerian degeneration (Be'eri *et al.* 1998, Lawson *et al.* 1994). Another marker, or possible measure of degeneration is an increase in the number of non-neuronal nuclei in the transected distal stump, which arise from proliferation of dedifferentiated Schwann cells and invading myleomonocytic cells (Brown *et al.* 1992).

"Digestive chambers" are formed from enlarged nodal spaces as the myelin sheath retracts from the nodes of Ranvier. These chambers are where the complete breakdown of axonal material proceeds inexorably to its conclusion. However, axonal debris and myelin may persist within the central nervous system for weeks or months (Lawson *et al.* 1994). The digestive chambers are removed by macrophages and phagocytosing Schwann cells, which simultaneously proliferate, and eventually join up end to end to

form "bands of Bungner". These structures are thought to play a role in guiding the regenerating proximal nerve stump to denervated sites (see Gillingwater & Ribchester, 2001). In explant systems in which macrophages have been excluded, the axons retain their structure for a much longer period of time, and in animals with depleted macrophage populations a similar result is seen (Ludwin and Bisby 1991). In the peripheral nervous system, basal lamina tubing ensheathing the nerve may retain dividing Schwann cells (columns of Schwann cells surrounded by basal lamina are commonly known as endoneural tubes). There is also evidence that Schwann cells actively promote regeneration by means of secreted factors (Lunn *et al.* 1989).

1.1.1. Differences between Wallerian degeneration in the CNS and PNS

There are temporal differences in the rate of Wallerian degeneration between the central and peripheral nervous systems (CNS and PNS respectively). It has been thought previously that this may be due to increased time delay in the activation of the mononuclear response (Lawson *et al.* 1994) and an inability of macrophages to adequately infiltrate the more densely packed regions of the brain. It is also said that the activation of the mononuclear phagocytes "occurs in response to Wallerian degeneration of axons rather than loss of electrical activity *per se*" (Lawson *et al.* 1994).

During Wallerian degeneration, lesioned axons in the CNS collapse and disintegrate at roughly the same time as in the PNS, however, the removal of myelin debris containing growth inhibitors is slowed considerably, i.e. it takes place over a time course of months (Stoll *et al.* 2002). Recruitment of macrophages could be dependent on loss of an inhibitory factor normally expressed by an intact nerve, or by the production of a chemotactic factor expressed by the injured nerve itself (Ludwin and Bisby 1991).

Increased knowledge of the mechanism and progression of Wallerian degeneration may be important in understanding axonal death, in a number of debilitating diseases such as

amyotrophic lateral sclerosis and multiple sclerosis, as well as a number of peripheral neuropathies (Coleman and Ribchester 2004).

1.1.2. What initiates Wallerian degeneration?

Theories about what initiates Wallerian degeneration include loss of trophic support from the cell body and activation of calpain by calcium influx. Interestingly, however, several groups have compared Wallerian degeneration to an active process similar to apoptosis (Buckmaster *et al.* 1995, Ribchester *et al.* 1995).

Calcium ions appear to be required to seal the damaged axon, and possibly to aid with the activation of later degenerative mechanisms. There are mechanisms within the neuron to help maintain the ion balance such as sequestration of calcium ions by mitochondria (Tsao *et al.* 1999, Xue *et al.* 2002). Buckmaster *et al.* (1995) also showed that increased cytoplasmic calcium levels could increase cell survival. However, calcium ions could be debilitating to the neuron after lesioning. Changes have been seen indicating Na^+-K^+-ATPase inhibition. For example, intact membranes exclude Na^+, while K^+ would continue to leak through open ion channels, along with Cl^- following passively to maintain the gradient. With the K^+ gradient dissipated, Na^+ can now enter the axon allowing Ca^{2+} entry through Na^+/ Ca^{2+} exchange, or through the failure of other mechanisms for Ca^{2+} extrusion or sequestration. Ca^{2+} could then enter the cell to the point where degradative enzymes are activated.

Importantly, Wallerian degeneration is known to begin at distal synapses. In the rat, recordings of action potentials over muscle membrane following sciatic nerve section show that all electrical activity declines by 24-36 hours (Miledi & Slater 1970), and it is after this that neuromuscular junctions begin to visibly degenerate. Complete disruption of the endplate takes between 3 and 5 hours (Miledi & Slater 1968).

Injury to an axon also has immediate effects on the Schwann cells surrounding it, including a considerable decrease in myelin protein mRNA expression (Ludwin and Bisby 1991). Inuiguez and Alvarez (1999) hypothesise that differentiated Schwann cells repress the sprouting programme of injured axons, and that on dedifferentiation Schwann cells lose their ability to repress the sprouting programme. They propose that this programme is then expressed by injured axons until they receive a signal that instructs them otherwise. However, degeneration and not regeneration is the focus of this thesis, and the biological tool I have used to study this is the *Wld*^{s} mouse.

1.2. The *Wld*^{s} mutant mouse

The *Wld*^{s} mouse occurred as the result of a spontaneous natural mutation in the C57Bl/6J line of mice. This mutation has a surprising, but covert, effect on the degeneration of axons and synapses (Perry *et* al. 1990, Andressen *et al.* 2001). The C57Bl/Wld^s (C57Bl/ Wallerian degeneration, slow) mutant mouse was first discovered in the course of experiments in which the authors were attempting to manipulate macrophage influx to damaged peripheral nerves, and by chance noted that these nerves showed delayed Wallerian degeneration (Lunn et al. 1989).

1.2.1. What are the effects of *Wld*^{s} on Wallerian degeneration?

Wallerian degeneration is normally complete within twenty-four to forty-eight hours of axotomy, but in the *Wld*^{s} mouse (initially named C57Bl/Ola) the process is delayed by up to three weeks (Lunn *et al.* 1989). That is, axons are still capable of conducting a compound action potential (CAP), and for this to be possible, the plasma membrane and associated trans-membrane voltage-gated channels must retain their integrity and maintain a balance of the normal intracellular ion levels.

In an ultrastructural study by Ludwin and Bisby (1991), a marked delay in Wallerian degeneration was seen most clearly at all stages up to four weeks post injury when

comparing *Wld*^{s} to wild-type. After this, the differences became indistinguishable from the wild type. Although the morphology of nerves is preserved up to 4 weeks after nerve lesion, physiological signs suggest an earlier deterioration in the ability to conduct action potentials (Gillingwater & Ribchester 2001).

The obvious differences in the degeneration rates of the nerves between *Wld*^{s} and wild-type mice, suggest that the *Wld*^{s} mutation is of great potential value in furthering our knowledge/understanding of mechanisms underlying nerve degeneration. Studies to elucidate the mechanism by which this mouse inherits its slow Wallerian degeneration phenotype could therefore aid in our understanding of diseases that have a primarily axonal pathology (Perry *et al.* 1989).

All of the above information relates to axonal protection. There is, however, also a synaptic protection component to the *Wld*^{s} phenotype. Normally, following separation of the axon from the cell body, the axon and the synapse are seen to degenerate. In *Wld*^{s} mice however, there appears to be a withdrawal of synapses rather than degeneration. This withdrawal has been said to be reminiscent of neonatal synapse elimination observed during development (Gillingwater & Ribchester 2001, Gillingwater *et al.* 2002/2003).

The majority of the studies carried out on *Wld*^{s} protection have been conducted on peripheral tissue (Gillingwater & Ribchester 2001, Gillingwater *et al.* 2002). With regards the study of central nervous tissue, there have been few *in vivo* (Gillingwater *et al.* 2004, Ferri *et al.* 2003, Gillingwater *et al.* submitted), studies of protection, and those *in vitro* studies have been limited to tissue easily accessible for culture (i.e. cerebellum, cortex and hippocampus (Buckmaster *et al.* 1995, Deckwerth & Johnson 1994, Araki *et al.* 2005, Wishart *et al.* submitted, Gillingwater *et al.* submitted).

Mice with the *Wld*^{s} gene are developmentally normal, that is they have normal numbers of axons and undergo synapse elimination as normal. In 1997, Parson *et al.* carried out a

study on elimination of motor nerve terminals. The conclusions of this study were three fold; first, that the *Wld*^{s} gene does not have a direct effect on the normal rate of synapse elimination in post natal mice; second, that muscle fibres can sustain polyneuronal synaptic inputs even after motor axons are separated from their cell bodies, and third, and perhaps most importantly, synapse elimination and Wallerian degeneration do not occur by the same mechanism.

1.2.2. The *Wld*^{s} phenotype is age dependent

Perry *et al.* 1992 were the first to suggest that the effectiveness of the gene that slows the rate of Wallerian degeneration in C57BL/Wld^s mice declines with age. In four-week-old mice they showed that action potentials could still be evoked up to five days after sciatic nerve section and that compound action potentials could be evoked up to three weeks after section in the distal nerve stump. They contrasted this with one-year-old *Wld*^{s} mice, where they saw no action potentials five days after nerve section. They also showed that there was no difference in the extent of axon decline between heterozygous and homozygous *Wld*^{s} mice. It was also noted that normally in C57BL/J6 mice there is a slowing in the degeneration of nerves with increasing age. However this can probably be attributed in part to a decline in immune response and by the general slowing down of other metabolic processes.

Tsao *et al.* (1999) stated that the rate of CNS Wallerian degeneration in *Wld*^{s} mice also accelerates with the advancing age of the animal. They speculate that the protein product of the *Wld*^{s} mutation, involved with generating the *Wld*^{s} phenotype, is associated with particular changes in energy status and metabolism of the cell involved, but not however through the generation of a "detectable novel metabolite". They conclude that tolerance to Wallerian degeneration does not correspond with an increased energy status of the resting state of the cell.

In contrast to both of these studies, Crawford *et al.* (1995) presented data suggesting that the C57BL/Wld^s phenotype of prolonged survival of transected nerves was unaffected by age. A study by Gillingwater *et al.* (2002) agreed with the axonal findings of Crawford and colleagues, but in addition clearly demonstrated that both structure and function of motor nerve terminals following nerve injury are related to the age of the individual *Wld^s* mouse. Thus, mice older than three months lose functional transmission after nerve section much faster than a younger mouse.

In neuromuscular junctions observed by Ribchester *et al.* (1995) & Gillingwater *et al.* (2002), two features were noted; 1) The centre of the synaptic boutons showed an accumulation of neurofilaments, and so called "giant" synaptic vesicles. They postulate that as *Wld^s* mice mature, the axotomy induced synaptic response changes from withdrawal to degeneration. 2) It has been found that it is not the age of the animal that affects degeneration in the *Wld^s* mouse *per se*, but the age of the axon. A newly regenerated axon in an older animal behaves as an axon in a younger *Wld^s* mouse. This was found by Gillingwater *et al.* (2002) through the use of a conditioning lesion to regenerate axons in old *Wld^s* mice, and following a second lesion the regenerated axons and synapses degenerate similar to that found in the young *Wld^s* mice. Therefore, it is likely that it is the age of the synapse rather than the age of the tissue surrounding it which determines the degenerative mechanism.

Thus it appears that *Wld^s* has a selective effect on neurones, protecting axons from degeneration, but not cell bodies, and providing an age related protection of synapses which is dependent on the maturity of the neuronal tissue examined, not the chronological age of the animal (Gillingwater and Ribchester, 2001, Gillingwater *et al.* 2002).

1.2.3. What has been learnt from studying the *Wld*^{s} mouse?

Given the need for more detailed information of how Wallerian degeneration progresses, it is therefore of interest to study aspects of this process in *Wld*^{s} mice where Wallerian degeneration is considerably slowed. The study of the *Wld*^{s} mutation allows us to glean information not only on how Wallerian degeneration proceeds, but also how it may be possible to intervene. The following experimental information could not have been obtained in wild-type nerves where Wallerian degeneration would proceed too quickly for an in-depth examination.

In 1990 it was suggested by Perry *et al.* that the gene product responsible for slow Wallerian degeneration in the PNS also affects the CNS. In the same paper they also ruled out Schwann cells as being the essential cell involved in the prolongation of axon survival (Perry *et al.* 1990). Schwann cells have however been shown (in trembler mice) to affect the local modulation of neurofilament, and therefore local cytoskeletal architecture (Tsao *et al.* 1994). The mutation responsible for the altered Wallerian degeneration phenotype was initially thought to act by slowing macrophage infiltration to a damaged nerve. This was later discounted due to an elegant series of experiments in which sciatic nerve chimeras were generated through transplanting sections of nerves from wild type mice and *Wld*^{s} mice and then allowing subsequent regeneration of host axons through the grafts containing the donor Schwann cells. These experiments demonstrate that fast or slow degeneration is a property conferred by the host and cannot be ascribed to the Schwann cells (Glass *et al.* 1993).

In 1991 Ludwin and Bisby presented evidence that once the actual process of degeneration has begun, the cellular mechanisms that are involved look the same as those in the normal animal but proceed at a slower rate. The *Wld*^{s} mouse has also been used to study movement of cytoskeletal proteins following transection (Glass and Griffin 1991). Nerves were examined at various intervals following transection. No evidence was found to suggest proximal to distal emptying as would be expected if anterograde

transport was predominating, instead gradual redistribution of neurofilament towards severed ends could be seen, with a higher concentration towards the proximal end of the distal stump. The authors suggest that this points towards an ability for bi-directional transport of neurofilament in transected fibres. In 1994 Tsao *et al.* state that up to fourteen days post transection, bi-directional transport of neurofilaments have been shown to continue. They suggest that this shows that axonal transport systems also remain intact, and that the mutation does not affect the ability of proteases, once they are activated, to proceed with protein degradation within the axon. IL-6 has also been shown to be up regulated 1 day after nerve injury. Given that axonal transport can continue for up to 2 weeks after axotomy, the increased levels of IL-6 may continue to be transported. Interestingly, mice lacking IL-6 show smaller action potentials and, after injury, they show slower regeneration of sensory nerves. However, motor nerve terminals are shown to regenerate normally. These findings are similar to what Brown *et al.* have shown in 1992 (b). But, where Wld^s mice showed delayed macrophage influx to the injured area, the IL-6 deficient mice showed no difference in macrophage numbers (Stoll *et al.* 2002).

In 1994 Deckwerth and Johnson argued that if in programmed death, the neurites and soma are not linked and degenerate autonomously, then in the Wld^s mouse, when the cell body dies the neurites should remain viable. This is exactly what they saw in a very simple and elegant experiment reproducing the Wld^s phenotype *in vitro* with primary explant cultures of dorsal root and superior cervical ganglion. The cells put out neurites in the presence of nerve growth factor. Deckwerth and Johnson (1994) showed that neurites would remain viable even after removal of NGF and apoptosis of the neuronal soma. Glass *et al.* (1993) also showed that survival of transected Wld^s dorsal root ganglia (DRG) in explant cultures survived longer than transected wild type DRG in explant. In 1995, Buckmaster *et al.* carried out similar experiments, showing extended neurite survival in culture and Raff *et al.* (2002) also showed that localised dying back occurs in sympathetic neurones. If the distal part of an axon is locally deprived of NGF, that part of the axon will degenerate leaving the rest of the axon and cell intact. This phenotype

can even be seen when neurons are plated as single cells without Schwann cells arguing that the *Wld*^{s} phenotype is a property of the axon/neurite in question, and not the surrounding support cells.

Ribchester *et al.* (1995) suggested that the rate of degeneration of terminals and some of the physiological characteristics of degenerating motor terminals in *Wld*^{s} mice are similar to those in muscles kept at a much lower ambient temperature than normal. Ribchester *et al.* (1995) also state that the time course of degeneration depends on the length of the distal nerve stump (about 48 hours per extra centimetre).

In 1999, Tsao *et al.* suggested that there are three distinct stages of Wallerian degeneration, and that this was revealed through the use of temperature modulation. The effect of lowering temperature on slowing the rate of Wallerian degeneration could be attributed to alterations of degradative enzyme activity and/or rates of axoplasmic transport. They found that 100% of compound action potential was preserved if the nerve was cooled from 37 to 25 degrees after axotomy. This suggests that there is a critical period after the initial injury and before Wallerian degeneration effects manifest themselves, during which the sequence of events leading to axonal destruction may have started but are not yet evident. The three stages of Wallerian degeneration elucidated by Tsao *et al.* (1999) through the use of the *Wld*^{s} mouse are as follows: 1) The initial response occurs during the first 12 hours after axotomy. This latency can be prolonged by lowering ambient temperatures. Events taking place in this stage appear to initiate processes giving rise to Wallerian degeneration, 2) 12 to 24 hours post axotomy, morphology is normal, CAP remains close to 100% (until 24 hours), but cooling cannot prolong this stage, and finally, 3) Rapid degeneration of the axon during the period 24-48 hours, and corresponds with the rapid enzymatic digestion of axonal components. It is suggested that catastrophic Ca^{2+} entry marks the transition from stage 1) to 2), which enables Ca^{2+} influx, and stage 3), resulting from protease and lipase activation due to Ca^{2+} influx. This suggests that the slower rate of Wallerian degeneration is an intrinsic

property of the axons, rather than, for example, a property of supporting glial cells (Ribchester *et al.* 1995, Glass *et al.* 1993).

The degradation of axons by Wallerian degeneration and its selective protection by the *Wld*^{s} gene has motivated the hypothesis that the cell body, axon and synapses are separate compartments with regards mechanisms of degeneration (Figure 1.1). The slow Wallerian degeneration phenotype has been of great importance in unmasking for example, synaptic withdrawal in response to axotomy, which is similar in both rate and appearance to neonatal synapse elimination (Gillingwater and Ribchester 2001). As mentioned previously, this is experimental data it would not have been possible to obtain from a wild-type animal, as axonal degeneration proceeds at such a rate as to make it impossible to see potential differences in synaptic degeneration.

1.3.0. What is known about the *Wld*^{s} mutation?

Mice carrying the *Wld*^{s} mutation are indistinguishable from their C57BL/6J strain mates in their appearance, behavior, histocompatibility and genotyping of more than 50 microsatellite markers and restriction fragment length polymorphisms (RFLPs, Coleman *et al.* 1998, Mi *et al.* 2002/2003).

The mutation responsible for the delay in Wallerian degeneration was identified by positional cloning and gene sequencing (Figure 1.2). The mutation maps to the distal portion of mouse chromosome four, homologous with the human chromosomal region 1p34-1p36 (Lyon *et al.* 1993). Perry *et al.* (1990) showed that the gene behaved as a single autosomal dominant gene, with heterozygotes slightly less affected than homozygotes. Lyon *et al.* (1993) mapped the locus (*Wld*^{s}) of the gene believed to be responsible for the *Wld*^{s} phenotype, and they showed that crossing did not impair the expression of the mutant phenotype with their linkage testing stocks. In the course of this investigation the mutant phenotype was found to vary with age (Perry *et al.* 1992). Ribchester *et al.* (1995) also commented that the capacity of motor nerve terminals to

withstand nerve injury is related to the age of the individual mouse, they showed that mice over three months of age lost functional transmission much more rapidly after nerve section than younger adult mice. Thus, a reduced "gene dose" (in heterozygotes) and aging (in homozygotes) appear to weaken the *Wld*^{s} phenotype (Figure 1.3).

Coleman *et al.* (1998) carried out the fine mapping of the gene responsible for the *Wld*^{s} phenotype through the generation of a 1.4Mb bacterial artificial chromosome (BAC), and contig mapping. They found that the *Wld*^{s} mutation comprises three genes, which are themselves arranged within a tandem triplication of about eighty-five kilobases (Kb) in size (Conforti *et al.* 2000, Coleman *et al.* 1998, Lyon *et al.* 1993, Figure 1.2).

1.3.1. How did this mutation arise?

Although the *Wld*^{s} mutation involves a spontaneous triplication of an 85 kb region, in some cases duplication was noted. Coleman *et al.* 1998 suggested that this could indicate some instability in the repeat copy number, which also suggests that the triplication arose from a duplication by unequal crossing over. The predominant genotype appears to have been the triplication for a number of years now. The duplication has only been observed post mortem, so it would be of interest to know how duplication affects phenotype. Mi *et al.* (2002) after examining 128 chromosomes from *Wld*^{s} mice using PFGE (pulse field gel electrophoresis), suggested that they can examine the instability of the triplication at the chromosomal level. They were all found to contain the triplication. This indicated the duplications may have been an original mutation rather that a partial reversion. They have also pronounced the triplication to be a stable mutation.

Coleman *et al.* (1998) also pointed out the presence of a mini-satellite array of eight bases (5'-GCCCCCAC-3', guanine and cytosine rich) at both the distal and proximal boundaries of each repeat unit, which they believe suggests recombination between short homologous sequences, either by "illegitimate" or "non-homologous" recombination. There is the possibility that this mutation arose from viral origin. A small viral sequence

would present the possibility of doing a pathogenicity island (PAI) study on gene compression if the viral sequence is actually linked to the gene. This has not been mentioned in any publications on *Wld*^{s} to date. The repeat sequence is present at the proximal boundary and also makes up part of a minisatellite repeat of twenty-two base pairs at the distal end. This eight base pair repeat should not, statistically be present by chance at each boundary. Statistically it should only appear in sequence once every sixty-four kilobases. There are of course, always exceptions. There was also an endogenous retroviral sequence found, 40-46 Kb from the proximal end of the repeat unit

Three genes are encoded within the eighty-five Kb tandem triplication. These include firstly, Rbp7; a novel member of the cellular retinoid binding protein family, and it is highly expressed in white adipose and mammary tissue. It was previously suggested that it was undetectable by Northern blot of *Wld*^{s} brain (Conforti *et al.* 2000, but see results chapter 5). It is likely to function in retinol storage and release. Given that retinoic acid can induce neuronal differentiation it was thought during the early characterisation of the *Wld*^{s} mutation that *Rbp7* may be involved in neuroprotection in the *Wld*^{s} mouse. However, the possibility that Rbp7 may play a critical role in the generation of the *Wld*^{s} phenotype was discounted by the demonstration that transgenic lines which express only the chimeric portion of the mutation (i.e. the N-70 Ube4b/Nmnat1 C-303 chimera) is sufficient to recapitulate the *Wld*^{s} phenotype (Adalbert *et al.* 2005; Mack *et al.* 2001). As *Rbp7* is not over expressed in these transgenic lines and the phenotype is expressed it is considerably unlikely to contribute to the phenotype. There has however been no direct test of the effects of *Rbp7* overexpression in a model system. Secondly, *D4Cole1e*; has since been shown to code for nicotanamide mononucleotide adenyltransferase (*Nmnat1*) that was previously undescribed. *Nmnat1* is involved in the regulation of NAD^{+} levels. This will be discussed below in more detail. Finally, *Ufd2*, ubiquitin fusion degradation protein, shown to have high homology with the N-terminal fragment of the ubiquitination factor E4B (*Ube4b*). *Ube4b* is a part of the ubiquitin proteasome system, which will also be discussed in more detail below. Both *Nmnat1* and *Ube4b* lie in the

same orientation and when brought together form the *Wld*^{S} chimeric gene. The chimeric mRNA is strongly expressed in the nervous system and codes for a fusion protein (in frame) that is made up of the N-terminal seventy amino acids of *Ube4b* (which are normally not expressed in *Ufd2* in yeast) and the C-terminal three hundred and two amino acids of *Nmnat1*, and an aspartic acid formed at the junction (Conforti *et al.* 2000, Figure 1.2). There are also two more potential exons spliced to the 5' end of the exon noted using a 3'-RACE (rapid amplification of cDNA ends) and RT-PCR, identified by Conforti *et al.* (2000) through exon trapping, which are not present in the expressed sequence tag (EST) database. The authors also did not give a sequence or any additional information about them. It is not known whether or not these potential exons have any significance.

The chimeric gene has been shown to be responsible for the slow Wallerian degeneration phenotype through the use of a viral vector to transform DRG (dorsal root ganglion) cells and induce a protective phenotype against toxic neuropathy in the peripheral nervous system (Wang *et al.* 2001) as well as by studying various transgenic lines (Mack *et al.* 2001, Adalbert *et al. 2005*) demonstrating that transgenic expression of the chimeric protein in rats and mice is sufficient to fully reproduce the gene dose dependent protective phenotype. Until this point the possibility remained, however unlikely, that the causative gene did not lie within the triplication, but may be subject to a positional effect (Conforti *et al.* 2000). There is a wide expression of the transcript, which is consistent with the observation that *Ube4b* (whose promoter is thought to drive the expression) has an EST in a wide variety of tissues, with particularly high expression in the brain (Conforti *et al.* 2000). The fusion protein has been shown to give a dose-dependent block of Wallerian degeneration (Mack *et al.* 2001, Figure 1.3), conferring protection of both the motor and sensory axons in the C57Bl/Wld^{S} and transgenic mice containing the same gene (Mack *et al.* 2001). I will now refer to the protein product of the gene (*Ube4b/Nmnat1*) as "Wld^{S} protein". Coleman *et al.* 1998 suggested that an increased dosage of the gene may cause an increase in its rate of transcription, and therefore a steady increase in the amount of protein product (Figure 1.3). All exons

within the fusion protein are in the same chromosomal orientation (5' proximal, 3' distal).

1.4.0. How might *Wld*^{s} work?

The exact mechanism by which the *Wld*^{s} mutation is protecting axons is unknown. However, every experiment undertaken leads us one step closer to an understanding.

Lunn *et al.* (1989) suggested that failure to recruit macrophages and polymorphonuclear cells were the reason for the resulting slow rate of Wallerian degeneration. They blocked recruitment with an antibody, and found that a reduction in myelomonocytic recruitment helped preserve a rapidly degenerating nerve for at least five days. Ribchester *et al.* (1995) suggests that nerve section normally activates cellular components or processes already present, but which are latent in axons and motor nerve endings. Could it be that in *Wld*^{s} mice, either the trigger or the cellular response is abnormal?

There is evidence suggesting that the phenotype is not due to the surrounding glia (Glass *et al.* 1993). However, examining axon-glia signalling with respect to CNTF (ciliary neurotrophic factor) that is a potential maintenance factor, in wild type animals following axotomy, the CNTF protein and mRNA levels decline rapidly, whilst in the *Wld*^{s} mice both CNFT protein and mRNA levels remain constant for at least four days following axotomy before declining slowly to be equal with wild-type levels at ten days (Subang *et al.* 1997).

Wallerian degeneration appears to occur via mechanisms distinct from those responsible for degeneration of the cell body, since over-expression of *bcl-2* which inhibits somatic apoptosis, appears not to affect its rate and that the degeneration appears to occur in a caspase independent manner suggesting a non-apoptotic mechanism (Ikegami & Koike 2003, Ferri *et al.* 2003). It is also known that caspase-3, which is important for apoptosis in neurones (Xue *et al.* 2001), is not activated in Wallerian degeneration indicating that

the mechanism of Wallerian degeneration is distinct from the caspase dependent apoptosis required for cell body apoptosis. Caspase inhibitors do not alter the progression of this type of degeneration and in cultures of sensory *Wld*^{s} neurones, removal of NGF will cause the cell body to undergo apoptosis immediately whilst axons may remain in culture for a following five days plus (Buckmaster *et al.* 1995, Deckwerth & Johnson 1994).

Buckmaster *et al.* (1995) showed that the rate of degradation could be slowed by increased time in culture before cutting or withdrawal reaching a maximum by about seven days. This suggests that the mechanism responsible for the protective phenotype requires time to activate in culture, i.e. the Wld^s protein is present in the adult cerebellar granule cells, but is not visible at the age (P4) from which the cultured cells were taken from (see chapter 4). So in this case, the delay in the onset of protection in culture could represent the time taken for the activation of the protective phenotype (further explanation will be given in chapter 4). Following culture of sympathetic neurones DRG and SCG, Buckmaster *et al.* (1995) observed the effect of removing NGF (nerve growth factor) as an initiator of SCG death (Edwards *et al.* 1991) from the culture media. Raised potassium in the media in conjunction with NGF withdrawal was found to extend cell survival by up to 3 times. In this case it was seen that cell bodies die first and that neurites would remain for some time. This indicates that neurite degradation is controlled by the neurites themselves (as suggested in section 1.2.3), or that the degradation of neurites is continuously inhibited by a signal from the cell body, and when this is removed the neurites begin to break down. With cerebellar granule cells, which were the authors CNS cells of choice for culture, after three days in culture neurites were cut, *Wld*^{s} cells survived for 3-4 days but wild type cells survived only 18-20 hours. After seven days in culture, the axotomised *Wld*^{s} neurites survived for up to and more than five days and the wild-type only survived for about 36 hours after section. This study formed the basis of an assay I will use to measure *Wld*^{s} phenotype in vitro (described in chapter 4).

It has been shown that the chimeric Wld^S protein is localised almost exclusively to neuronal nuclei, and is therefore not present in large amounts in axonal or synaptic compartments (Mack et al. 2001; Fang *et al.* 2005, Wishart et al. submitted). I will also demonstrate that Wld^S protein co-localises with transcriptional regulators such as HDAC5 and SMRT, as well as part of the UPS (VCP, see chapter 4). This suggests that *Wld^S* is not capable of directly protecting axons and synapses, but rather that downstream effector targets, present in non-somatic neuronal compartments, are required to generate the neuroprotective phenotype (Coleman & Ribchester, 2004). Several lines of investigation appear to lend support to the hypothesis that gene expression patterns could be regulated by *Wld^S* (Gillingwater and Ribchester 2001, Araki *et al.* 2004, Fang *et al.* 2005).

In protecting axons that have been severed, the fusion protein localised to the nucleus in areas of the nervous system showing a protective phenotype (Mack *et al.* 2001, Fang *et al.* 2005, Wishart *et al.* submitted) is protecting a part of a neuron that has effectively been disconnected from the cell body and nucleus. This, importantly, suggests an indirect mechanism of neuroprotection.

1.5.0. Dissecting the molecular mechanism of *Wld^S*-induced axon protection

I have described how the *Wld^S* gene is an amalgamation of three genes in the spontaneous mutant: *Nmnat1* (Nicotanamide mononucleotide adenyltransferase 1), *Rbp7* (Retinoid binding protein 7) and *Ube4b* (Ubiquitination factor E4b). I have also stated that the portion of the mutation sufficient to reproduce the *Wld^S* neuroprotective phenotype is the N70-Ube4b-Nmnat1-C303 chimera. The sequestration of the Wld^S chimeric protein to neuronal nuclei suggests that it is incorrectly located to have a direct effect on axonal and synaptic protection following disease and injury.

Three strong hypotheses concerning the mechanism of action are therefore;

1. Over expression of *Nmnat1*; Over expression of this protein within nuclei may lead to high local concentrations of *Nmnat1*, which if functional could affect neuronal survival through the NAD pathway via several routes.
2. Dominant negative effect of *Ube4b*; *Ube4b* is a component of the ubiquitin proteasome pathway. One speculated mode of action is that because the Wld^S mutation only incorporates the N70 amino acids of *Ube4b*, it may act by interfering with native *Ube4b*. It could also be a case that a large amount of "foreign" protein within the nucleus leads to sequestration of the majority of the cells chaperone system, resulting in an alteration of the ubiquitin proteasome system.
3. Gene regulation by either or both *Ube4b/Nmnat1;* Both *Nmnat1* and *Ube4b* have been shown to be capable of affecting transcriptional regulation, either directly or indirectly.

These possibilities will be explored in more detail below.

1.5.1. *Nmnat1*/NAD hypothesis

In humans the nuclear enzyme Nmnat1 catalyses an important step in the NAD (NADP) biosynthetic pathway (Raffaelli *et al.* 2002, Figure 1.4) and therefore also plays an important role in the oxido-reducatse pathway in mitochondria. It has been demonstrated that in yeast and *C.elegans*, life span can be extended through manipulation of the NAD^+ pathway. This is through the activation of the NAD^+ dependent histone deacetylase Sirt2p. It has been shown that an increase in *NPT1*, which encodes a nicotinate phosphoribotransferase critical for the NAD^+ salvaging pathway, increases Sir2 dependent silencing, stabilising the rDNA locus (which would otherwise give rise to circular forms of rDNA termed extrachromosomal rDNA circles that replicate, but do not segregate to daughter cells and eventually kill cells, by titrating essential transcription factors and replication factors once the numbers exceed 1000 copies) and can extend yeast life span by up to 60% (Anderson *et al.* 2002). Both *Npt1* and *SIR2*

have been demonstrated to provide resistance against heat shock suggesting that they can also act in a more general manner, which can promote cell survival.

A recent publication by Araki *et al.* (2004) suggested that it is an increase in nuclear NAD biosynthesis that prevents axonal degeneration in the *Wld*^{s} mouse. This was based on the effects of adding exogenous NAD to DRG cultures before insult, to show that this was sufficient for protection. Although the protection demonstrated was not as strong as that seen in the *Wld*^{s} mouse, it was an improvement on the situation normally seen in the wild-type mouse. Furthermore, Araki *et al.* also suggested that this protection was mediated through a Sirt1 dependent pathway. The evidence for this was that when cultures incubated with exogenous NAD were exposed to sirtinol, an inhibitor of Sirt1, the cultured neurones no longer displayed a neuroprotective phenotype. This study has generated a controversy within the field of *Wld*^{s} research, mainly because generation of transgenic lines which over express *Nmnat1* were previously thought to have no neuroprotective phenotype (Coleman and Perry 2002). Until recently, no one has published confirmation of the work published by Araki *et al.* (2004). A recent paper presents results which did not completely agree with all of Araki's findings (Wang *et al.* 2005). At the time of writing this thesis, Coleman *et al.* were preparing a paper for publication (M.P.Coleman, personal communtication) showing that several transgenic lines over-expressing *Nmnat1* fail to show the neuroprotective phenotype described by Araki *et al.* (2004). This highlights the importance of validating work carried out *in vitro*, *in vivo* models when investigating phenotype.

Wang *et al.* (2005) are the first group to publish data relating to the Araki study. The suggestion by Wang *et al.* that NAD is important in regulating neuroprotection supports some of the findings of the Araki *et al.* paper. Moreover, Wang *et al.* suggest that there is a Sirt1 independent local pathway which could be involved in the NAD dependent protection. That is, local bioenergetics pathways may be important as suggested by the ability of 10mM methyl-pyruvate (a membrane permeable version of the glycolytic end point, pyruvate) to prevent a decrease in axonal ATP levels and protect against axonal

degeneration. It was also shown that inhibition of the Sirt1 pathway did not affect neuroprotection in their model system. This also is not consistent with the observations reported by Araki *et al.* (2004) and suggests that the action of NAD in a Sirt1 dependant fashion is not sufficient to fully reproduce the *Wld*^{S} neuroprotective phenotype *in vitro*. Thus, the role of NAD levels in conferring the *Wld*^{S} phenotype still remains unclear.

1.5.2. Ube4b and the ubiquitin proteasome hypothesis

Proteasome inhibitors have been demonstrated to block Wallerian degeneration both *in vitro* and *in vivo*, and for this reason, until the publication of the study by Araki *et al.* (2004), the *Ube4b* portion of the *Wld*^{S} gene has been considered the most likely candidate for neuroprotective regulation in *Wld*^{S} (Zhai *et al.* 2003).

Ubiquitin is a highly conserved 76 amino acid protein. This protein acts as a tag, and the length of this tag is very important in its recognition. The ubiquitin proteasome is "a complex macromolecular tube whose inner aspect is lined with proteases" (Grey, 2001). The ubiquitin proteasome system and ubiquitin, until relatively recently, were thought to only be involved in preventing protein misfolding and removal of proteins which have become so misfolded that this cannot be prevented. I discuss in more depth below, the emerging view that ubiquitination is a very versatile process, whose complexity should be considered to rival that of the phosphorylation signalling system. Monoubiquitination has been shown to be involved in various activities ranging from histone regulation and transcriptional regulation to endocytosis and budding of retroviruses from the plasma membrane in yeast (Hicke, 2001). The most important point to note is that there is a mechanism for determining ubiquitin chain length, and that the ubiquitin proteasome system has a threshold length of four ubiquitin subunits before the chain and attached protein cargo are directed to the proteasome for degradation.

In yeast, members of the E4 family ubiquitination factor proteins (of which Ube4b is a member) are involved in multiubiquitin chain assembly, and their activity is linked with

cell survival under stress conditions. This suggests that eukaryotic cells may use E4 dependent proteolysis pathways for many cellular functions (Kogel *et al.*1999, Figure 1.5). See below.

Substrates of the ubiquitin/proteasome pathway can be "recognised" by the ubiquitin conjugation system and are then signalled for degradation by the addition of ubiquitin molecules (Kogel *et al.* 1999, Figure 1.5). For ubiquitin molecules to be added to a protein, several events must take place which utilise combinations of several different interacting proteins;

1) E1-Ubiquitin activating enzymes. E1s hydrolyse ATP to produce energy for the reactions that are about to occur, and a high-energy thioester bond is formed between a cysteine of E1s active site and the C-terminus of a ubiquitin molecule, which becomes "active".

2) E2-Activated ubiquitin is then passed from E1s on to E2s, which are a family of ubiquitin conjugating enzymes. The E2s then form a thioester link with ubiquitin in a similar fashion to E1. These can then in some cases interact directly with the substrate protein and add ubiquitin directly to the side chain of a lysine residue, or it can go via another protein family, the E3s.

3) E3-Ubiquitin is attached covalently to the substrate protein by ubiquitin protein ligases (E3s).

4) E4- binds to conjugated ubiquitin moeties and working in conjunction with E1, 2 and 3 can drive the addition of more ubiquitin to yield longer chains (Figure 1.5).

What is the significance of this? The preferred substrate of the 26S proteasome are multiubiqiutinated proteins, whilst mono-, di- and tri- ubiquitinated substrates appear to be persistent for longer within the cell and are later subject to degradation by different degradation pathways (Kogel *et al.* 1999). So, there appears to be a hierarchy for protein degradation, akin to a "green", "amber", "red" hierarchy of alert states for protein removal, where multiubiquitination via E4 facilitates more rapid removal of these proteins than shorter ubiquitin chains, which are slower acting. In contrast to E3,

the E4 (including Ube4b) proteins do not interact directly with the substrate, but with the ubiquitin moeties of the ubiquitin-substrate conjugates (Kogel *et al.* 1999). E4 is apparently essential for cells under stress conditions, at least in yeast (Kogel *et al.* 1999). When a cell under stress conditions is examined, there will be a large increase in the percentage of aberrant proteins within the cell, with the potential to interfere with normal cell function, and chaperones will be overwhelmed. So ubiquitination is the next step in rapid removal of proteins tagged with a "code red" degradation signal. It has also been speculated that ubiquitin can be used to completely coat misfolded proteins and keep them out of circulation if the degradation pathways are overwhelmed such as in Huntington's disease (Arrasate *et al.* 2004). Ubiquitinated deposits are also observed in brains of patients with Alzheimer's disease where it accumulates in the form of neuritic plaques. Intranuclear inclusions also appear in other polyglutamine diseases such as Myotonic Dystrophy.

Ubiquitination to the point of recognition by the proteasome for degradation is probably not the only function of the ubiquitination system. It may not always be necessary to degrade misfolded or aggregated proteins. There is a large pool of de-ubiquitinating enzymes within the cell. This may act as a means of rescuing tagged protein from definite degradation through the proteasome. This may also be a way of reclaiming ubiquitin back to the system for use in the event of severe stress. Imagine that there is the formation of large aggregates within the cell, and that more protein is being misfolded. A coating of ubiquitin to stop these aggregates from interacting with other processes within the cell may be all that is needed. The production of misfolded protein may be so great that the proteasome cannot keep up and there is insufficient ubiquitin to fulfill the needs of the cell. Reclamation of ubiquitin from ubiquitin chains may be the only way to deal with these aggregates.

Addition of ubiquitin is important. However, there are several possible steps that could follow on from the ubiquitin tagging of substrate proteins, and which add further complexity and flexibility to the system. One other step in this chain is VCP (valosine

containing protein/p97/CDC48), which is a member of the AAAfamily (ATPases with multiple cellular activities), involved in a range of different functions including membrane fusion, nuclear envelopes, nuclear envelope reconstruction, post mitotic Golgi reassembly and ubiquitin dependent degradation (Wojcik 2002). Interactions with *Ube4b* could also indirectly affect transcriptional regulation (see chapter 4).

In mammals, *Ube4b* (in yeast, *Udf2*) is a protein needed for the addition of multiubiquitin chains to a ubiquitinated substrate. The predicted amino acid sequence within the *Wld*^{s} gene is identical to the human *Ufd2* sequence, but Conforti *et al.* (2000) state that it represents an N-terminal extension of the yeast *Ufd2* protein. In the presence of active E1, E2 and E3 enzymes, *Ufd2* is known to be required for the multiubiquitination of already ubiquitinated substrates in yeast. The presence of the N-terminal 70 amino acids of *Udf2* in the fusion protein was therefore of interest due to the rise in reports of altered ubiquitination in neurological disease.

1.6.0. Gene regulation hypothesis

Both the *Nmnat1*/NAD and *Ube4b*/ubiquitination hypotheses support the idea that either or both of these pathways can be involved in transcriptional regulation. Once again, given that the Wld^{s} chimeric protein (comprising the N-70 amino acids of Ube4b and all of Nmnat1) is localised exclusively to the nucleus, it is important to fully explore the possibility of an indirect action through transcriptional regulation.

1.6.1. *Nmnat1*/NAD pathway and transcriptional regulation

Sir2 in yeast is a silencing protein believed to be a component of the heterotrimeric Sir2/3/4 complex. This complex catalyses the formation of silent heterochromatin at telomeres. It is also a regulator of nucleolar silencing and has also been shown to directly stimulate transcription of rRNA by polymerase I (Anderson *et al.* 2002; Blander and Guarente, 2004). Its deacetylase activity is dependent on NAD^{+}. Sir2 are a family of

protein deacetylases and have been shown to deacetylate and therefore inactivate p53 (Blander and Guarente 2004). Sir2 have also been implicated in the regulation of the FOXO transcription factors, specifically FOXO3a through deacetylation and therefore repression of activity (Brunet *et al.* 2004, Motta *et al.* 2004). It has also been demonstrated that negative control of p53 by a member of the Sir2 family (specifically Sir2α) can promote cell survival under stress conditions (Luo *et al.* 2001) by specifically repressing the p53-dependent apoptotic response. In yeast Sir2 is the only protein exclusively localised to nuclei whose activity is of great importance for both gene silencing and extension of yeast life span. Sir2α and its human orthologue SIRT1 are the closest homologous to yeast Sir2 and both of them are exclusively localised to nuclei. Sirt1 has also been shown to regulate the transcriptional activity of NF-kappaB. Sirt1 has been demonstrated to interact directly with the RelA/p65 subunit of NF-kappaB and therefore inhibit transcription by deacetylating this subunit. As stated previously, Sirt1 activity can affect apoptosis. Yeung *et al.* (2004) suggest that one pathway for this control may be in response to TNFalpha deacetylation inhibiting the transactivation potential of the RelA/p65 protein (Yeung *et al.* 2004).

1.6.2. *Ube4b*/ubiquitination pathway and transcriptional regulation

The very fact that there is a threshold mechanism for recognition by the ubiquitin proteasome system means that degradation mediated by ubiquitin proteasome system is not an all or nothing system. At first glance, gene transcription and ubiquitin-mediated proteolysis are two processes that do not appear to have anything in common. However, ubiquitylation of RNA polymerase II itself is an important step in transcription coupled DNA repair, in which the presence of DNA damage in a transcribed gene stops transcription and allows for the co-ordinated entry of the DNA repair machinery (Muratani and Tansey, 2003). More recent research by Muratani *et al.* (2005) has added significantly to our knowledge of transcriptional regulation, as can be affected by ubiquitination. As already mentioned, polyubiquitination targets a protein for degradation, but monoubiquitination, although it can lead to destruction, can also simply

alter the function of the "tagged" protein without signaling its destruction. There is support for the idea that the ubiquitination system should be considered as versatile a signaling mechanism as phosphorylation. Gal4, which is a transcriptional activator in yeast, is known to bind to specific regulatory sites in the regulatory regions of the *GAL* genes. It can activate transcription to a high level when the yeast *S.cerviciae* is grown with galactose as a carbon source, i.e. under activating conditions. Gal4 ubiquitination, and in this case subsequent destruction, are required for activation by Gal4 (Muratani *et al.* 2005). Gal4 is not unique in having an overlap of activation and "destruction" domains. It has now been shown that this is a more general phenomenon that occurs in unstable transcription factors with a close correlation between the ability of an acidic activation domain to activate transcription as well as signaling proteolysis. Salghetti *et al.* (2000) showed that this is the case for Myc and in doing so, may have been the first to hypothesise that transcription factors could be "destroyed" because of their ability to activate transcription.

There are other examples where ubiquitination is important in transcriptional regulation, for example, monoubiquitination of histone H2B is known to be associated with activation of transcription and transcriptional activation. (Xiao *et al.* 2005, Laribee *et al.* 2005). The role of ubiquitination in transcriptional regulation has been suspected for many years now. A review published in 1998 (Hershko and Ciechanover) makes the case specifically for the role of ubiquitination in the NF-κB (Nuclear Factor κB) system. NF-κB is a transcription factor involved in many processes including immune, stress, inflammatory and developmental processes. NF-κB is a collective name for inducible dimeric transcription factors that are made of members of the Rel family of DNA binding proteins (Jesenberger and Jentsch, 2002). There are five Rel proteins in mammals; NF-κB1 (p50 and its precursor p105), NF-κB2 (p52 and its precursor p100), c-Rel, RelA (p65) and RelB. The latent form of NF-κB1 is located within the cytoplasm through association with inhibitory molecules termed IκBs (inhibitors of κB which mask nuclear localisation signal and inhibit DNA binding ability of NF-κBs). When the cell is stressed, IκBs are degraded and the active heterodimers are transported to nuclei to

affect transcriptional regulation. It has been demonstrated that through phosphorylation at serine residues 32 and 36, is strongly recognised by the ubiquitin conjugation machinery at lysine 21 and 22, followed by degradation by the proteasome (Hershko and Ciechanover, 1998). Mutations in TAF250 that inhibits its ubiquitination activity cause defects in transcriptional activation in Drosophila embryos, indicating that TAF250 dependent H1 ubiquitination may control gene expression (Hicke, 2001). There are many other proteins in transcriptional systems which can be affected by ubiquitination, including; Mdm2, c-Jun (but not v-Jun), β-Catenin (better known for its involvement in the "wingless" pathway) and the EF2 family of transcription factors.

VCP (VCP/p97/Cdc48p AAA chaperone) as mentioned earlier is a link in the ubiquitination pathway (in some cases directly interacting with UFD2 in yeast) which may, indirectly, be able to effect transcription. It has been demonstrated that VCP can interact with HDACs to alter acetylation and therefore other processes within the cells (Seigneurin-Berny *et al.* 2001). This is therefore a link between the ubiquitination and acetylation pathways, adding another level of complexity to the ubiquitination system. Class I HDACs are homologous to yeast RPD3, class II HDACs are related to HDA1 and class III members are related to yeast SIR2 deacetylases. The interaction of VCP with class III HDACs (SIR2 homologous) may not appear significant at first glance. However, when this information is take in context with the earlier description of the *Nmnat1* portion of the *Wld*^{S} gene and its possible interactions, this information becomes more interesting. Another interesting point is that a number of proteins show an association with HDACs, and within this group of HDAC associated proteins are mammalian homologues of the yeast UFD pathway (Seigneurin-Berny *et al.* 2001). HDACs are involved in transcriptional regulation, and HDACs 4, 5, 6 and 7 have been shown to shuttle between the nucleus and the cytoplasm.

1.7. Protein aggregates in neurodegenerative disease

Taking into account that the Wld^S chimeric protein is localised exclusively to neuronal nuclei (Fang *et al.* 2005, Wishart *et al.* submitted) it is perhaps important to know whether inclusions observed in neurodegenerative diseases are pathogenic, incidental or even beneficial? Opinions are divided into two camps; 1. Those adherent to the view that the formation of a protein aggregate is pathogenic, as the aggregates have the ability to absorb other important cellular proteins. 2. Those who think that the formation of aggregates in disease models represent an attempt to protect the cell by sequestering mutant/abnormal proteins, reducing interference with vital cell processes.

A number of neurodegenerative diseases feature progressive cell loss in specific sub populations of cells that appear to have some level of susceptibility to the formation of certain protein aggregates. There are a number of processes that induce neurodegeneration and may lead to abnormal protein aggregation. For example, unusual protein interactions leading to altered degradation and aggregation (i.e. through the UPS), oxidative stress and free radical formation leading to altered chaperone activity, and altered bioenergetics (as may be the case with *Nmnat1* in Wld^S). A recent study by Arrasate *et al.* (2004) suggests that the formation of protein inclusions in models of neurodegenerative diseases may actually be protective for the cell involved. Through following neurones transfected with GFP tagged mutant protein, they were able to demonstrate that those cells which formed neuronal inclusions were at a "significantly" reduced risk of dying.

Ubiquitin is detectable in a number of human neurodegenerative diseases whose most distinctive traits are the formation of protein aggregates. It has most frequently, been assumed that these inclusions and the presence of ubiquitin may be the consequence of failure to remove these abnormal protein structures by the cell. However, there is the possibility that the presence of ubiquitin may serve a protective function to the cell. That is, a surface coating of ubiquitin may 1) prevent further growth of the aggregate, 2)

prevent interaction of this aggregate from interfering with normal cell processes and 3) conceal the aggregate from detection mechanisms which may, ultimately lead to the destruction of the cell (Gray, 2001).

VCP has previously been demonstrated to suppress the formation of polyQ aggregates in a *C.elegans* system and as such it has been suggested that VCP/p97/Cdc48p homologues (AAA chaperones) may have a protective role in polyQ aggregation (Yamanaka *et al.* 2004). It has also been demonstrated that mutations in VCP can lead to inclusion body myopathy, which is associated with Paget disease of bone and frontotemporal dementia (IBMPFD). The identification of VCP mutations as being important in IBMPFD could be an important step in the understanding of common ubiquitin based disease pathways (Watts *et al.* 2004, Schroder *et al.* 2005). A large protein deposit within the nucleus may not appear to be a good thing, however, if it is coated with ubiquitin, it may be preferable to, say, expanded polyglutamine tracts, potentially interfering with transcriptional machinery or other potential cell functions (Grey, 2001).

So, alterations in ubiquitin pathways overall play an important role in axon degeneration. Synaptic changes in neuromuscular synaptic form and function are known to be altered in *Drosophila* mutants which display up or down regulated deubiquitinating proteases or ubiquitin ligases (Gillingwater *et al.* 2002). Coleman and Perry (2002) in their review suggest that all available evidence for the mechanism of protection in Wld^S leans towards ubiquitination-proteasome pathway being involved for three reasons: First, that the basal level of NAD is unaltered in the unlesioned Wld^S nervous system, although that does not necessarily negate the possibility that the situation will not undergo rapid alterations in a lesioned system. Secondly, that transgenic expression of *Nmnat1*, when fused to a shorter *Ube4b* sequence does not delay Wallerian degeneration, indicating that the *Ube4b* fragment is necessary for slow Wallerian degeneration. Thirdly, that mutations in other ubiquitin-proteasome pathways have been shown to alter neuronal degeneration, for example in recessive juvenile Parkinson's disease and *gad* (gracile axonal dystrophy) mice. *Gad* mice carry a mutation in UCH-L1,

which is associated with inclusions in a variety of neurodegenerative disorders, and which was recently shown to have the ability to shorten ubiquitin chains on specific substrates (Grey, 2001). This suggests that *gad* mice may be predisposed to the formation of inclusions/aggregates through the depletion of monomeric ubiquitin pools.

1.8. Neurodegenerative diseases shown to be affected by *Wld*^{s}

Crossbreeding *Wld*^{s} mice with models of neurodegenerative diseases has given cause for optimism that there may be some functional use for the application of knowledge gained from the study of *Wld*^{s} (Figure 1.6). For example, in the treatment of neurodegenerative disorders including; myelin related neuropathy (Samsam *et al.* 2003), motor neurone disease (Ferri *et al.* 2003), Parkinsons disease (Sajadi *et al.* 2004) and Gracile axonal dystrophy (Beirowski *et al.* 2005) it has been shown that the *Wld*^{s} gene leads to attenuation of symptoms and extension of life span in the models studied. This suggests the plausible hypothesis that these diseases converge on one or more pathways that are also impacted upon by *Wld*^{s}. This also suggests that by testing to determine which disease and other conditions i.e. stroke (Gillingwater *et al.* 2004) are affected by *Wld*^{s}, it should then be possible to determine common pathways which may be affected.

Several groups worldwide are currently using this strategy. It is therefore important to identify the genetic status of mice crossbred with *Wld*^{s} mutants especially in order to be certain that the crossbreeding has proceeded to a homozygous *Wld*^{s} state. As previously mentioned, only homozygous animals show the *Wld*^{s} synaptic phenotype. Heterozygous animals show neither any overt constitutive phenotype that would allow identification without a neurological examination, nor any identifiable polymorphisms that may lead to their genotyping by conventional methods. Genotype cannot be resolved by conventional PCR, and southern blots are too insensitive to allow a confident identification of genotype. The current method for genotyping *Wld*^{s} mice is accurate and reliable, based on pulse field gel electrophoresis (Mi *et al.* 2002). However, this method

is time consuming and technically difficult to perform. A more rapid, reliable method for genotyping the mutation would be highly desirable for genotyping multiple crosses.

1.9. Aims

The aim of this thesis is to advance our understanding of the mechanisms controlling nerve degeneration, by examining the molecular interactions of the *Wld*^{S} gene and its chimeric protein product. Given the extent of knowledge currently available on the mechanism by which the *Wld*^{S} mutation provides a neuroprotective phenotype, the objectives of this thesis were three fold;

1. To develop a rapid and cost effective method for genotyping using quantitative real time PCR on genomic DNA from the spontaneous *Wld*^{S} mutant mouse and transgenic lines. This method should allow the determination of *Wld*^{S} copy number (specifically a region of the N70-*Ube4b* portion of the *Wld*^{S} gene) for genotyping and calculating insertion number in transgenic lines.

2. To advance knowledge of the localization of the Wld^S protein product throughout the nervous system through immunohistological mapping. Available to me was a highly specific antibody generated against the Wld-18 peptide, which has previously been used to confirm that the *Wld*^{S} protein product is localised to neuronal nuclei in the PNS. I will use this antibody to determine the location of the Wld^S protein product in various regions of the *Wld*^{S} nervous system. I also used the antibody to compare protein levels in some key areas. Colocalisation studies were also carried out to determine possible interacting partners.

3. To test the hypothesis that the *Wld*^{S} protective phenotype is an indirect effect and that it is acting through affecting expression of other genes. This was carried out through the use of microarray analysis and quantitative real time PCR of genes whose expression is altered by *Wld*^{S}. I will also demonstrate through the generation of various constructs that different components of the *Wld*^{S} gene can have effects on RNA levels of other genes.

Figures

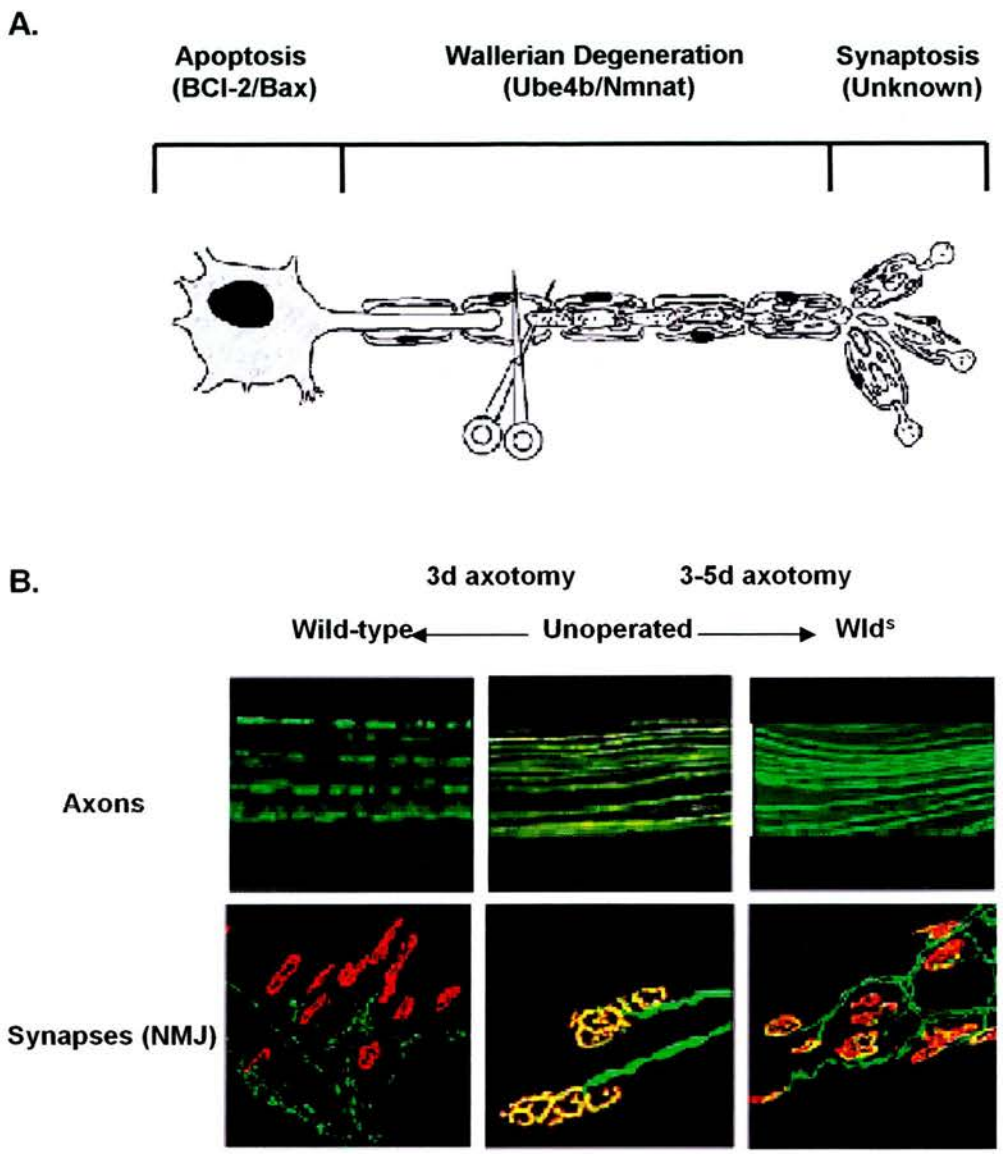

Figure 1.1. Compartmentalisation of the neurone.
A. Schematic diagram of the early stages of Wallerian degeneration showing granular disintegration of the cytoskeleton, axon and synapse fragmentation and myelin breakdown.The *Wld*^{s} mutant mouse was instrumental in working out that a neurone has separate comparments with regards to degeneration, and that the slowed degeneration exhibited by neurones in the *Wld*^{s} mutant mouse allows visualisation of these events. B. Wallerian degeneration and its delay by the Wld^s in peripheral nerves and NMJ of YFP-H and YFP-16 transgenic mice, visualized directly by fluorescence microscopy. The middle panels show an uncut nerve and the left and right panels show axons and synapses 3 to 5 days post lesion. In the wild type animal both the axons and synapses have degenerated, but the corresponding Wld^s animal shows intact axons with occupied endplates as show by bungarotoxin labelling (Red). Adapted from Coleman and Ribchester (2004).

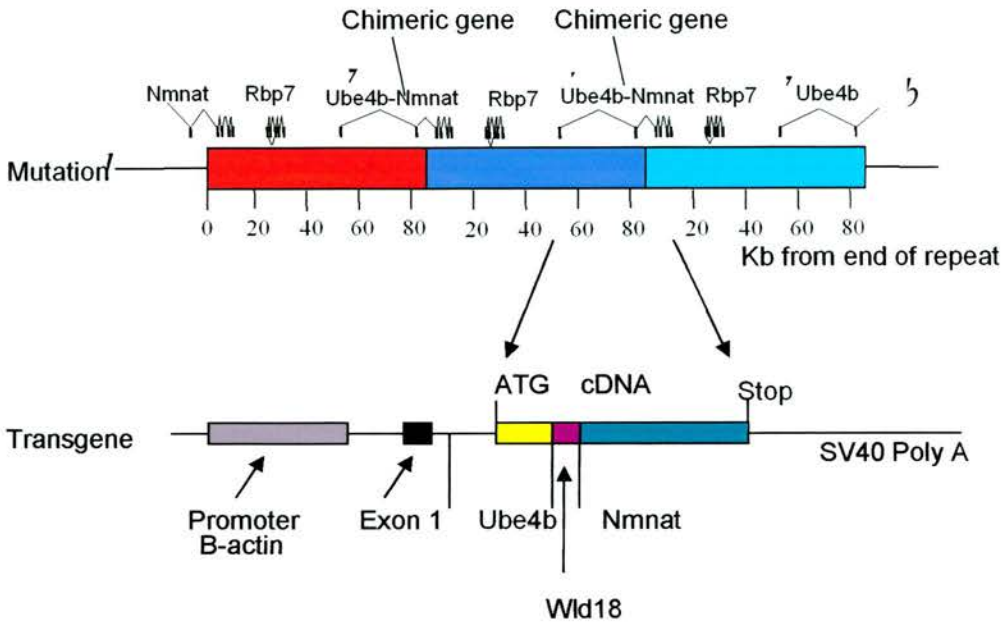

Figure 1.2. The *Wld*^{S} mutation comprises an 85Kb tandem triplication of a region already present in the wild-type animal.

The triplicated region contains the genes for Nmnat, Rbp7 and Ube4b. The boundaries of this triplication result in the formation of a chimeric gene consisting of the N-70 amino acids of Ube4b and the c-terminal 303 amino acids of Nmnat. This chimeric gene has been shown to be sufficient to provide the Wlds protective phenotype through the generation of transgenic mice and rats using the transgene shown above. The chimeric gene is expressed with the noncoding region of exon 1 of β-actin under the control of the human β-actin promoter. The protein product of the fusion gene contains 18 amino acids that are not normally expressed because they are part of the 5' untranslated region of Ube4b. This allowed the generation of a highly specific antibody which can be used to identify the protein through immunocytochemistry. This figure was adapted from Conforti et al (2000).

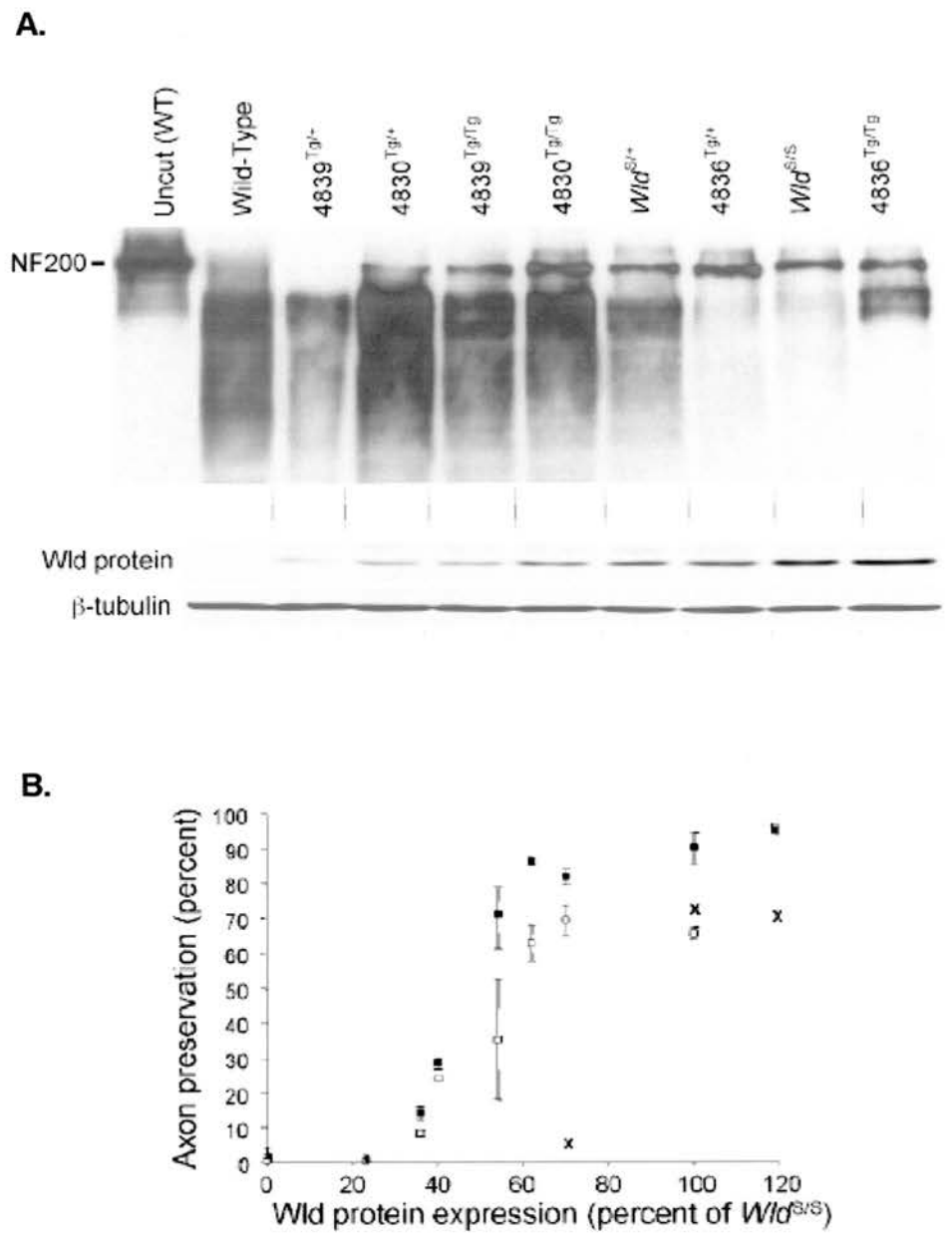

Figure 1.3. Dose-dependence of axon protection by the Wld^s protein.
A. Western blot probed for NF-200 shows the extent of 200-kD neurofilament protein degradation in distal sciatic nerve 3 days after transection (5 days for 4836 and *Wld*^{s} homozygotes). Complete preservation of NF-200 in uncut contralateral nerve (lane 1) indicated degradation occurred only in vivo. Although preservation of NF200 protein can be seen there is also a "smearing" below this band which may be degraded neurofilament. Western blot For Wld^s protein shows the expression level of the Wld^s protein in brain homogenates (detected by N70 antiserum). Western blot probed with control monoclonal antibody β-tub 2.1 against β-tubulin demonstrates that the lanes have been correctly loaded. B. The graph shows axon preservation as a function of the expression level of Wld^s protein. Axon preservation after 3 (black circle), 5 (white square) and 14 (cross) days as measured using light microscopy; means ± s.e.m. where n > 1. Wld^s protein expression level is the signal quantified from Gel 2 standardized against β-tubulin and expressed as a percentage of the expression in Wld^s homozygotes. This figure was adapted from Mack et al (2001).

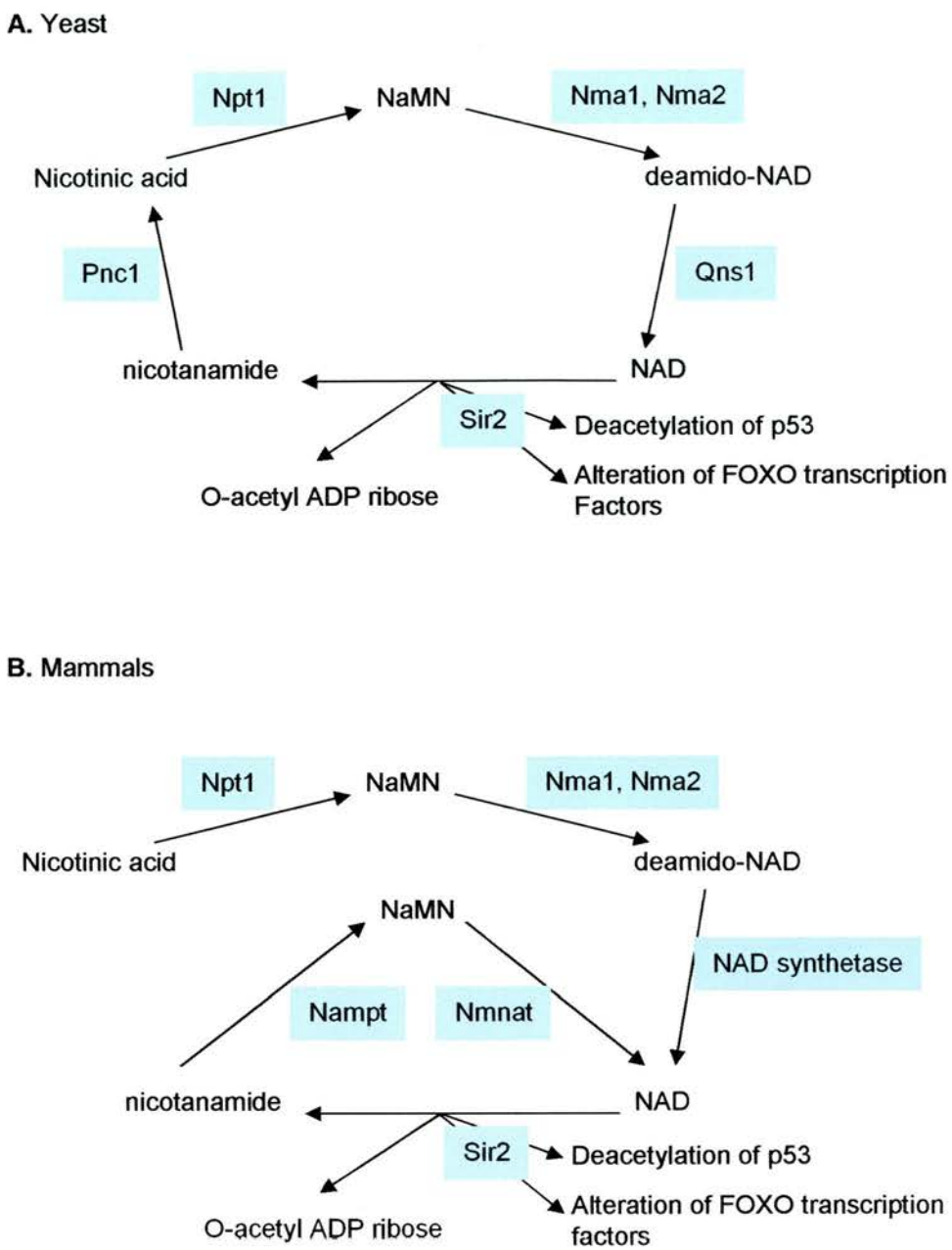

Figure 1.4 . The NAD biosynthesis pathways from nicotinamide in yeast and mammals.

A, NAD biosynthesis from nicotinamide in *S. cerevisiae*. *Pnc1*, *Npt1*, *Nma1*, *Nma2*, and *Qns1* are nicotinamidase, nicotinic acid phosphoribosyltransferase, nicotinic acid mononucleotide adenylyltransferase 1 and 2, and NAD synthetase, respectively. This pathway is also conserved in *C. elegans*, *Drosophila*, and other invertebrates. *B*, NAD biosynthesis from nicotinamide and nicotinic acid in mammals is shown. These pathways are also conserved throughout vertebrates. Nicotinamide is the main precursor for NAD biosynthesis in mammals. *Npt*, *Nampt*, and *Nmnat* are nicotinic acid phosphoribosyltransferase, nicotinamide phosphoribosyltransferase, and nicotinamide/nicotinic acid mononucleotide adenylyltransferase, respectively. Several enzymes break down NAD into nicotinamide, but only Sir2 is shown. Sir2 is also implicated in deacetylation of p53 and affecting FOXO transcription factors. *NaMN*, nicotinic acid mononucleotide *NMN*, nicotinamide mononucleotide. Adapted from Revollo *et al.* 2004.

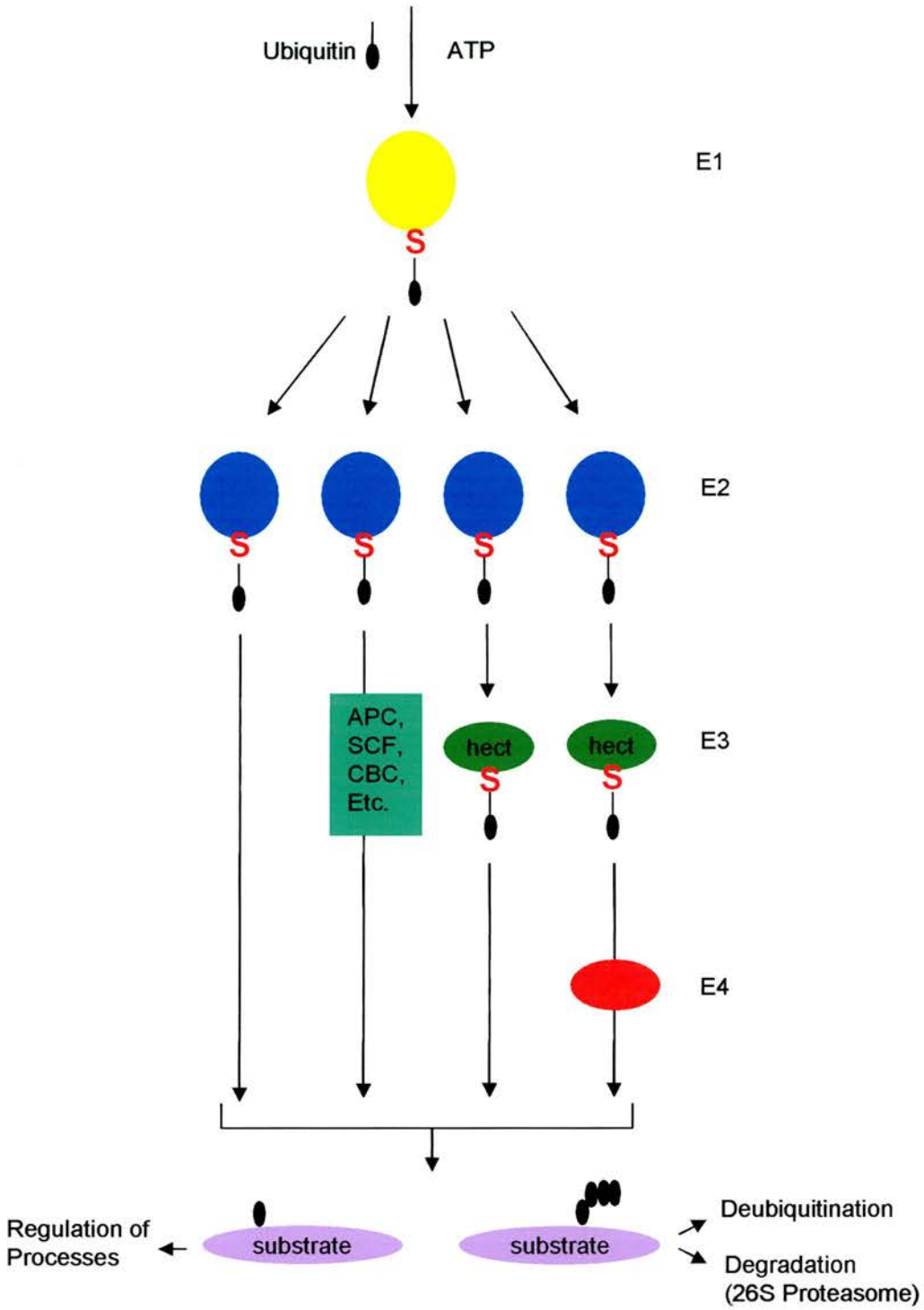

Figure 1.5. UFD2 Protein family and ubiquitination pathways.
Multiubiquitination of proteins proceeds via variations of ubiquitin-enzyme thioester cascade. E1 (yellow) is always required, forms a thioester –linked complex (S) with ubiquitin, and transfers activated ubiquitin onto E2s (blue). In some reactions, E2s can directly multiubiquitinate substrates, whereas others involve E3s (different shades of green). In contrast to some E3s (APC, SCF, CBC, etc), a subfamily of E3s (hect) can form thioester –linked complexed with ubiquitin, similar to E1 and E2. At least one E1, E2, E3-thioester cascade involves an additional E4 (red) activity for efficient substrate multiubiquitination. Protein is finally tagged either for degradation or regulation of other processes. Adapted from Kogel *et al.*(1999).

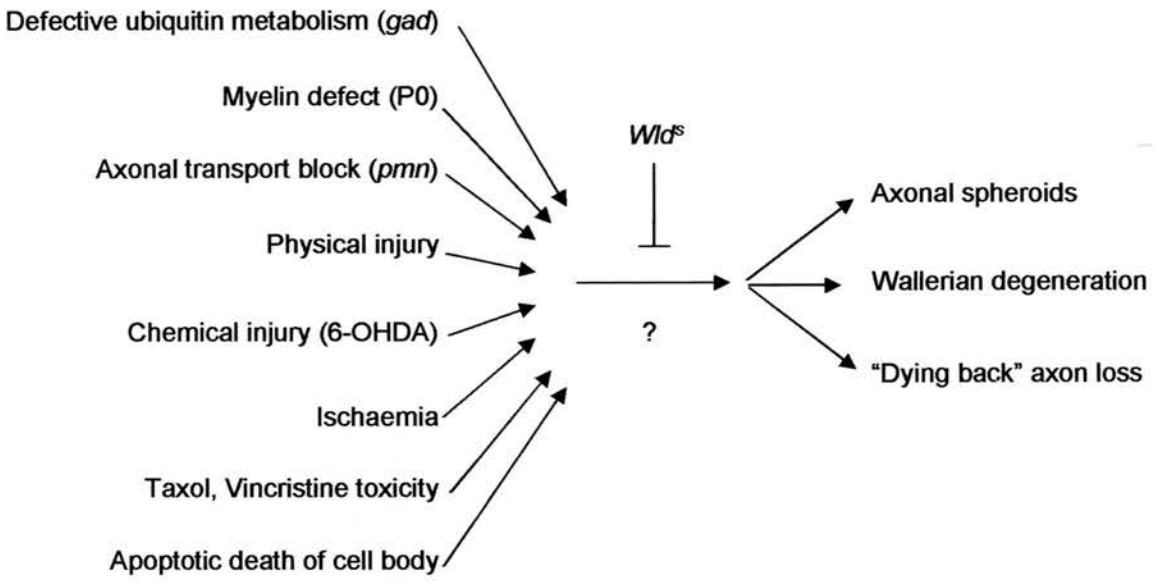

Figure 1.6. Axon degeneration mechanisms may converge at a *Wld*^{s} sensitive point. The *Wld*^{s} mutation is able to delay axon degeneration not only after injury, but following a wide range of degenerative insults. It follows that all degeneration mechanisms shown must converge on a pathway that is delayed by *Wld*^{s}. Therefore, understanding the mechanism of injury-induced Wallerian degeneration is highly relevant to axon degeneration in disease. Adapted from Coleman and Ribchester (2004).

Chapter 2:
Materials and Methods

2.1.0. Tissue culture

2.1.1. Cerebellar granule cell preparations:

Rat:

Cultures of cerebellar granule cells were obtained via a dissociative method described previously by Courtney *et al.,* 1990 and Gallo *et al.,* 1989 with some modifications. Seven day old Wistar rat pups were killed by cervical dislocation and decapitated in accordance with Home Office rules. The cerebellum was aseptically removed, and cut at 375μm intervals orthogonally on a nylon disc using a motorised McIllwain tissue chopper.

Mouse:

A variation of the technique used to culture rat cerebellar granule cells was used as described previously (Buckmaster *et al.* 1995). The optimal age of mice used was P4 (C57/Bl6 or C57/Wld^s). Four day old C57Bl/6J or C57Bl/Wld^s mice were killed by cervical dislocation and decapitated in accordance with Home Office rules. The cerebellum was aseptically removed by the "flip top" method, and cut at 375μm intervals orthogonally on a nylon disc using a motorised McIllwain tissue chopper.

Rat and Mouse continued:

Following crude dissociation with a McIllwain tissue chopper, Cells were separated in dissociation solution (0.1mM glucose, 0.3% fatty acid free BSA, 15nM $MgSO_4.7H_2O$ and 1 tablet of PBS (5mM Phosphate buffer, 1.4mM Potassium chloride, 50mM Sodium Chloride, pH 7.4) and 0.685mM EDTA, all made up to 100ml with fresh milli Q water).

The cells in solution were placed in a water bath for 40 minutes at 37°C and gently agitated every 5 minutes. During this time three sterile, 9 ml glass pipettes were flame polished. Each pipette was heated gently until its bore was half that of the last. After incubation for 20 minutes the tube was removed from the water bath and this was then taken and centrifuged at about 1000g for one minute. The supernatant was then removed, and the pellet re-suspended in up to 3ml dissociation of solution using the wide bore pipette. Following this the small bore pipettes were used to thoroughly triturate the cell suspension. After trituration, the suspension of cells were layered on top of 10ml of EBSS solution (EBSS from GIBCO with 4% BSA and 3mM $MgSO_4$) and centrifuged for 10 minutes at 1500g. The purpose of the EBSS was to remove debris caused by the trituration. The resulting pellet was re-suspended in up to three ml of culture medium as detailed by Buckmaster *et al.* 1995 (containing DMEM with 32mM KCl, 30mM glucose, 10μg/ml insulin, 10% FCS, 5ml/500ml Penicillin/streptomycin and 0.15g/500ml L-Glutamine). 10μl of this solution, diluted with 90ml of the culture medium was then used to measure cell density with a haemocytometer. The cells counted within a four by four square are used in the following calculation:

Cell number x volume (μl, i.e. up to 3000μl) x 100 (conversion number for grid system) = total yield of cells from preparation.

400 000 cells in suspension were then added to coated cover slips or about 2 000 000 cells per 35mm dish to give high density. The cover slips or dishes were put back into an incubator for between 30 and 60 minutes and following this, 2 ml of the culture medium were added to the cells and then replaced in the incubator. The following day the medium was changed to medium containing Ara-C (cytosine arabinosidase to inhibit proliferation of astrocytes. The medium used was as detailed above, but with 10μM Ara-C from 10mM aliquots added and filtered through a syringe filter), usually 2ml. Six days post plating the cells were-fed again with medium containing Ara-C.

Cells were plated out on Cellstar dishes (Greiner), which have built in rings designed to hold four 10mm diameter glass coverslips These protected the cells from detachment or damage during re-feeding. The rings were coated with Poly-D-Lysine two days before pre-preparation, and left in the incubator at 37°C until one hour pre-preparation, at which time any excess poly-D-lysine was removed and the rings were coated with laminin (200ml of 50μg/ml frozen stock, thawed at 4°C and made up to one ml with EBSS). At the time of plating the excess laminin was removed and cells were plated directly into the rings. Mouse cerebellar granule cells from the C57/B6J background will not grow on glass. CellStar wells with the required number of cells were placed in the incubator for 30 minutes, then flooded with culture media. The medium was then changed at 24 hours and again at six days with culture media containing 10μM Ara-C.

The table below details the dissociation solution as detailed by (Van Vliet *et al.* 1989, Buckmaster *et al.* 1995)

Reagent	Dissociation solution
Glucose	250mg (0.1mM)
BSA	300mg (0.3%)
$MgSO_4$ (from 1.5mM stock)	1ml (15nM)
PBS tablet (contents as detailed above)	1 unit
EDTA	26mg (0.685mM)
Autoclaved milliQ water	100ml

2.1.2. Withdrawal of serum and potassium from cerebellar granule cell cultures.

I used a low serum and potassium challenge to test phenotype *in vitro*. It is possible to induce neurite degeneration by removing serum and potassium from the culture media. At 7 days in culture, the neurons were re-fed with medium containing a normal potassium concentration (5mM) and no serum to initiate neuronal degeneration, as previously described (Gallo *et al.* 1987). It is of interest to note that to begin with, the cells are cultured in media containing 25mM potassium which is a non-physiological concentration. The cells then become dependent on this level of potassium, and upon returning the cells to physiological concentrations (5mM) wild-type cultures begin to degenerate. The table below shows the contents of the culture medium (Buckmaster media) and the media used as a challenge to the cells (low serum and potassium).

Reagent	Buckmaster media	Low serum and potassium media
DMEM	250ml	30ml
Insulin(50mgml^{-1} stock)	50µl (1.8μM)	6µl (1.8μM)
Pen/Strep	2.5ml (0.1%)	0.3ml (0.1%)
L-Glutamine	0.7g (19mM)	0.08g (19mM)
Glucose	1.3513g (30mM)	0.1622g (30mM)
FCS	25ml (10%)	0.75ml (2%)
KCl (1M stock)	6.675ml (25mM)	0.15ml (5mM)

2.1.3. Quantification of the Neurite degeneration in Cerebellar granule cell cultures

Following serum/potassium withdrawal, one wild type and one *Wld*^{s} culture dish per day were fixed in 4% paraformaldehyde with 4% sucrose, stored in PBS and imaged on an a Nikon microscope with Hoffman optics. Up to 20 random pictures were taken per dish at 40 X magnification. Total neurite length was assessed by measuring the length of every neurite in the visual field using an image processing and analysis software package, Scion image (www.scioncorp.com). Neurite lengths were summed to reach a total neurite length for each image (Büttner *et al.* 2002). Mean neurite length was then calculated for each experiment.

2.1.4. HEK 293 Cells

HEK cells were cultured in DMEM supplemented with 10% FBS and 1% penicillin/streptomycin (Invitrogen) at 37°C in 5% CO2. Cultures were split every 3-4 days.

Transfection of HEK293 cells was done using the calcium phosphate method (see below) one day post split. Wld^{s}-eGFP construct was used at 5μg per well. Cells were incubated at 2.5% CO_2 for 4 hours. The cells were then washed twice with fresh filtered PBS, and then returned to fresh media and incubated at 5% CO_2 until required. Control cells were treated the same way as transfected cells.

When experiments required the incubation of cells in various reagents, they were incubated for 4 days in HEK293 media containing combinations of the following reagents:

NAD (Sigma, product number N-1511) at 1mM.
Sirtinol (Calbiochem, product number 566320) at 100μM made up in DMSO.
Vincristine (Sigma, product number V-8879) at 0.5μM.

Control cells were incubated for the same period of time in HEK293 media containing the same volume of the vector used in the experimental sample (i.e. DMSO).

2.2.0. Sectioning

2.2.1. Vibratome Sectioning

High magnesium ACSF (artificial cerebrospinal fluid) was prepared and cooled in freezer to the point of becoming slush. Animals were sacrificed by decapitation according to Home Office rules and regulations (Project license 60/3277). The brain was removed and dropped into the cold oxygenated high Mg^{2+} ACSF to maintain the integrity of the brain and increase firmness for cutting. Brains were mounted by supergluing a block of agar (2long x 1deep x 1high cm) onto the cutting dish to provide a firm flat surface into which the blade would slice. The brain was then mounted for slicing (saggital/coronal) by gluing to the cutting surface and resting against the agar block. The cutting chamber was filled with cold oxygenated high Mg^{2+} ACSF and sliced are cut to desired thickness (100-150μm). Slices were cut using a Vibratome 1000 plus sectioning system. Cut slices were removed with a large ended pasture pipette and dropped into fixative (4% paraformaldehyde& 4% sucrose). Slices were then removed from fixative and immunostained. The constituents of high Mg^{2+} ACSF are detailed below.

High Mg^{2+} ACSF

Reagent	Molarity	Stock	L^{-1}
NaCl	125mM	58.4 (molecular weight)	7.3g
$NaHCO_3$	26mM	84 (molecular weight)	2.1g
Glucose	25mM	180.2 (molecular weight)	4.5g
KCl	2.5mM	74.6 (molecular weight)	0.186g
$NaH_2PO_4(.2H_2O)$	1.25mM	119.98 (molecular weight)	0.150g
$CaCl_2$	1mM	1M Solution	1ml
$MgCl_2$	4mM	1M Solution	4ml

2.2.2. Cryostat

Tissue was mounted on a rotatable chuck on OCT (optimal cutting temperature) gel in the cryostat at an ambient temperature of -16°C. OCT was allowed to solidify for at least 5 minutes. The tissue was mounted and sections were cut utilising the anti-roll plate at 10μm thickness. Cut sections were then collected onto poly-l-lysine coated slides and stored at -20°C until used.

2.3.0. Immunocytochemistry

Appropriate controls were always carried out for every immunocytochemical experiment. For example, wild type samples were always processed alongside

experimental samples (data not shown unless otherwise stated), and secondary antibody controls were always undertaken.

2.3.1. Fluorescent Immunocytochemical staining

2.3.1.1. Fixation

Tissue was washed with oxygenated PBS (phosphate buffered saline) and fixed with 4% paraformaldehyde (containing 4% sucrose) for up to 60 minutes. The cells were then washed with PBS for 30 minutes, then again with PBS containing 0.1M glycine for 30 minutes. The final wash was PBS for 30 minutes. Tissue was permeabilised and antigenic recognition sites were masked with blocker (PBS, 4% BSA, 0.5% Triton X [Sigma]) overnight, on a rotating tantibodyle top in the cold room.

2.3.1.2. Primary antibodies

Primary antibodies were made up in blocker and applied overnight on a rotating table top at 4°C.

Staining for the protein product of the *Wld*^{s} gene was accomplished using a primary antibody we refer to as Wld^{18}, which was raised in a rabbit and very kindly supplied to us by Dr M.P.Coleman. The antibody binds to 18 amino acids of *Nmnat1* which are not normally expressed in the wild type animal, but which are expressed in the *Wld*^{s} mice. The primary antibody was used at dilutions ranging from 1 in 4000 to 1 in 2000.

Staining for astrocytes in culture was achieved using GFAP (Chemicon). The primary antibody was raised in mice and was used at a dilution of 1 in 20.

Staining for ubiquitin was carried out using FK2 (Santa Cruz) mouse primary antibody at a concentration of 1 in 200 which was used to stain monoubiquitinated proteins, a

Ubiquitin (Sigma) rabbit primary antibody which is specific for polyubiquitinated proteins.

Staining for neurofilament was carried out using NF2H3 (Developmental Studies Hybridoma Bank, University of Ioah) mouse antibody which recognises the 165KDa form, normally at a dilution of 1 in 200.

2.3.1.3. Secondary antibodies

After primary antibody incubation, the cells were typically washed for up to six hours in blocker before the addition of the secondary antibodies. The secondary antibodies FITC/TRITC anti-mouse/rabbit (Dako) were typically made up in blocker, but sometimes in PBS.

Secondary antibodies were used at a dilution of between 1 in 40 and 1 in 20, and left overnight on a rotating table top 4°C. The samples must be kept away from light as fluorescent secondary antibodies photo-bleach.

2.3.1.4. Mounting

After overnight incubation with secondary antibodies cells were washed for at least six hours in a combination of blocker and PBS. CellStar culture dish wells were filled with MoOil, and 13mm diameter glass coverslips are placed over the top of the wells. The dishes were then left overnight to set. When mounting slices on slides a single drop of MoOil was added to the slice and the coverslip was dropped in place gently to avoid damaging the tissue.

2.3.1.5. Direct visualisation

TOPRO3 is a distinct one step nuclear stain which may be added to cells during their final wash with PBS before mounting. It was typically used at a dilution of 1 in 1000 and left on the sample for 5 minutes before washing again with PBS and mounting. However, TOPRO3 photo-bleaches much faster than the secondary antibodies. It emits in the far red (excitation 644nm & emission 657nm), and as I typically used a red label for the Wld^{s} protein, confocal images shown with TOPRO3 were typically pseudocoloured blue.

2.3.2. DAB immunocytochemistry

If necessary (for example following paraffin embedding) tissue was rehydrated as follows, 60°C for 30 minutes, Xylene for 10 minutes, 100% alchol for 10 minutes and then 5 minutes. Endogenous peroxidase was blocked by incubating in 0.5% H_2O_2 in methanol for 30 minutes. Tissue was then washed in running tap water for 10 minutes, washed with PBS and then blocked with blocking solution for 1 hour (PBS with 3% fish skin gelatine [or 1ml goat serum and 0.5ml BSA] and 0.5% Triton-X). Wld^{18} antibody was used at a dilution of 1:500 overnight in blocker. Following this tissue was washed in PBS twice for 10 minutes, then incubated in secondary antibody (biatinylated anti-rabbit) 1:100 in PBS for 1 hour. The tissue was washed with PBS twice for 10 minutes. And then the Vectastain elite kit was used as per manufacturers instructions (solution made 30 minutes prior to use). Tissue was washed twice with PBS for 10 minutes. The DAB was prepared and applied for 2 to 5 minutes then washed in running tap water and Haematoxylin stained (10 to 15 seconds) followed by another wash in tap water. Acid alcohol was used for 10 seconds and tissue washed in Scots tapwater substitute for 10 minutes followed by a final wash with water. If desired tissue could then be dehydrate as

follows: 70% 2 minutes, 90% 2 minutes, 100% 2 x 5 minutes, xylene 10 minutes. Finally, tissue was mounted in DPX.

2.4.0. Microscopy

2.4.1. Confocal microscopy

Immunostained preparations were viewed using a Radiance 2000 confocal microscope (Biorad) via a Nikon Eclipse E600 microscope equipped with a 60x Oil immersion objective. Images were captured using Lasersharp 2000 software running on a Dell Poweredge 1400 computer. Tiff files were exported into Adobe Photoshop and/or Scion Image for assessment/analysis.

Wld^S protein mapping values in chapter 4 were obtained by confocal microscopy as detailed above at 2x zoom and with a step size of 0.3μm. Images were captured to include 2 cell layers in the desired area. For example, cerebellar granule cell layer images were 25μm thick and a 3D rotation was compiled and incomplete cells were excluded from the TOPRO3/Wld^S percentage count. Averages were calculated from multiple images per brain (N=4).

2.4.2. Transmission Microscopy

Images were captured on an inverted Nikon microscope with Hoffman modulation contrast optics. Images were captured with a chilled 3CCD camera (Hamamatsu C5810)connected to an Apple Mac G4 computer running Openlab (Improvision) and Adobe Photoshop software.

2.5.0. Molecular techniques

2.5.1. Transfection

2.5.1.1. High efficiency transformation using calcium phosphate-DNA precipitate formed in BES

A transfection solution was made up of 12.5µl $CaCl_2$, 5µg DNA (mini prep. is clean enough), made up to 125µl with water. 125 µl BES solution (2.5M $CaCl_2$, TE buffer pH7.4, 2 x N,N-bis(2-hydroxyethyl)-2-aminoethanesulfonic acid (BES) buffered solution and filtered PBS) was added and mixed by pippetting briefly and added dropwise immediately to cerebellar granule cells, or a precipitate was allowed to form for 5 minutes before adding to HEK 293 cells dropwise.

The cells were incubated at 2.5% CO_2 for 1 hour (cerebellar granule cells) or 4 hours (HEK 293 cells), washed twice with PBS and the media replaced and the cells incubated again at 5% CO_2. Transfection had no overt effect on the survival or morphology of either the transfected or non-transfected sub-population of HEK293 cells.

2.5.1.2. Nucleofector kit.

Efficient gene delivery into primary culture is difficult to achieve. Viral transfer is probably the most effective way of getting a high transfection rate. Construction of viral vectors is often time consuming and limits the size of DNA to be inserted. Viral infections can also interfere with the host cells metabolic processes such as hijacking the cells protein synthesis machinery. Other methods of transfection also include calcium phosphate, cationc lipids, micro injection or ballistics (i.e. gene gun). These methods can often be toxic to neurones and are unlikely to give a rate of greater than 20% (Berry *et al.* 2001). However, these methods are not as efficient or simple as the Nucleofector kit.

This kit works around the principal of electroporation, but utilises a "super secret expensive special" solution.

Cells were transfected using the commercially available Rat Neuron Nucleofector kit according to manufacturer's instructions (Amaxa Biosystems). Briefly, a maximum of 6 million cerebellar granule cells (counted by haemocytometer) were centrifuged at 900rpm for five minutes. They were then resuspended in 100µl of Nucleofector solution for primary neurones, and mixed with a maximum of 3µg of construct before transfer to cuvettes provided (Dityateva *et al.* 2003). The cuvettes were then placed within the Nucleofector electroporator and treated using programme G-014. 500µl of media was added to cells and they were then plated out onto poly-D-lysine (Sigma) coated coverslips in a multiwell plate using the disposable pipettes provided. Cells were then placed in an incubator for one hour thirty minutes before flooding each well with media. Media was then changed one and six days later.

2.5.3. Extraction of genomic DNA

Tail biopsies or ear punches were taken from mice of ages P4 to adult. Genomic DNA was extracted using a modified proteinase K digestion/isopropanol precipitation protocol (Laird *et al.* 1991). Tissue was incubated in tail lysis buffer (100mM Tris-HCl, pH 8.5, 5mM EDTA, 0.2% SDS, 200mM NaCl, 100µg/ml Proteinase K). Samples were incubated overnight at 55°C. Lysed tissue was vortexed for 1 minute and spun at 15800 g for 10 minutes to remove hair and bone. The supernatant was decanted into a new tube and isopropanol was added (equal volume to the tail lysis buffer used earlier). The solutions were inverted until a white precipitate can be seen. The solution was centrifuged and the pelleted DNA is washed with 70% ethanol and air dried before it was resuspended in an appropriate volume of 1 x TE buffer.

2.5.4. Extraction of RNA

RNA extraction was carried out using tri-reagent (Sigma) as per manufacturers instructions. Tissue was rapidly plunged into liquid nitrogen for 1 minute, then placed in 1ml of tri-reagent (Sigma) on dry ice. Tissue was homogenised in tri-reagent and left for 15 minutes on ice. 0.2ml $CHCl_3$ was added and left to stand for 10 minutes at room temperature before centrifuging for 15 minutes at 13000rpm at 4°C. The aqueous layer was removed and 0.5ml of isopropanol was added before re-centrifugation for 15 minutes at 13000rpm at 4°C. The RNA pellet was washed with 200μls of 70% ethanol before re-centrifugation for 5 minutes at 13000rpm at 4°C. Pellets were re-suspended in DEPC-treated water and stored at -80°C. Quality was checked by assaying levels using a spectrophotometer and running on a gel to check integrity.

2.5.5. Microarrays

Total RNA was prepared from the cerebellum for microarray analysis (initially by Dr P.Chen, and subsequently by me) as follows.

RNA quality was initially assessed using formaldehyde gels and by measurement of absorbance at 260/280nm following standard procedures (by me). A further assessment of RNA quality was then undertaken using an Agilent Bioanalyser (Agilent Technologies, GmBH, by K.Robertson). Samples (10μg) were labelled, hybridised to Affymetrix MOE-430A GeneChip arrays and scanned according to standard Affymetrix protocols (K.Robertson). All analyses were undertaken in Affymetrix Microarray Suite 5.1 software as follows: arrays were scaled (normalised) to an overall target intensity of 100 prior to comparison and notable differences in gene expression were identified by pair-wise comparison of appropriate samples. Differentially expressed genes were annotated using the Affymetrix online analysis resource 'NetAffx' (www.affymetrix.com/analysis).

2.5.6. Reverse-transcriptase (RT) and real time-RT (QRT) PCR

Reverse transcriptase PCR (RT-PCR) was carried out in 'ready-to-go' RT-PCR tubes (Amersham Biosciences) using a T-Personal PCR machine (Biometra). Beta-tubulin was used as a loading control for all RT-PCR experiments. Quantitative real-time PCR (QRT-PCR) was carried out using a Sybr-Green '1 step QRT-PCR kit' (Invitrogen) on a Model 7700 instrument (Applied Biosystems). For all QRT-PCR experiments, actin was used as a control gene. Where possible, primers were designed to span an intron eliminating the possibility of any genomic DNA contamination. For all genes, PCR bands were removed from gels and the product extracted using a Q-gel extraction kit (Qiagen). The bands were sequenced to confirm product identity. We were unable to obtain human Dap3 primers that worked well enough to quantify transcriptional changes in HEK293 cells, thus Dap3 analysis was not included in any transfection or NAD experiments. Primers used, and the full names for all genes, are shown below. Conventional RT-PCR products were analysed in a 2% agarose gel containing ethidium bromide in 1 x TAE buffer run at 120mV for 40 minutes. The primer sequences are listed below.

Microarray validation RT and QRT primer list

Gene	Forward Primers	Reverse Primers
Mouse		
Beta-tubulin	AGTTCACTAAGGGTGCACACTGTAT	AGAGCAACATGAATGACCTGGTGTC
Ccl21	GAAGCACTCTAAGCCTGAGCTATGT	TCAGTTCTCTTGCAGCCCTAGGAGC
Dap3	AGATAGAACCTTGATTGCCCCAGAG	CTAAGTAGTACTGGAAGGAACTTTC
D11Ertd730e	TCAGTCCTCTGGTCTCTTGAATGTA	AACCAAGAAAATCTTAGATGGCAAA

Edr1-L	TTTCTCTGTTTATGGACCCGGATCC	TTGAGAATCGTGAGAGTGGCTCCAT
EST	GTATCTGAACAAACATCTCTCTGGC	AGCAGTATTTTAATCTCAAGGGCCC
Fabp7	AAGATGGTCGTGACTCTTACCTTTG	ACTTATAATTAGTGACCAGTGCTTC
Mybpc3	AAATCGCTCCATCATTGCAGGCTAT	CCAGGCCATTCTTGAACCAGGAAAT
Pttg1	GGCATCTAAGGATGGGTTGA	TTCGGCAACTCTGTTGACTG
Rbp7	TCAGCGGTACCTGGAATCTTCTCAG	CTGTACGCAAGTGAGTTTGTCATTC
Src-LA	GCTGAATGCTGCCATAGATGATTGT	ACAGGGATGAATAGCCATGACTATC
Ssr1	TAAATGTTGTGTGTGCCGCAGTGCA	TTTCAGCAATCGTATGGCCACAGAC
Tnip1	ATGAGGTGCAACAAGACCCCATTCT	TCTGCTCTAGAGACAAAGCCCTCTC

Human

Actin	CAAGAGATGGCCCACGGTGCT	TCCTTCTGCATCCTGTCGGCA
Ccl21	CACCAACGCTTGAAGCCTGAACCCA	CAGGTCCAGGGTCCTGATGATTCTC
D11Ertd730e	AGCCAGCAGCTGTTACTTTGTTTGT	ACACCACTGTTTCTGAGATGCTGAC
Edr1-L	TTTCTCTGTTTATGGACCCGGATCC	TTGAGAATCGTGAGAGTGGCTCCAT
EST	AGATGAATGCTGTGCACCACCACGC	AATCGTGAGAGTGGCTCCATCCTGG
Fabp7	GGTTATGACCCTTACTTTTGGTGAT	TGTTGTAATAGGATAGCACTGAGAC
Mybpc3	CCCCTCCCTACTGTTGGATGTATGT	ACATAGCAGGCCAGAAAGGCCTGTC
Pttg1	GAGAGAGCTTGAAAAGCTGTTTCAG	TCCAGGGTCGACAGAATGCT

Src-LA	CTCCCATCCAAATCCTACTAGGAAG	CACATACCAGTAGCACGATGAGCTT
Ssr1	CACATGGTTTGTTCAAGCACACTTA	ACATTATTCTCACACATCCGGGGAT
Tnip1	TTTTTGCTTCAAGCTCTGTAGCAGG	AAATAGCATACCAGGGATGGACAGC

2.5.7. Quantitative real time-PCR on genomic DNA for genotyping *Wld*^{S} mice

The primers and probes (TaqMan Probes) were designed using Primer Express software as described in the ABI Primer Express User Bulletin (P/N 4317594). Wld^{S} primers were based on Genbank entry AF260927 and recognise a region of exon 1. The Wld^{S} probe was tagged with a FAM flurophore and a TAMRA quencher producing a 75bp amplicon. Tubulin primers were based on Genbank entry M28739. The probe was tagged with a VIC flurophore and a TAMRA quencher producing an 81bp amplicon. The sequences used are detailed below.

The following sequences were used:

Component	Sequence (5'-3')
Wld^{S} forward	GGCAGTGACGCTCAGAAATTC
Wld^{S} reverse	GTTCACCAGGTGGATGTTGCT
Wld^{S} probe	TCTACGAGTCCGATGTGCTGTGGAGACA
Tubulin forward	GCCAGAGTGGTGCAGGAAATA
Tubulin reverse	TCACCACGTCCAGGACAGAGT
Tubulin probe	CAAGGCTTTCCTGCACTGGTACA

The optimal primer concentrations used were 900nM and the optimal probe concentrations were found to be 250nM. The PCR mix was made up to manufacturer's instructions. DNA was used at a concentration of 1:200 dilution of the original sample. The machine used was an ABI Prism 7000 sequence detection system. Standard PCR cycles were used as designated in the ABI user guide.

2.5.8. Assaying DNA concentration

There are 2 main ways of assaying DNA concentration, a crude method and a more accurate method.

The crude method: A 1 in 200 dilution of the resuspended DNA in ddH_2O was made. Using a quartz cuvette and a spectrophotometer the absorbance of this dilution at 260 and 280nm was measured. The value obtained for the absorbance at 260nm, multiplied by 10 gave the concentration of DNA in the undiluted sample in µg/µl. The ratio given on dividing the absorbance at 260nm by the absorbance at 280nm gave an indication of the possible level of contamination of the sample with RNA.

The more accurate method: As a cheaper alternative to Pico Green, DNA was assayed accurately using Hoechst 33258, excited at 365nm, emission at 460nm. Standards were made up using 20 µl of a 1mg/ml stock calf thymus DNA diluted in 1000µl of TE buffer giving a solution of 20µg/ml. This solution was then be serially diluted 1:1 with TE buffer giving concentrations of 20, 10, 5, 2.5, 1.25, 0.625 & 0.312 µg/ml. TE buffer was used for a reference solution. Typically 2µl of sample containing 20 – 10000ng DNA was added to TE for dilutions in a flurometer. Standard cuvette assay is linear from 10ng to over 5000ng/ml DNA. The non-specific fluorescence should be less than 1% of the fluorescence that can be attributed to the DNA-dye complex. The Hoechst 33258 dye was dissolved at 2µg/ml per sample. (Teare, J.M. *et al.* 1997)

2.5.9. Assaying RNA concentration

A 1 in 250 dilution of the resuspended RNA in DEPC treated H_2O was made. Using a quartz cuvette and a spectrophotometer the absorbance of this dilution at 260 and 280nm was made. The value obtained for the absorbance at 260nm, multiplied by 10 gave the concentration of RNA in the undiluted sample in μg/μl. The ratio given on dividing the absorbance at 260nm by the absorbance at 280nm gave an indication of the possible level of contaminants in the sample.

2.5.10. RNA gel electrophoresis

A 60ml 0.8% agarose SeaKem GTG (Flowgen) RNA denaturing gel was made with the following components:

Component	Volume
5 x MOPS (0.1M MOPS-BDH-Merck, pH 7.0, 40mM NaAc, 5mM EDTA, pH 8.0) buffer	12ml
40% formaldehyde (Gibco)	11ml
0.48g agarose SeaKem GTG (Flowgen) DEPC-water	37ml

The agarose was dissolved in water before the 5 x MOPS buffer and the formaldehyde was added. RNA samples were loaded in the following way. Sample buffer (for each 1.0μl RNA) was composed of 1.5μl 5 x MOPS buffer, 2.6μl formaldehyde and 7.5μl formamide. Loading buffer contained 2.0μl Ficoll loading buffer and 0.5μl 1mg/ml ethidium bromide. Both buffers and RNA sample were heated to 65°C for 2 minutes before 11μl sample buffer and 2.5μl loading buffer was mixed with the RNA sample. The mixture was loaded onto the gel immediately. The gel was run at a speed of 15/V in

1 x MOPS buffer for 1 hour. A 4μl sample of RNA marker (1μg/μl Promega) was run with the sample to identify the molecular size of the RNA sample.

2.5.11. Western blot

Western blots were performed as described previously (Mack *et al.*, 2001). Briefly, tissue or cells were extracted and homogenised. Protein was homogenized using a fine bore syringe and the solublised protein extracted in RIPA buffer with 10 % protease inhibitor cocktail (Sigma) through centrifugation at greater than 10 000g. Protein concentration was determined through the use of a MicroBCA assay kit (Pierce Biosciences) as per manufacturers instructions. Protein was separated by SDS/Polyacrylamide gel electrophoresis on a 4 - 20% pre-cast gradient gel (Invitrogen) and then transferred to PVDF membrane overnight at 25 volts in CAPS buffer (pH 11.5). After blocking with 10% milk the membrane was incubated in the presence of either Wld-18 (1:2000 dilution) primary antibody and/or VAP-A primary antibody (rabbit 1:4000 dilution; gift from Dr P.Skehel, University of Edinburgh) for 1 hour. The PVDF membrane was further processed using horseradish peroxidase conjugated secondary antibody and a chemiluminescence system (Amersham) and exposed to film.

2.5.12. Southern Blotting and radiolabelled probe hybridization

DNA for *Wld*^{S} genotyping was extracted from spleen and digested for 3 to 4 hours at 37°C and then run in 0.6% agarose TBE gel at 1.75V/cm overnight. Gels were then denatured (1.5M NaCl, 0.5M NaOH) for up to two hours for genomic DNA and then neutralized (1.5M NaCl, 0.5M Tris-HCL pH 7.2, 1mM EDTA) for 30 minutes with gentle shaking. Gels were rinsed in MilliQ-water to remove excess neutralization solution. Genomic blots were transferred overnight via capillary transfer in 10 x SSPE (20 x SSPE stock- 3M NaCl, 200mM $Na_2PO_4 \bullet H_20$, 20mM EDTA, pH 7.4). After blotting, nylon membranes (Hybond-N, Amersham Pharmacia Biotech) were crosslinked in a Stratalinker® UV crosslinker 2400 (exposure = 120000 μJ) (Stratagene)

and then prehybridised (10ml 2 x hybridization solution-(12 x SSPE, 10 x Denhardt's reagent and 100μg/ml yeart tRNA), 10ml formamide and 1ml 10% SDS) for overnight at 42°C. Additionally 150μl 10mg/ml fragmented single-stranded salmon sperm DNA (Sigma) was added to further reduce non-specific binding. DNA fragments used for probe making were digested with restriction enzymes and run at 2V/cm in a low-melting point 0.7% agarose gel. The appropriate fragment was excised and water was added according to the ratio 3ml of water to 1g gel slice (under the guidance of Dr M.Coleman). Radioactive probes were generated using the Primer-It© labeling kit (Stratagene) and incorporated the radioisotope (α-^{32}P)-dATP (Specific activity:3000 Ci/mmol) (Amersham Pharmacia Biotech). Probes were hybridized to membranes (in a smaller volume of prehybridisation solution, by Dr M.Coleman) overnight at 42°C and these were washed the next day in 5 x SSPE, 0.1% SDS for 30 minutes at 65°C and twice in 0.3 x SSPE, 0.1% SDS for 10 minutes at 65°C. Blots were exposed overnight to X-ray film (X-OMAT/AR, Kodak) at -80°C.

2.6.0. General Cloning

2.6.1. Bacterial strains

For transformations the DH5α *E.coli* strain from Invitrogen was used with the following genotype:

*sup*E44 Δ*lac* U169 (φ80*lacZ*ΔM15) *hsd*R17 *rec*A1 *end*A1 *gyr*A96 *thi*-1 *re*1A1

2.6.2. Restriction Enzymes

All restriction enzymes were obtained from either Boehringer Mannheim or New England Biolabs. Enzymes were used with buffers provided according to the manufacturers instructions.

2.6.3. Bacterial medium and preparation of electrocompetent cells

TB (Terrific Broth) medium - 11.8g SELECT peptone 140, 23.6g Yeast extract, 9.4g Dipotassium hydrogen sulphate, 2.2g Potassium dihydrogen phosphate (Gibco, 47g/L).

LB (Lennox Broth) medium – 10g bactotryptone, 5g bactoyeast extract, 5g NaCl (Sigma, 25g/L).

LB Agar – (Gibco, 32g/L).

All transformations were carried out using frozen stocks, which were prepared according to the technique described by Dower *et al* 1998. Bacteria were streaked (from a glycerol stock kept at -80°C) on an LB-agar plate and incubated overnight at 37°C. This was used to start a large scale culture using 500ml LB-medium. Cells were grown up until the density reached OD_{600} = 0.5-1.0. Cells were then centrifuged at +4°C for 15 minutes at 4000g and the medium removed. The pellet was resuspended carefully in 500ml ice-cold Milli-Q water and centrifuged again at 4000g. This process was repeated twice, again in ice cold Milli-Q water and then in 20ml 10% glycerol. Finally the cell pellet was resuspended in 10% glycerol in a 1:1 (cells:10% glycerol) ratio. The cells were aliquoted and stored at -80°C. Electrocompetence was tested by transforming 10pg SKII-Bluscript circular vector (Stratagene), using the protocol described later. Cells usually gave 1-2 x 10^7 colonies on an LB agar plate supplemented with 200μg/ml ampicillin.

2.6.4. Digestion reactions

A typical analytical digestion reaction was made of the following components:

Component	Volume
10x restriction enzyme buffer	1.0μl
Mini/maxi-prep DNA	1.0μl (approx. 0.5μg)
(10x Bovine Serum Albumin)	1.0μl if required
Restriction enzyme	0.5μl (approx 5U)
(2^{nd} restriction enzyme)	0.5μl if required
Milli-Q water	made up to 10μl final volume

Preperative digestion reactions of DNA contained 1x restriction enzyme buffer (NewEnglandBiolabs/BoehringerMannheim), 1-5μl mini/maxi-prep DNA backbone/insert, 0.5μl restriction enzyme at a concentration of 5U/μl NewEnglandBiolabs/BoehringerMannheim) and Milli-Q water (Millipore) making a final volume of 10μl. Reactions were carried out usually at 37°C for 1 hour unless otherwise stated. For preparative digests, fragments were separated by gel electrophoresis in a 0.8% SeaKem GTG agarose (Flowgen) gel made in 1x TAE buffer (40mM Tris-acetate, 1mM EDTA (pH8.0)). This was carried out in an electrophoresis tank (Flowgen) filled with 1x TAE buffer. Voltage was provided by a Power pac 300 power supply (Biorad) at a speed of 2.5-5V/cm. To estimate the size of the DNA bands 1.0μg λ-bacteriophage (Pharmcia Biotech) digested with Sty I, was added in an adjacent well. To visualise the DNA under UV Light (wavelength 302nm) 3μl 10mg/ml ethidium bromide was added to 100ml liquid agarose. The DNA band of appropriate size was excised from the gel and extracted using the Qiagen gel extraction kit (Qiagen) according to manufacturers instructions. The isolated DNA fragment was then resuspended in 20μl 1x TE buffer for ligation reactions.

For analytical digestions, DNA was analysed by gel electrophoresis in a 0.8% SeaKem LE agarose gel (Flowgen) made in 1x TAE buffer. 10% Ficoll loading buffer was added to all DNA reactions prior to loading (15% Ficoll, 0.25% Xylencyanol FF, 0.25% Bromophenol blue dissolved in water).

2.6.5. Constructs

cDNA sequence encoding full-length Wld^S protein, Nmnat-1 or Ube4b amino acids 1-70 (N70) was PCR amplified from the *Wld^S* transgene template (Mack et al., 2001) using the high fidelity enzyme *Pfu* (Stratagene) and appropriate combinations of the following primers (1+2, 4+2 and 1+3 respectively) . 5' restriction enzyme tags, added for cloning purposes, are shown in bold and the first or last three bases of sequence derived from the *Wld^S* gene are underlined. A single base change to repress the stop codon of Wld^S Rev and allow read through of the C-terminal EGFP is double underlined. The restriction enzymes required to make the full-length Wld^S, Nmnat-1 or Ube4b amino acids 1-70 (N70) fragments were:

Fragment	Enzymes
Full-length Wld^s	*Hind*III and *Bam*HI
Nmnat-1	*Nhe*I and *Bam*HI
Ube4b amino acids 1-70 (N70)	*Hind*III and *Sac*II

The primers used in the reactions as detailed above were:

(1) Wld^S forward:

5'-TAGATCCC**AAGCTT**AACCTTTCACCATTAAGAGGAAAGCGATG-3'

(2) Wld^S reverse:

5'- GCG**GGATCC**CGTCCCAGAGTGGAATGGTTGTG-3'

(3) N70 reverse

5'-TCCTCC**CCGCGG**GTCTGCTGCACCTATGGGGGA-3'

(4) Nmnat-1 forward:

5'-GACTA**GCTAGC**ATGGACTCATCCAAGAAGACAG-3'

Fragments were the ligated into the pEGFPN1 vector from Clontech.

2.6.6. Ligation reactions

Ligation reactions contained 1x T4 ligase buffer (Boehringer Mannheim), the appropriate concentrations of backbone/insert DNA for efficient ligation, 0.5μl T4 ligase (5U/μl) (Boehringer Mannheim) and Milli-Q water to make the final volume up to 10μl. Reactions were left overnight at 14°C.

2.6.7. Electroporesis of bacteria

1-2μl of a ligation reaction was added to a 1mm gap BTX disposable electroporation cuvette on ice (BTX inc.) 40μl of electrocompotent DH5α *E.coli* was added to the cuvette and mixed on ice. Bacteria was transformed in a BTX electro-cell manipulator®-600 with a resistance of 129Ohms and a voltage of 1.6kV. Immediately after, 600μl of pre-warmed SOC medium (2.0% w/v bacto-tryptone, 0.5% w/v bacto-yeast extract, 8.5mM NaCl, 0.25mM KCl, 10mM $MgCl_2$, 20mM glucose) was added to the cuvette and the cells allowed to recover for 15-20 minutes at 37°C in a shaking incubator (250rpm). Cells were then spread on LB-agar plates supplemented with 50μg/ml Kanamycin (Sigma) unless otherwise stated.

2.6.8. Small scale preparation of plasmid DNA from bacterial cultures (Mini-prep)

Single well isolated antibiotic resistant colonies appeared after 12-16 hours incubation at 37°C Individual colonies were picked with a sterile toothpick and grown as a small scale

culture at 37°C and shaken at 250rpm. Cells from overnight small scale cultures (3ml) were centrifuged (8000g) in a benchtop centrifuge-5415C (Eppendorf) and the medium aspirated. The pelleted bacteria were the used for plasmid extraction. Small scale mini-preparations of plasmid DNA was carried out using Qiagen Mini-prep kits as per manufacturers instructions.

2.6.9. Large scale preparation of plasmid DNA from bacterial cultures (Maxi prep)

The protocol for a Maxi-prep (Qiagen) is the same as that for the Mini-prep except that the small scale culture is then used to start a large scale culture (50ml) before centrifuging at 4000g for 15 minutes. This pellet was then used to extract plasmid DNA with a Maxi-prep kit (Qiagen) as per manufacturers instructions.

2.6.10. Conformation of positive clones

Clones were confirmed by analytical restriction enzyme digests and automated dye sequencing (Dye-Deoxy-Terminator Cycle sequencing kit). PCR reactions were carried out and the product was sent to SBS Sequencing Service (Ashworth Laboratories, University of Edinburgh). Returned sequences were checked using the programme Sequencher 4.2 (demo version) for the PC. Clones were sequenced along the entire length of the PCR segment inserted into the DNA construct. Sequencing was carried out in both sense and anti-sense directions.

The primers used for sequencing Nmnat1 were:

Forward Primers (5'-3')	Reverse Primers (5'-3')
ATTCGGTGGTGGGCTGGGATGA	CATCTCGTCCACCAAGATCCGGAGGGC
ACGTGGGAAAGTCTTCAGAAGGAG	GCGGGATCCCGTCCCAGAGTGGAATGGTTGTG
ATTTCTGAGCGTCACTGCCAGC	GACTAGCTAGCATGGACTCATCCAAGAAGACAG

The primers used for sequencing N70-Ube4b were:

Forward Primers (5'-3')	Reverse Primers (5'-3')
TAGATCCCAAGCTTAACCTTTCACCATT AAGAGGAAAGCGATG	TCCTCCCCGCGGGTCTGCTGCACCTATGGGGGA

Chapter 3:
An improved method for detecting multiple alleles in *Wld*^{S} expressing rodents

3.1.0. Introduction

The neuroprotective effects of the *Wld*^{S} gene have been shown to be gene-dose dependent. That is, the greater the amount of Wld^S protein expressed, the greater the level of axonal and synaptic protection conferred after nerve injury (Mack et al., 2001; Gillingwater et al., 2002). Moreover, the *Wld*^{S} mouse has been cross-bred with several mouse models of neurodegenerative diseases, and shown to mitigate the onset and progression of disease in these models, including the P0 demylinating neuropathy (Samsam, M. *et al.* 2003.), and the PMN model of motor neurone disease (Ferri, A. *et al.* 2003). In addition, *Wld*^{S} mutant and transgenic mice have been crossbred with lines expressing neuronal markers such as derivatives of Green Fluorescent Protein (Feng et al., 2000; Gillingwater et al., 2002; Beirowski et al., 2004). Since the extent of protection in these models is also likely to be *Wld*^{S} -gene dose-dependent, it is important to have reliable methods for genotyping *Wld*^{S} -expressing mice and/or determining the extant *Wld*^{S} gene copy numbers.

The *Wld*^{S} mutation is a triplication of a region already present in the wild-type animal (see General Introduction), therefore the only quantifiable measures of the number of mutant *Wld*^{S} alleles are: 1. by the strength of the neuroprotective phenotype. 2. Copy number of the mutation. The principal disadvantages of the first are ethical and temporal: an invasive procedure (nerve injury or biopsy) is required to test for strength of neuroprotection over a period of several days. Thus, the second is more appealing. Initially, attempts to PCR across the chimeric boundary were unsuccessful because of the very high GC content at that point in the sequence. Conventional PCR of any other intron-exon boundary in the triplicated region is insufficient to distinguish the different genotypes (figure 3.2). Some success was found through the use of Southern blots in identifying homozygous animals from heterozygous animals as it can be used to some extent to distinguish the genotype by band strength. However, Southern blotting is not recommended for genotyping animals where important experiments are to be carried out, as the results can be affected by inefficient digestions, blotting efficiency, time and

other factors that affect the quantifiable intensity of blots and their signal-noise ratio. The most accurate published method for genotyping *Wld*^{S} - expressing mice to date, has been the method reported by Mi et al (2002) based on Pulse Field Gel Electrophoresis (PFGE). The PFGE method is based on fragment size rather than band intensity.

The current methods for assaying *Wld*^{S} DNA include; 1. conventional PCR, 2. southern blots and 3. pulse field gel electrophoresis. By contrast, the use of quantitative real time PCR (QRT-PCR) to assay DNA has been relatively neglected. In this Chapter, I report the development of a more rapid and efficient alternative to PFGE as a method for genotyping the *Wld*^{S} mutation. This method is based on QRT- PCR using genomic DNA.

3.1.1 Quantitative real time PCR

Quantitative reverse transcriptase (QRT) PCR was developed to fill a niche in quantifying differences in mRNA expression. Possible methods used to analyse RNA levels include; 1. Northern blots; 2. ribonuclease protection assays. Both of these methods require significant amounts of RNA, frequently more than may be available. They do not use amplification steps; they are only semi-quantitative; and they can be very time consuming. 3. *In-situ* hybridisation. This method is also more qualitative than quantitative and can also be very time consuming to perform. 4. Conventional reverse transcriptase (RT) PCR.

Conventional PCR and RT-PCR can be misleading with respect to actual differences in DNA/RNA levels compared to a standard due to cycle number used i.e. it is difficult to visualise in the linear phase (i.e. the phase of the reaction where the amount of PCR product doubles, in theory, with every cycle) because of the amplification process and inefficient incorporation of ethidium bromide into the product. Conventional PCR should therefore only be used to gauge direction of change. By contrast, quantitative (Q)-PCR requires very small amounts of RNA and after some calibration experiments can be very quick and easy to use. The two methods of assessing the level of amplicon being produced in real-time reactions are SYBR green and TaqMan.

3.1.2. SYBR Green

SYBR Green becomes incorporated in new double stranded (ds) DNA, but not to single stranded (ss) DNA. It can therefore be used to monitor the synthesis of new dsDNA in real-time PCR reactions. Upon incorporation into dsDNA SYBR green fluoresces brightly. The fluorescence is significantly better for visualising new DNA production than ethidium bromide because of reduced background levels of fluorescence. The ratio of the fluorescence produced when SYBR green is bound to dsDNA compared to ssDNA is much higher than that of ethidium bromide.

3.1.3. TaqMan

The TaqMan system utilises a primer pair and a probe, which is located between the two PCR primers and has a melting temperature 10°C higher than the primers. The binding of the TaqMan probe to the region of interest before binding of primers is important because without it, the PCR products would be produced without fluorescence and as a result would not be detected. The TaqMan probe has two fluorescent tags attached to it. One is a reporter dye, for example 6-carboxyfluorescein (FAM), which has its emission spectra quenched because a second fluorescent dye or quencher, for example, 6-carboxy-tetramethyl-rhodamine (TAMRA) is attached to the other end of the probe. The result of this is that the probe is effectively silent in this state. TaqMan assays are therefore based on the 5' exonuclease activity of the enzyme Taq DNA polymerase. This enzyme cleaves the probe to release the reporter dye from the proximity and therefore, activity of the quencher. The result is an increase in fluorescence which is proportional to the amount of new PCR product formed.

3.1.4. Multiplex PCR

This utilises the ability of ABI TaqMan Sequence Detection System (SDS) to distinguish between two different flurophores. It is therefore possible to use two separate

primer pairs, each interacting with its own probe linked to different reporter and quencher dyes, to monitor two different reactions taking place in the same tube. The implications of this kind of reaction are quite exciting. Given that the dual fluorescence SDS is a more advanced version of a sequencer, it should be possible in the future to detect the progress of up to four reactions taking place in the same tube. The logistics of this would be quite complicated and the calibration required to set up such a reaction would be no mean task, but it should be possible. However, the use of two flurophores is enough for the present purpose. The implication is that it is possible to monitor an internal control gene versus a gene of interest, for example *β-tubulin* versus *Wld*^{s}.

Because both reactions take place in the same tube and my interest was in calculating the *Wld*^{s} copy number, it was not necessary to add exact amounts of template to the tube. It was sufficient simply to add very dilute template and then calculate the ratio between *β-tubulin* versus *Wld*^{s} of product formed within that tube through the comparative C_T method. Because two independent reactions are monitored within the same tube, the calibration steps must be performed first in individual reactions and then together. This involves determining; 1. Abundance of reference and target genes. Through testing primers as separate reactions it is possible to adjust the primer concentrations so that accurate threshold cycles (C_T) are obtained for both species. By doing so it is possible to stop the amplification of the majority species before it can limit the availability of the common reactants to the minority species. 2. Optimal primer and probe concentrations, which give the maximum ΔR_n and the lowest ΔC_T values. 3. Linear dynamic range, is the range of initial template concentration that accurate C_T values can be gained. The lower the amount of template required the more sensitive the assay becomes.

3.1.5. Selecting optimal amplicon sites

According to guidelines set out by ABI, primers can be designed as close as possible to each other provided that they do not overlap. Generally, the smaller the amplicon the more efficient the amplification. However, the smaller the amplicon the greater the risk

of amplification of a homologous region. It is therefore important to keep the GC content as low as possible, as increased CG will raise the melting temperature of the primers. According to the primer express software (ABI) the T_m should be kept between 58-60°C, and the 5 nucleotides at the 3' end of the primer should have no more than 2 G/C bases (*Primer Express User Bulletin,* P/N 4317594).

DNA:

Optimal amplicon sites will allow the amplification of DNA without amplifying any contaminating RNA sequences. This can be achieved by designing primers to span an intron-exon boundary, thus allowing the amplification of the target DNA without amplifying the target genes RNA product. If however there are no introns present in the gene of interest then amplification of RNA cannot be ruled out without adding RNAse to the extract.

RNA:

Optimal amplicon sites will allow the amplification of RNA without amplifying any contaminating genomic DNA sequences pseudogenes or other related genes. This can be achieved by designing primers to span one or more introns, thus allowing the amplification of the target RNA without amplifying the target gene DNA sequence. If however there are no introns present in the gene of interest then amplification of genomic DNA cannot be ruled out and for this reason no reverse transciptase (no-RT) controls should always be carried out.

3.1.6. Efficiency of amplification

One of the main problems when comparing the level of the gene of interest to an "internal control" gene is the effect of primer efficiency. This can be explained by saying that if the primer pairs are running at 100% efficiency, then after 1 cycle the

amount of product present should be double the starting amount.. However if the primer efficiency is only 90% then after 1 cycle there would be 1.9× the amount of product and so on (80% = 1.8×, 70% = 1.7× etc). Thus, after 10 cycles this effect would be magnified, i.e. if the primer efficiency is 100% after 10 cycles there will be 2.0^{10}× product, 90% will give 1.9^{10}× product and so on (80% = 1.8^{10}×, 70% = 1.7^{10}× etc). So, the effect of comparing two primer pairs that may have slightly different efficiencies can be minimised by setting the threshold for measurement as low as possible where the effects of this unequal amplification will not be so apparent.

Therefore, with each set of primers it is important to carry out several checks on the primer efficiency. It is important to calculate the optimal primer concentrations required the dynamic range of these primers and the limiting concentrations. Checks should include; 1. melting curves, 2. the slopes of the curves are in parallel when viewed in the log output graph, 3. there are 4 or 5 dilution points and 4. that the correlation coefficient is greater than 0.90.

When intending to carry out duplex real time PCR i.e. TaqMan involving the use of a probe, those primers must first be tested in separate tubes to allow the reactions to proceed without interference from the other primer i.e. eliminating any competition for reagents within the tube. The optimal primer and probe concentrations will be those that give the highest ΔR_n and the lowest ΔC_t values. It is important that the primers can work with a small amount of template because the reaction will give a more sensitive assay at lower concentrations so a linear dynamic range test involving titrations of the template to calculate the dynamic range of the primers.

3.1.7. Contamination

"The exquisite sensitivity of the polymerase chain reaction means DNA contamination can ruin an entire experiment. Tidiness and adherence to a strict set of protocols can avoid disaster" (Kwok *et al.* 1989). Potential contamination can be introduced by

samples with high DNA concentrations, DNA template controls or PCR carryover contamination (Peters *et al.* 2004). The need to analyse product through gels or dissociation curve for non specific product formation is therefore high.

3.1.8. Miss-priming

One way of stopping the formation of non-specific product is through the use of Applied Biosciences Ampli-tTaq Gold which is a chemically modified version of Taq DNA polymerase. This modification renders the enzyme inactive until a certain temperature is reached, therefore any mispriming which may have occurred will not be enzymatically extended and amplified. The enzyme does not become active until 48°C, which is especially important if carrying out 1 step QRT-PCR. This is because the production of cDNA from RNA is carried out by a primary extension step at 42-45°C.

3.1.9. False positives

Non specific amplification including primer dimers can affect the amplification data, for this reason dissociation curves should be checked. Primer dimers are likely to be most prevalent in no template control wells and in wells with a very low template concentration.

Single stranded contamination can lead to false positives, provided by the ability of the PCR process to amplify single strands (Higuchi *et al.*1989). This can be controlled for through the incorporation of dUTP instead of dTTP into new product via the PCR mix (SYBR). Subsequent treatment of PCR reactions with uracil-N-glycosylase (UNG) prior to amplification will lead to the degradation of miss-primed, non-specific products that may have been produced before specific amplifications. It will not however degrade the native nucleic templates.

Fluorescent contaminants can also lead to false positives, so it is wise to use no-amplification control tubes (sample but no enzyme). Following the PCR reaction, if the no-amplification tube has greater fluorescence than the no-template control tube there is likely to be a fluorescent contaminant, either in the sample or in the heat block of the cycler.

3.1.10. Relative quantitation of gene expression

Amplification of an endogenous control may be used to standardise the amount of sample RNA or DNA added to a reaction. The two main methods for calculating RNA levels are the standard curve method and the delta C_T (change in cycle number at set threshold) method.

3.1.11. The delta CT method of relative gene quantitation

The amount of target when normalised to an endogenous reference and relative to a calibration sample can be expressed as:

$$2^{-\Delta\Delta C_T}$$

Derivation of the formula (ABI user bulletin number 2) through the equation that describes the exponential amplification of a product through PCR is:

$$X_n = X_0 \times (1 + E_x)^n$$

Where: X_n = number of target molecules at cycle n.

X_0 = initial number of target molecules

E_x = efficiency of target amplification

n = number of cycles

Threshold cycle (C_T) indicates the cycle number at which the amount of amplified target reaches a fixed threshold:

$$X_T = X_0 \times (1 + E_X)^{C_{T,X}} = K_X$$

Where : X_T = threshold number of target molecules
$C_{T,X}$ = threshold cycle for target amplification
K_X = constant

A similar equation for the endogenous reference reaction is:

$$R_T = R_0 \times (1 + E_R)^{C_{T,R}} = K_R$$

Where: R_T = threshold number of reference molecules
R_0 = initial number of reference molecules
E_R = efficiency of reference amplification
$C_{T,R}$ = threshold cycle for reference amplification
K_R = constant

Dividing X_T by R_T gives the following expression:

$$X_T \div R_T = [X_0 \times (1 + E_X)^{C_{T,X}}] \div [R_0 \times (1 + E_R)^{C_{T,R}}] = K_X \div K_R = K$$

The exact values of X_T by R_T depend on a variety of factors including; 1. the reporter dye used, 2. the effects of the amplified sequence on the fluorescent properties of the reporter, 3. the efficiency of reporter incorporation (SYBR green) or cleavage of the

probe (Taq Man), and 4. the purity of the reporter/probe and the setting of the fluorescence threshold. For these reasons the constant K does not necessarily need to be equal to one. However, if we assume that the efficiencies of the target and reference amplification are the same:

$E_X = E_R = E$,

$$X_0 \div R_0 \times (1+E)^{C_{T,X} - C_{T,R}} = K$$

Or,

$$X_N \times (1+E)^{\Delta CT} = K$$

Where: $X_N = X_0 \div R_0$, the normalised amount of target

$\Delta CT = C_{T,X} - C_{T,R}$, the difference in threshold cycles for target and reference.

This can be rearranged to give:

$$X_N = K \times (1+E)^{-\Delta C_T}$$

Finally XN can be divided for any sample q by XN for the calibrator (cb):

$$X_{N,q} \div X_{N,cb} = [K \times (1+E)^{-\Delta C_{T,q}}] \div [K \times (1+E)^{-\Delta C_{T,cb}}] = (1+E)^{-\Delta\Delta C_T}$$

Where: $\Delta\Delta C_T = \Delta C_{T,q} - \Delta C_{T,cb}$

So, if the efficiency is close to 1, the amount of target normalised to an endogenous reference and relative to a calibrator is:

$$2^{-\Delta\Delta C_T}$$

The use of the comparative C_T method can be preferable to the standard curve method for several reasons, including increased throughput due to less reagents being used to construct a standard curve, elimination of any adverse effects introduced through dilution errors when making a standard curve and decreased sample preparation time.

3.1.12. Limitations of the delta C_T method

The first limitation of the delta CT method is that it assumes that the efficiency of amplification is 100% i.e. $2^{-\Delta\Delta C_T}$. However, this can be corrected for by adjusting the equation to compensate for a large variance in efficiency. If the efficiency was only 90% the equation would be $1.90^{-\Delta\Delta C_T}$. The second limitation of the delta CT method is that it assumes that as the samples are diluted, the amplification of the gene of interest relative to the internal control gene may not be consistent. Example, two genes A and B; B is slightly less abundant than A. However, the primers for gene A are only 90% efficient when compared to the primers for B. The more the samples are diluted the more the amplification levels of B will begin to reach the amplification levels of A at higher cycle numbers. This is another reason why it is important to set the threshold at as low a level as possible. This is due to the fact that this possible difference in the efficiency of amplification may not affect the results at lower threshold levels. The error will become more obvious as the reaction progresses.. It is also another reason that multiple repeats (at least triplicate) should be run for each sample.

Results

3.2.0. Results

3.2.1. Efficiency of amplification

Serial dilution of genomic DNA from wild-type C57Bl/6J mice was used as a template for PCR to test the efficiency of amplification of the two primer pairs. The genomic DNA was diluted 1 in 10 each time and correlation coefficients were obtained for each primer pair (figure 3.3). Primers against a region of *Wld*^{S} and *β- tubulin* gave correlation coefficients of 0.9982 and 0.9928 respectively, with slopes of -3.3647 for *β-tubulin* and -3.3867 for *Wld*^{S}. The reactions were found to proceed similarly when primers were used both separately and together, indicating that the two separate primer pairs are not interacting with each other.

3.2.2. Change in cycle number (ΔC_T)

Amplification plots for wild-type, heterozygous-*Wld*^{S} and homozygous-*Wld*^{S} show clear differences for the ΔC_T between each group (figure 3.4). The difference between *β-tubulin* and *Wld*^{S} amplicon product at the set threshold can be used to determine *Wld*^{S} genotype. A difference giving less *Wld*^{S} than *β-tubulin* product is a wild-type animal, a difference of 1 cycle more *Wld*^{S} than *β-tubulin* product is a heterozygous *Wld*^{S}, and a difference of 2 cycles more *Wld*^{S} than *β-tubulin* product is a homozygous *Wld*^{S} (figure 3.3). The product of a PCR for the *Wld*^{S} amplicon alone run on ethidium bromide gel does not allow for determination of genotype (figure 3.2).

Plotting the cycle difference result for animals of known genotype in a box and whisker plot (n=36) allows the illustration of 95% confidence limits for each genotype. When genotyping animals it should be good practice to repeat the genotyping if the sample of interest falls outwith the 95% confidence limits for all of the plotted genotypes (figure 3.5). However, plotting on the same axis a scatter of the results for animals of unknown genotype (n=91) there is a trend towards banding into the 3 genotypes as demonstrated

previously by the box and whisker plot (figure 3.5). A representative set of unknown genotype whose identity was determined by real time PCR, were also confirmed via southern blot (Dr M.P.Coleman, personal communication).

3.2.3. Determining copy number in transgenic animals

Transgenic animals have been generated which express the *Wld*^{s} chimeric gene (Adalbert *et al.* 2005). These animals show a strong neuroprotective phenotype. It has previously been shown that *Wld*^{s} neuroprotective phenotype is dose dependent on the level of Wld^{s} protein product being expressed (Mack *et al.* 2001). It is therefore of benefit to determine the number of copies which have been integrated into the genome of these transgenic animals. In this case there are 2 rat models of *Wld*^{s}, the transgenic line 23 and line 79 (Adalbert *et al.* 2005). Through the use of real time PCR on genomic DNA it is possible to calculate the copy number of insertions into the rat genome. The results examining the number of inserts in two of the *Wld*^{s} transgenic lines can be seen in Figure 3.6. This is not an exact determination as the primers are designed against a short sequence of *Ube4b* and may also amplify any endogenous rat *Ube4b* that may or may not be present. There is also some variability in the amplification process at higher copy number as previously described (Ballester *et al.* 2004).

As previously mentioned, wild-type animals are expected to have 2 copies, Heterozygous *Wld*^{s} are expected to have 4 copies and homozygous *Wld*^{s} should have 6 copies. Analysis of the data detailed in figure 3.6 show that wild-type mice have 1.15±0.68 (mean±SEM) copies (n=13), heterozygous *Wld*^{s} 3.87±0.36 copies (n=7), homozygous *Wld*^{s} 6.10±0.53 copies (n=7), Tg23 12.34±2.05 (n=10) and Tg79 19.49±1.52 (n=14).

Discussion

3.3.0. Discussion

I have described here a new method for genotyping *Wld*^{S} mice. PFGE has hitherto been the only method reliable enough to distinguish homozygotes from heterozygotes of this genotype.

It is not possible to generate a *Wld*^{S}-specific product suitable for conventional PCR: the nature of the mutation means the product would also appear in samples from wild-type animals. Conventional PCR does not produce bands of significantly different intensity for each genotype, when run on an agarose gel (See figure 3.2). A Southern blotting method relies on the strength of the *Wld*^{S} specific band to distinguish between homo-/hetero-zygous animals which can lead to ambiguity. The most recent method employing PFGE, is based on altered fragment size rather than a difference in fragment intensity and as such is a more reliable assay. However, this method is itself fallible: there can be problems, for example with incomplete digestion of the sample in question. The tissue normally required for extraction of DNA for PFGE is the spleen, the genotyping is effectively carried out post mortem, and therefore if the animal was homozygous it is no longer available for breeding. It also means that substantial sums are spent on animal husbandry and breeding only to determine the genotype of the animals being generated post mortem.

Through the use of real time PCR, animals can be genotyped using DNA extracted from small pieces of tissue, e.g. ear punch. This is a regulated procedure often used to mark animals within a breeding programme. This means that the genotype of the subject in question can be tested before an experiment, and checked during or after use in breeding or experiments. The main benefits of this method over others are; 1. The time scale in which it can be performed. Samples can be digested overnight, the DNA extracted the next morning, quantity assessed if desired and PCR performed the same afternoon. 2. The animals can still be available for breeding and use once the genotype has been determined which would not be the case after pulse field. 3. Real time PCR is very cost

effective. By sourcing other suppliers in this case Sigma, primers and probe can be acquired for about 30% of the cost from ABI. 4. This method is much more convenient when mass screening for genotype. For example, each plate has 96 wells, excluding a few wells for controls it would be possible to genotype (in triplicate) up to 30 animals at once. Given that the time consuming part of the genotyping is the DNA extraction, but that the PCR itself only takes about 90 minutes, which is a theoretical turnover of 30 animals every 90 minutes.

Initial experiments with SYBR green were promising but ultimately proved unreliable, reflected in a series of conflicting data. Because only one flurophore (SYBR Green) could be used it was not possible to run the control gene and the gene of interest in the same tube. Pippetting errors are a significant potential source of such inconsistencies. For example, if the reaction requires the addition of 1µl of sample per tube, then 0.25µl on the outside of the pipette tip will make a considerable difference to the contents of the reaction. This is especially true when seeking a very small change in copy number i.e. 2 copy difference between wild-type and heterozygous *Wld*^{S}. A standard curve must also be run for both genes against which the samples can be compared. The need for a standard curve for comparison means that an accurate way to assay the DNA samples is required. The samples must all fall within the range of concentration set out by the standard curve. This requires the use of a method to accurately assay DNA. Initially thought was given to using Pico Green to assay the DNA, but the cost of this system was prohibitive. Instead an assay system was set up based on the use of Hoechst 33258 (Lopukhov *et al.* 2002). This method, though more cost effective and based on the PCR results, more accurate than measurement via spectrophotometry, is also time consuming. The need for this therefore results in an increased in expense and in the amount of time required for set up.

TaqMan Real time PCR was the best solution to the genotyping problem. Because the comparative C_T is being used, as long as both primer pairs are running with the same efficiency (see figure 3.3) standard curves are not required. It also means that there is no

need to accurately assay the concentration of the DNA as each sample will be referenced to its own control gene within the same tube. The samples, although much quicker to assay by examining the curves produced (see figure 3.4), can also be assayed by cycle number difference between the *Wld*^{S} amplicon and the *β-tubulin* control product at the set threshold (see figure 3.5). 95% confidence limits based on samples of known genotype assayed suggest that the number of *β-tubulin* cycles minus the number of *Wld*^{S} cycles gives a reliable indication of when a result should be accepted or when it should be re-genotyped for definite conformation. Genotyping of unknown samples with representative samples checked for genotype by Southern blot, show that the samples do in-fact fall within certain patterns consistent with the three genotypes.

Transgenics

The determination of copy number in transgenics is important to establish if, as in the case of *Wld*^{S}, the effect of the mutation is gene dose dependent. However, it is the level of protein expression rather than the number of copies of the transgene incorporated in the transgenic that leads to the "level" of protection. As previously mentioned, the accuracy of real time PCR varies with increasing copy number (Ballester *et al.* 2004). Figure 3.6 shows that the estimate of copy number is consistent with that of PFGE at lower copy numbers. The discrepancy in results between animals from the same line at higher copy number has been described in detail before (Ballester *et al.* 2004). They showed that standard deviation of copy number between animals of the same transgenic line increases as the number of copies increases. Ballester *et al.* also showed that the discrepancies became most obvious in their line which had 18-20 copies, and that when 40 copies are reached the change in cycle number becomes unreadable in the linear range of quantification. I suggest that this may be corrected by diluting samples of high copy number to a greater extent before assay to obtain a more accurate measure of copy number at a lower threshold. This however, may become a problem itself if the endogenous reference used has a low copy number. The method of estimating insertion copy number is therefore adequate providing the factors already mentioned are taken

into account. This method will still not provide an indication of area/orientation of insertion and whether or not those copies are all functional.

Figures

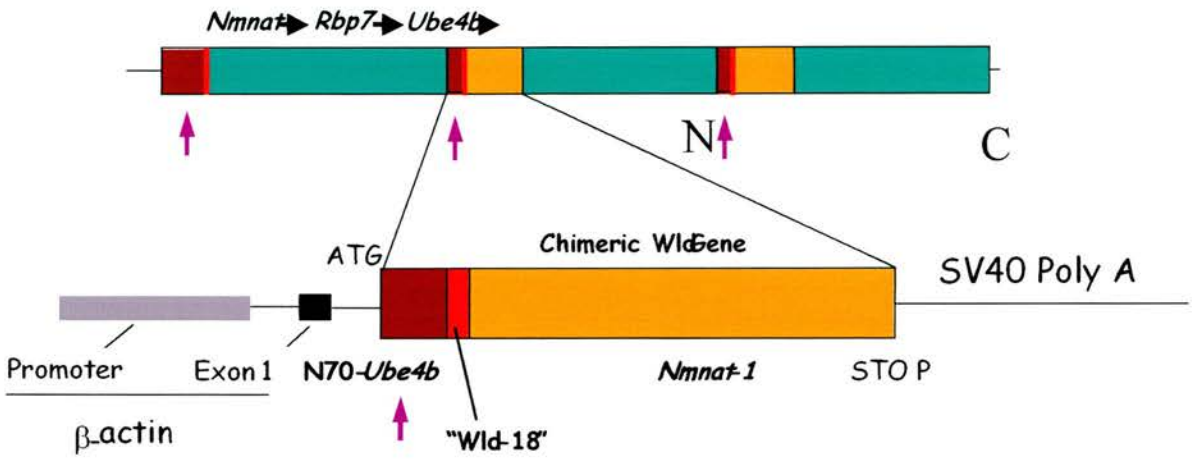

Figure 3.1. Primer annealing sites on the *Wld*^{S} mutation and transgene. The spontaneous mutation discovered in the *Wld*^{S} mouse and the transgene used to make the various transgenic *Wld*^{S} animals including Tg4836 mouse, Tg23 and 79 rat lines. The above diagram is not to scale but gives an indication of where the primer annealing sites (purple arrows) are located. Primers were designed against a region of exon 1 in the Genbank sequence AF260927 for the chimeric *Wld*^{S} product. See methods (section 2.5.7) for more detail.

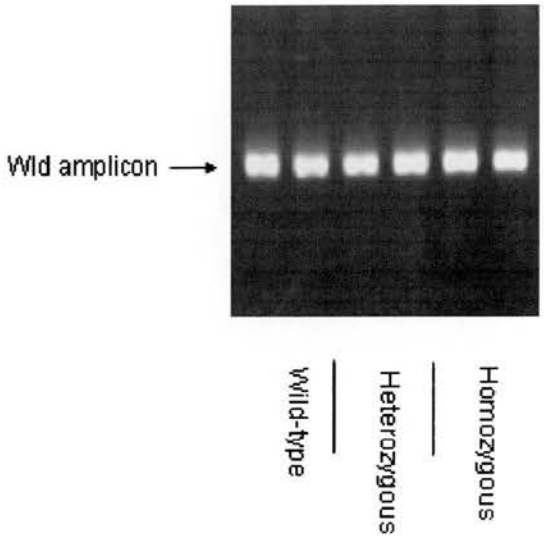

Figure 3.2. Conventional PCR on genomic DNA does not allow for differentiation between the 3 genotypes.
The product of a conventional PCR using the Wld primers displayed on an agarose gel (2%) containing ethidium bromide. There is no obvious difference between wild type, heterozygous and homozygous animals.

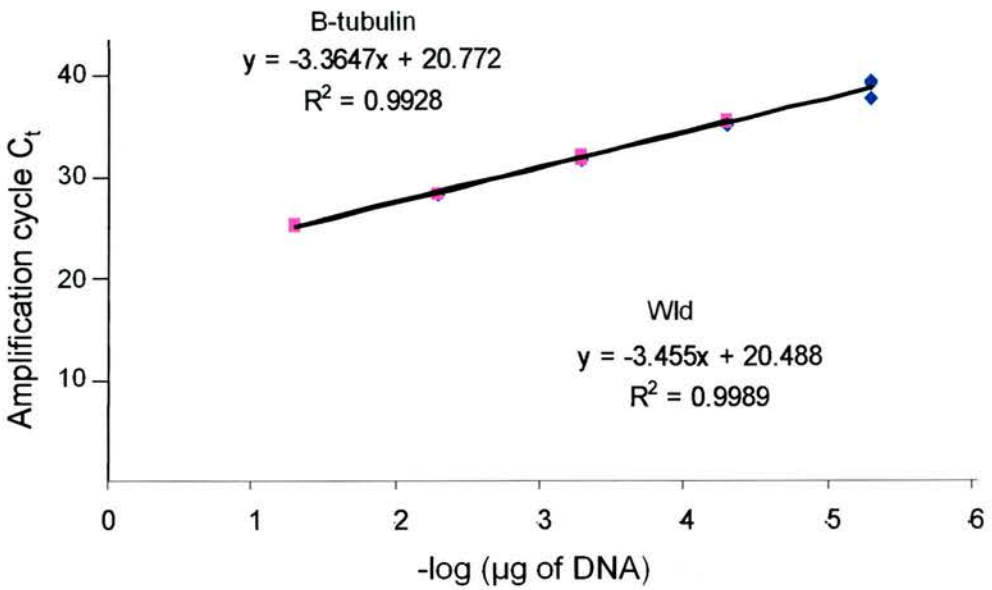

Figure 3.3. Primers for *Wld*^{S} and *β-tubulin* have very similar R^2 values.

Standard curves for the *Wld*^{S} and *β-tubulin* gene in serially diluted (1 in 10) template genomic DNA sample from wild-type (C57Bl/6J) mice from Harlan-Olac. Very efficient amplification was obtained as demonstrated by the slopes of linear regression of the standard curves, and good correlation coefficients. C_t is cycle threshold.

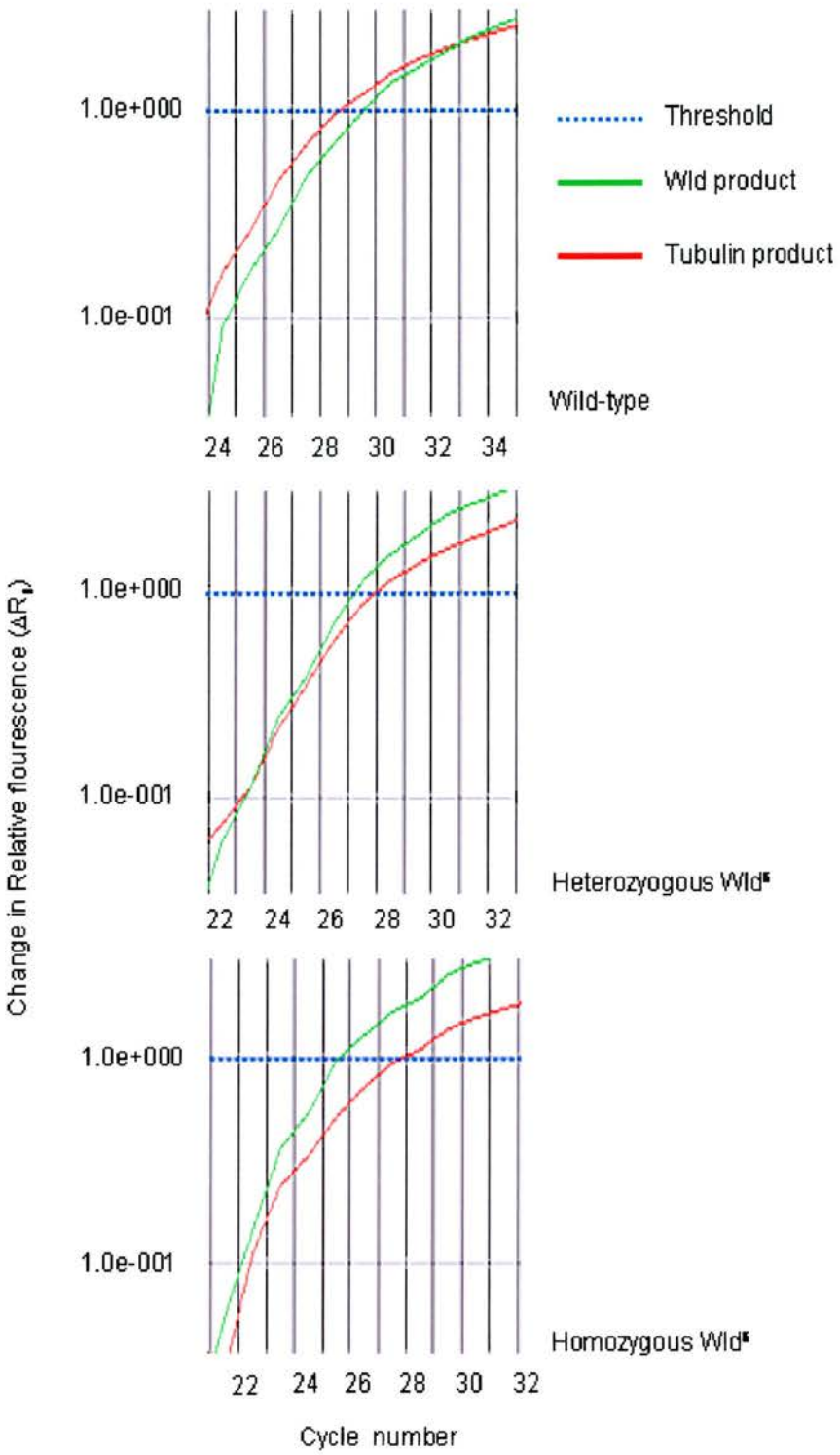

Figure 3.4. Real time data shows differences between wild-type, heterozygous and homozygous animals.
Screen grabs from ABI software. The curves show the difference in cycle number (ΔC_t) between tubulin (red) and Wld^s (green) for each genotype at 1.0e+000, i.e. wild type -0.65, heterozygous +1, and homozygous +2.

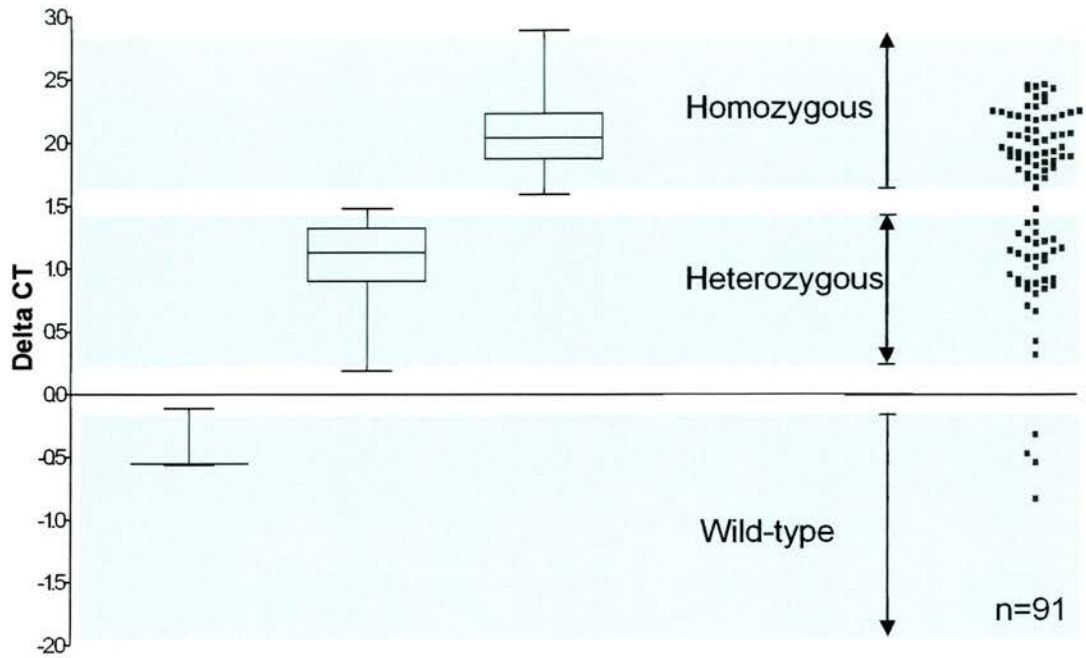

Figure 3.5. Real time PCR on genomic DNA shows clear difference in ΔC_t for the 3 genotypes.

The above is a graphical representation of ΔC_t between the tubulin and Wld amplicons, for animals of known genotype (n=36, box and whisker) and animals of unknown genotype (n=91, scatter). The areas shown in blue represent the 95% confidence limits for each particular genotype as determined from the box and whisker plots. There is a clear trend for each particular genotype. If however the animal of interest falls out-with the predetermined 95% confidence limits it should be re-genotyped.

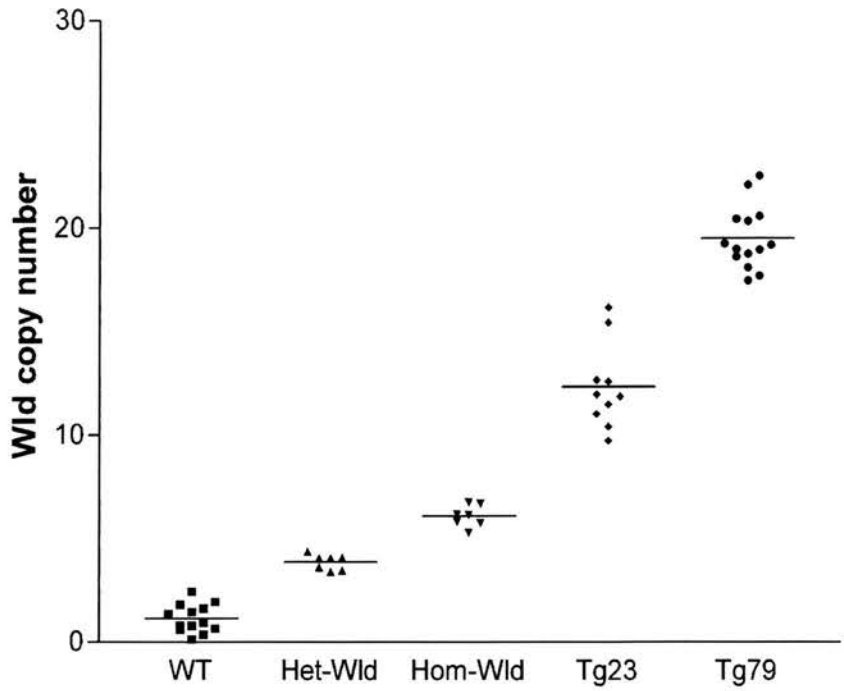

Figure 3.6. Real time PCR can be used to determine copy number in transgenic animals.
Real time PCR carried out on pre-determined samples of genomic DNA can be used to determine copy number of an insert in rat transgenic lines (Tg) 23 and 79. This does not show functionality or orientation of insertion. Although there is some fluctuation in the determined copy number, wild-type (WT) animals are expected to have 2 copies Heterozygous *Wld*^{s} (Het-Wld) are expected to have 4 copies and homozygous *Wld*^{s} (Hom-Wld) should have 6 copies. Analysis of the above data show WT 1.15±0.68 (mean±SEM) copies (n=13), Het-Wld 3.87 ± 0.36 copies (n=7), Hom-Wld 6.10 ± 0.53 copies (n=7), Tg23 12.34 ± 2.05 (n=10) and Tg79 19.49 ± 1.52 (n=14).

Chapter 4:
Mapping the Distribution of Wld^S Protein in the Brain

4.1.0. Introduction

Although the *Wld*^{s} mutation (Figure 3.1) itself has now been quite well characterised (Conforti *et al.* 2001) the mechanism by which it provides its neuroprotective effect is still unknown. As stated previously, the chimeric Wld^{s} protein (see chapter 3, figure 3.1) is sufficient for its protective effect: transgenic lines that express the chimeric gene show a strong neuroprotective phenotype (Adalbert *et al.* 2005). One feature that the transgenic animals and the spontaneous *Wld*^{s} mutant all share is localisation of Wld^{s} protein to nuclei (Mack *et al.* 2001, Adalbert *et al.* 2005). A recent report shows that Wld^{s} protein is absent from the cytoplasm of neurones (Fang *et al. 2005*). It is therefore logical to hypothesise that the neuroprotective effect of *Wld*^{s} is not caused by the protein directly, but rather by some cascade of interactions that are a function of Wld^{s} protein concentration within nuclei.

The expression of Wld^{s} protein and its localisation within nuclei in the peripheral nervous system has already been described, but until recently has not been extensively studied within the central nervous system. I have made use of an antibody "Wld-18" which targets an eighteen amino acid peptide. This peptide is coded by DNA normally contained within the 5' untranslated region of *Nmnat1*, but which is expressed between the *Ube4b* and *Nmnat* portions of the *Wld*^{s} chimeric gene because of the resultant in frame insertion and continuous read through from the *Ube4b* portion of the gene (Figure 4.1). This antibody is both very specific and versatile, as it allows the visualisation of the Wld^{s} protein through either Western blot or immunocytochemistry.

A search for conserved interactive domains using the Wld^{s} protein sequence was carried out using Prosite (http://kr.expasy.org/tools/scanprosite/). This search revealed possible casein kinase II phosphorylation, N-myristoylation, protein kinase C phosphorylation, amidation and N-glycosylation sites (Figure 4.2).

Western blots on whole brain lysate have previously shown strong Wld^S protein expression in the brains of *Wld^S* mice and transgenic equivalents (Mack *et al.* 2001). Thus a reasonable hypothesis is that the protein should be evenly distributed throughout neuronal nuclei in the brains of these mice, as seen previously in motor neurone nuclei (Mack *et al.* 2001). Evaluation of this hypothesis will be described in this chapter. I present evidence that:

1) Wld^S protein is not uniformly distributed in CNS neurones, either in the spontaneous mutant or the transgenic equivalents.
2) Intra-nuclear distribution of Wld^S varies considerably between and within cell types. Some neurones show intense, diffuse staining. Other neurones show fine speckling, while some display large nuclear inclusions that can vary in shape from spheres to more irregular structures.
3) The various patterns of Wld^S protein distribution develop postnatally *in vivo* and *in vitro* in isolated neurones.
4) Wld^S protein aggregates co-localise with other proteins involved in ubiquitination and transcriptional regulation.
5) Redistribution of the Wld^S protein occurs following stressful or damaging stimuli to the cells in which it is expressed.

Therefore, the protection of axons which has previously been demonstrated in neurones of the PNS may not be anticipated for all neurones in the CNS of *Wld^S* expressing models.

Results

4.2.0. Results

4.2.1. Western Blot analysis of Wld^S protein expression in the Brain

Previous analysis of Wld^S protein expression by Western blot was limited to protein extracts made from whole brain. I first refined this analysis by examining Wld^S protein levels in different regions of *Wld*^{S} mouse brain, specifically cerebral cortex, hippocampus and cerebellum. All these regions appeared to contain Wld^S protein in both immature postnatal mice and in adults. However, expression appears greater in the cerebellum, where it increased with the age of the *Wld*^{S} mutant mice (Figure 4.3). Thus, the adult cerebellum showed increased levels of Wld^S compared to either P6 cerebellum or adult hippocampus and cerebral cortex. Levels of Wld^S protein in the immature hippocampus and cortex were not discernibly different compared to adult mice. However, the expression pattern in the hippocampal and cortical neurones appear to be very different (Figure 4.4). The levels of VAP-33 (a synaptic protein which does not alter during postnatal development) were constant across all these brain regions, and did not change with age. The increase in Wld^S expression in cerebellum with age, can be also be detected immunocytochemically, both *in vivo* and *in vitro* (Figure 4.3, 4.6 & 4.7).

4.2.2. Distribution of Wld^S protein in the *Wld*^{S} mouse brain is not uniform

Through the use of the Wld-18 antibody in immunocytochemistry I confirmed that Wld^S protein is expressed in the central nervous system of the adult *Wld*^{S} mouse when visualised using fluorescent secondary antibodies or DAB immunohistochemistry. Both methods show Wld^s confined to the nucleus (Mack *et al.* 2001, Sajadi *et al.* 2004 & Fang *et al.* 2005). However, I found that the expression pattern is not uniform, which has not been reported in the previous studies (Figure 4.4). A comparison of the two immuno-labelling techniques demonstrated that although DAB immunocytochemistry has been assumed to be more sensitive than fluorescent labelling, I could not discern any difference in protein labelling between the two techniques (Figure 4.5). However,

fluorescence imaging provides a more fine grained resolution of Wld^S puncta distribution within nuclei of cells in different regions of the nervous system (Figure 4.4, Table 4.1 & 4.2). There was both regional variation and inter-cellular variation within regions. To analyse the expression patterns observed with confocal microscopy I grouped the cells into four categories;

1) large inclusions in the nucleus (dots),
2) numerous small nuclear inclusions (speckles),
3) strong diffuse nuclear expression (diffuse),
4) very weak diffuse/no staining in the nucleus (weak).

The number of cells in each category were counted through the use of low power confocal microscopy (Figure 4.4). The nuclei containing Wld^S positive inclusions were expressed as a percentage of the total number of visible TOPRO-3 positive nuclei. This would also include TOPRO-3 positive non-neuronal cells. Therefore, the numbers are probably an underestimate of the percentage of neurones expressing Wld^S protein (Table 4.1 and 4.2). Attempts were made to count only neurons using Neu-N a neuronal marker, but this proved too difficult to accurately quantify in the more neuronal dense regions (data not shown). Some cells fell into more than one category (e.g. large inclusions plus strong diffuse staining were evident in some layers of cortex (Figure 4.3, Table 4.1). Table 4.1 and 4.2 lists the percentages of cells in each category within each of the major brain regions analysed.

Cerebellum

The cerebellum showed a very striking distribution pattern; 90% of cerebellar granule cells and 82% of cells in the molecular layer. However, Purkinje cells showed no nuclear Wld^S protein (Figure 4.4, Table 4.1 and 4.2).

Hippocampus

In contrast, where I have shown there is Wld^S protein present by Western blot, the hippocampus has no discernable Wld^S protein within nuclei of either dentate gyrus granule cells or CA1 neurones. However, most CA3 neurones show nuclear speckling.

This variability in distribution patterns is in contrast to spinal motor neurones, where there is a uniform strong diffuse nuclear staining pattern (Mack *et al.* 2001).

Ganglia

On the other hand, *Wld*^{S} expression in peripheral (autonomic and sensory) ganglia showed similar diverse staining patterns. No discernible nuclear staining was seen in *Wld*^{S} mouse superior cervical ganglion (SCG), which is reported to show a strong protective axonal phenotype *in vitro*. There were large, clear nuclear inclusions in the nuclei of small neurofilament positive neurones in the dorsal root ganglion (DRG). Some DRG neurones contained unusual shaped inclusions. These neurones showed a reproducible array of unusual shapes including; large circular structures, smaller tight ring shaped structures and strings of protein (Figure 4.4). Without deconvolution software it is not easy to determine whether these are hollow structures, i.e. a coating of protein around an internal core, or whether they represent "solid" aggregates of Wld^S protein. In order to simplify classification, these structures were grouped together and termed "tubes" (Table 4.1 and 4.2). There were also examples where inclusions appear to be joined by threads of Wld^S protein. Interestingly, these complex nuclear inclusions were not observed in the large neurones in the DRG which display a more diffuse, rather faint staining pattern. Although these patterns were not seen elsewhere in the regions of the spontaneous mutant I examined, they were present in certain areas in the transgenic animals (see below). Interestingly, these structures and faint diffuse Wld^S staining have not been mentioned in any other studies, and yet the DRG have a very strong neuroprotective phenotype in the majority of fibres following axotomy (Mack *et al.* 2001).

4.2.3. Changes in protein distribution during development

A comparison of neonatal and adult brain revealed developmental changes in Wld^S protein expression (Figure 4.6, 4.7, Table 4.1 and 4.2). These were particularly striking

in the cerebellum. Only 3% of cerebellar granule cells from P6 animals showed discernable levels of Wld^S protein in the nucleus, compared with over 90% in the adult (Table 4.1). Figure 4.6 illustrates the formation of the characteristic large nuclear inclusions in cerebellar granule cells *in vivo*. Very little Wld^s protein was visible at P6. This was followed by an increase in the number of cells with a "speckling" of protein (Panel B, Figure 4.6) which appear to aggregate and form the nuclear inclusions characteristic of the adult cerebellar granule cell. It appears as though there is an increase in the amount of speckling and strong diffuse protein which may aggregate to form the large inclusions seen in the adult.

Cultures of dissociated cerebellar granule were prepared from neonatal P4 mice. I anticipated that Wld^S protein would initially be undetectable *in vitro*. When dissociated granule cells from *Wld*^{S} mice were fixed and stained for Wld^S protein immediately following plating and adhesion, no Wld^S protein expression was observed (Figure 4.7, Panel A). However, after 7 days in culture, Wld^S-containing inclusions could clearly be seen in the cultured cell nuclei (Figure 4.7, Panel B). This suggests that cerebellar granule cell neurones mature in culture. The observation that these inclusions reach a maximum size by seven days is interesting because a previous study by Buckmaster *et al.* (1995) showed that the *Wld*^{s} protective phenotype developed over seven days. It is also possible to demonstrate that Wld^s positive inclusions can be formed in rat cerebellar granule cell dissociated cultures following transfection with a Wld^s-eGFP construct (Figure 4.7). These reached a maximum size approximately 9 days after transfection and look similar in both appearance and size to cerebellar granule cell inclusions in the *Wld*^{s} mutant mouse (Figure 4.7). Interestingly, in the adult cerebellum Figure 4.8 shows a size calculation for the size of the nuclear Wld^s protein aggregates in cerebellar granule cells. The average aggregate size is 1.12±0.36 (Mean±SD, n=10) μm^3. If we assume there are 10^{10}-10^{11} granule cells per cerebellum (Llinás, 1975) there is about 1.12×10^{10}(-10^{11}) μm^3 of visible Wld^s protein aggregate in the cerebellar granule cell layer.

There was also an interesting developmental change in the pattern of staining visualised in the primary-, secondary- motor cortex and the somatosensory cortex. At P6 when Wld^S protein expression was seen, it was mostly in the form of small speckles. As the animals matured, *Wld*^{S} expression appeared as a strong diffuse pattern, suggesting that the strong staining may possibly represent a myriad of tiny inclusions that it is impossible to fully resolve at the confocal/light microscope level (Table 4.1). Thought was given to a more detailed examination using immuno-electron microscopy, but it was beyond the scope of the current study.

4.2.4. *Wld*^{S} expression in transgenic mouse and rat brains

Dr M.P.Coleman provided brains from transgenic *Wld*^{s} animals, made by non-targeted insertion of the chimeric *Wld*^{s} gene under the control of the β-actin promoter. Although the mouse line 4836 and rat line 23 both show a strong neuroprotective phenotype in axotomy of peripheral nerve (Mack *et al.* 2001, Adalbert *et al.* 2005), the expression pattern of Wld^S protein in the *Wld*^{S} transgenic mouse is markedly different from the spontaneous *Wld*^{S} mutant.

Surprisingly, for example, cerebellar granule cells show no Wld^S, in either the transgenic mouse or rat (Figure 4.9, 4.10 & Table 4.3). Instead, there was clear Wld^S protein expression in a subset of neurones at the interface between the granule cell layer and molecular layer in both of the transgenic lines. The transgenic rat shows large inclusions in what appeared to be basket cells. The transgenic mouse had very unusual inclusions, resembling 'tubes' of Wld^S protein, in the nucleus of what may be Golgi cells. Similarly, in the hippocampus the transgenic expression patterns were unlike the spontaneous *Wld*^{S} mouse; dentate gyrus granule cells and CA1 cells of the hippocampus, regions mostly devoid of Wld^S protein in the *Wld*^{S} mouse (Table 4.1), show strong Wld^S expression in the transgenic mouse. However, these regions showed very little evidence of Wld^s staining in the line 23 transgenic rat (Table 4.3).

4.2.5. Where in the nucleus is the Wld^S protein?

Currently it may be easier to say where the protein is not. Wld^S protein does not co-localise with either Cajal (or coiled) bodies, PML bodies or the splicing factor SC35 (M.P.Coleman personal communication). Dr Haley and I have also shown that Wld^S does not co-localise with SMN, ConA or mono-ubiquitin or poly-ubiquitin (data not shown). However, the fact that we have not seen the Wld^S protein in these areas may simply be due to our inability to adequately detect it given the limitations of the current protocols.

Perhaps not surprisingly given that native Ube4b (in yeast) is known to interact with VCP (Berny *et al.* 2001), a pull down assay revealed an interaction between Wld^S and VCP, through interaction at a specific binding site located on the N70-portion of Ube4b, contained within the chimeric protein (Laser *et al.* 2005, Submitted). I therefore examined cerebellar granule cells, which I found to be a rich source of Wld^S protein, for evidence of co-localisation with VCP.

4.2.6. Colocalisation of Wld^S protein with VCP

Valosin containing protein (VCP; p97/Cdc48) is a protein with diverse cellular roles including an important involvement with the ubiquitin proteasome system. A recent study by Laser *et al.* (2005, unpublished but submitted at the time of writing) shows that Wld^S lacking its N-terminal 16 amino acids (N16) does not bind or redistribute VCP, but the Wld^S protein will still form nuclear aggregates. This means that the binding site for VCP on the Wld^S chimeric gene is in the N-terminal 16 amino acids, which are part of Ube4b. Laser *et al.* also state that wild-type Ube4b also requires N16 for binding to VCP, even though the yeast homologue has its binding site towards its C-terminus.

Figure 4.11 demonstrates colocalisation of Wld^S protein with VCP in cerebellar granule cells and Wld^S positive cells within the cerebellar molecular layer. Figure 4.12 shows

colocalisation in the DRG. In the DRG the co-localisation is not absolute. That is, not every Wld^S positive inclusion is VCP positive. VCP staining on wild-type tissue shows that it normally does not aggregate in nuclei (Figure 4.13). Not all Wld^S inclusions showed evidence of VCP co-localisation, suggesting that aggregation of Wld^S protein does not require interactions with VCP, but that VCP does require Wld^S.

VCP is known to interact with histone deacetylases (HDACs, Berny *et al.* 2001). A recent publication by Araki *et al.* (2004, explained in more detail later) suggested that the Wld^S phenotype is mediated through the NAD pathway in a Sirt1 dependent fashion, and it is known that Sirt1 is a member of the histone deacetylation family (NAD dependent deacetylases, Kyrylenko *et al.* 2003). Following a fruitful discussion with Dr Hardingham (Edinburgh University) it became apparent that a subset of HDACs and another pathway related protein, silencing mediator for retinoic acid and thyroid hormone receptors (SMRT), show a similar distribution to Wld^S protein within neurones. For these reasons I decided to test for co-localisation of Wld^S with SMRT and HDAC5.

4.2.7. Colocalisation of Wld^S protein with SMRT & HDAC5

The silencing mediator for retinoic acid and thyroid hormone receptors (SMRT) mediates transcriptional repression by recruiting histone deacetylases (HDACs) to DNA bound receptor complexes. SMRT contains an N-terminal sequence that is highly conserved in the nuclear co-repressor N-CoR. It has previously been demonstrated that SMRT aggregates in cell nuclei and forms nuclear speckles. This can lead to recruitment of HDAC4 & 5 to these speckles. HDAC4 is primarily diffuse in the cytoplasm, and HDAC5 has a primarily diffuse localisation within the nucleoplasm. SMRT movement is followed by translocation of these into discreet nuclear foci (Wu *et al.* 2001).

Figure 4.14 shows some evidence of colocalisation of Wld^S protein with SMRT in transfected cortical cells. A colocalisation "map" (Figure 4.14 panels D and H) shows colocalisation in a low power and higher power confocal micrograph. The co-localisation is not complete. In some cells there was no evidence of colocalisation. The

results were similar when either cortical cells or HEK 293 cells were cotransfected with Wld^S-eGFP and SMRT-Flag.

However, Figure 5.15 shows co-transfection of cortical cells with Wld^S-eGFP and HDAC5-Myc. In this case all the cells examined appear to show complete co-localisation with HDAC5. This co-localisation is strongly evident in both dissociated cortical cells and HEK293 cells when transfected with either Wld^S-eGFP and HDAC-Myc or Wld^S-RFP and HDAC-GFP. This apparent preference for co-localisation of Wld^S with HDAC5 over SMRT could perhaps be related to an interaction between HDACs and VCP (see discussion).

4.2.8. Wld^S protein may move in response to stress

At this point I would like to report observations I have made in relation to some preliminary experiments undertaken initially to test whether Wld^S localisation may be related to electrical activity of neurones that express it. These observations may be of general interest, although I feel that to cover them in detail would distract the reader from the overall direction of this thesis. Further information can be found in appendix 4.1.

Could the formation of connections in the CNS could be the reason for the change in localisation of Wld^S protein during development? I have already shown that Wld^S protein accumulates into inclusions over a period of more than a couple of weeks *in vivo*, but rapidly accumulate in culture reaching a maximum size at about 7 days in vitro, which would correspond in time with the formation of a complete network of connections in dissociated cerebellar granule cell cultures.

Electrical activity has previously been shown to affect the localisation of HDACs (Chawla *et al.* 2003, Lin *et al.* 2005). It has been demonstrated that spontaneous electrical activity is sufficient to drive nuclear export of HDAC4 but not of HDAC5 in

cultured hippocampal neurones, and that HDAC5 translocation to the cytoplasm can be induced, following stimulation of calcium flux through synaptic NMDA receptors or L-type calcium channels (Chawla *et al.* 2003). In order to test the possibility that electrical activity may involved in the localisation of the Wld^S protein (as it can affect the localisation of HDACs), whole brain vibratome cut slices were incubated in oxygenated ACSF with either PTX (picrotoxin, blocks the gamm-aminobutyric acid activated chloride channels) or TTX (tetrodotoxin, specifically blocking voltage-gated sodium channels) over a time period of 4 hours. This caused an interesting change in distribution of the Wld^S protein within the nuclei of neurones. In the cerebellar granule cells protein became localised towards the edges of the nuclei. However, this visual effect was no different between treatments with PTX, TTX or if the slices were just maintained in oxygenated ACSF. An example of the protein redistribution seen in cerebellar granule cells is given in Figure 4.16. It was initially thought that the reason for this lack of difference between treatments could be that the tissue, following slicing and incubation in ACSF are reacting to the severing of synaptic connections that must have occurred during the process. It is not the case that the cells are simply dead because incubation with the dying-cell marker, propridium iodide, showed very few cells with uptake at 4 hours (data not shown).

The images shown in Figure 4.16 give an impression that there is an increase in the visible amount of protein. To confirm overall protein levels a Western blot was carried out on protein extracted from different brain region of slices, which have undergone incubation in ACSF for 0 and 4 hours. However, the Western blot in Figure 4.17 demonstrates further that there is no discernable change in the overall protein levels.

Discussion

4.3.0. Discussion

Wld^S protein is localised to nuclei of neurones in both the PNS and the CNS of the *Wld^S* mouse (Figure 4.4 and Table 4.1; Mack *et al.* 2001). The data presented here show, however, that the distribution of the Wld^s protein throughout the nervous system is not uniform from region to region. There are also intra region variations. For example, although there is as much protein within the hippocampus as there is in the cortex as estimated by Western blot (Figure 4.3), the distribution of visible protein is very different both between and within the two regions, and varies greatly within the hippocampus itself (Table 4.1). Almost 50% of cortical cells are Wld^s positive, ranging from large inclusions to speckling, to strong diffuse immunostaining, whilst the hippocampus shows no discernable Wld^s immunostaining in the dentate gyrus, with only 10% of cells in the CA1 and over 80% of cells in the CA3 with speckled immunostaining. This variation suggests that there is cytoplasmic Wld^s protein, which is so diffuse that we cannot visualise it either by DAB or fluorescence immuno-cytochemistry, or that there are two pools of Wld^s protein both with different configurations, one which allows visualisation with the Wld-18 antibody, and another which does not. However, due to the fact that transfection with an eGFP tagged *Wld^s* construct shows a similar pattern as visualised by immunocytochemistry on the *Wld^s* mouse, I am tempted to assume that the protein is just diffuse, and therefore below detection levels. Fang *et al.* (2005) also appear unable to detect any Wld^s protein within the cytoplasm of neurones, and although their publication has validated the methods used in this study, they were unable to show co-localisation of Wld^s with any possible candidate downstream factors and have not provided any form of quantification of expression profiles throughout the nervous system.

The formation of visible aggregates also appears to develop postnatally (Figure 4.6). In the regions examined by Western blot (Figure 4.3), all the areas appear to have the same levels of protein at P6 and P70 except the cerebellum, which shows an increase. Large nuclear Wld^s protein aggregates within every cerebellar granule cell were not evident until after P17.

It therefore becomes important to ask if these inclusions serve any function; for example, does the phenotype vary with pattern of nuclear aggregates of Wld^S protein? In particular, the inclusions must contain very high local concentrations of Nmnat1, reported to be the active component of the Wld^S protein (Araki *et al.* 2004). This increased local Nmnat1 content within the nucleus may be important in activating local downstream effector pathways and subsequently causing the *Wld*^{S} neuroprotective effect through a cascade of events.

The formation of these inclusions could have implications for neuroprotection, both *in vivo* and *in vitro*. Experimentally, neurones are cultured normally from very young tissue, and if it can be determined that the formation of inclusions within nuclei are important for phenotype, then when neurones are first cultured there may be no protection. In cerebellar granule cell cultures from *Wld*^{S} mice, although there is no obvious nuclear Wld^S protein at postnatal day 4 when the cultures are prepared, inclusions do develop *in vitro* over 7 days by which point the distribution of protein resembles that of the adult *in vivo*. This timescale is accelerated compared to the *in vivo* development of inclusions but correlates well with the time course of development of an *in vitro* neuroprotective phenotype in DRG, SCG and cerebellar granule cells from *Wld*^{S} mice where maximal protection of neurites was observed only after the cells had been in culture for 7 days (Buckmaster *et al.* 1995). This slow development of the phenotype *in vitro* suggests that perhaps the development of nuclear inclusions is necessary for the protective phenotype. Other studies have utilised dissociated cells and/or explants of the SCG to demonstrate and assay the axoprotective *Wld*^{S} phenotype (Deckwerth and Johnson, 1994; Buckmaster *et al.* 1995). The fact that cerebellar granule cells look like adult tissue after 7 days *in vitro* (i.e. chronologically P11) reinforces the idea that tissue from the developing animal can subsequently be treated as adult tissue.

Thus, it has become critical to ask whether nuclear localised Wld^S and/or nuclear Wld^S inclusions are required for the full axonal protection phenotype. If they are essential,

then not all neurones in the CNS or PNS of the *Wld*^{S} mouse or transgenic mouse/rat would exhibit axonal protection. This issue might be addressed by comparing the strength of the neuroprotection observed in the spontaneous Wld^S mouse with that seen in comparable neurones in the transgenic equivalents. The mosaic expression pattern of Wld^s protein makes this feasible. Regardless, it is clear that Wld^S neurones are able to survive and develop normally despite the presence of large inclusions of abnormal protein within the nucleus. Recent evidence suggests that some neurones survive by accumulating aggregates of abnormal protein (Arrasate *et al.* 2004). Although the aggregates themselves are probably not directly effecting survival, they are more likely acting through some cascade of events initiated in the nucleus.

It is difficult to correlate Wld^S inclusions with the strength of the neuroprotective phenotype since there is a wide variety of expression patterns, even within a particular cell type. However, there are some cell types where there is a more homogeneous distribution of Wld^S protein and it may be possible to draw some conclusions from these:
1) Motor neurones have very strong diffuse nuclear Wld^S protein (which could be numerous small inclusions that it is not possible to resolve) and there is clear neuroprotection of motor neurone axons following axotomy (Gillingwater & Ribchester. 2001 & 2003, Coleman & Ribchester. 2004).
2) The majority of cortical cells in the adult have strong diffuse nuclear staining similar to that seen in motor neurones. Dr T.Gillingwater has recently provided evidence that these cells exhibit protection of synapses following cortical ablation (Gillingwater *et al.* Submitted).
3) 90% of cerebellar granule cells from *Wld*^{S} mice have single large inclusions of Wld^S protein (Figure 4.4 and Table 4.1) and clear neuroprotection is observed *in vitro* following removal of serum and potassium (Explained in more detail in chapter 5, Figure 5.1, Buckmaster *et al.* 1995, Haley *et al.* submitted).
4) Small DRG neurones contain very large and unusually shaped inclusions of Wld^S protein (Figure 4.4) and sensory axons are protected following axotomy *in vivo* and *in vitro* and vincristine toxicity (Perry *et al.* 1990, Buckmaster *et al.* 1995, Wang *et al.*

2001 & Araki *et al.* 2004). However, large DRG neurones appear to have only faint, diffuse Wld^S staining and yet they are also protected following axotomy.

5) Superior cervical ganglion neurones are also protected *in vitro* after 5-7 days of culture (Deckworth and Johnson 1994, Buckmaster *et al.* 1995), but there is only faint Wld^S staining in these neurones *in vivo*. I have not seen strong nuclear expression of Wld^S in adult SCGs *in situ*. This could be a function of the growth factors present in the culture medium, inducing SCG neurones to express Wld^S *in vitro*.

6) Recent electrophysiological studies by Dr Haley demonstrate that the axons of hippocampal CA3 cells, which do have visible Wld^s protein inclusions are protected against axotomy, whilst those axons from CA1 cells, which do not have visible aggregates are not protected (Dr J.Haley, unpublished data, Appendix 4.2).

The diverse pattern of Wld^S protein expression in the *Wld*^{S} mouse is also reflected in the transgenic mouse and transgenic rat (which express the *Wld*^{S} gene) although the actual patterns of expression differ from each other and from the *Wld*^{S} mouse (Figure 4.9, 4.10 and Table 4.3). A possible reason for the different expression patterns in the transgenic lines, relative to the spontaneous mutant is that both transgenics are driven by a β-actin promoter, whilst in the spontaneous mutant, transcription is regulated by the native promoter for Ube4b (Conforti *et al.* 2000). I might predict that Wld^S protein distribution between neuronal subsets in the *Wld*^{s} mouse would parallel the distribution pattern of Ube4b expression. This is not the case. In the mouse cerebellum, Ube4b is expressed predominately in Purkinje cells (Kaneko *et al.* 2003) whereas nuclear Wld^S expression is very weak in these neurones. However, the β-actin promoter used in the transgenic lines is almost ubiquitously expressed in neurones and yet Wld^S protein also has a very varied distribution pattern in these animals. The differences between the expression in the transgenic lines, could also be due to the fact that the lines are generated by a non-targeted insertion. This means that the constructs have probably inserted in different regions of the genome and are probably being affected by local factors. Referring back to Figure 3.6, I have already demonstrated that the transgenic lines have a different

number of insertions, although as stated previously, this does not mean that all of the inserts are functional.

Whatever underlies the inter-cellular distribution pattern of Wld^S, the intra-cellular localisation of this protein to the nucleus appears to result from the full-length *Nmnat1* present in the protein. Recently, Araki *et al.* (2004) provided evidence that elevated NAD synthesis by *Nmnat1* is sufficient to confer neuroprotection. They suggested that this would need to occur locally in the nucleus since overall NAD levels are not altered in the *Wld*^{S} mouse (Mack *et al.* 2001). *Nmnat1* is known to have a nuclear localisation signal as part of its structure (Figure 4.1, Schweiger *et al.* 2001). This portion is required for the nuclear localisation of Wld^S protein in cell lines since the removal of the *Nmnat1* region results in the cytoplasmic localisation of Wld^S protein (Explained further in chapter 5, Figure 5.11, Araki *et al.* 2004). In contrast, the ubiquitin ligase Ube4b is normally cytoplasmically located (Figure 5.11, Kaneko *et al.* 2003), or possibly shuttled between cytoplasm and nucleus. Thus, the truncated N70 portion of Ube4b (which constitutes part of the Wld^s protein), might be inappropriately located in the *Wld*^{S} mouse and is sequestered away from its normal cytoplasmic location, into the nucleus by the attached Nmnat1 region.

Whether this relocation of the truncated Ube4b has any consequence for the neuroprotective phenotype remains to be demonstrated, but it may be required for the formation of inclusions. In HEK293 and COS-7 cells, only the full length Wld^S construct produced inclusions in addition to nuclear expression of the protein (Figure 5.11, Laser *et al.* submitted).

I have also demonstrated that Wld^s co-localises with VCP and HDAC5. HDAC5 is a class II HDAC, and the class II members are related to yeast SIR2 deacetylase. The possible significance of this will become apparent in the next chapter. As previously described, class II HDACs, which include HDAC 4,5,6 & 7 are capable of shuttling between the cytoplasm and the nucleoplasm, and their localisation is highly regulated by

a number of factors (Chawla *et al.* 2003), including electrical activity and cell stress. Through immunoprecipitation in yeast, HDAC6 associated proteins have been shown to have high homology to proteins involved in the regulation of ubiquitination. These homologous proteins include UFD3 (phospholipase A2 activating protein) and Cdc48p AAA ATPase (i.e. VCP). It has been demonstrated that Ube4b (the mammalian homologue of Ufd2) has a binding site for VCP (Laser *et al.* 2005), and also that HDAC6 can interact with VCP (Seigneurin-Berny *et al.* 2001). It is known that HDACs can act as transcriptional regulators, but only when they have translocated to the nucleus. I have shown that VCP is distributed diffusely and does not aggregate in a wild type mouse, but in the presence of Wld^S protein, VCP does form aggregates. This may be because VCP binds Wld^S protein at an identified binging site on N70-Ube4b and is "dragged" into the nucleus due to the nuclear localisation signal incorporated in the sequence of Nmnat1. I have also shown co-localisation of Wld^S with HDAC5 (another class II HDAC), and it could be that class II HDACs in general interact with VCP, resulting in its movement to the nucleus, and in its new position exert transcriptional regulatory effects. This suggests a possible mechanism by which Wld^S protein localised to nuclei may effect protection of axons and synapses, following separation from the cell body. However, this is just untested speculation.

Furthermore, it remains to be determined what intranuclear structures house both the inclusions and the extraordinary loop structures highlighted by the Wld^S protein. Further characterisation of these structures could provide insight into the mechanism of Wld^S-conferred neuroprotection.

To summarise, I have mapped the Wld^S protein in various different regions within the nervous system, and have never found it outwith the nucleus. A pressing question remains: how can a protein localised to the nucleus protect axons and synapses from degeneration when separated from the cell body by a cut or a crush injury? The easiest hypothesis is that through its nuclear localisation, and now proven interaction with members of the ubiquitin proteasome system and possible regulators of transcription, it

is altering transcriptional regulation within those cells. This hypothesis was examined in chapter 5.

Figures

MEELSADEIRRRRLARLAGGQTSQPTTPLTSPQR
ENPPGPPIAASAPGPSQSLGLNVHNMTPATSPIGA
ADNIAVRGLHVGQHHQLLPMDSSKKTEVVLLACG
SFNPITNMHLRLFELAKDYMHATGKYSVIKGIISPV
GDAYKKKGLIPAHHRIIMAELATKNSHWVEVDTWE
SLQKEWVETVKVLRYHQEKLATGSCSYPQSSPAL
EKPGRKRKWADQKQDSSPQKPQEPKPTGVPKVK
LLCGADLLESFSVPNLWKMEDITQIVANFGLICITR
AGSDAQKFIYESDVLWRHQSNIHLVNEWITNDISS
TKIRRALRRGQSIRYLVPDLVQEYIEKHELYNTESE
GRNAGVTLAPLQRNAAEAKHNHSTL

Figure 4.1. Wld^{s} protein sequence.
The protein product of the *Wld^{s}* mutation showing the location of the N70 amino acids of *Ube4b* (black). The 18 amino acids normally located in the 5' un-translated region of *Nmnat1* but which are expressed in the chimeric protein (red) allowing the generation of the highly specific Wld-18 antibody. The C-terminal 303 amino acids of *Nmnat1* (the whole coding region in blue), including a constitutively expressed nuclear localisation signal (green). This sequence was obtained from PubMed: AF260924.

Hits for all PROSITE (release 18.48) motifs on sequence USERSEQ1 :

Found: 14 hits in 1 sequence; USERSEQ1 (373 aa)

MEELSADEIRRRRLARLAGGQTSQPTTPLTSPQRENPPGPPIAASAPGPSQSLGLNVHNMTPATSPIGAADNIA
VRGLHVGQHHQLLPMDSSKKTEVVLLACGSFNPITNMHLRLFELAKDYMHATGKYSVIKGIISPVGDAYKKKGLI
PAHHRIIMAELATKNSHWVEVDTWESLQKEWVETVKVLRYHQEKLATGSCSYPQSSPALEKPGRKRKWADQK
QDSSPQKPQEPKPTGVPKVKLLCGADLLESFSVPNLWKMEDITQIVANFGLICITRAGSDAQKIYESDVLWRHQS
NIHLVNEWITNDISSTKIRRALRRGQSIRYLVPDLVQEYIEKHELYNTESEGRNAGVTLAPLQRNAAEAKHNHSTL

hits by patterns with a high probability of occurrence or by user-defined patterns:
[14 hits (by 5 distinct patterns) on 1 sequence]

PS00006 **CK2_PHOSPHO_SITE** *Casein kinase II phosphorylation site* :

5 - 8: SadE

345-348: TesE

PS00008 **MYRISTYL** *N-myristoylation site* :

19 - 24: GGqtSQ

68 - 73: GAadNI

77 - 82: GLhvGQ

147 - 152: GLipAH

PS00005 **PKC_PHOSPHO_SITE** *Protein kinase C phosphorylation site* :

91 - 93: SsK

92 - 94: SkK

126 - 128: TgK

183 - 185: TvK

312 - 314: StK

324 - 326: SiR

PS00009 **AMIDATION** *Amidation site* :

211 - 214: pGRK

PS00001 **ASN_GLYCOSYLATION** *N-glycosylation site* :

369 - 372: NHST

Figure 4.2. Scan Prosite Results Viewer.
This view shows ScanProsite results together with rule-based predicted features inside (profile) matches. For further information visit: http://kr.expasy.org/tools/scanprosite/

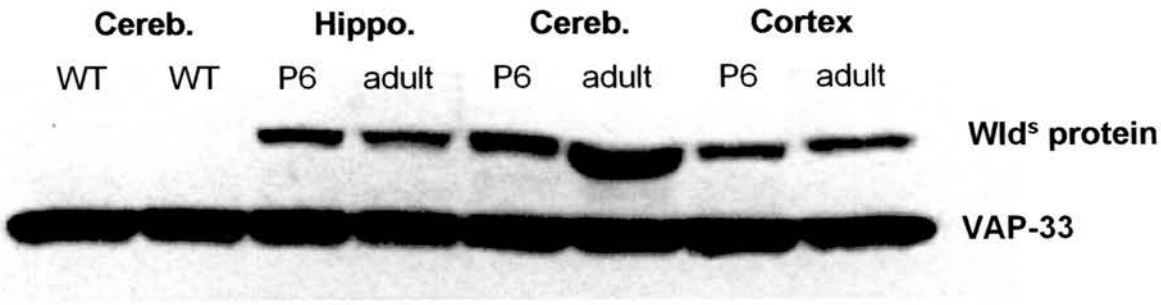

Figure 4.3. Western blot analysis confirms the absence of Wld^s protein in wild type mice.
Levels in P6 mice are detectable and similar in hippocampus (hippo.), cerebellum (cereb.) and cortex as well as adult hippocampus and cortex ($P>0.13$; N=3, 2 tailed T-test welch corrected from band density analysis). There is a clear increase ($P<0.03$), in the level of Wld^s protein (43KDa) present in the adult cerebellum compared to the neonate. However, protein levels are consistent between the hippocampus and cortex. Similar levels of protein were loaded in each lane, as demonstrated by the uniform VAP-33 (33KDa) staining in all lanes.

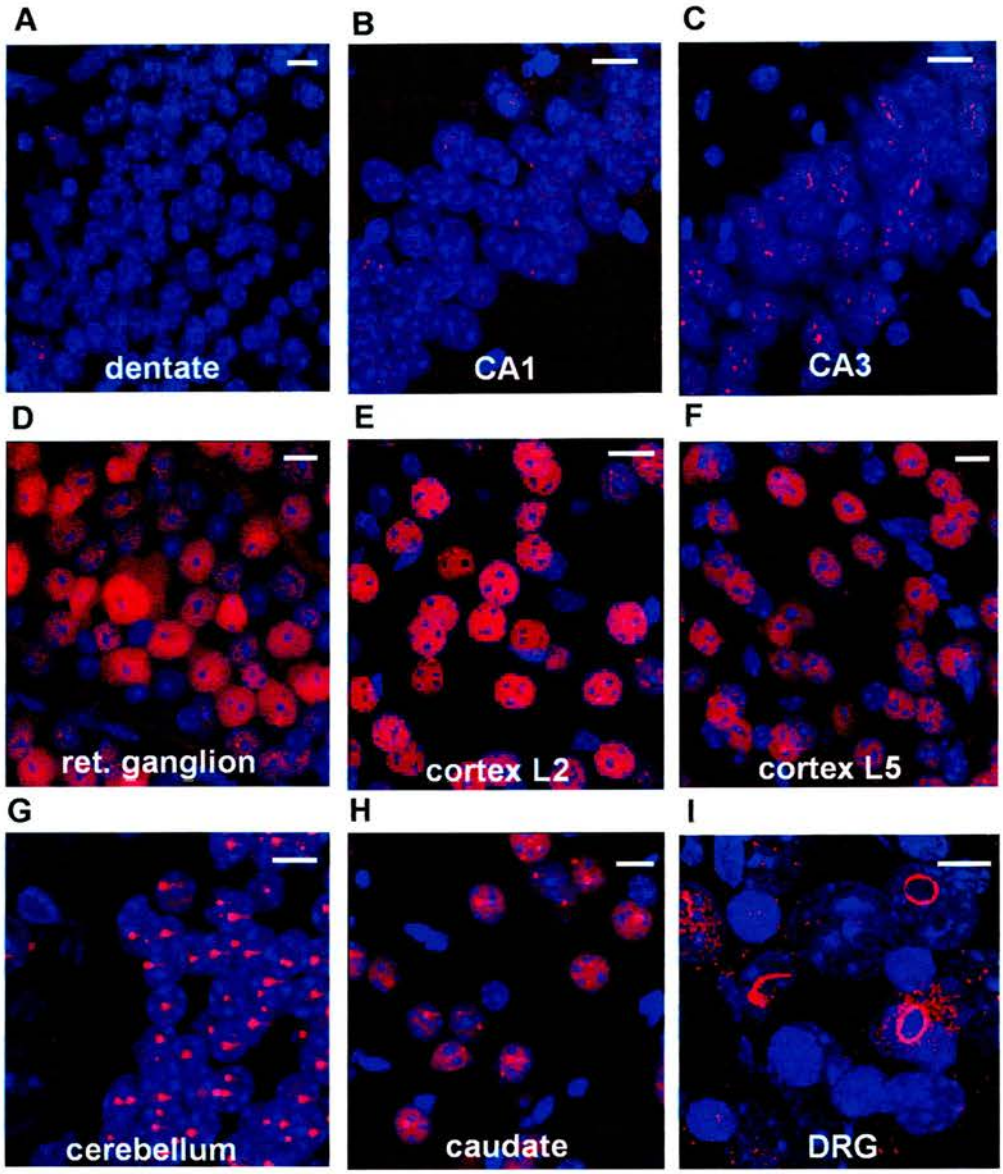

Figure 4.4. Wld^s protein staining in the Adult *Wld^s* mouse is not uniform in its distribution.

Confocal micrographs illustrating that the expression of Wld^s protein (red) in various regions of brain slices from *Wld^s* mice, plus dorsal root ganglion (DRG) and retinal ganglion cells. Slices were counterstained with TOPRO-3 (blue) to show nuclei. Distribution patterns have a wide range including; clear strong diffuse staining in the nucleus of retinal ganglion cells and motor cortex layer 2 cells (D & E), to large or small punctuate inclusions in hippocampal CA3 neurones, cerebellum and caudate (C,G &H) and no obvious staining in dentate gyrus and hippocampal CA1 neurones (A & B). Staining in the small neurones of the DRG was unusual with circles and tubular structures occurring within the nuclei (I). Scale bar = 10μm.

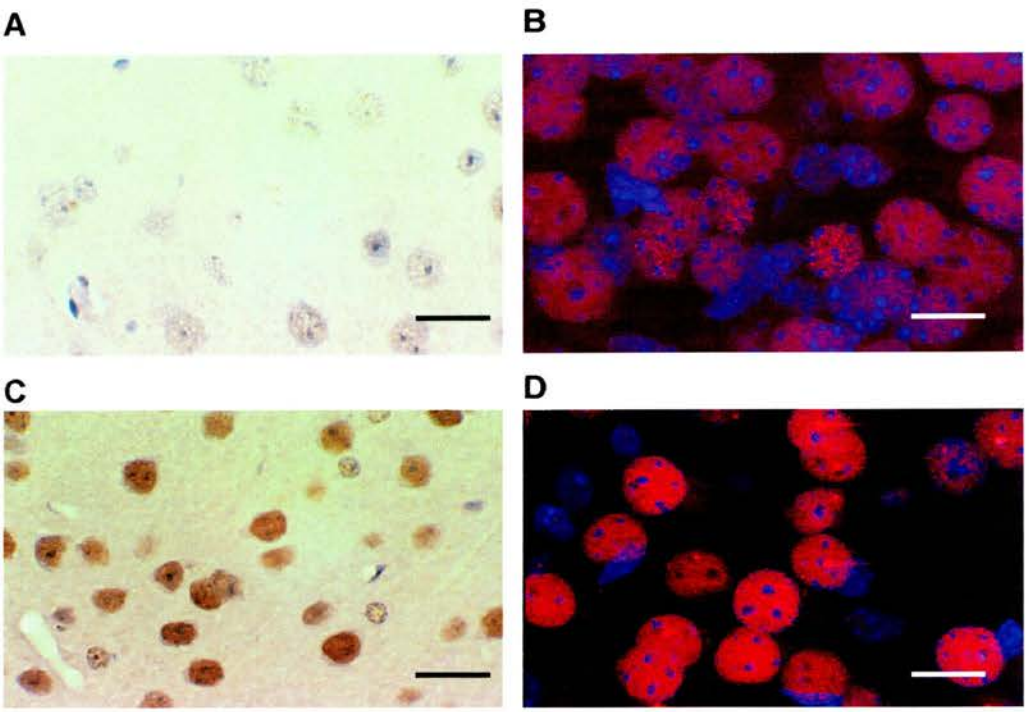

Figure 4.5. DAB immunocytochemistry does not appear to reveal any Wld^s protein that fluorescent immunocytochemistry may not detect.

DAB (A & C) and fluorescence (B & D) immunocytochemistry on *Wld*^{s} primary motor cortex at P6 (A & B) and P70 (C & D). Using both DAB and fluorescence it is possible to see strong nuclear staining with large inclusions in the adult cortex (C & D), and nuclear speckling of Wld^s protein in developing cortex (A & B). The 2 main disadvantages of DAB are 1. That the length of the staining protocol can affect the appearance of the DAB and 2. That with Wld^s protein immunocytochemistry the use of a nuclear marker can obscure the protein of interest. Scale bar = 20μm A & C, 10μm B & D.

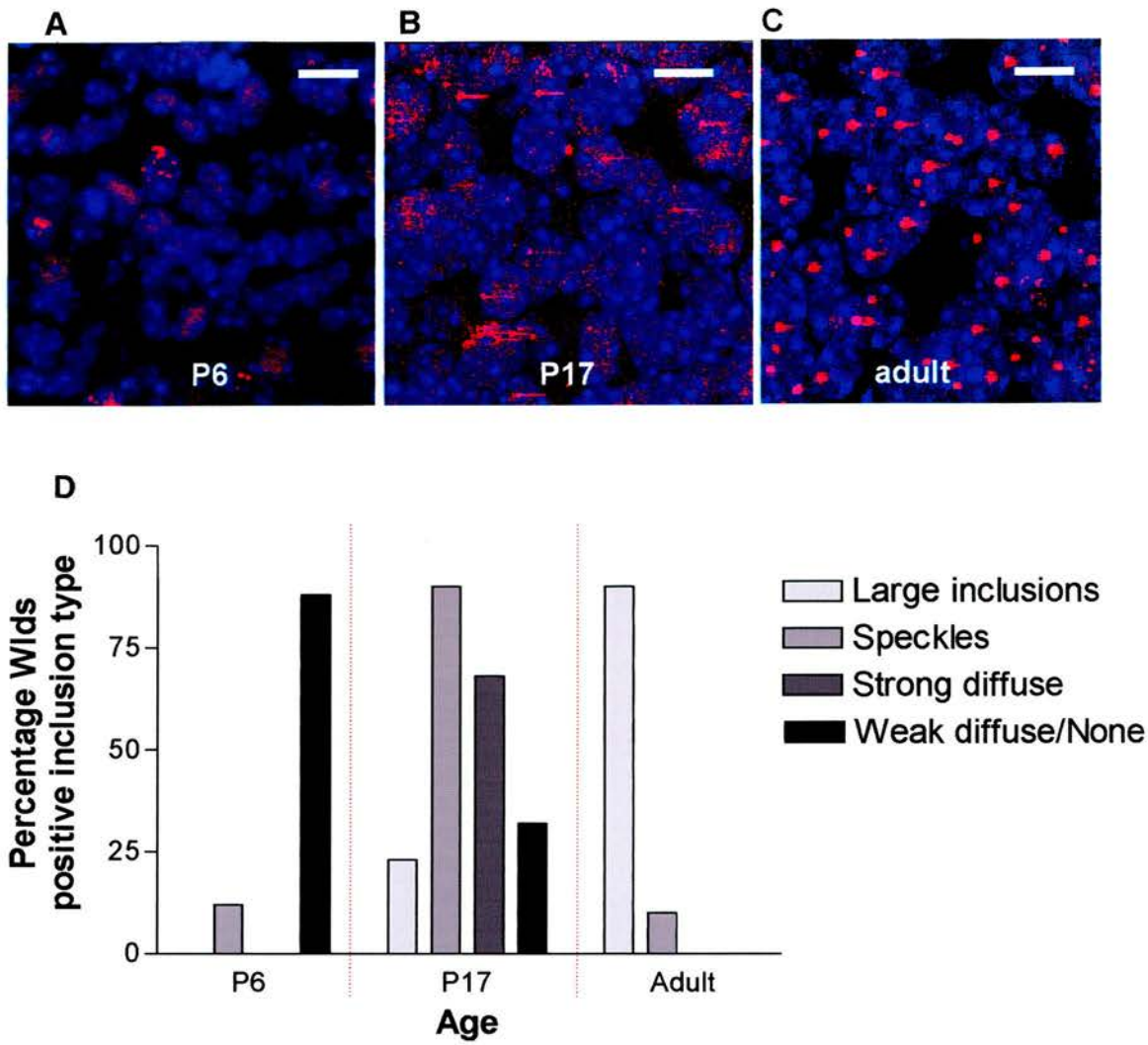

Figure 4.6. Wld^s distribution in *vivo* alters during the first few weeks of postnatal life.

Confocal micrographs of *Wld^s* cerebellar granule cells immunocyochemically labelling Wld^s protein in red and the nuclear marker TOPRO-3 in blue. Very few nuclear inclusions are present in the cerebellar granule cells at P6 (A) while about 90% of granule cells have large nuclear inclusions by 2 months (C). Panel B shows an intermediate stage of inclusion formation. (D). Graphical representation of nuclear inclusion type in cerebellar granule cells during development shown in panels A-C. Scale bar = 10μm (A-C)

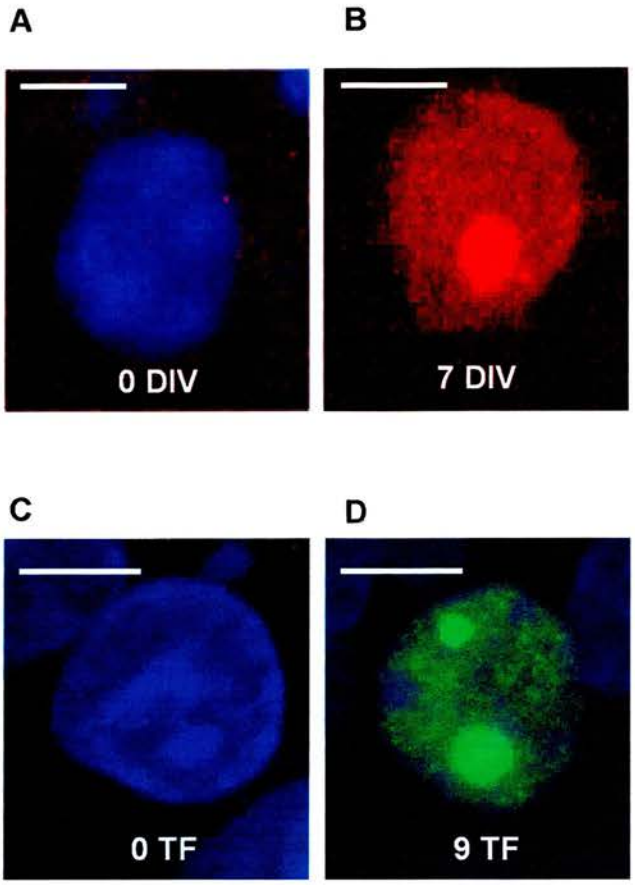

Figure 4.7. Wld^s protein inclusions develop in *vitro* at an accelerated rate.
Confocal micrographs show dissociated cerebellar granule cells cultured from P6 *Wld^s* mice have no obvious Wld^s protein expression when initially plated (A). Nuclear Wld^s protein inclusions develop in culture reaching an apparent maximum size after 7 days in culture (B). Inclusions also develop in dissociated cerebellar granule cell cultures from P7 Rats, 9 days after transfection with a Wld^s-eGFP construct (C & D). Scale bars = 5µm (A-D).

A

B

Nucleus	Inclusion	
93.80	11.51	Diameter in Pixels
9.38	1.151	Approx. diameter μm
476.24	1.12	Approx. volume μm^3
	0.23	% nuclear volume

Figure 4.8. Wld^s protein inclusions in adult cerebellar granule cells make up less than 0.5% of their nuclear volume.
Panel A shows an example of an adult cerebellar granule cell nucleus and its Wld^s protein inclusion taken from a confocal micrograph. Images like this were analysed using Scion image. Panel B details volume calculations for 10 example cerebellar granule cell nuclei and their Wld^s protein inclusions, as calculated with Scion image.

	tubes	inclusions	speckles	diffuse	weak/none
					
Caudate	0	55	0	0	45
Cerebellum: granule cells	0	90	10	0	0
Cerebellum: Purkinje cells	0	0	0	0	100
Cerebellum: molecular layer	0	82	0	0	18
Cortex: primary motor, layer2/3	0	20	5	75	25
Cortex: primary motor, layer4	0	5	40	50	50
Cortex: primary motor, layer 5	0	10	50	60	40
Cortex: somatosensory, layer2/3	0	0	24	50	50
Cortex: somatosensory, layer4	0	3	82	85	14
Cortex: somatosensory, layer5	0	2	29	63	37
Dentate	0	0	<10	0	100
DRG	5	1	12	16	70
Hippocampus: CA1	0	0	10	0	100
Hippocampus: CA3	0	0	84	0	100
Medial Habenulla	0	0	79	94	6
Retina: ganglion cells	0	11	13	86	12
SCG	0	1	11	2	88
Thalamus	0	0	21	0	100
P6 caudate	0	0	0	25	75
P6 cerebellum: midlayer	0	0	3	0	97
P6 cortex: primary motor, layer 5	0	0	14	0	86
P6 cortex: somatosensory, layer 5	0	0	1	0	99

Table 4.1. Quantification of Wld^S protein distribution profile in the *Wld^S* mouse nervous system.

The percentage of cells in each region displaying a particular nuclear Wld^S protein distribution pattern was assessed from low power confocal pictures. Percentages are calculated as a percentage of TOPRO-3 labelled nuclei. The distribution pattern was divided into large inclusions, multiple small inclusions (speckles), strong diffuse and weak diffuse/no obvious staining. A cell could therefore fall into more than one category (e.g. a cell with a large inclusion which also showed strong diffuse staining) and would be counted twice.

	% tubes	% large inclusions	% speckles	% strong diffuse	% weak diffuse/none
					
Anterior commissue	0	0	5	0	95
Corpus callosum	0	0	0	0	100
Cortex: cingulate	0	8	62	38	30
Cortex: secondary motor, layer2/3	0	20	0	36	64
Cortex: secondary motor, layer4	0	17	4	38	62
Cortex: secondary motor, layer 5	0	0	11	35	65
Geniculate nucleus	0	0	9	0	91
Retina: bipolar cells	0	0	9	7	93
Retina: innerplex	0	0	0	0	100
Retina: rods	0	0	27	73	28
PVP	0	0	70	97	3
P6 cerebellum: inner layer	0	0	12	0	88
P6 cerebellum: outer layer	0	0	0	0	100
P6 corpus callosum	0	0	0	0	100
P6 cortex: cingulate	0	0	23	0	77
P6 cortex: primary motor, layer 2/3	0	0	0	0	100
P6 cortex: primary motor, layer 4	0	0	6	0	94
P6 cortex: secondary motor, layer 2/	0	0	19	0	81
P6 cortex: secondary motor, layer 4	0	0	80	0	20
P6 cortex: secondary motor, layer 5	0	0	85	0	15
P6 cortex: somatosensory, layer 2/3	0	0	0	0	100
P6 cortex: somatosensory, layer 4	0	0	0	0	100

Table 4.2. Quantification of Wld^S protein distribution profile in the *Wld^S* mouse nervous system.

This table details other areas that were not included in table 4.1. The percentage of cells in each region displaying a particular nuclear Wld^S protein distribution pattern was assessed from low power confocal pictures. Percentages were calculated as a percentage of TOPRO-3 labelled nuclei. The distribution pattern was divided into large inclusions, multiple small inclusions (speckles), strong diffuse and weak diffuse/no obvious staining. A cell could therefore fall into more than one category (e.g. a cell with a large inclusion which also showed strong diffuse staining) and would be counted twice.

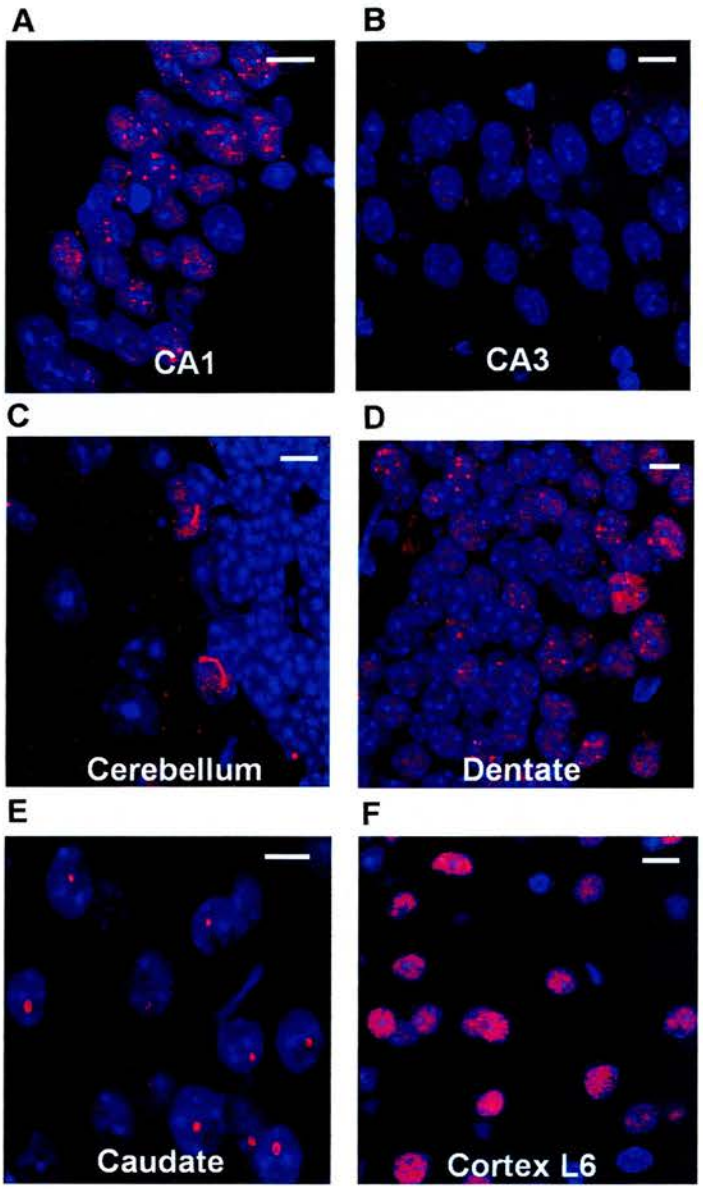

Figure 4.9. The transgenic line 4836 mouse has a different expression pattern of Wld^S protein to that of the spontanious *Wld^S* mouse.

Expression of Wld^S protein (red) in various regions of brain slices from transgenic mouse expressing the *Wld^S* gene. Slices were counterstained with topro-3 (blue) to highlight the nuclei. The distribution patterns differed from that seen in the *Wld^S* mouse but also varied between cell types. Speckled inclusions can be seen in CA1 (A) neurones but there is no obvious expression in CA3 (B), whereas in the caudate there are single nuclear inclusions (E) and in the cerebellum there are tubes of Wld^S protein in a subset of neurones similar in shape to that seen in the *Wld^S* mouse DRG. Scale bar = 10μm.

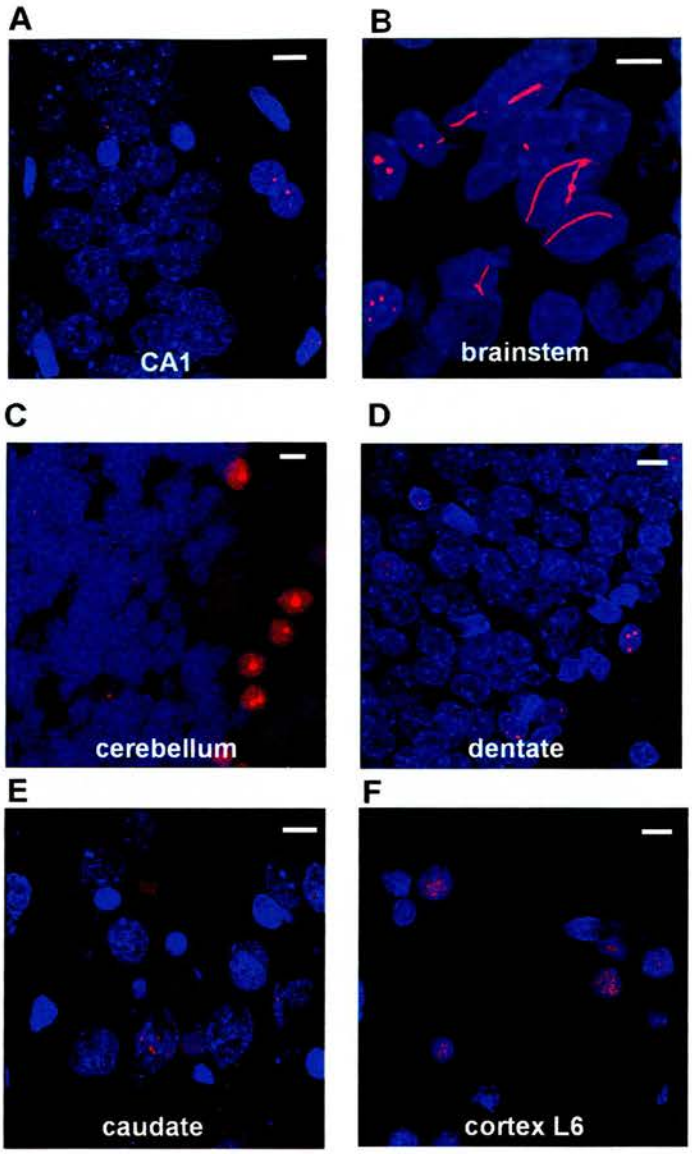

Figure 4.10. The transgenic line 23 rat has a different expression pattern of Wld^s protein to that of the transgenic line 4836 mouse and spontanious *Wld*^{s} mouse.

Expression of Wld^s protein (red) in various regions of brain slices from transgenic mouse expressing the *Wld*^{s} gene. Slices were counterstained with topro-3 (blue) to highlight the nuclei. Wld^s protein expression differed from that seen in either the transgenic mouse or *Wld*^{s} mouse. There is little staining in the CA1(A) and dentate (D) but very large inclusions in the basket cells of the cerebellum (C) and tubes of Wld^s protein in the dorsal brainstem (B) similar in shape to those seen in the *Wld*^{s} mouse DRG and transgenic line 4836 mouse cerebellum. Scale bar = 10μm.

	% tubes	% large inclusions	% speckles	% strong diffuse	% weak diffuse/none
					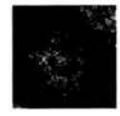
Transgenic Mouse					
Caudate	0	55	0	0	55
Cerebellum: granule cells	0	2	0	0	98
Cerebellum: Purkinje cells	0	0	0	0	100
Cerebellum: molecular layer	6	2	0	0	94
Cortex: layer 4	0	8	8	73	27
Cortex: layer 6	0	8	0	72	28
Dentate	0	7	15	0	85
Hippocampus: CA1	0	1	65	20	35
Hippocampus: CA3	0	0	3	0	97
DRG	0	0	4	0	96
motorneurone	0	0	0	100	0
Transgenic rat					
Caudate	0	3	15	0	85
Cerebellum: granule cells	0	2	0	0	98
Cerebellum: Purkinje cells	0	0	0	0	100
Cerebellum: molecular layer	0	17	0	17	83
Cortex: layer 4	0	0	2	15	85
Cortex: layer 6	0	5	0	27	73
Dentate	0	4	6	0	94
Dorsal Brainstem	4	18	10	12	82
DRG	0	0	18	19	81
Hippocampus: CA1	0	6	50	0	50
Hippocampus: CA3	0	7	4	4	93
motorneurone	0	0	0	100	0

Table 4.3. Distribution profile of Wld^S protein in the transgenic mouse line 4836 and rat line 23.

The percentage of cells in each region displaying a particular Wld^S protein nuclear distribution pattern was assessed from low power confocal pictures. The distribution pattern was divided into large inclusions, multiple small inclusions (speckles), strong diffuse and weak diffuse/no obvious staining. A cell could fall into more than one category (e.g. a large inclusion with strong diffuse staining as well) and would therefore be counted twice.

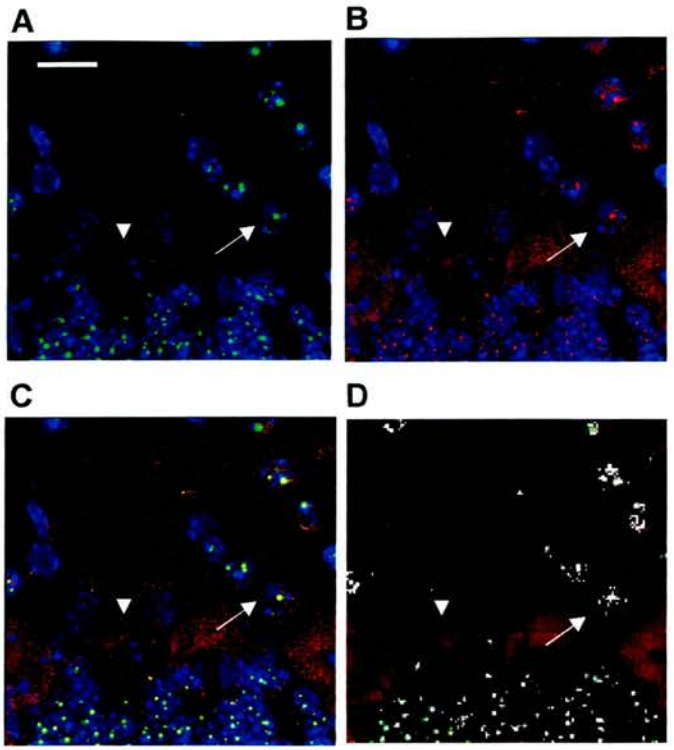

Figure 4.11. Co-localisation of Wld^s protein and VCP. Confocal micrographs show immunolabelling of Wld^s protein (green) and VCP (red) in cerebellar slices from *Wld^s* mouse. Slices were counterstained with topro-3 (blue) to highlight the nuclei (merged C). A-D show cerebellum with evidence of Wld^s protein in granule cell and molecular layers (arrow) (A), and VCP inclusions in the same regions, with diffuse VCP staining in purkinjie cells (arrow head) (B). There are some examples of cells with VCP but no Wld^s protein (C). Image J allows areas of co-localisation to be marked on an overlay image using white pixels (D). Scale bar = 20μm.

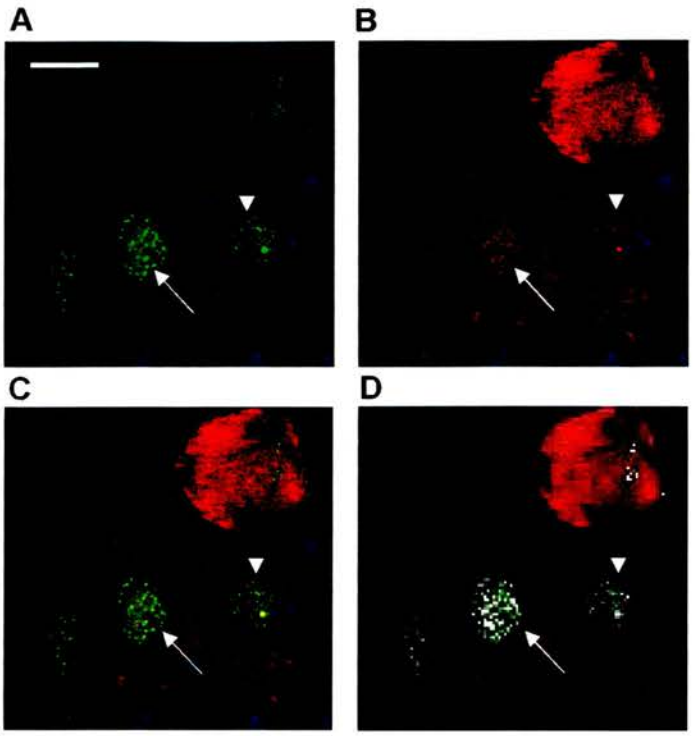

Figure 4.12. Co-localisation of Wld^s protein and VCP (2). Confocal micrographs show immunolabelling of Wld^s protein (green) and VCP (red) in DRG slices from *Wld^s* mouse. Slices were counterstained with topro-3 (blue) to highlight the nuclei (merged C). A-D. Show DRG cells with evidence of Wld^s inclusions both with, and without corresponding VCP aggregates (arrow head), and other cells with complete co-localisation (arrow). Image J allows areas of co-localisation to be marked on an overlay image using white pixels (D). Scale bar = 10μm.

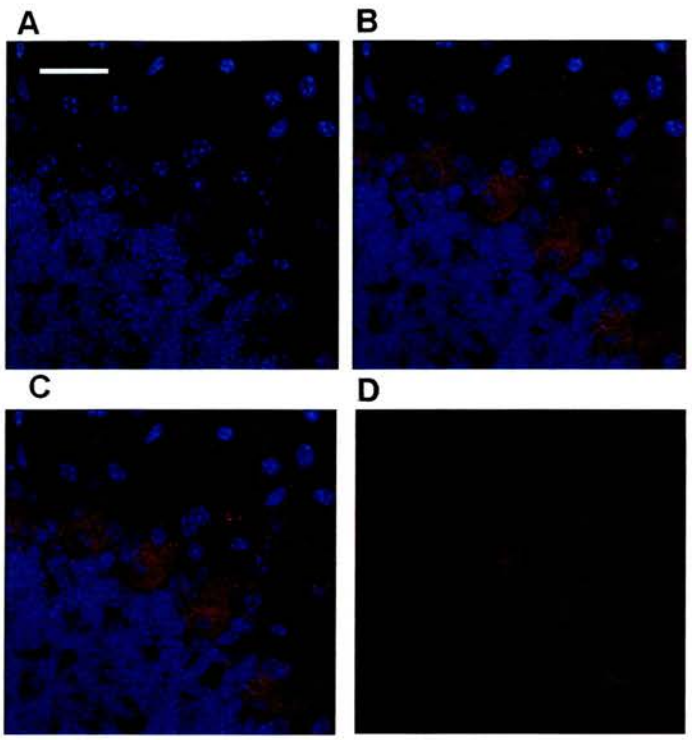

Figure 4.13. Co-localisation of Wld^s protein and VCP (3). Confocal micrographs show immunolabelling of Wld^s protein (green A) and VCP (red B) in cerebellar slices from wild-type mouse. Slices were counterstained with topro-3 (blue) to highlight the nuclei (merged C). A-C. Show immunostaining in a non-*Wld^s* control cerebellum. There is no visible Wld^s protein (A) with visible diffuse VCP in the purkinjie cells (B) and no VCP puncta elsewhere in the section. Image J allows areas of co-localisation to be marked on an overlay image using white pixels (D). Scale bar = 30µm.

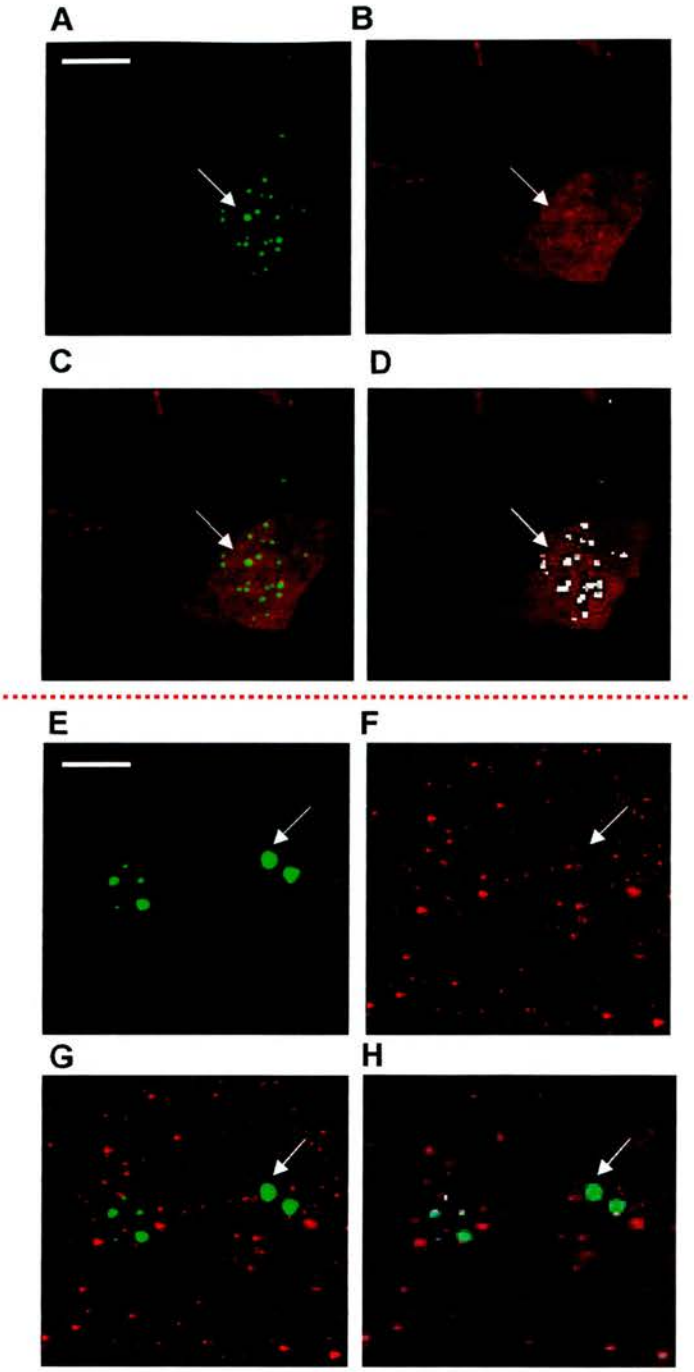

Figure 4.14. Co-localisation of Wld^s protein and SMRT.
Cortical cells in dissociated culture co-transfected with Wld^s-eGFP and SMRT (Myc or Flag tagged). **A-D.** Green Wld^s (A) and Red SMRT (B) shows some evidence of co-localisation (C) at low power magnification. **E-H.** High power confocal micrographs of some cells show very little/no co-localisation of SMRT and Wld^s. Image J allows areas of co-localisation to be marked on an overlay image using white pixels (D, H). Scale bar = 10μm (A-D), 5μm (E-H).

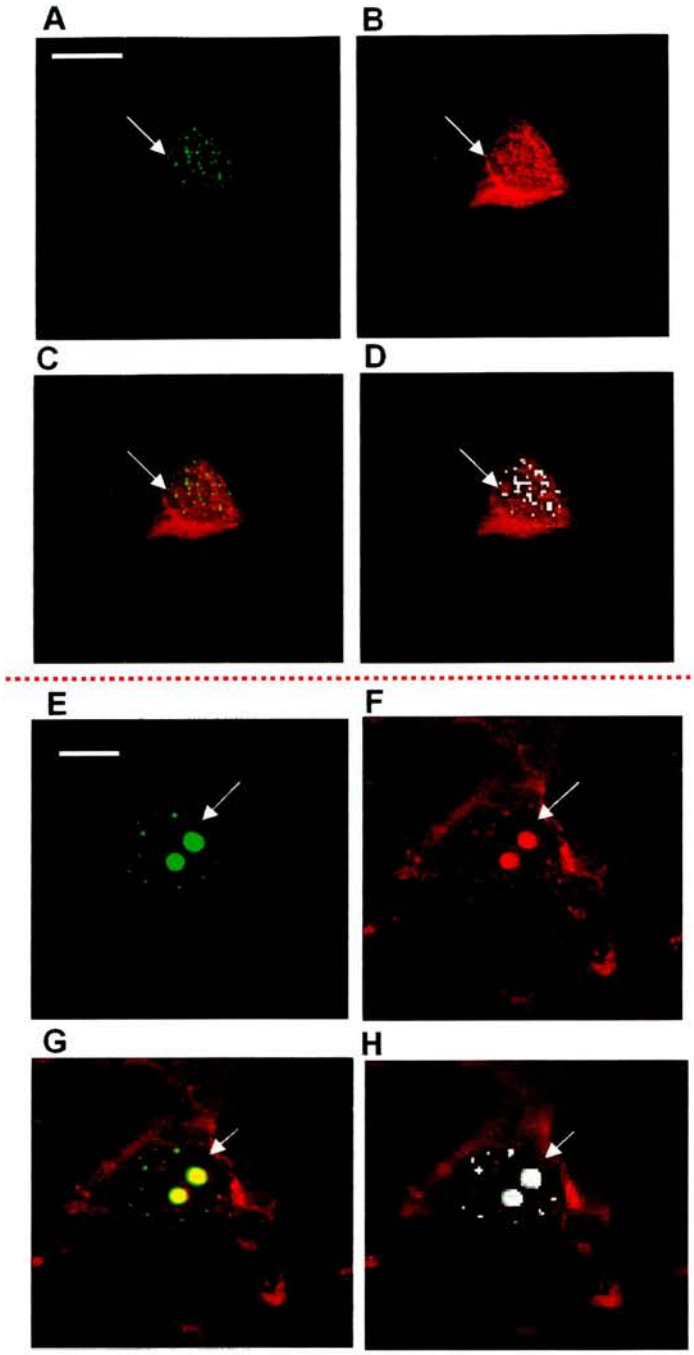

Figure 4.15. Co-localisation of Wld^s protein and HDAC.
Cortical cells in dissociated culture co-transfected with Wld^s-eGFP and HADC (Myc or Flag tagged). **A-D.** Green Wld^s and red HDAC show some evidence of co-localisation at low power. **E-H.** Wld^s and HDAC show co-localisation at high power. Image J allows areas of co-localisation to be marked on an overlay image using white pixels (D, H). Scale bar = 15μm (A-D), 5μm (E-H).

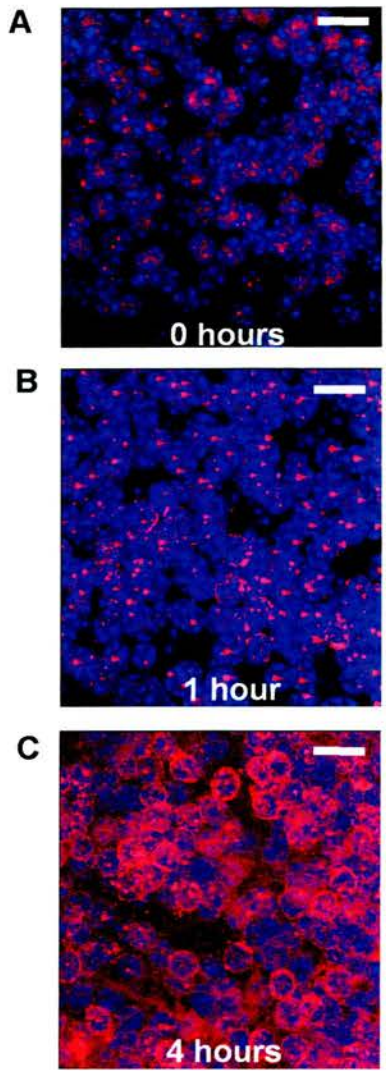

Figure 4.16. Movement of Wld^s protein following slicing and incubation in oxygenated ACSF.
Tissue was vibratome cut and incubated in oxygenated ACSF for various time intervals before fixation and immunohistochemistry for Wld (red) and TOPRO-3 (blue). Propridium iodide staining showed that all cells imaged were still viable (not shown). A. Cerebellar granule cells following section, 0 hours incubation. B. Cerebellar granule cells following section and 1 hour incubation in ACSF. C. Cerebellar granule cells following section and 4 hours incubation in ACSF. Scale bar = 12μm.

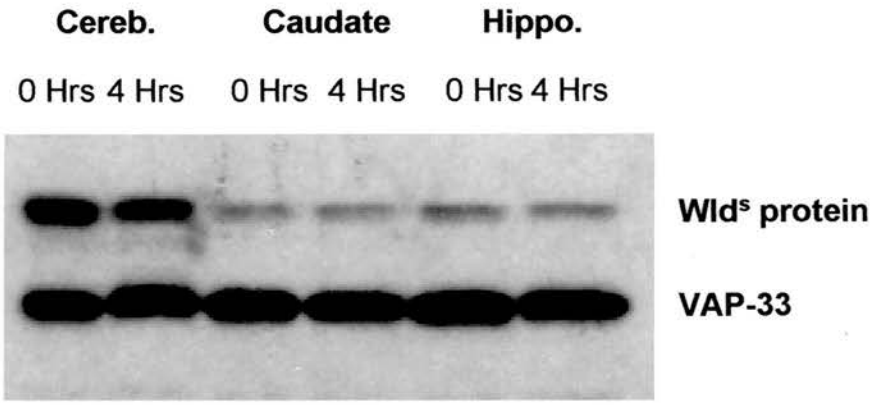

Figure 4.17. Western blot analysis demonstrates that Wld^s protein levels are not changed after incubation in ACSF. Levels are detectable and similar in hippocampus (hippo.), cerebellum (cereb.) and caudate at the two time points. There is a clearly more protein in the cerebellum compared to the other regions as shown previously in Figure 4.3. Similar levels of protein were loaded in each lane, as demonstrated by the uniform VAP-33 staining in all lanes.

Appendix 4.1

Appendix 4.1. Wld^S protein appears to move in response to stress

I have already shown that there is Wld^S protein present in areas such as the hippocampus where there are no visible aggregates (Table 4.1, Figure 4.3). There are examples of other nuclear proteins (BARD1 and BRCA1) that are known to form nuclear aggregates, and are present and obvious on Western blots, but are not visible as protein aggregates with immunocytochemistry until a set point in the cell cycle is reached (Jin *et al.* 1997). Jin *et al.* suggest that BARD1 polypeptides are distributed diffusely within nuclei of cells at concentrations too low for antibody detection, but that at certain cell cycle points are accumulated into inclusions and therefore raising their local concentration at that position in the nucleus allowing detection. This accumulation of protein into aggregates may be what is happening in response to stress in the CA1, where there are more cells showing nuclear Wld^S inclusions following slicing and 4 hours incubation in ACSF. "Nuclear dots" belong to a heterogeneous group of nuclear bodies and do not co-localise with any other known nuclear structures (Sternsdorf *et al.* 1999). Their localisation can change in response to stress as a result of hyper-SUMOylation (i.e. modification by SUMO-1). This could be viewed as an indicator as one of the initial events of apoptotic induction in leukemic cells (Sternsdorf *et al.* 1999).

An analysis of the fluorescence levels in the slices at set time points allowed the generation of a graphical representation of protein "levels" (Appendix figure 4.1.1). An analysis of the areas under the curves given at each time point in the experiment show that the overall levels of fluorescence have not changed, suggesting that this is a redistribution of existing protein and not simply new protein synthesis. Incubation of slices in puromycin, an inhibitor of new protein synthesis, also failed to stop this redistribution of Wld^S protein (Appendix figure 4.1.2).

Apoptosis has been interpreted as a failure to correctly re-enter the cell cycle. Will an inhibitor of a component of the cell cycle regulatory mechanism (the CDKs) alter the redistribution of Wld^S protein observed following slicing and incubation in ACSF?

Incubation with the CDK inhibitor roscovitine shows that it does not affect the redistribution of the Wld^S protein (Appendix figure 4.1.2).

It is also know that HDACs can shuttle and in response to staurospaurine (as a trigger for cell stress) move from the nucleus into the cytoplasm. The redistribution seen in cerebellar granule cells following vibratome sectioning may be attributed to a stress response, and the formation of the "halo" like shapes (Figure 4.16) could be an accumulation of the protein at the edge of the nucleus. If the movement of the Wld^S protein is linked to the possible movement of HDACs, the Wld^S protein may be unable to leave the nucleus due the constitutive nuclear localisation signal contained within the protein (Figure 4.1).

Could the change in Wld^S protein localisation simply be a reversion to a localisation seen during development? Appendix figure 4.1.3 illustrates the change in localisation of Wld^S protein in the cerebellum and cortex following incubation in ACSF for 4 hours, and what the localisation is like in those areas at P6. Could this suggest that the protein is moving in response to changes in connectivity following sectioning?

A.

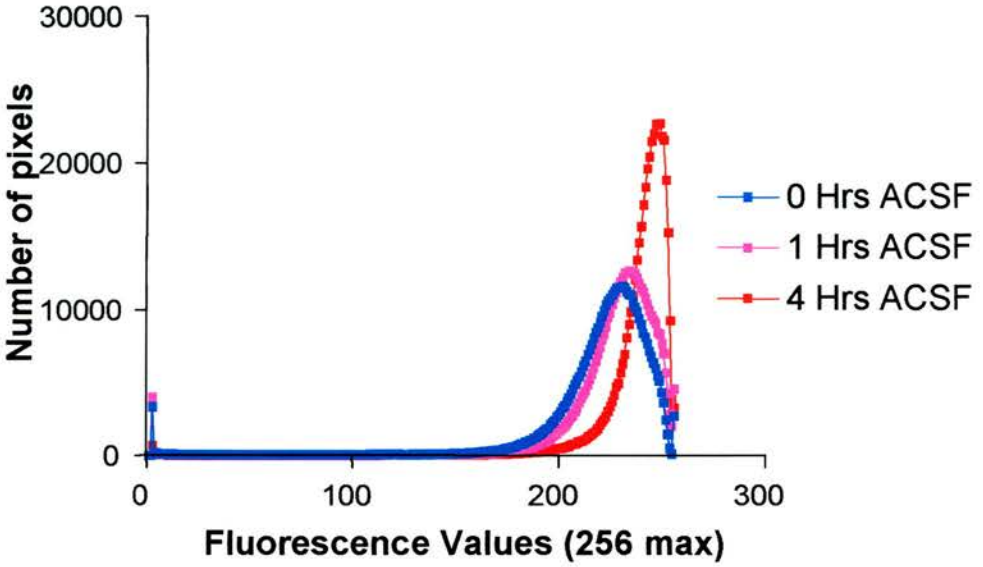

B.

ACSF Time course	0 Hours	1 Hour	4 Hours
Baseline	0	0	0
Total peak area	458328	457418	458052
Number of peaks	1	1	1

Appendix 4.1.1. Redistribution of Wld^s protein in cerebellum following slicing and incubation in oxygenated ACSF.
A. Graphical representation of protein movement. Pixel intensity for Wld^s protein immunostaining was measured and plotted for each time point, with 256 as the maximum fluorescence intensity. B: Area under each curve was measured and all the curves match at each time point suggesting that this phenomenon is the result of redistribution of existing protein rather than new protein synthesis.

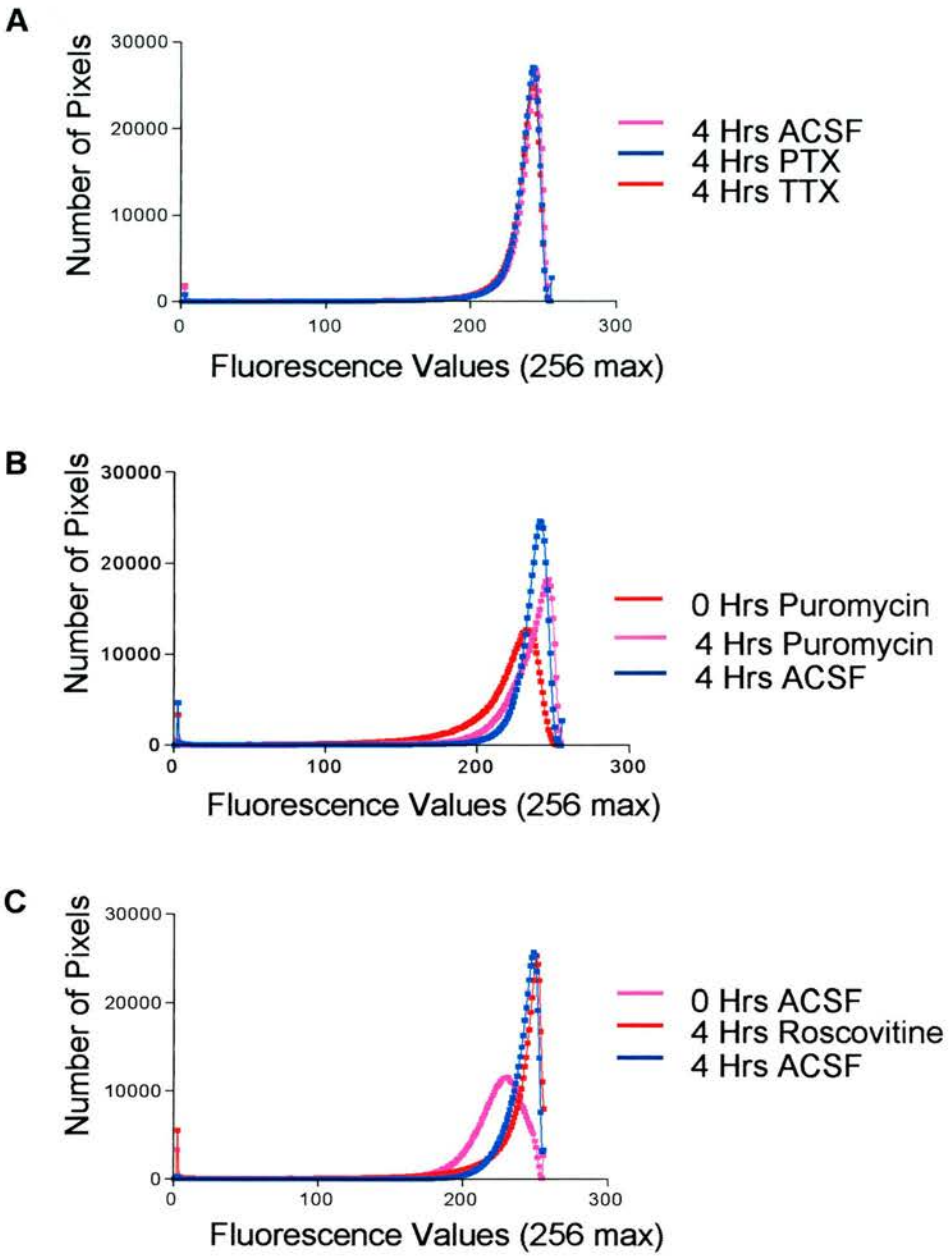

Appendix 4.1.2 Redistribution of Wld^s protein in cerebellum following slicing and incubation in oxygenated ACSF.
Graphical representations of protein movement. Pixel intensity for Wld^s protein immunostaining was measured and plotted for each time point, with 256 as the maximum fluorescence intensity. A. Incubation in TTX (500nM **)** and PTX (50μM**)**. B. Incubation in Puramycin (500μM**)**. C. Incubation in Roscovitine (10μM) .

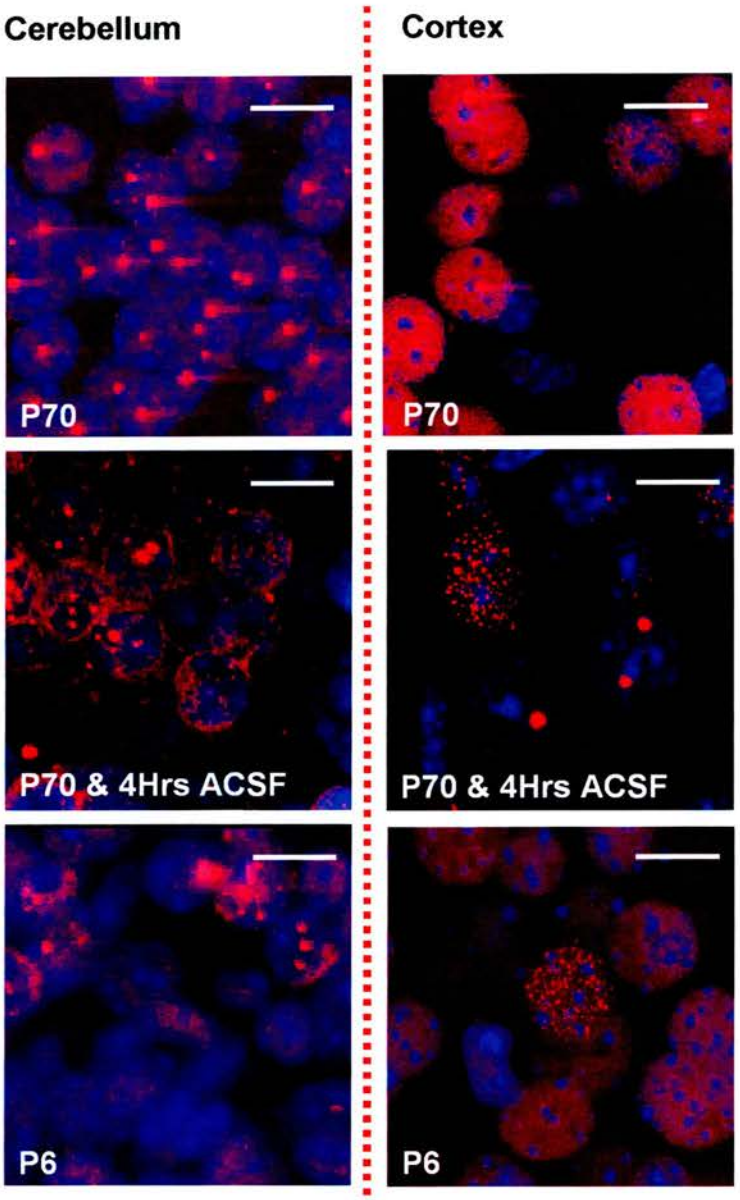

Appendix 4.1.3. The Wld^s protein redistributing is reminiscent of a previous developmental localisation.
Confocal micrographs showing Wld^s protein (red) and the nuclear marker TOPRO-3 (blue). Protein is redistributed to give patterns similar to that seen at P6 in the cerebellar granule cells and cortex. Scale bar = 10μm

Appendix 4.2

Appendix 4.2. Nuclear Wld^S protein is required for axonal protection in the hippocampus

The work detailed in this appendix was all carried out by Dr Jane Haley and is identified here in order that I may refer to the experiment in discussion.

Hippocampal slices were cut and stored in O_2/CO_2 bubbled artificial cerebrospinal fluid (ACSF) containing elevated Mg^{2+}. Slices were recorded on the day of slicing (acute), 24 and 48 hours later. Extracellular field recordings were made in stratum radiatum of CA1 (stimulating the CA3 Schaffer-collateral pathway) and from stratum radiatum of CA3 (stimulating the mossy fibre pathway). At the time of slicing, half the slices had the Schaffer-collateral pathway axotomised and half had the mossy fibre pathway axotomised.

The fibre volley on Wild type mice was not present 48 hours after slicing/axotomy of Schaffer-collateral pathway. In *Wld*^{S} mice stimulation of this pathway revealed a clear fibre volley still present after 48 hours (appendix figure 4.2.1.). In contrast, the mossy fibre pathway did not show protection and the fibre volley was not present after 48 hours in *Wld*^{S} mice.

The axons that constitute the mossy fibre pathway originate in the dentate gyrus, which does not exhibit nuclear Wld^S protein aggregates (Figure 4.4). By contrast, the Schaffer-collateral pathway originates from CA3 neurones, which do show nuclear Wld^S protein aggregates. This region specific protection suggests that the formation of nuclear Wld^S protein aggregates may be important for the *Wld*^{S} neuroprotective phenotype, adding value to mapping data presented in this thesis. It may also have wider implications for others who are testing the ability of *Wld*^{S} to protect against neurodegenerative disorders through cross breeding. The ability to protect may be linked to whether the affected cells show nuclear Wld^S aggregates in the spontaneous mutant.

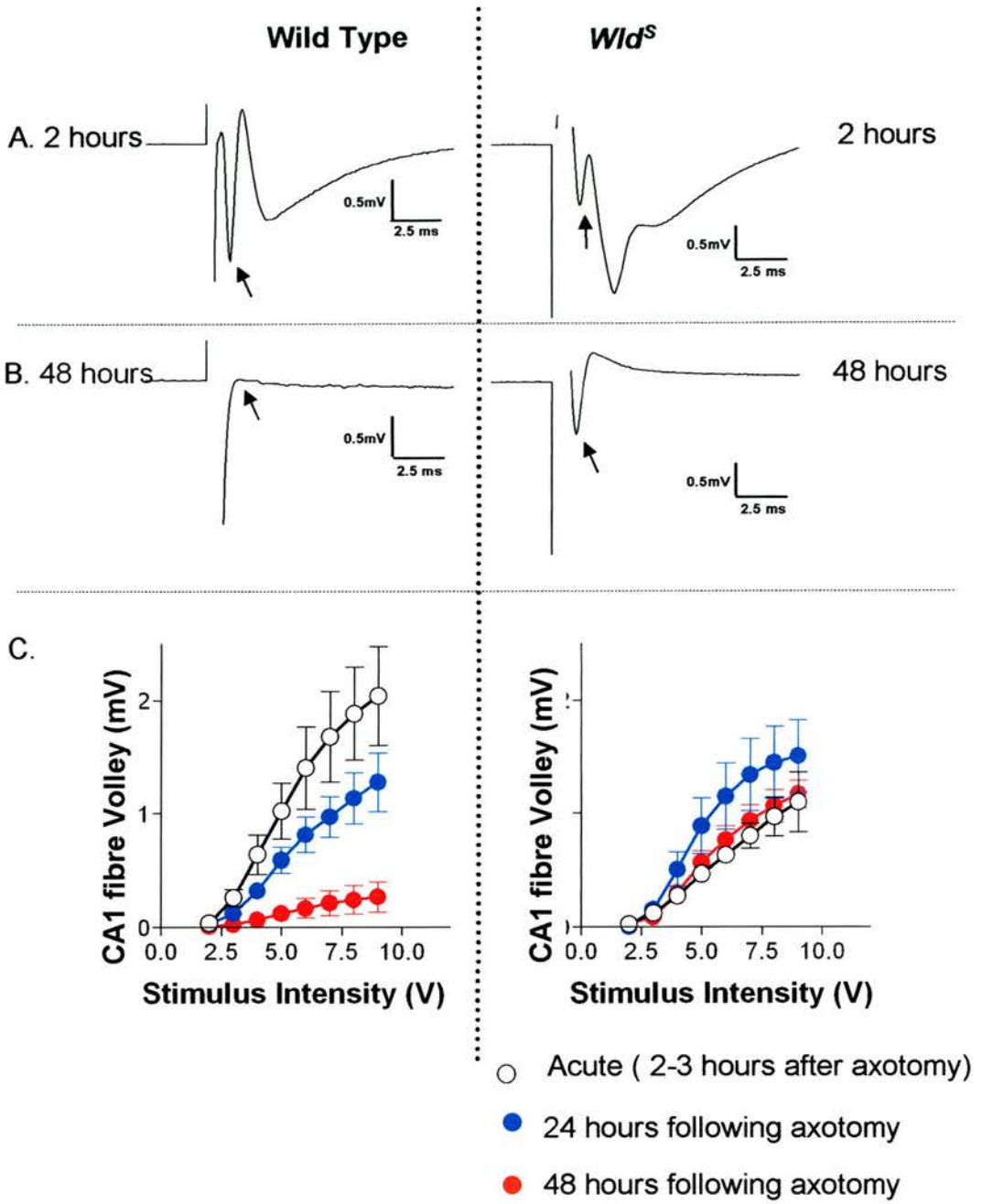

Appendix 4.2.1. Nuclear Wld^S protein is required for axonal protection in the hippocampus.

Extracellular field recordings were made in stratum radiatum of CA1 (stimulating the CA3 Schaffer-collateral (SC) pathway) and from stratum radiatum of CA3 (stimulating the mossy fibre (MF) pathway). The fibre volly (arrows in A & B) in Wild-type mice was not present 48hrs post slicing of the SC (C). *Wld^S* mice revealed a clear fibre volly at this time point (C). In contrast, the MF pathway did not show protection and the fibre volly was absent in *Wld^S* at 48hrs.

Chapter 5:
Transcriptional regulation by the *Wld*^{S} gene

5.1.0. Introduction

Transgenic expression of the chimeric *Ube4b/Nmnat1* gene alone has previously been shown to be sufficient to confer the neuroprotective phenotype (Mack et al., 2001). As detailed in the previous chapter, the Wld^S protein product localises to neuronal nuclei. How can the protein product of a gene, known to affect axon and synapse survival following injury, act when the cell body is severed from those compartments by a cut or a crush? I have already shown that the Wld^S protein can co-localise in nuclei with VCP and HDAC5. These factors could affect other processes in the cell, for example through ubiquitination and acetylation pathways. The hypothesis addressed in this chapter is therefore that the *Wld^S* chimeric gene exerts its neuroprotective effect indirectly, through a cascade of downstream events. More specifically, I address the hypothesis that the Wld^S protein regulates expression of other genes, one or more of which may be more directly responsible for the *Wld^S* phenotype. A priori analysis of this hypothesis leads me to focus attention on the *Ube4b* and *Nmnat1* components of the *Wld^S* chimeric gene.

5.1.1. *Ube4b*

The incorporation of an E4 ubiquitination factor in the *Wld^S* gene has previously led to speculation that protein tagging and degradation via the ubiquitin-proteasome system may be altered in these mutant mice (Coleman & Ribchester, 2004). The yeast homologue of *Ube4b*, (*Ufd2*) gives clues to the function of *Ube4b* in mammals. An alignment of Yeast *Ufd2* and mammalian *Ube4b* show that the N-terminal portion of *Ube4b* is absent from *Ufd2* (NCBI blast alignment). This suggests that the ability of *Ube4b* to multi-ubiquitinate target protein is a function of the C-terminal region of the gene as *Ufd2* homologues display the same functionality as *Ube4b*. If the *Ube4b* portion of the gene is responsible for the *Wld^S* phenotype then it is probably not through multi-ubiquitination as only the N-terminal 70 amino acids of *Ube4b* (*N70-Ube4b*) are included in the *Wld^S* chimeric gene. What are the remaining possibilities for its action? One could be a dominant negative effect on other functions of *Ube4b*. For example,

Ube4b incorporated in the Wld^s mutant protein could bind native Ube4b and therefore interfere with VCP interactions. This hypothesis is supported by data from studies showing that the ubiquitin-proteasome system can regulate synaptic and axonal degeneration in a variety of systems (Zhai *et al.*, 2003; Korhonen & Lindholm, 2004).

Zhai *et al.* (2003) showed that axon degeneration can be prevented through the use of protease inhibitors, but is protected only by pre-treatment with these inhibitors. The proteasome inhibitors were unable to prevent the earliest signs of Wallerian degeneration. Proteasome inhibitors did not retard microtubule fragmentation which is one of the earliest signs of axon degeneration and is UPS dependent. Proteasome inhibitors can block the degradation of neurofilaments, but Zhai *et al* considered this to be a secondary effect to the UPS activating a subset of E3s, causing degradation of a subset of proteins which themselves trigger a secondary phase of degeneration. This suggests the involvement of the ubiquitin proteasome system only at the early stages of Wallerian degeneration. Zhai *et al.* also suggested that the UPS inhibitors were unable to counteract Wallerian degeneration instigated by microtubule destabilising agents such as vincristine. However, it has also been shown that *Wld^s* mice neurones are resistant to vincristine neuro-toxicity (Wang *et al.* 2001). Therefore, *Wld^s* must act via some mechanism other than that employed by general protease inhibitors which cannot prevent microtubule degradation. *Gad* mice show spheroid body formation and dying back axon degeneration through a mutation in the *Uch-l1* gene. This mutation highlights the importance of the UPS in axon integrity and maintenance. The Gad neurodegenerative phenotype can be partially rescued by crossing with *Wld^s* (Mi *et al.* 2005) suggesting that it can protect against UPS disorders. This suggests that if *Wld^s* does act by UPS dominant negative inhibition of *Ube4b* that it is not the whole story.

Another possibility is that the *Ube4b* portion of the chimera could affect the UPS through its interactions with VCP or other nuclear proteins such as HDAC (see chapter 4). One possible chain of events could be that N70-Ube4b interacts directly with VCP

and that this then interacts with HDAC to alter acetylation and therefore other processes within the cells (Wu *et al.*2001).

5.1.2. Nmnat1

Many studies in yeast have been carried out in order to identify cellular factors which could be required for transcriptional silencing, and among proteins identified are those encoded by yeast SIR genes. These genes are responsible for silencing at repeated DNA sequences in yeast mating type loci, telomeres and rDNA. SIR2 is required for silencing in the rDNA, causing closed regions of chromatin structure making it inaccessible (Blander and Guarente, 2004). This silencing requires lysine residues in the N-terminal tail of histones H3 and H4, which are acetylated in active chromatin and deacetylated in inactive/silenced chromatin. SIR2 is the yeast homologue of a mammalian protein, Sirt1. Sirt1 is a forkhead transcriptional regulator which can also regulate the activity of p53 through deacetylation at Lys182 (Blander and Guarente, 2004). The Sir2 family of conserved proteins require NAD to upregulate deacetylase activity and as such, can regulate a variety of processes including aging, metabolism and stress response. *Nmnat1* codes for the enzyme responsible for the production of NAD. NAD and its derivatives have previously been implicated in transcriptional regulation through various pathways (Revollo *et al.* 2004).

A recent study by Milbrandt and colleagues suggested that the *Wld*^{S} phenotype is caused, at least in part, by increased nuclear NAD biosynthesis, mediated by the *Nmnat-1* component of the *Wld*^{S} gene (Araki *et al.*, 2004). These authors also reported that increased nuclear NAD acts through the nuclear transcriptional regulator Sirt1, suggesting that modification of gene expression patterns is required to produce NAD-dependent neuroprotection.

In this chapter I set out to test whether the *Wld*^{S} gene regulates mRNA levels of other genes. I show that 11 non-associated genes are altered in the mouse cerebellum in *vivo*. I also reproduced and quantified this response in a human (HEK293) cell line following

transfection with an eGFP-tagged *Wld*^{S} construct. In addition, I show that some of the transcriptional changes induced by *Wld*^{S} expression are regulated via NAD-/Sirt1-dependent pathways, whereas others are NAD-/Sirt1-independent. Following the observation that some genes are NAD dependent and others are independent. I demonstrate that the different components of the *Wld*^{S} mutation independently regulate two of the genes with the largest expression changes in the *Wld*^{S} mouse.

Results

5.2.0. Results

5.2.1. Microarray analysis of RNA from *Wld*^{S} mouse cerebellum

In order to identify potential candidate genes whose expression may be regulated by *Wld*^{S}, preliminary microarray experiments were performed comparing RNA levels in *Wld*^{S} and wild-type (C57Bl6) mouse cerebellum. The intial experiments were instigated by Dr T.H.Gillingwater and the microarray analysis carried out by Kevin Robertson at the Scottish Centre for Genomic Technology and Informatics (University of Edinburgh).

The cerebellum was chosen as an ideal preparation for several reasons. First, it is composed predominately of large numbers of cerebellar granule cells (10^{10}-10^{11}), resulting in an almost homogenous cell population (Llinás, 1975). Cellular heterogeneity as is present in most other anatomically distinct brain regions such as the hippocampus, hampers gene expression profiling due to large region-specific divergence in expression patterns (Datson et al., 2004). Second, as I showed in chapter 4, the vast majority (>90%) of cerebellar granule cells strongly express Wld^S protein (Figure 5.1; Wishart et al., submitted). Third, the *Wld*^{S} neuroprotective phenotype can be shown through neurite survival assays in cerebellar granule cell dissociated culture following a death stimulus (Figure 5.2). Four days following withdrawal of serum and potassium from the culture medium, wild-type cultures are reduced to 13.73±3.70% of neurites remaining (see figure 5.2), while the *Wld*^{S} cultures still have 74.77±2.38% of neurites remaining. Finally, the cerebellum is a discrete anatomical unit, suitable for precise and rapid removal before subsequent RNA extraction. Thus, the cerebellum is perhaps the most unique, identifiable structure in the brain, but fortuitously also shows exceptionally strong expression of Wld^S protein in *Wld*^{S} mice.

Patterns of RNA expression were compared in cerebella from 3 independent microarray experiments, each pairing a *Wld*^{S} and wild-type mouse. The arrays highlighted 11 out of ~23,000 genes whose expression patterns were consistently altered across all 3 runs by,

on average, more than a factor of 2 (Table 5.1). As expected, Rpb7 (contained within the triplicated *Wld*^{S} region, but previously discounted as contributing to phenotype; Mack et al., 2001) was also up-regulated (Figure 5.3). A small number of candidate genes were identified, including both up-regulated and down-regulated examples (Table 5.1). These findings suggest that the *Wld*^{S} gene may be directly targeting specific down-stream genes, and is not acting as a non-specific, broad-spectrum repressor/instigator of gene expression. All of the candidate genes are known, with the exception of 1427820_at and 1427055_at. A BLAST (NCBI) search using the sequence for the Affymetrix EST 1427820_at a BLAST sequence comparison showed a 91% homology to a genbank sequence submitted by Strausberg *et al.* (2002) (*Erd1*; public ID NM_133362). I will therefore refer to this EST as "erythroid differentiation regulator 1-like" (*Edr1-L-EST*). However, our novel transcript is unlikely to be an exact match for this gene as levels of erythroid differentiation regulator 1 transcripts were below the detectable threshold in all experiments and were not altered on any of our microarray chips (Affymetrix 1439200_x_at; data not shown). Biochemical analysis of this novel transcript and its possible products is beyond the scope of the current study, so I have therefore named this transcript *Edr1-L-EST* for the purposes of this paper. This gene consistently showed the greatest up-regulation on the *Wld*^{S} cerebellar microarray, about 3.4 fold higher than in wild type mice.

A similar BLAST search for Affymetrix EST 1427055_at yielded no overt homology and hence its identity remains unknown, and I therefore simply refer to this gene as "*EST*". Of the 11 identified genes, the most significantly down-regulated candidate was pituitary tumour transforming gene 1 (*Pttg1*), whose expression was virtually silenced. The most significantly over-expressed candidate, was the sequence coding for Erythroid differentiation regulator 1-like EST (*Edr1-L-EST*). A preliminary assessment of potential functional genetic linkages was undertaken using Pathway Assist software (Ariadne Genomics). However, no specific pathway in which two or more of the candidate genes were a significant component could be identified (data not shown).

5.2.2. Validation of provisional microarray screen on *Wld*^{S} cerebellar RNA

I confirmed provisional modifications in RNA expression for those genes which were consistently altered across all 3 microarray runs semi-quantitatively using triplicate RT-PCR analysis. All 11 genes were confirmed to be up- or down-regulated, as indicated by the microarray data (Figure 5.4.A). Conventional RT-PCR can be quite insensitive to small variations in RNA levels. This is due to several factors (for more information see chapter 3). This inherent insensitivity means that some of the smaller changes as indicated by the microarray were not so apparent when the RT-PCR product was visualised on an agarose gel, for example myosin binding protein C3 (*Mybpc3*, Figure 5.4 A). I therefore used QRT-PCR to determine the change in mRNA levels of the two most highly altered genes: *Pttg1* and *Edr1-L-EST* (Figure 5.4 B). This analysis showed that *Pttg1* mRNA levels were 14.1±2.2 (mean±S.E.M, N=3) fold down-regulated in *Wld*^{S} mouse cerebellum compared to wild-type tissue. *Edr1-L-EST* mRNA, on the other hand, was 8.6±1.4 fold up-regulated in *Wld*^{S} cerebellum. Examples of raw QRT-PCR data in the form of amplification curves can be seen in Figure 5.5.

5.2.3. Mimicry of alterations in an independent (HEK293) cell line

My QRT-PCR endorses the changes in gene expression level shown by microarray of *Wld*^{S} cerebellar RNA. It is possible however, that such changes are a result of some other irregularity within the *Wld*^{S} mouse and not as a direct result of *Wld*^{S} expression. Therefore, in order to test whether the observed in *vivo* changes in gene transcription could be directly attributed to *Wld*^{S} gene expression, RNA levels were measured in a stable Human Embryonic Kidney (HEK293) cell line after transfection with a *Wld*^{S}-construct. The eGFP-*Wld*^{S} construct comprised the N70 amino acids of *Ube4b* and the C-terminal 303 amino acids of *Nmnat1*, which includes the Wld18 region, normally in the 5' untranslated region of *Nmnat1* in the wild-type (Mack et al., 2001, Figure 5.10). The *Wld*^{S} component was then inserted into the pEGFP-N1 vector under the control of a CMV promoter (Clontech). To confirm that *Wld*^{S} expression was present in all cells

containing GFP signal, and that all cells expressing *Wld*^{S} also expressed GFP, HEK293 cultures were fixed 4 days after transfection and stained immunocytochemically for Wld^S protein (Figure 5.6). Transfection efficiency, as measured by the relative numbers of cells showing both GFP fluorescence and Wld-18 immunostaining, was 17.9±8.7% of total cells (mean±S.E.M, N=4). These cells localised the fluorescent *Wld*^{S} gene product to their nuclei, forming either discrete puncta of staining, or diffuse nuclear fluorescence. A similar diversity of nuclear localisation patterns to those seen in the *Wld*^{S} mouse brains was observed (e.g. motor neurones show diffuse labelling; CGC show punctate labelling; different cortical neurones show both types of labelling; see chapter 4). All cells expressing GFP were also positive for Wld^S protein, and Wld^S protein expression without co-localisation with GFP was never seen (Figure 5.6). Transfection had no overt effect on the survival or morphology of either the transfected or non-transfected sub-population of HEK293 cells. The effects of transfection with *Wld*^{S} were consistent and reproducible (Figure 5.13).

5.2.4. Alterations of mRNA levels are *Wld*^{S} gene dose dependent

Semi-quantitative RT-PCR of HEK293 cells after transfection was first used to examine expression patterns of those genes previously seen to be altered in the *Wld*^{S} cerebellum (with the exception of Dap3, see methods; data not shown). To rule out the possibility that any changes in gene expression were due to a 'hijacking' of cellular RNA and/or protein synthesis machinery, rather than specific expression of the *Wld*^{S} gene, I preformed a 'squelching' experiment. Under many circumstances, the presence of abnormally large amounts of a foreign protein can result in altered gene expression patterns (Everett and Wood, 2004). HEK293 cells were therefore transfected with 5μg of total construct, with varying amounts of *Wld*^{S}-eGFP in the total transfect. For example, when the concentration of *Wld*^{S} was reduced to 3μg, the difference was made up using 2μg of plain eGFP (Clontech).

Figure 5.7 A-C shows an example of a conventional RT-PCR from one of these experiments focussing on *Pttg1* and *Edr1-L-EST*. The data clearly demonstrate a Wld^S-eGFP dose-dependent response. Figure 5.7 D shows that as expected, with transfection of more *Wld^S* construct more Wld^S protein is produced. Thus, the transcriptional changes observed when *Wld^S* is also present occur as a direct result of *Wld^S* gene expression, and are not simply due to large amounts of a foreign construct and/or protein. These findings also underscore the gene-dose dependence of the neuroprotective phenotype conferred by *Wld^S* expression, as measured in different transgenic lines in *vivo* (Mack et al., 2001).

5.2.5. Quantification of mRNA levels in *Wld^S* transfected HEK293 cells

Subsequently, real-time PCR (QRT-PCR) was used to confirm and quantify the changes in response to transfection with 5μg *Wld^S*-eGFP (Figure 5.8). Most genes examined (9 out of 10; Figure 5.8) showed significant changes in transcription compared to actin controls ($P<0.05$ for all genes except *TNFAIP3_IP*, ANOVA with Tukey's Post Hoc Test; N=3 for all genes except *Pttg1* and *Edr1-L-EST*, N=6). The other gene *TNFAIP3_IP1* was altered with a $P>0.05$ compared to actin, but were still clearly responding to *Wld^S* transfection (Figure 5.8).

The largest changes in expression detected were for the genes *Pttg1* and *Edr1-L-EST*. *Pttg1* expression was down-regulated by 13.97±1.8% (mean±SEM). At the other extreme, *Edr1-L-EST* expression was up-regulated by 18.55±4.8%. Importantly, it should be noted that RNA from HEK293 cells was extracted from the entire cell culture preparation, where ~75% of cells were not transfected with *Wld^S* (see above and Figure 5.6C). Thus, changes in expression of about 10-20% in the entire cell preparation probably represent a 40-80% change in expression at the level of individual *Wld^S* positive cells. As expected, actin controls showed no change in expression following transfection with *Wld^S* (-1.35±0.53%). So, to calculate the changes which may be occurring at the level of the individual cell it is necessary to compensate for the average transfection efficiency. This calculation suggests the levels of expression for *Pttg1* and

Edr1-L-EST, are downregulated by 77.6±10%, and upregulated by 103.0±10.8% per *Wld*^{S} positive cell.

5.2.6. *Wld*^{S} can change some mRNA levels through the NAD/Sirt1 Pathway

Araki *et al* (2004) provided evidence that the *Wld*^{S} phenotype is due to the *Nmnat1* portion of the gene alone in a Sirt1 dependent fashion. I therefore tested whether changes in gene transcription following *Wld*^{S} expression might occur due to modifications in the NAD and Sirt1 pathway. Instead of DRG cultures or fibroblasts (used by Araki *et al.*), I added 1mM NAD to HEK293 cultures and examined mRNA levels 5 days later using QRT-PCR. Of the 11 candidate genes regulated by *Wld*^{S} (excluding *Dap3* as no reliable human primers were available) *Ccl21*, *EST*, *TNFAIP3_IP1*, *Mbp-C*, *Ssr* and *Edr1-L-EST* all responded with less than 5% change in expression following NAD addition (Figure 5.9 and Table 5.2). Thus, a significant proportion of *Wld*^{S} mediated changes in transcription are not regulated by NAD-dependent pathways. However, the other 4 genes (D11, *Fabp7*, *Src-LA* and *Pttg1*) did respond with a greater than 5% altered expression pattern after 4 days of NAD incubation (Figure 5.9 and Table 5.2). All of these changes were in the same direction as those indicated by the microarray and after *Wld*^{S} transfection. The largest change was found for *Pttg1* (-14.9±2.7%; $P<0.001$; ANOVA with Tukey's Post Hoc Test; N=5). However, it should be noted that the magnitude of expression changes are not directly comparable to those seen after *Wld*^{S} transfection. NAD addition to the culture medium should affect every cell in the preparation, whereas only ~25% of cells would be exposed to the effects of *Wld*^{S} following transfection (see above). Thus, the magnitude of transcriptional modifications for *Pttg1* at the level of individual cells were in the order of 70-80% following transfection, yet were only in the order of 10-15% following NAD addition. It therefore remains possible that these NAD-dependent gene changes are potentiated by a non-NAD dependent mechanism in *Wld*^{S}-expressing cells.

Araki and colleagues demonstrated that the neuroprotective effects of NAD were mediated through activating the deacetylase Sirt-1 (Araki et al., 2004). Of the 4 genes altered by the addition of NAD, only one showed a significant decrease ($P<0.05$) in responsiveness following pharmacological inhibition of the Sirt-1 pathway using sirtinol (Figure 5.9). *Pttg1* downregulation was reduced from (-14.9±2.7%; to –2.49±0.59% ($P<0.02$; Mann-Whitney test; N=3). Interestingly, Ssr-α expression was significantly increased above those levels observed with NAD only by the addition of sirtinol ($P<0.05$, Table 5.2). This may suggest that Sirt-1 normally acts as a repressor of *Ssr-α*, and that alleviation of this repression via the addition of sirtinol can increase expression of *Ssr-α*.

5.2.7. Dissecting *Wld*^{S} induced gene regulation

Araki *et al.* (2004) showed that over-expression of *Nmnat1* was sufficient to reproduce the *Wld*^{S} phenotype in *vitro*, but that over-expression of *Ube4b* was not. I have demonstrated that exogenous NAD affects the regulation of *Pttg1* but not *Edr1-L-EST* (the two transcripts most highly altered by the presence of the full length *Wld*^{S} chimeric gene). I therefore asked whether transfection of HEK293 cells with either component of the *Wld*^{S} gene (Figure 5.10), would produce changes in expression of the two most strongly regulated genes. I used QRT-PCR to measure mRNA levels following transfection of HEK293 cells with either eGFP-*Nmnat1* or eGFP-N70-*Ube4b* constructs (Figure 5.10).

Interestingly, transfection with N70-*Ube4b* produced protein product diffuse throughout the cytoplasm (Figure 5.11B), with no more present within the nucleus than would be seen with transfection of just eGFP alone. N70-*Ube4b* does not produce any aggregates, nuclear or otherwise. Transfection with the *Nmnat1* portion of the gene produced fluorescent protein localised to nuclei in a strong diffuse pattern (Figure 5.11C), with no visible aggregates. This suggests that to obtain aggregates the two components of the

gene must be at least within the same cell and possibly attached (via their 18 amino acid bridge).

Nmnat1 transfection alone caused a significant down-regulation of *Pttg1* (Figure 5.11C, 5.12; -7.34±0.8%, (-40.77±4.44% normalised) $P<0.001$ compared to actin controls, ANOVA with Tukey's Post Hoc Test, n=6). As may have been expected, since NAD had no effect, transfection with *Nmnat1* did not alter the level of *Edr1-L-EST* mRNA (-1.57±0.7%, (8.31±4.16% normalised) $P>0.05$). However, the *Ube4b* construct caused a significant up-regulation of *Edr1-L-EST* mRNA levels (Fig 5.11B, 5.12; 7.84±1.3%, (43.52±7.21% normalised) $P<0.01$). This construct had no effect on the expression level of *Pttg1* mRNA (-1.71±0.9%, (9.49±4.99% normalised) $P>0.05$). Surprisingly, transfection with full length Wld^S construct produced greater changes in expression levels of both *Pttg1* and *Edr1-L-EST* than either of the separate constructs (Figure 5.11 A, 5.12). Therefore, it appears that *Ube4b* increases the efficacy of *Nmnat1* as a gene expression regulator; and similarly *Nmnat1* must affect the capability of N70-*Ube4b* to independently regulate expression of other genes.

Discussion

5.3.0. Discussion

The data presented here provide the first direct evidence that the neuroprotective *Wld*^{S} gene acts as a transcriptional regulator for a conserved set of genes in both mouse and human cells. In addition, I have demonstrated that this transcriptional regulation is mediated through both NAD/Sirt1-dependent and -independent pathways. Furthermore, I have shown that transcriptional regulation by *Wld*^{S} is species independent, since the same transcriptional responses to *Wld*^{S} are present in both mouse and human cells. If the *Wld*^{S} phenotype is conferred due to changes in mRNA levels of the other genes detailed above, the findings highlight the potential transferability of the neuroprotective phenotype to the human nervous system. This is cause for optimism that the utilisation of *Wld*^{S} induced specific pathways could be exploited for therapeutic intervention in neurodegenerative disease. The data suggest that further examination of genetic pathways regulated by *Wld*^{S} may identify novel therapeutic targets for the treatment of neurodegenerative diseases in humans where axonal and/or synaptic degeneration is a major pathological event.

Remarkably, expression levels were substantially altered (greater than two fold) for only a small number of genes, and yet for some of these, the change was as great as tenfold. As the *Wld*^{S} mutation confers a neuroprotective phenotype without affecting normal development and function of the nervous system (e.g. Parson et al., 1997), it seems appropriate to suggest that the chimeric fusion protein is acting on a very specific step in the degeneration process (Coleman & Ribchester, 2004). As the Wld^S neuroprotective phenotype can be transferred to other species through the generation of transgenic lines, it must be acting on a conserved pathway(s). Preliminary assessment of potential functional regulatory linkages could not identify any common molecular pathways connecting the candidate genes. The hypothesis that *Wld*^{S} is targeting a specific step in the degeneration process is supported by the fact that none of the identified genes with altered expression levels are thought to play a major regulatory role in normal cell development or maintenance pathways. Otherwise a non-degeneration related phenotype

would perhaps be expected in *Wld*^{s} mice. To date, no study of either mutant or transgenic mice or rats expressing the *Wld*^{s} gene has identified any overt phenotypic, developmental or behavioural abnormality (Gillingwater & Ribchester, 2001). It is however, unlikely that the phenotype could be recapitulated through alterations of the product levels of one gene. An example of this is given in appendix 5.2 where a *Pttg1* null mutant is examined for a neuroprotective phenotype.

The data suggest that both NAD-dependent and –independent pathways may underlie the *Wld*^{s} neuroprotective phenotype. I demonstrated that increased levels of exogenous NAD are sufficient to alter the expression patterns of at least some of the genes modified in *Wld*^{s} neurons in *vivo*. However, not all genes altered by *Wld*^{s} in *vivo* were affected by NAD application, suggesting that transcriptional regulation is also expected by NAD-independent pathways. None of the changes we observed following NAD application approached the relative levels obtained via transfection with a Wld^{s}-eGFP construct. Thus, while NAD-dependent pathways are apparently sufficient to regulate axon degeneration (Araki et al., 2004), it seems likely that other modifications of other pathways may be required to generate full transcriptional changes at the level observed in *Wld*^{s} tissue in *vivo*. It is tempting to suggest that the ubiquitin-proteasome system, modified by changes in *Ube4b*, may provide this additional regulation. This hypothesis is supported by recent data showing that the ubiquitin-proteasome system does not act as a general effector of protein degradation in axonal degeneration, but rather can function in the regulation of signalling pathways that control these degeneration processes (MacInnis & Campenot, 2004).

None of the genes identified here have previously been shown to play a critical regulatory role in neuronal degeneration. Nevertheless, previous research on *TNFAIP3_IP1*, *Dap3* and *Ccl21* suggest that they may be able to directly influence neurodegenerative pathways associated with axonal and/or synaptic degeneration. *TNFAIP3_IP1* acts on TNFAIP3, which is a component of the NF-κB/Rel signaling pathway (Baltathakis et al., 2001). Activity of this molecular pathway has been observed

in neurodegenerative disorders and rodent models of seizure and stroke (Mattson & Calmandola, 2001). *TNF-α* has also been shown to be a pro-inflammatory cytokine, induced during Wallerian degeneration (George et al., 2004). However, exactly how, and to what extent, *TNFAIP3_IP1* may influence these pathways remains unclear. Interestingly, *Dap3* may act on similar pathways to *TNFAIP3_IP1*, as it is known to be a positive mediator of TNF-α- and Fas-induced cell death (Kissil et al., 1999), although any potential interaction was not highlighted by our functional linkage assessment. *Ccl21* is another chemokine signalling molecule, responsible for signalling between neurons and microglia following nerve injury (Dijkstra et al. 2004). Loss of expression of *Ccl21*, on its own or in addition to altered TNF-α activity, could therefore perturb inflammatory responses in the nervous system. However, it should be noted that changes in expression levels for a cytokine do not necessarily indicate changes in their functional involvement in neuronal degeneration (Shamash et al., 2002).

Several of the other identified genes have been independently implicated in regulation of cell survival mechanisms, suggesting that they may also have the potential to directly regulate axonal and/or synaptic degeneration pathways. The human homologue of *Pttg1* (securin) has been shown to interact with p53, regulating its transcriptional and apoptosis-inducing behaviour (Bernal et al., 2002). It also modulates cell proliferation and FGF-2 expression in the developing human foetal brain (Boelart et al., 2003). It should be noted that I have been unable to determine a change in *Pttg1* protein levels with the currently available antibodies (Figure 5.14). *Edr1* is a newly characterised gene involved in haemoglobin synthesis induction, but which is also present in brain and can act as a stress-related survival factor (Dormer et al., 2004).

A recent publication detailing cell type specific gene expression of midbrain dopaminergic neurones, specifically, differences between A9 and A10 neurones gave a detailed microarray analysis. This analysis included a list of mRNA differences which may relate to their different vulnerabilities to Parkinson's Disease. In the middle of a large table of gene changes is an up-regulation of *Edr1* in A10 cells, which show

resistance to PD (Chung *et al.*2005). None of the genes I have detected changes in are typically associated with neuronal protection. As a result the authors of this particular paper may have overlooked the possible importance of *Edr1* alterations and focused on genes which are already thought to be involved in neuronal pathways. Another recent paper carried out microarray analysis on *Sod1* mutants. The authors of this paper noted a decrease in NADPH and in their published microarray table there is a decrease in levels of EDR which was not mentioned in the text of the paper (Kirby *et al* .2005). This may be significant in so much as Wld^S mice have increased nuclear *Nmnat1* which gives rise to the production of NAD, and I have shown an upregulation in an EDR like transcript, as well as a possible upregulation in EDR levels as gauged by P.Dormer (Figure 5.15).

One facet of this study should remind us that we should not rule out the involvement of one, or several, of the other genes yet to be implicated in any neuronal survival pathways. These genes will need to be the subject of further investigation to identify any potential role they may play in regulation of neurodegenerative pathways. Thus, it remains possible that modifications in the expression of either a single candidate gene, or multiple candidate genes, are required to confer phenotype, with or without changes in other genes which we may have failed to identify in the current experiments.

This finding begs the major question, beyond the scope of the present thesis, whether any of the genes here identified, either alone or in combination are responsible for the Wld^S phenotype. Answers to this question could have a major impact on our understanding of neurodegenerative mechanisms and possibly for treatments for neurodegenerative diseases as well. To address this would require the development and implementation of a high throughput analysis where transcription of more than one gene at a time can be controlled experimentally with a clear readout of Wld^S phenotype.

In summary, the transcriptional effects of Wld^S expression on conserved sub-sets of genes in mouse and human cells suggest it may be possible to extend the neuroprotective phenotype into large animals, including man.

Figures

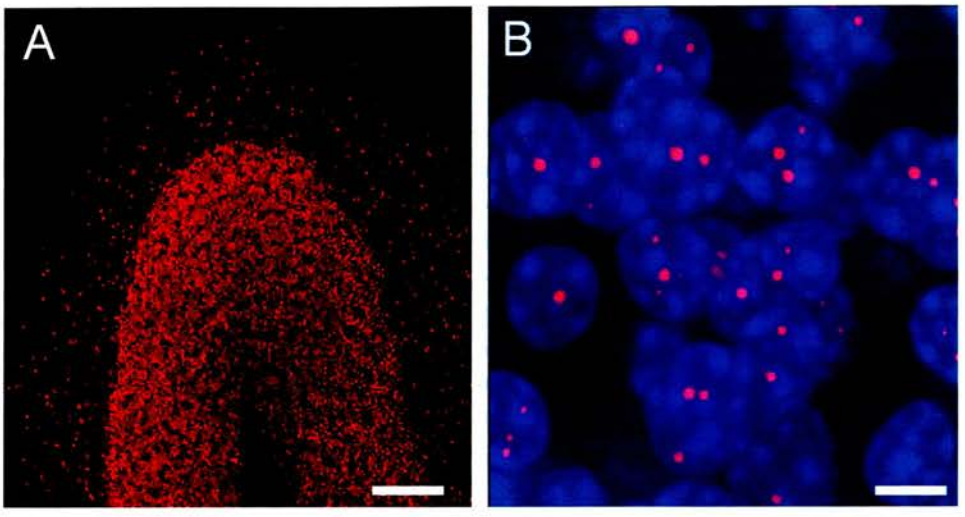

Figure 5.1. The cerebellum is an enriched source of Wld^s protein product.
(A) Confocal micrograph of cerebellar folium immuno-cytochemically labelled for Wld^s protein (red). There is strong labelling in the cerebellar granule cell layer. (B) High power confocal micrograph of cerebellar granule cells immunocytochemically labelled for Wld^s protein (red) and the nuclear marker TOPRO-3 (blue). Every cerebellar granule cell has a large nuclear Wld^s protein inclusion. Scale bar = 50μm (A); 6μm (B).

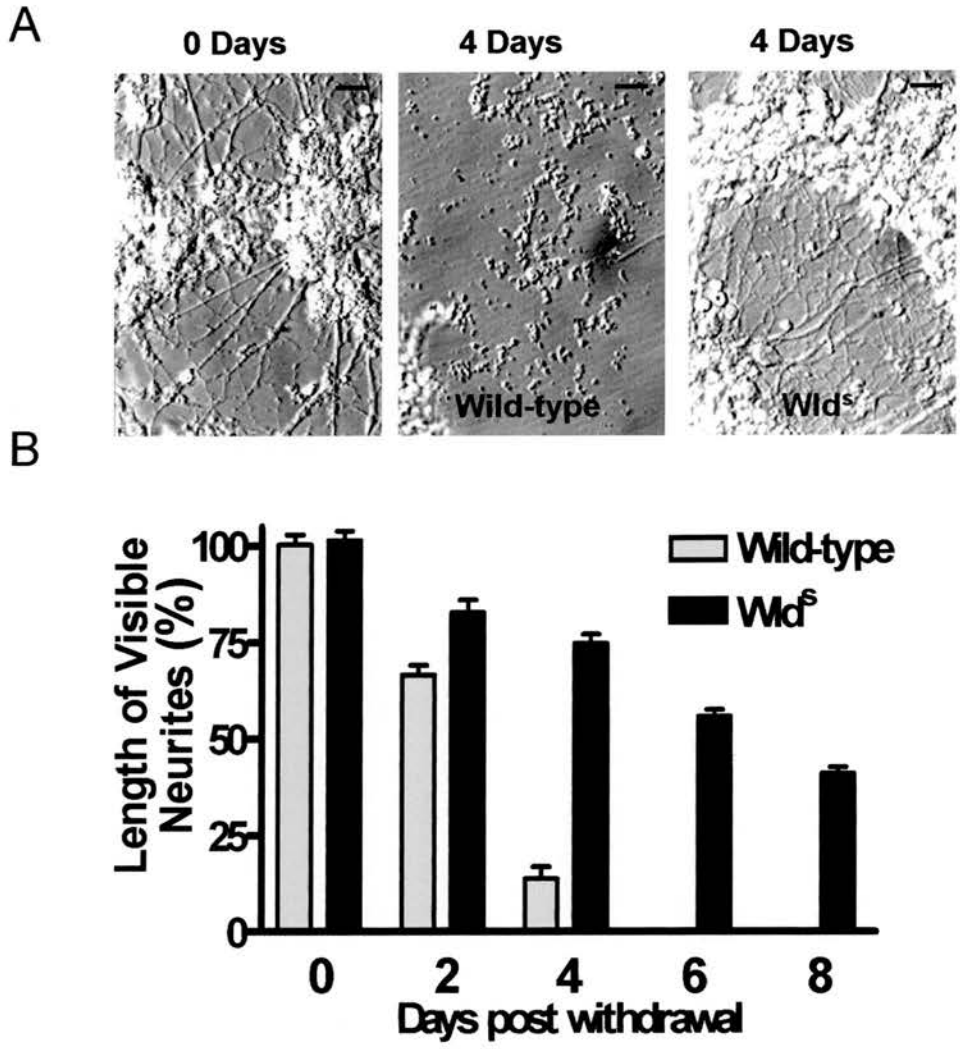

Figure 5.2. The *Wld*^{s} cerebellum displays a neuroprotective phenotype.

(A) Phase contrast micrographs of dissociated cerebellar granule cell neurones in culture showing protection of neurites in preparations from Wld^s compared to wild type mice, 4 days after withdrawal of serum and potassium. (B) Bar chart showing quantification of neurite retention in cultures of cerebellar granule cells from wild-type and Wlds mice up to 8 days after serum and potassium withdrawal (mean±SEM). Scale bar = 80μm.

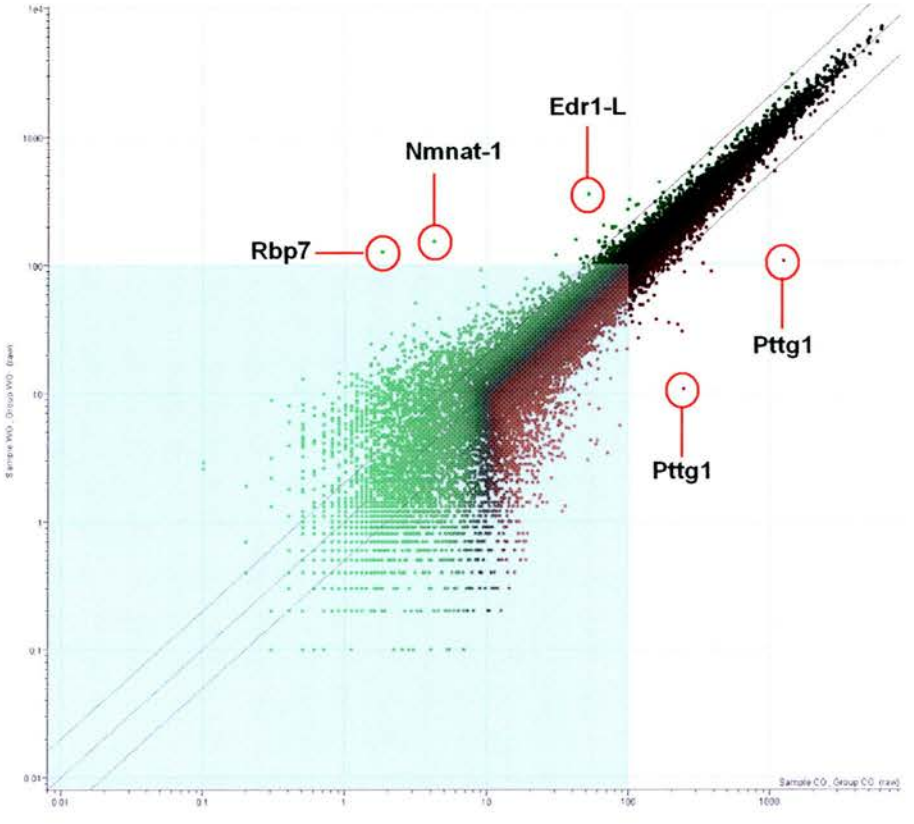

Figure 5.3. Microarray analysis of *Wld*^{S} cerebellar mRNA shows both up- and down- regulated genes.
A scatter plot comparing mRNA expression in *Wld*^{S} and wild-type cerebellum from a single (of 3) microarray experiment. The *Wld*^{S} signal (y axis) is plotted against the wild-type signal (x axis) for each gene probe set present on the Affymetrix MOE-430A array. 3 Diagonal lines are guides, centre is line of no change, 2 outer lines indicate a 2 fold level of up or down regulation. Transcripts for *Rbp-7*, *Wld*^{S} and *Edr1-L* are evidently up-regulated. Transcripts for *Pttg1* are evidently down regulated (Graph courtesy of T.H.Gillingwater and K.Robertson, RNA extracted by myselft and P.E.Chen).

Affymetrix ID	Gene Title	Gene Symbol	Approx Fold Change
Up-regulated			
1427820_at	Erythroid differentiation regulator 1 - like	Edr1-L	3.4
1418551_at	Myosin binding protein C, cardiac	Mybpc3	2.1
1417764_at	Signal sequence receptor, alpha	Ssr1	2.0
1450779_at	Fatty acid binding protein 7, brain	Fabp7	1.7
1427689_a_at	TNFAIP3 interacting protein 1	Tnip1	1.5
1420819_at	Homologous to Human/Rat Src-like adaptor	Src-LA	1.5
Down-regulated			
1450848_at	Death associated protein 3	Dap3	-1.7
1427055_at	RIKEN cDNA 4921507I02 gene	EST	-2.0
1447146_s_at	DNA segment, Chr 11, ERATO Doi 730, expressed	D11Ertd730e	-2.5
1419426_s_at	Chemokine (C-C motif) ligand 21b (serine) Chemokine (C-C motif) ligand 21a (leucine) Chemokine (C-C motif) ligand 21c (leucine)	Ccl21b Ccl21a Ccl21c	-8.1
1438390_s_at	Pituitary Tumor Transforming 1	Pttg1	-7.1

Table 5.1. Affymetrix analysis shows mRNA levels for 11 of ~23 000 genes on the chip are altered.

This table lists those genes with a change consistently greater than 1.5 fold across the 3 affymetrix gene chip comparisons. 6 genes show a higher presence in *Wld*^{S} mRNA and 5 genes show decreased presence in *Wld*^{S} mRNA. The table indicates the affymetrix gene identification code, the gene name, symbol and approximate fold change averaged across all 3 microarray comparisons.

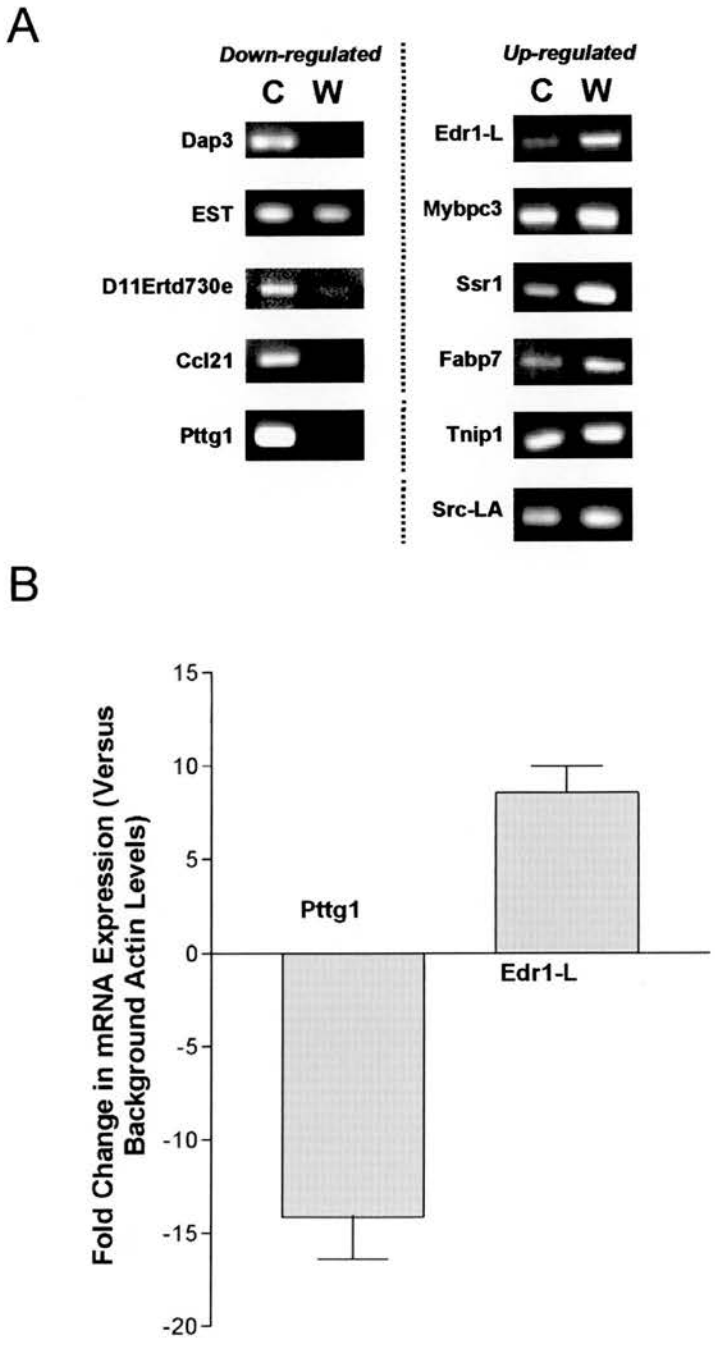

Figure 5.4. Bidirectional changes in mRNA expression in *Wld*^{S} cerebellum. (A) RT-PCR validation of microarray data on cerebellar mRNA. Each of these semi-quantitative experiments was performed in at least triplicate. An example band for each is shown. (B) QRT-PCR validation of *Pttg1* and *Edr1-L* fold expression changes in *Wld*^{S} mouse cerebellum (Mean±SEM).

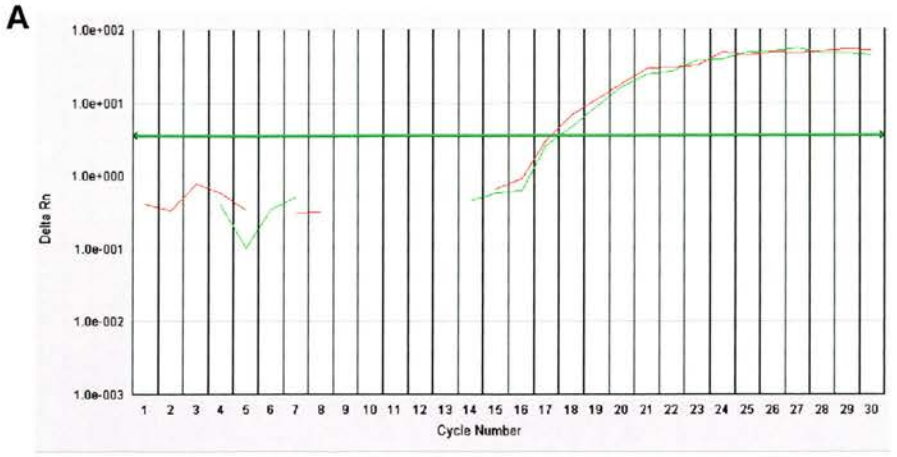

B-tubulin mouse

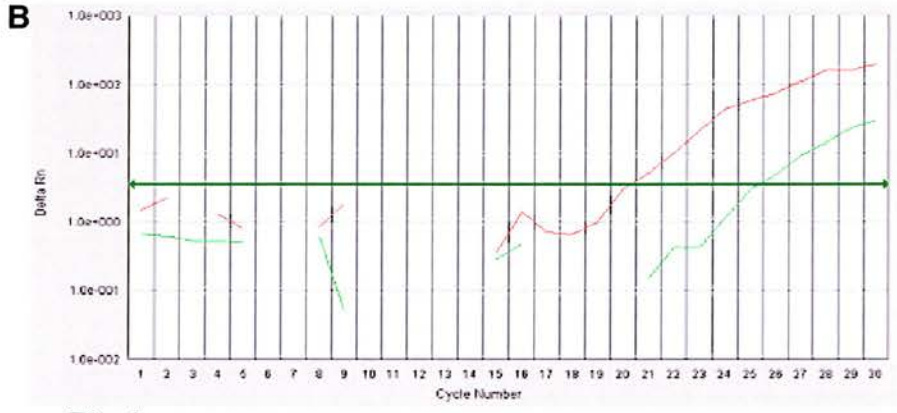

Pttg1 mouse

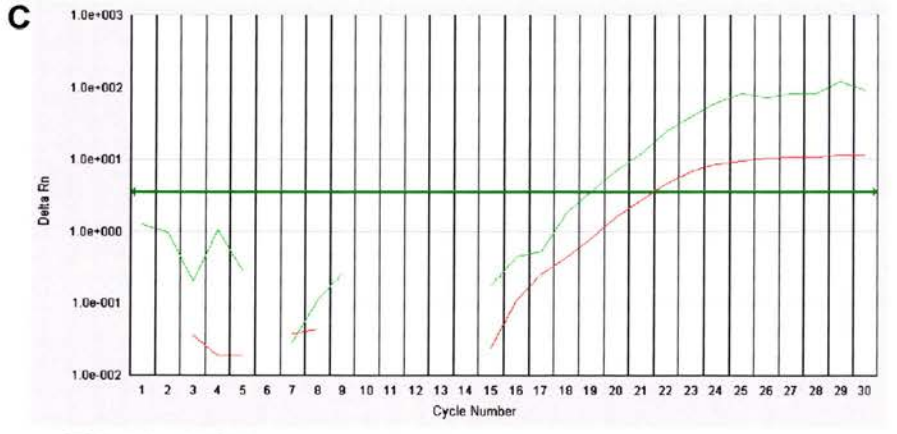

Edr1-L –EST mouse

Figure 5.5. Example curves from QRT-PCR on mouse cerebellar RNA.
Green line indicates *Wld*^{S} RNA and red line indicates wild-type RNA. Screen grabs are shown for *β-tubulin* (A), *Pttg1* (B) and *Edr1-L-EST* (C).

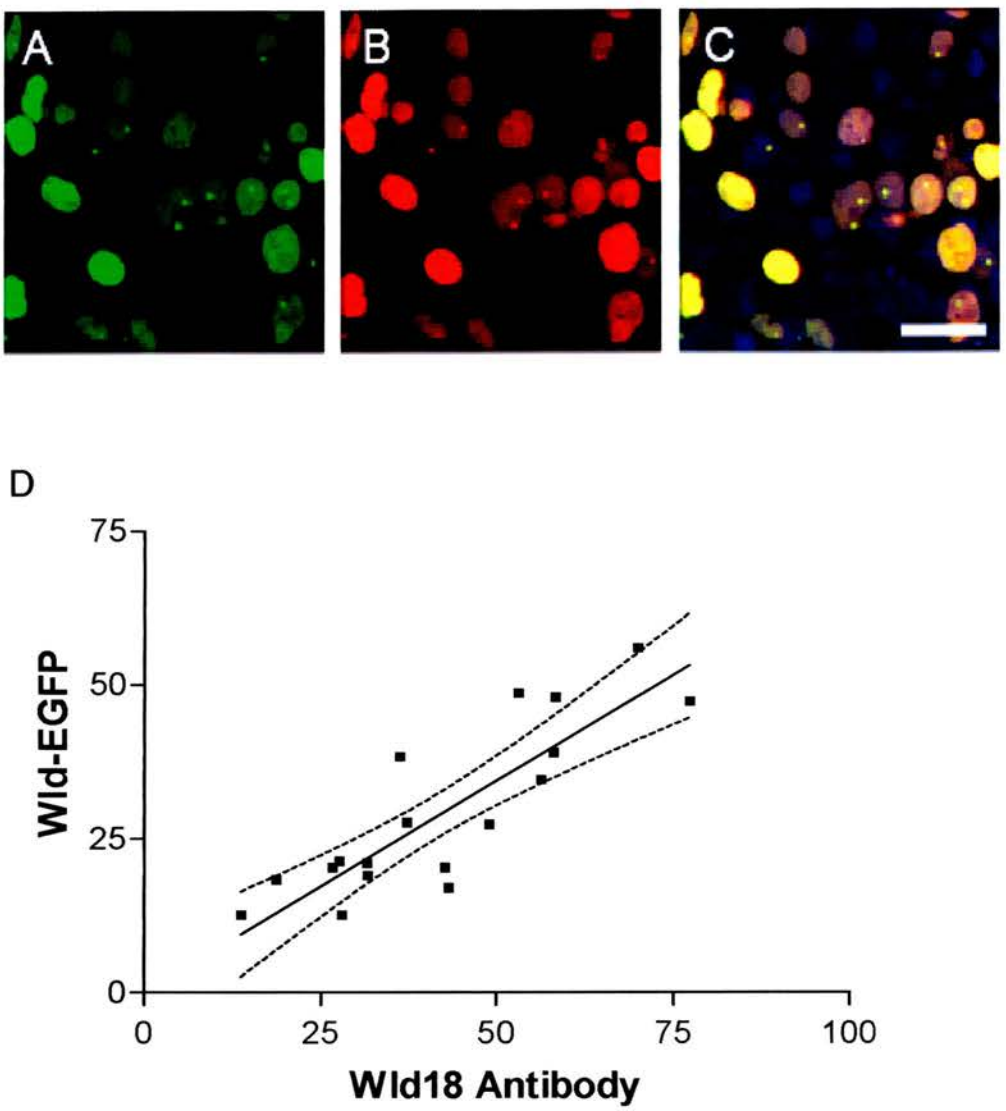

Figure 5.6. *Wld*^{S} can be transfected and expressed in a human (HEK293) cell line.

(A-C) Confocal micrographs of HEK293 cells 4 days post transfection with Wld^{S}-eGFP. These cells shown were also immuno-labelled for Wld^{S} protein using the Wld-18 antibody, to demonstrate that all of the eGFP visible is attached to Wld^{S} protein. Panel A shows the eGFP image alone (green), panel B shows immuno-labelling for Wld^{S} protein (red) and panel C shows the overlay of (A) and (B) and labelling of nuclei with TOPRO-3 (blue). Panel C shows ~25% transfection efficiency in this particular example. (D) – A graphical representation of the correlation between eGFP and Wld-18 antibody labelling as a measure of fluorescence intensity (100 being the most intense). Scale bar = 15μm.

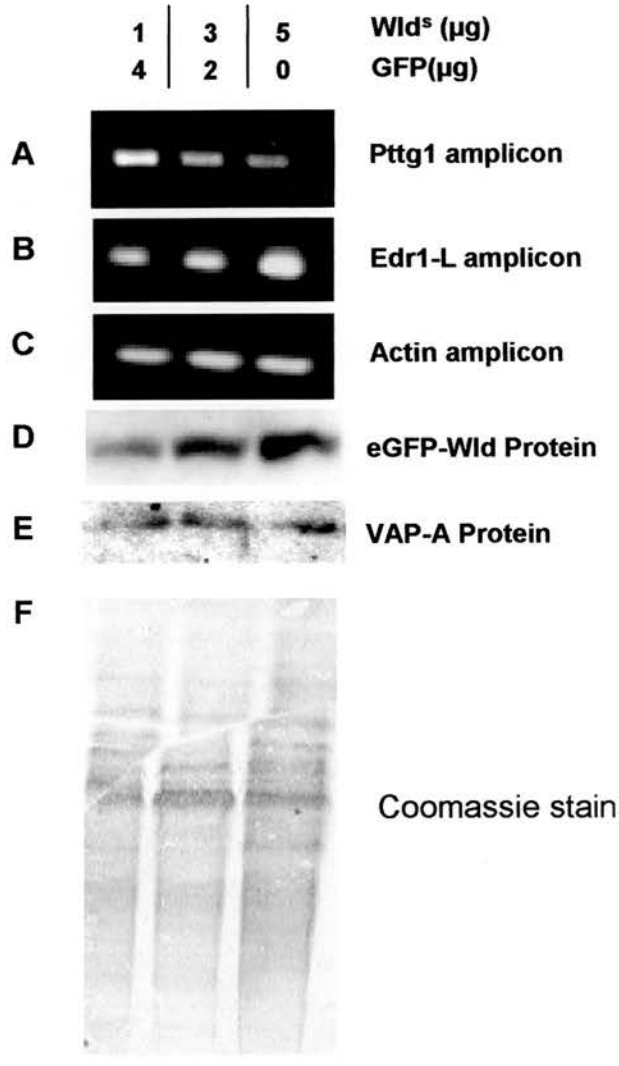

Figure 5.7. Transfection of HEK293 cells with Wld^s-eGFP regulates mRNA levels in a dose dependant fashion.
HEK293 cells were transfected with 5µg of total construct. The proportion of Wld^s-eGFP and "plain" eGFP in that mix was varied in order to demonstrate that the effects shown are not only due to the presence of a large amount of foreign DNA. (A-C) RT-PCR. (A) *Pttg1* amplicon levels decrease with increasing *Wld^s*. (B) *Edr1-L-EST* amplicon levels increase with increasing *Wld^s*. (C) *Actin* amplicon levels remain constant. (D-E) Western blot. (D) Wld^s-eGFP protein levels increase with increasing Wld^s-eGFP construct. (E) VAP-A controls remain roughly constant. (F) Commassie stain. Analysis of band intensity shows that all 3 lanes are within 4%.

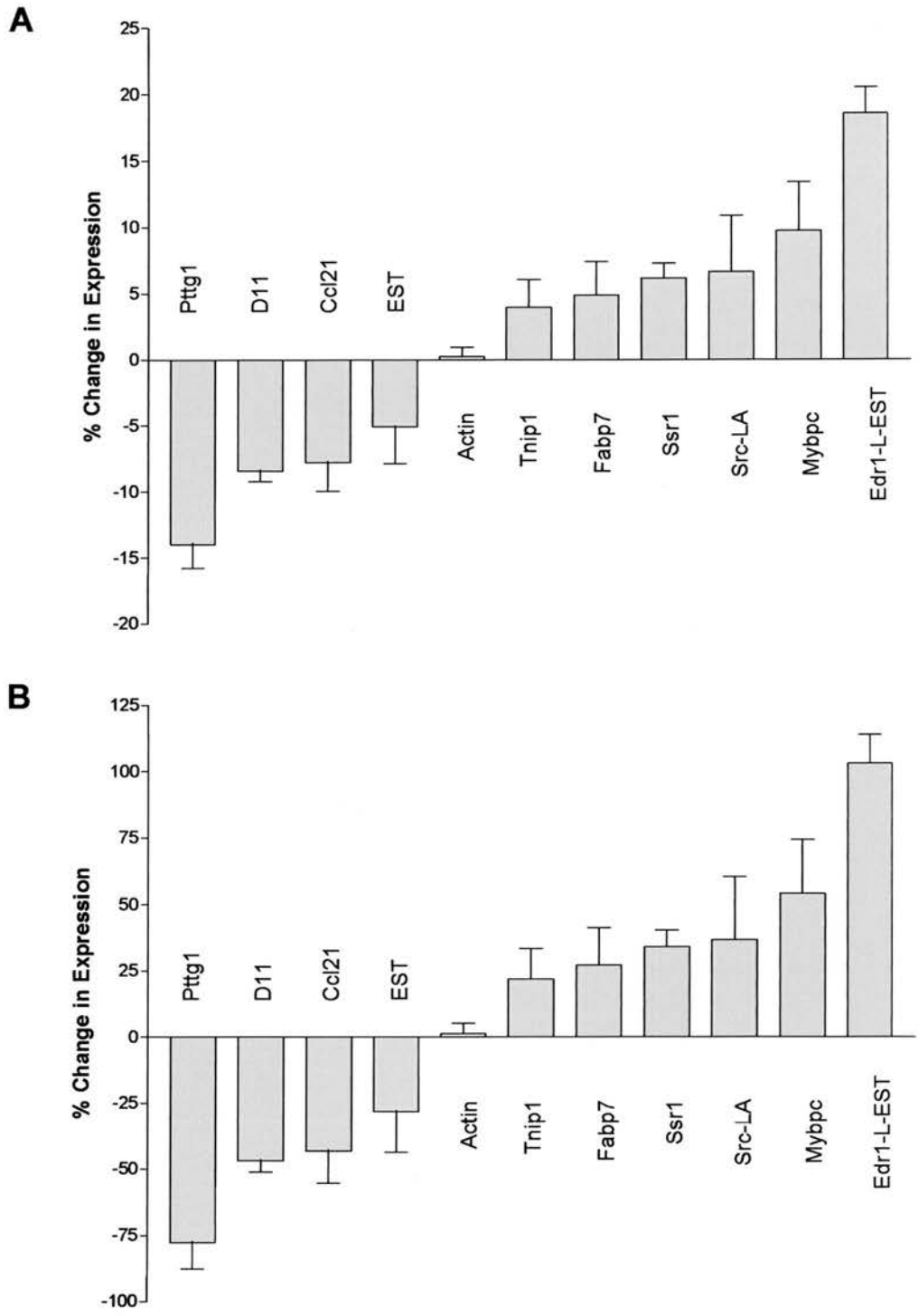

Figure 5.8. Alterations in mRNA levels mimicked in Wld^S-eGFP transfected HEK293 cells.

Transfection with 5µg of construct and subsequent QRT-PCR assay of mRNA levels for 10 of the 11 genes indicated by the initial microarray studies show changes in the same direction as the *Wld^S* mouse. Note that the 2 largest changes in the HEK293 cells are *Pttg1* and *Edr1-L* as in the *Wld^S* mouse. (A) Raw values, (B) Normalised to transfection efficiency.

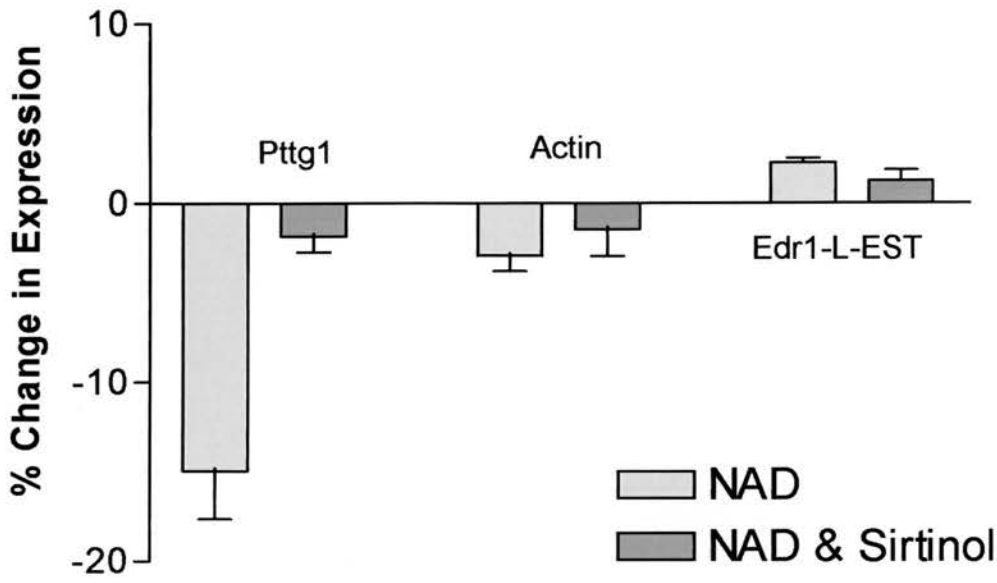

Figure 5.9. Changes in *Pttg1* mRNA levels are mimicked by NAD in a Sirt1 dependant fashion.
The bar chart shows QRT-PCR responses of *Pttg1* and *Edr1-L-EST* mRNA levels with actin controls, 4 days post application of exogenous NAD (1mM) or NAD (1mM) and sirtinol (100μM). Note that only Pttg1 showed a significant response to NAD application and that this response can be blocked by addition of the sirt1 inhibitor sirtinol.

Gene	NAD (Mean)	NAD (SEM)	Change vs Actin	NAD+ Sirtinol (Mean)	NAD+ Sirtinol (SEM)	Change NAD/Sirtinol vs NAD
Actin	-2.92	0.85	N/A	-1.45	1.495	NS
Pttg1	-14.95	6.60	P<0.001	-1.80	1.587	P<0.02
Ccl21	-4.33	0.90	NS	-2.74	2.551	NS
D11Ertd730	-5.32	1.49	NS	-1.69	0.468	NS
EST	-1.99	1.23	NS	-1.03	0.411	NS
Fabp7	10.21	2.75	P<0.0001	3.42	0.453	P<0.04
Mybpc3	3.60	0.94	NS	1.53	0.288	NS
Src-LA	6.89	1.78	P<0.01	1.23	1.494	P<0.04
Ssr1	4.82	2.10	NS	13.03	1.295	P<0.05
Tnip1	2.33	1.08	NS	3.73	2.996	NS
Edr1-L-EST	2.27	0.58	P>0.05	1.27	1.035	P>0.05

Table 5.2. Changes in mRNA levels for most of the indicated genes are not mimicked by NAD in a Sirt1 dependant fashion.

The table illustrates QRT-PCR responses of mRNA levels for all the *Wld*^{S} altered genes, 4 days post application of exogenous NAD (1mM) or NAD (1mM) and sirtinol (100μM). Note that *Fabp7* and *Src-LA* show "significant" changes in response to NAD addition and that these changes can be averted when NAD and sirtinol are added together. However, *Ssr1* shows a significant increase in response to NAD and sirtinol. This also occurs in response to sirtinol alone suggesting that Sirt1 is acting to "suppress" levels of *Ssr1*.

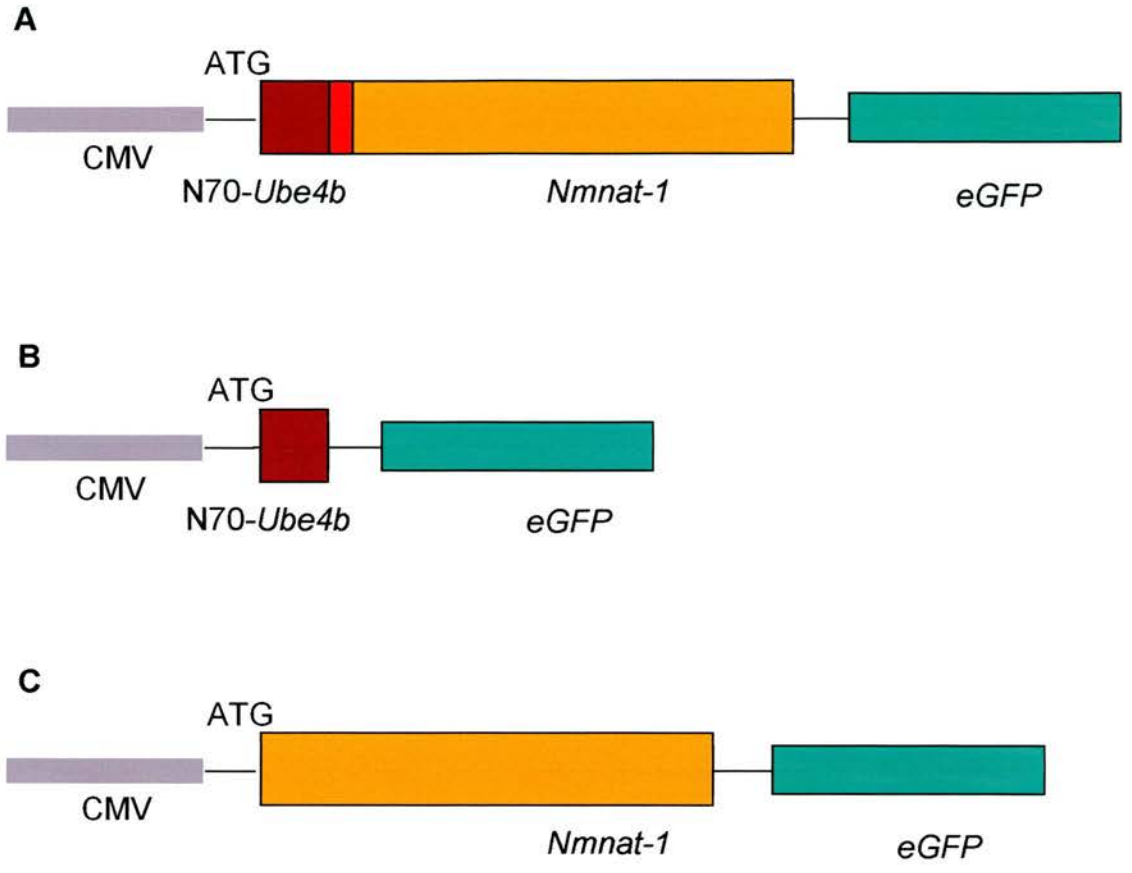

Figure 5.10. Constructs produced for in vitro transfection.
Diagrammatical representations of constructs used to introduce and visualise (with an eGFP tag) (A) full length chimeric *Wld*^{S}, (B) N70-*Ube4b* and (C) *Nmnat-1* in *vitro*.

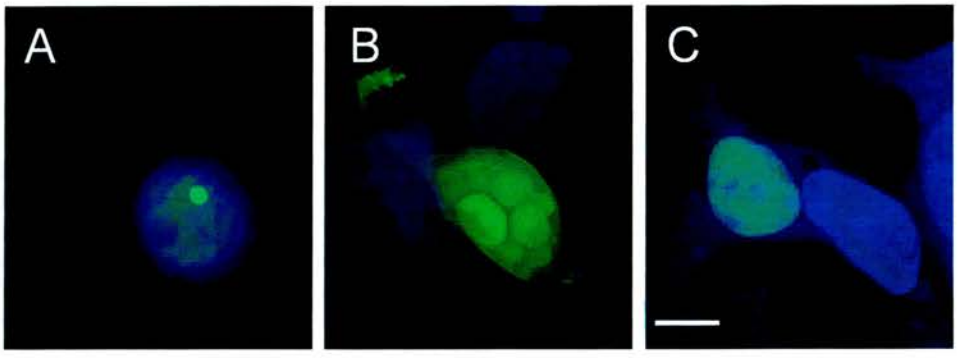

Figure 5.11. *Pttg1* and *Edr1-L* are independently regulated by the Nmnat-1 and Ube4b portions of the *Wld*^{S} chimeric gene. Transfection with 5µg of each construct was carried out and followed by visualisation and QRT-PCR analysis. (A-C) Confocal micrographs. (A) Transfection with the full length chimeric Wld^{S}-eGFP construct shows localisation of the protein product to the nucleus and in this case a large single inclusion. (B) Transfection with the N70-Ube4b-eGFP construct shows the protein product dispersed throughout the whole cell, nucleus and cytoplasm. (C) Transfection with the Nmnat-1-eGFP construct showing localisation to the nucleus without the formation of inclusions. Scale bar = 6µm (A-C).

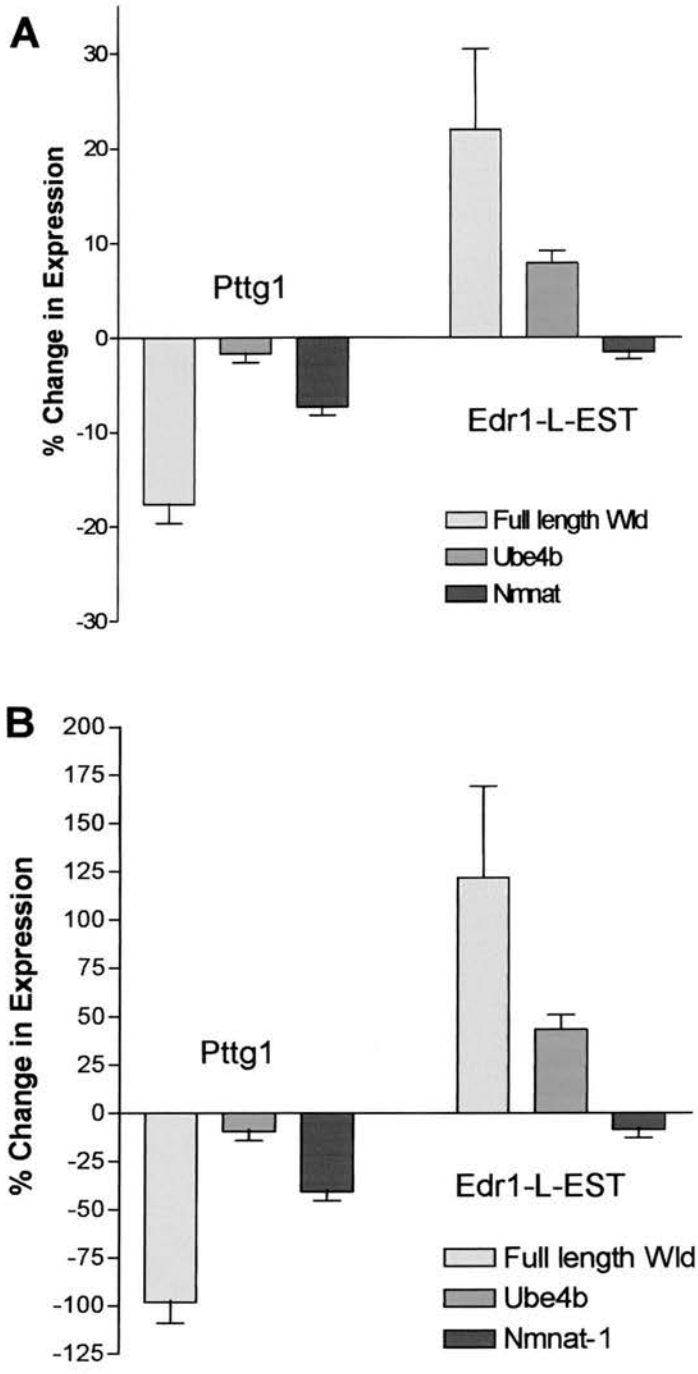

Figure 5.12. *Pttg1* and *Edr1-L* are independently regulated by the Nmnat-1 and Ube4b portions of the *Wld*^{s} chimeric gene.
Transfection with 5µg of each construct was carried out and followed by QRT-PCR analysis. (A) Raw values for gene levels following transfection with each construct. (B) The values normalised according to transfection efficiency. *Pttg1* levels are changed following transfection with chimeric Wld^{s} and Nmnat-1 but not N70-Ube4b. *Edr1-L-EST* levels are changed by chimeric Wld^{s} and N70-Ube4b, but not Nmnat-1.

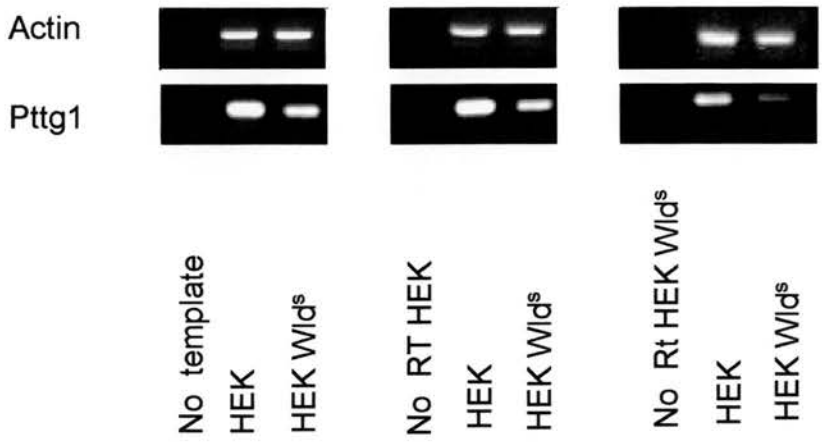

Figure 5.13. The effect of *Wld*^{s} transfection were reproducible and consistent.

Conventional RT-PCR for Pttg1 on HEK293 RNA from non transfected cells and Wld^s transfected cells. It is important to note the inconsistency between the different lanes. Although *Pttg1* levels are always at lower levels in the *Wld*^{s} RNA in comparison to non transfected controls, it is obviously only possible to note the direction of change and not relative difference. This is the main reason for the need of QRT-PCR to determine levels of change.

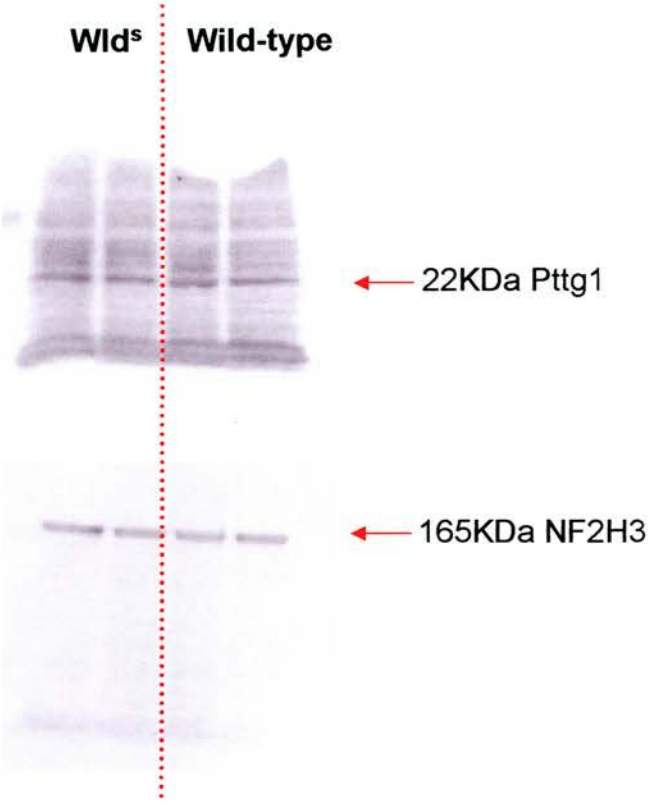

Figure 5.14 It is not possible to detect alteration of Pttg1 protein levels in *Wld*^{s} mice.
The antibodies available for western blotting and immunocytochemistry of Pttg1 protein are poor. The western blot of Pttg1 above was carried out using antibody kindly donated by S.Melmed (Cedars-Sinai Research Institute, UCLA).There are too many bands at the expected size of 22KDa for the Pttg1 protein to be sure which is the correct band. Western blots were also attempted using commercially available antibodies from Santa Cruz, and the outcome was equivocal. Immunocytochemistry with either antibody was poor.

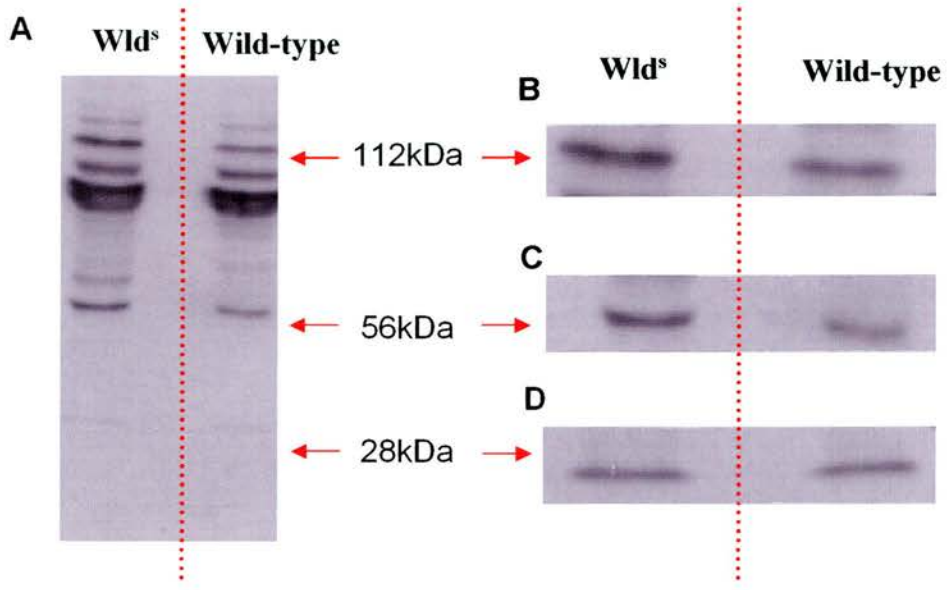

Figure 5.15. Edr1 levels appear to be increased in *Wld*^{s} mice.
The antibodies available for western blotting and immunocytochemistry of Edr are poor. The western blot shown in figure A was prepared using an antibody kindly donated by P.Dormer (GSF-Department of Experimental Hematology, Gaunting, Germany). There is a detectable increase in the trimer (B) and dimer (C) forms (112 and 56KDa respectively) of Edr, but not the monomer (D, 28KDa). Immunocytochemistry carried out with this antibody was inconclusive.

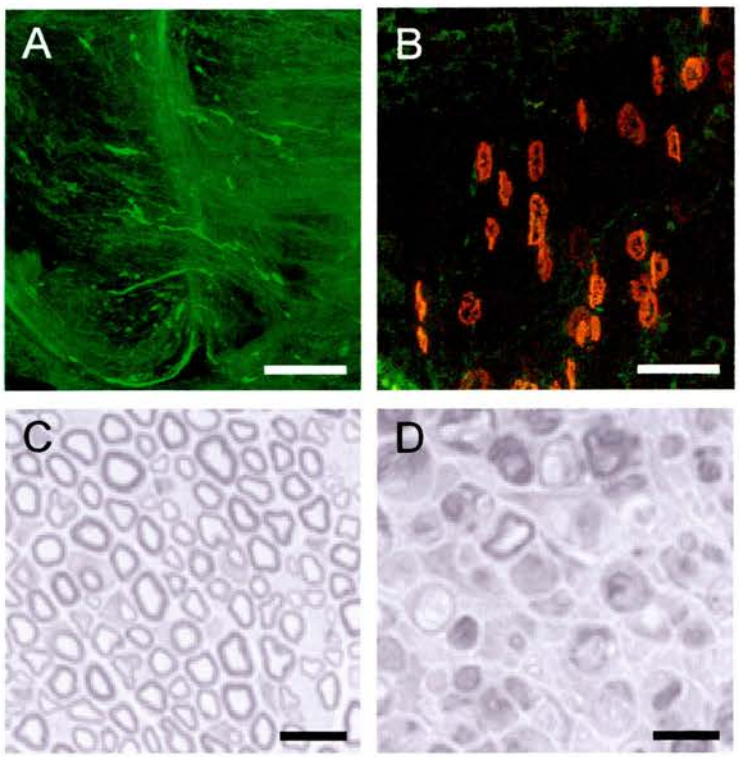

Appendix 5.2.1. *Pttg1* knock out animals do not show a neuroprotective phenotype.
(A) *Pttg1 -/-* mouse tibial nerve immunostained for 165kDa neurofilaments, showing fragmentation of axon profiles 3 days after sciatic nerve lesion. (B) *Pttg1 -/-* mouse deep lumbrical muscle 2 days after sciatic nerve lesion. Evidence for functional motor nerve terminals was sought using FM1-43 (green), and motor endplates were labelled with TRITC-conjugated alpha-bungarotoxin (red). No functioning motor nerve terminals were found in any of the muscles examined (n=6) 2 days after sciatic nerve lesion, whereas nearly all terminals in contralateral unoperated muscles were stained with FM1-43 (data not shown). (C) Micrograph of unlesioned *pttg1 -/-* mouse tibial nerve stained with toluidine blue. (D) P*ttg1 -/-* mouse tibial nerve 6 days after sciatic nerve lesion. Almost all axon profiles appeared to be undergoing degeneration. Scale bars = 50μm (A,B) 10μm (C,D). Taken from Gillingwater *et al. (2005) Under review.*

Appendix 5.1

Appendix 5.1. Colony specific strain variations can affect microarray results

Although it detracts from the flow of this chapter I believe it is interesting to point out a possible problem with microarray analysis. An initial list of mRNAs whose expression was highly different between wild-type and *Wld*^{S} and showed an apparent alteration in levels during aging. That is, changes in levels between *Wld*^{S} and wild-type and an alteration in levels from young to old *Wld*^{S}, but not across all 3 comparisons were also identified. As described earlier, the *Wld*^{S} shows an age related synaptic protective phenotype, therefore an age related change in mRNA levels could be very exciting. An example of one of these was *Kcne2*, a potassium channel, which registered as a down-regulation in *Wld*^{S}. Validation showed that it was down-regulated in *Wld*^{S} mice compared to wild-type. In this case the control was a C57Bl/6J from Harlan-Olac, which is also known to be α-synuclein negative. When the levels of *Kcne2* are compared to a C57Bl/6J from Charles River they are very similar to that in *Wld*^{S}. Therefore, the apparent down-regulation of *Kcne2* in *Wld*^{S} mice could be an α- synuclein related alteration in expression. The spontaneous loss of α-synuclein from the Harlan-Olac C57Bl/6J appears to have occurred after the spontaneous triplication forming the *Wld*^{S} mutation in that line. This assumption can be made as both the *Wld*^{S} and the C57Bl/6J from Jackson Labs are α-synuclein positive (Appendix figure 5.1.1.). Whether or not the alterations shown by the microarray are a function the presence or lack of α-synuclein, remains to be seen. This should serve as a cautionary note to those who wish to carry out microarray analysis. It is important to be aware of the history of the control strain used for analysis.

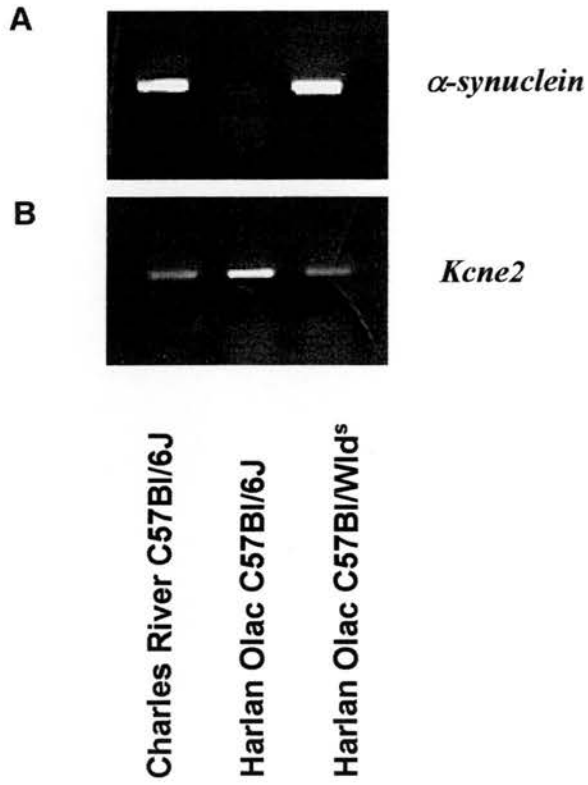

Appendix 5.1.1. *Kcne2* mRNA level alterations may be α-synuclein linked.
Conventional RT-PCR for *α-synculein* (A) and *Kcne2* (B) show that *α-synculein* is present in Charles River C57Bl/6J and Harlan Olac C57Bl/Wld^s but not Harlan Olac C57Bl/6J and that Kcne2 is present at greater levels in Harlan Olac C57Bl/6J.

Appendix 5.2

Appendix 5.2. *Pttg1* knock out animals do not show a neuroprotective phenotype

The only available mutant for the genes of interest identified by the microarray screen and subsequently verified was a null mutant (knockout) *pttg1* -/- mouse. This mutant was located in Los Angeles. Experiments performed by Dr T.Gillingwater and Prof. R.Ribchester showed that these mice do not show axonal or synaptic protection after sciatic nerve injury (Appendix figure 5.2.1 and 5.2.2). This should not exclude the possibility that an alteration of *Pttg1* levels may contribute to the phenotype, however, as it may be important in conjunction with alterations in any of the other genes identified by this study. It is also important to note that these *Pttg1* knock out mutants may have redundant genes that may compensate for the low levels of *Pttg1* in a constitutive knock out.

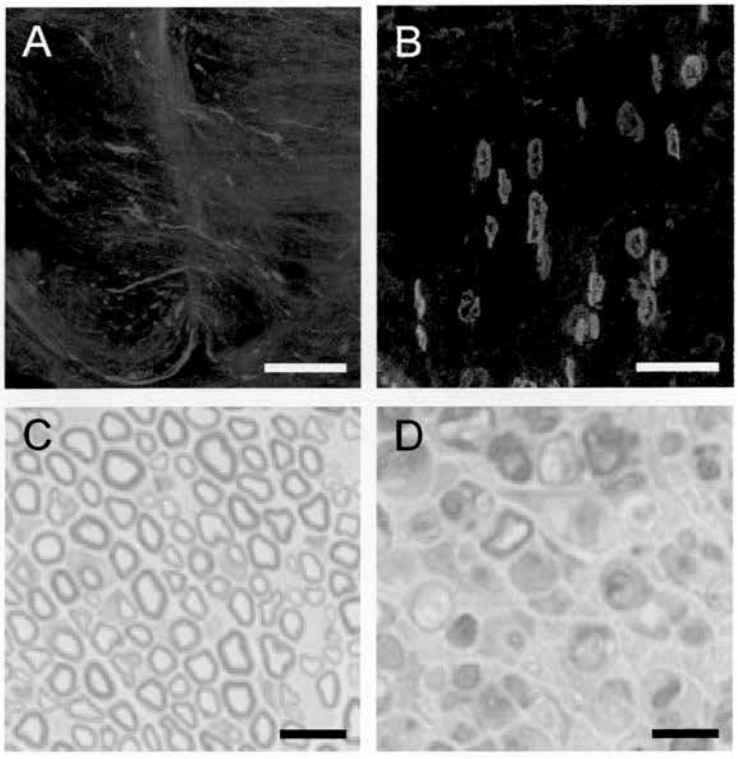

Appendix 5.2.1. *Pttg1* knock out animals do not show a neuroprotective phenotype.
(A) *Pttg1* -/- mouse tibial nerve immunostained for 165kDa neurofilaments, showing fragmentation of axon profiles 3 days after sciatic nerve lesion. (B) *Pttg1* -/- mouse deep lumbrical muscle 2 days after sciatic nerve lesion. Evidence for functional motor nerve terminals was sought using FM1-43 (green), and motor endplates were labelled with TRITC-conjugated alpha-bungarotoxin (red). No functioning motor nerve terminals were found in any of the muscles examined (n=6) 2 days after sciatic nerve lesion, whereas nearly all terminals in contralateral unoperated muscles were stained with FM1-43 (data not shown). (C) Micrograph of unlesioned *pttg1* -/- mouse tibial nerve stained with toluidine blue. (D) P*ttg1* -/- mouse tibial nerve 6 days after sciatic nerve lesion. Almost all axon profiles appeared to be undergoing degeneration. Scale bars = 50μm (A,B) 10μm (C,D). Taken from Gillingwater *et al. (2005) Under review.*

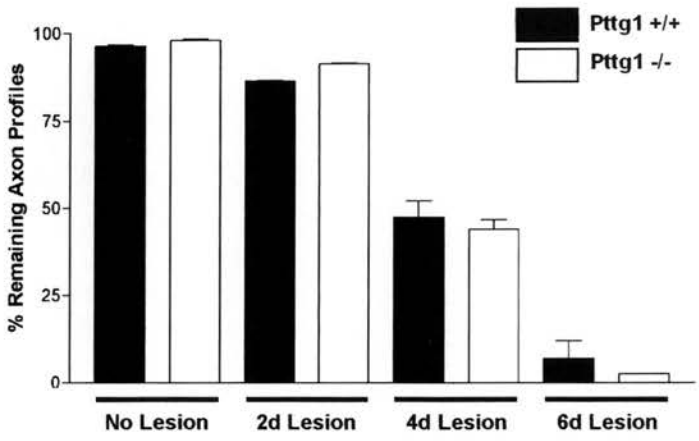

Appendix 5.2.2. *Pttg1* knock out animals do not show a neuroprotective phenotype.

Bar chart showing quantification of axon profile preservation in the tibial nerve of *pttg1-/-* (ko) and +/+ (wt) mice at 2, 3, and 6 days post sciatic nerve lesion (mean±SD; n = 2-/- and 1 +/+ per time-point). There was no difference in the onset or rate of degeneration between the two experimental groups.

Taken from Gillingwater *et al. (2005) Under review.*

Chapter 6:
General discussion

6.0. General discussion

Before the discovery of the *Wld*^{S} mutant mouse (Lunn *et al.* 1989), it was assumed that one of two things were happening in response to injury by axotomy; either 1. The injury starves the isolated distal axon of essential maintenance factors, which are normally synthesized in neuronal cell bodies and propagated through the neuron by axonal transport, or 2. The injury generates a signal at the site of the injury itself which triggers a rapid necrosis in the distal stump. The delay of Wallerian degeneration in *Wld*^{S} mice suggests that Wallerian degeneration is an active, highly regulated process (Gillingwater *et al.* 2005 submitted). More recently a third possible hypothesis has become apparent. This hypothesis does not preclude either of the above hypotheses. The *Wld*^{S} mutation affects expression levels of RNAs or proteins that may be ordinarily involved in regulating the programme of axon degeneration.

As more work is carried out in the field of cell death there appears to be increasing overlap in some of the complex pathways involved in necrosis and apoptosis. Wallerian degeneration was once thought to be a passive necrotic process in response to the separation of the axon from the cell body. It appears now to a highly regulated programme involving genes and proteins that have yet to be fully characterised, but which is distinct from apoptosis. It is gradually becoming accepted that Wallerian degeneration is involved in numerous neurodegenerative diseases/injuries where axons and synapses are the primary pathological targets. This may include diseases where aggregates are formed and/or axonal transport is blocked. It is therefore important that the mechanism underlying Wallerian degeneration is elucidated.

6.1. Genotyping

By crossing various neurodegenerative disease models with *Wld*^{s} mice, it has become possible to test what type of neuronal insults *Wld*^{s} can help to protect against. The development of an efficient genotyping system (as detailed in chapter 3) through QRT-PCR should be of help to others working in this field in the future. It is also important to note that this method should, in theory, be applicable to other mutations and transgenic animals where there is a need to determine mutation/insert copy number.

6.2. Mapping

The mapping of Wld^{s} protein expression to neuronal nuclei throughout the CNS was one of the first clues that the *Wld*^{s} mutation may be affecting neuroprotection by some form of transcriptional regulation. The discovery that the pattern of protein localisation within neuronal nuclei changes during development, but is still never seen outside the nucleus may also be of some importance. The development of Wld^{s} protein inclusions within cerebellar granule cells (*in vivo* and *in vitro*) in particular, is especially important to note when taken in context with the discovery that cerebellar granule cells in culture take time to display the neuroprotective phenotype (Buckmaster *et al.* 1995).

Recent work carried out by my colleague Dr Jane Haley demonstrates electrophysiologically that cells in the hippocampus which develop Wld^{s} protein inclusions (CA3) display the *Wld*^{s} phenotype, but those which do not form inclusions (CA1) are not protected (Wishart et al. submitted, appendix 4.2). All of this information suggests that the formation of nuclear Wld^{s} protein aggregates are important for the neuroprotective phenotype. However, I have also demonstrated through the generation of constructs for *N70-Ube4b* and *Nmnat1* that neither portion of the *Wld*^{s} chimera is sufficient to form aggregates alone. Both are required for the formation of nuclear protein aggregates *in vitro* (Figure 5.11).

Whether or not the pattern of Wld^s immunostaining in nuclei is functional or not, the fact that it occurs offers the opportunity to discern which other molecules may associate with (or be segregated from) Wld^s as I have shown in the case of VCP and HDAC5. This could provide further data on the mechanism of *Wld^s* action.

6.3. Microarray

Mapping the Wld^s protein product throughout the nervous system showed that the richest source of Wld^s protein aggregates localised to neuronal nuclei, is the cerebellum. This tissue is an almost homogeneous cell population, due to the large number of cerebellar granule cells. Therefore it seemed appropriate that this should be the tissue to carry out a Microarray analysis.

Microarray analysis revealed 11 genes which were altered above the set threshold. The two most highly changed were *Pttg1* and *Edr1-L-EST*. The scope of the present data does not allow determination of whether the changes in transcript level are due to altered rates of RNA synthesis, altered turnover rate for existing levels of the RNAs examined or both of the above.

Both *Pttg1* and *Edr1-L-EST* remained the most highly altered RNAs examined following transfection of a Human cell line (HEK293). I cannot at this point say whether any of the genes examined are involved in the *Wld^s* phenotype. The changes in gene expression levels may have nothing to do with phenotype and may in fact be an unrelated but highly reproducible response to the presence of a large amount of Wld^s protein within the nucleus of the cells examined. The response will not simply be a response to a large amount of foreign protein within the cells (demonstrated in figure 5.7).

6.4. The NAD link

The recent study by Araki *et al.* (2004) suggested that the *Wld*^{s} phenotype is caused mainly by the *Nmnat1* portion of the *Wld*^{s} mutation, and can be mimicked through the addition of exogenous NAD. It was also shown that the mimicry of the phenotype occurs in a Sirt1 dependent fashion.

Addition of exogenous NAD to HEK293 cultures showed that few of the genes studied were affected by NAD addition and only *Pttg1*, *Fabp7* and *Src-LA* was affected in an NAD/Sirt1 dependent fashion. The other genes shown to be altered in the micrarray and HEK293 validation were not affectd by NAD and/or sirtinol addition. There was one exception to this; *Ssr-*α levels were potentiated by the addition of sirtinol alone suggesting that Sirt1 normally acts to suppress *Ssr-*α levels.

With the exception of the Araki study, there have been no other publications validating the NAD dependent protection of axons as the mechanism through which the *Wld*^{s} mutation is working, apart from a recent study by Wang *et al.* (2005). However, although the study by Wang *et al.* agree that it may in fact be NAD dependent protection of axons, mediated through local mechanisms, they suggest that NAD alone is not enough and do not completely agree with the findings of Araki *et al.*

6.5. Dissecting the *Wld*^{s} gene

However, as *Pttg1* and *Edr1-L-EST* showed the largest changes in the preliminary Microarray and transfection experiments I focussed on these. Transfection with separate constructs for the *Nmnat1* and *N70-Ube4b* portions of the *Wld*^{s} chimeric gene showed that *Pttg1* and *Edr1-L-EST* are differentially regulated by the two separate portions of the chimera respectively.

It is unlikely however, that either *Pttg1* or *Edr1-L-EST* alone, will be sufficient to induce a neuroprotective phenotype. The reasoning for this is as follows; *Nmnat1* overexpressing mice do not show delayed Wallerian degeneration *in vivo*. Overexpression of *Ube4b* also fails to induce the phenotype (M.P.Coleman personal communication). The only available mutant for any of the genes examined, *Pttg1* null mice, do not show delayed Wallerian degeneration (Gillingwater *et al.* 2005 submitted, Appendix 5.2).

6.6. How does *Wld*^{s} protect?

How might the *Wld*^{s} gene be affecting mRNA levels of these 11 genes? A preliminary examination of the Wld^{s} protein sequence did not highlight any zinc fingers or other motifs known for transcription factor interaction. However, the protein product of the mutation has not been the subject of much examination prior to this body of work. The most in depth study to date on Wld^{s} protein and its interactions was carried out recently by Laser *et al.* (2005 submitted) who have built on previous work detailing that Ufd2 in yeast is known to interact with VCP. It appears that the N70 portion of *Ube4b* contained within the *Wld*^{s} chimera is sufficient to interact with VCP. This protein functions as a chaperone for ubiquitinated proteins, ER associated degradation, nuclear envelope reconstruction, cell cycle, postmitotic Golgi reassembly and suppression of apoptosis, and may indirectly regulate transcription (Zhang *et al.* 2000).

The finding that the Wld^{s} protein aggregates co-localise with HDACs is also an interesting discovery as HDACs are also capable of affecting transcription via activating and repressing effects on target transcription factors, including retinoic acid receptor, thyroid hormone receptor and centromere binding factor-1 (as discussed in chapter 4).

As previously discussed, the *Wld*^{s} gene protects axons and synapses in both the central and peripheral nervous system from physical injury (Gillingwater & Ribchester 2003), toxic injury (Wang *et al.* 2001) and disease induced neurodegeneration e.g. Parkinson

disease (Sajadi *et al.* 2004) and motor neurone disease (Ferri *et al.* 2003). The inability to detect a non neuroprotective phenotype coupled with the ability to perpetuate the phenotype cross species suggests that the effect is limited to a few very specific conserved pathways. The work carried out by the Ribchester lab and its collaborators in combination with the work presented in this thesis could represent a significant step forward in elucidating these pathways. I would speculate that mimicry of the down stream effects of the *Wld*^{s} mutation could be sufficient to protect injured or diseased neuronal populations without having a detrimental effect on the surrounding non affected neuronal tissue.

Understanding the *Wld*^{s} protective phenotype may therefore be a very productive strategy for the development of therapies for neurodegenerative diseases or injuries where axons and/or synapses are the primary pathological targets.

6.7. Future directions

There are several main points that need to be addressed in the future;

1. *Are changes in expression of the candidate genes a conserved response in different neuronal populations which show the Wld*^{s} *neuroprotective phenotype?*

Do different areas of the *Wld*^{s} brain with different protein expression patterns show the same gene changes? If they don't, do those areas show a protective phenotype? The use of transgenic lines generated by Dr M.P.Coleman may also be of use in this respect as I have also mapped the protein distribution in 2 of his transgenic lines which show poor Wld^{s} protein expression in the cerebellum.

2. *Which components of the Wld*^{s} *gene are required to control the expression of the candidate genes?*

I have already shown differential regulation by the *Nmnat1* and *N70-Ube4b* portions of the Wld^{s} gene for the two most highly altered genes *Pttg1* and *Edr1-L-EST* as detailed

by the initial microarrays. The main problem with analysing the smaller changes at the moment is the transfection efficiency. This may however, have been overcome by the generation of an enriched population of Wld^S positive NSC34 immortalised motorneurone cell line (Dr P.Skehel).

3. *Which genes are the primary changes and which are downstream events?*

Examination of gene expression changes by QRT-PCR in HEK293 cells and/or NSC34 cells could illuminate temporal changes in gene expression. Following transfection at 6h, 12h, 24h, 2d, 3d and 4d it may be possible to determine which genes are altered by which time point. For example, if *Pttg1* and *Edr1-L-EST* are changed within 24 hours of transfection but the other genes are not altered until 3-4 days later, then they may be downstream compensatory changes which occur in response to the early changes in gene expression.

4. *What about protein?*

Studying changes in transcript level is interesting, but RNA levels do not necessarily relate to protein levels. For example, the attempt at identifying changes in Pttg1 protein levels were a failure due to poor antibody availability. Although Edr1 levels are not changed in *Wld^S* mice, the Edr1-L-EST levels are changed. I am not suggesting that there is definitely a protein product associated with this EST. It is a short sequence and could very well be a natural RNAi. However, the use of an Edr1 antibody (P.Dormer) suggested an increase in 2 forms of the Edr1 protein levels in *Wld^S* cerebellum. Depending on where about in the protein this antibody binds it may pick up the product of the EST. It is also important to carry out a more indepth study of the Wld^S protein itself. X-ray crystallography may provide insights into potential binding sites that conventional web based protein sequence analysis can not.

5. *Are changes in expression of these candidate genes necessary and/or sufficient to confer the Wld^S neuroprotective phenotype?*

Overexpression of a candidate gene that has increased expression levels in wild type tissue and look for a gain of phenotype. Overexpress a candidate gene that has decreased expression levels in *Wld^S* tissue and look for loss of phenotype. Knock down a candidate gene that has increased expression levels in wild type tissue and look for a gain of function. Any of these processes should help determine if any one gene is necessary and/or sufficient to confer the *Wld^S* neuroprotective phenotype. However, a combination of these processes may be required to test out combinations of candidate genes.

6. *What if we missed something?*

There may be many transcripts with altered levels in the Wld^S mouse but which were either excluded from the screen as they fell below the set cut off point, of they were classed as below detectable levels by the Microarray. Re-analysis of the Microarray output as a bioinformatics project may throw up something we missed. More microarrays may be required, but it will take a long time to exhaust the list of genes currently being investigated.

7. *What about synaptic phenotype?*

This will probably require more microarrays on young versus old homozygous *Wld^S*. It may also be worth carrying out the same microarrays on heterozygous *Wld^S* tissue as it is known that they have the axonal protection, but not the synaptic protection. For example, the levels of *Basp1* were altered in 2 of the 3 microarrays and the change was just below the set threshold level. However, preliminary RT-PCR showed that *Basp1* appears to be upregulated in *Wld^S* mouse cerebellum. *Basp1* is also known as *NAP22* and also has very high levels in the DRG, and declines with age in motor and sensory nerve terminals. Could this be a potential factor in the synaptic protection seen in *Wld^S* mice?

6.8. Summary

As a result of this body of work the following has been determined:

1. The mutation can be genotyped rapidly and effectively through the use of QRT-PCR on genomic DNA.

2. This process can also be applied to the determination of insertion copy number in transgenic lines.

3. The protein product of this mutation localizes exclusively to neuronal nuclei.

4. The conformation of localisation of this protein changes during development.

5. The protein product is mobile under some conditions.

6. The formation of nuclear aggregates is required for axonal protection (in conjunction with Dr Jane Haley and Dr Tom Gillingwater).

7. Wld^S protein aggregates colocalise with a member of the ubiquitin proteasome system (VCP) and histone deacetylase family (HDAC5), which can affect transcriptional regulation amongst other processes. It also colocalises to some extent with SMRT.

8. Expression of the *Wld*^{S} chimeric gene (N70-Ube4b- Nmnat-C303) is sufficient to give rise to altered RNA levels for at least 11 genes, in the spontaneous mutant and HEK293 cells.

9. Alteration of one of these genes alone (*Pttg1*) is not sufficient to provide the *Wld*^{S} neuroprotective phenotype (Dr Richard Ribchester and Dr Tom Gillingwater).

10. There is still a long way to go!

References

References

Amaxa Biosystems, http://www.axaxa.com Optimised protocol for primary mouse hippocampal neurons.

Adalbert, R., Gillingwater, T.H., Haley, J.E., Bridge, K., Beirowski, B., Berek, L., Wagner, D., Grumme, D., Thomson, D., Celik, A., Addicks, K., Ribchester, R.R. & Coleman, M.P. (2005). A rat model of slow Wallerian degeneration (WldS) with improved preservation of synapses. *European Journal of Neuroscience* **21,** 271– 7.

Anderson, R.M., Bitterman, K.J., Wood, J.G., Medvedk, O., Cohen, H., Lin, S.S., Manchester, J.K., Gordon, J.I. & Sinclair, D.A. (2002). Manipulation of nuclear NAD^+ salvage pathways delays aging without altering steady state NAD^+ levels. *The Journal of Biological Chemistry* **21,** 18881-18890.

Araki, T., Sasaki, Y & Milbrandt, J. (2004). Increased nuclear NAD biosynthesis and SIRT1 activation prevent axonal degeneration. *Science* **305,** 1010-1013.

Arrasate, M., Mitra, S., Schweitzer, E.S., Segal, M.R. & Finkbeiner, S. (2004). Inclusion body formation reduces levels of mutant huntingtin and the risk of neuronal death. *Nature* **431,** 805-10.

Avery, O.T., MacLeod, M.C. & McCarty, M. (1944). "Studies on the Chemical Nature of the Substance Inducing Transformation of Pneumococcal Types." *Journal of Experimental Medicine* **79,** 137-158.

Ballester, M., Castello. A., Sanchez, A. & Folch, J.M. (2004). Real-time quantitative PCR based system for determining transgene copy number in transgenic animals. *BioTechniques* **37,** 610-613.

Baltathakis, I., Alcantara, O. & Boldt, D.H. (2001). Expression of different NF-κB pathway genes in dendritic cells (DCs) or macrophages assessed by gene expression profiling. *Journal of Cellular Biochemistry* **83,** 281-290.

Be'eri,H., Reichert,F., Saada,A. & Rotshenker, S. (1998). The cytokine network of Wallerian degeneration:IL-10 and GM-CSF. *European Journal of Neuroscience* **10,** 2707-2713.

Benavides, E. & Alvarez, J. (1998). Peripheral axons of Wld^s mice, which regenerate after a delay of several weeks, do so readily when transcription is halted in the distal stump. *Neuroscience Letters* **258,** 77-80.

Bernal, J.A., Luna, R., Espina, A., Lazaro, I., Ramos-Morales, F., Romero, F., Arias, C., Silva, A., Tortolero, M. & Pintor-Toro, J.A. (2002). Human securin interacts with p53 and modulates p53-mediated transcriptional activity and apoptosis. *Nature Genetics* **32,** 306-311.

Berry. M., Barrett. L., Seymour. L., Baird. A. & Logan A. (2001). Gene therapy for central nervous system repair. *Current Opinion Molecular Therapy* **3,** 338-349.

Bisby, M.A. & Chen, S. (1990). Delayed Wallerian degeneration in sciatic nerves of C57BL/Ola mice is associated with impaired regeneration of sensory axons. *Brain Research* **530,** 117-120.

Bisby, M.A., Tetzlaff, W. & Brown, M.C. (1995). Cell body response to injury in motorneurones and primary sensory neurones of a mutant mouse, Ola (Wld), in which Wallerian degeneration is delayed. *Journal of Comparative Neurology* **359,** 653-662.

Blander, G. & Guarent, L. (2004). The Sir2 family of protein deacetylases. *Annual Review of Biochemistry* **73,** 417-435.

Boelart, K., Tannahill, L.A., Bulmer, J.N., Kachilele, S., Chan, S.Y., Kim, D., Gittoes, N.J., Franklyn, J.A., Kilby, M.D. & McCabe, C.J. (2003). A potential role for PTTG/securin in the developing human fetal brain. *FASEB Journal* **17,** 1631-1639.

Brown, M.C., Lunn, E.R. & Perry, V.H. (1992a). Poor growth of mammalian motor and sensory axons into intact proximal nerve stumps. *European Journal of Neuroscience* **3,** 1366-1369.

Brown, M.C., Lunn, E.R. & Perry, V.H. (1992b). Consequences of slow Wallerian degeneration for regenerating motor and sensory axons. *Journal of Neurobiology* **23,** 521-536.

Brown, M.C., Perry, V.H., Hunt, S.P. & Lapper, S.R. (1994). Further studies on motor and sensory nerve regeneration in mice with delayed Wallerian degeneration. *European Journal of Neuroscience* **6,** 420-428.

Brunet, A., Sweeny, L.B., Sturgill, J.F., Chua, K.F., Greer, P.L., Lin, Y., Tran, H., Ross, S.E., Mostolavsky, R., Cohen, H.Y., Hu, L.S., Cheng, H.L., Jedrychowski, M.P., Gygi, S.P., Sinclair, D.A., Alt, F.W. & Greenberg, M.E. (2004). Stress-dependent regulation of FOXO transcription factors by the SIRT1 deacetylase. *Science* **303,** 2011-2015.

Buckmaster,E.A., Perry, V.H. & Brown, M.C. (1995). The rate of Wallerian degeneration in cultured neurons from wild type and C57Bl/Wld^{s} mice depends on time in culture and may be extended in the presence of elevated K^{+} levels. *European Journal of Neuroscience* **7,** 1596-1602.

Büttner, B., Kannicht, C., Schmidt, C., Löster, K., Reutter, W., Lee, H.Y., Nöhring, S. & Horstkorte, R. (2002). Biochemical Engineering of Cell Surface Sialic Acids Stimulates Axonal Growth. *The Journal of Neuroscience* **22,** 8869-8875.

Cech, T.R. (1986). A model for the RNA-catalyzed replication of RNA. *PNAS USA* **83,** 4360-4363.

Chawla, S., Vanhoutte, P., Arnold, F.J.L., Huang, C.L.H. & Bading, H. (2003). Neuronal activity-dependent nucleocytoplasmic shuttling of HDAC4 and HDAC5. *Journal of Neurochemistry* **85,** 151–159

Chen, S. & Bisby, M.A. (1993). Long-term consequences of impaired regeneration on facial motoneurones in the C57BL/Ola mouse. *Journal of Comparative Neurology* **335,** 576-585.

Chung, C.Y., Seo, H., Sonntag, K.C., Brooks, A., Lin, L. & Isacson, O. (2005). Cell type specific gene expression of midbrain dopaminergic neurons reveals molecules involved in their vunerability and protection. *Human Molecular Genetics* **14,** 1709-1725.

Clayton, D.F. & George, J.M. (1999). Synucleins in synaptic plasticity and neurodegenerative disorders. *Journal of Neuroscience* **58,** 120-129.

Coleman M.P. & Ribchester R.R. (2004). Programmed axon death, synaptic dysfunction and the ubiquitin proteasome system. *Current Drug Targets – CNS & Neurological Disorders* **3,** 153-160.

Coleman, M.P. & Perry, V.H. (2002). Axon pathology in neurological disease: a neglected theraputic target. *Trends in Neurosciences* **25,** 532-537.

Coleman, M.P., Conforti, L., Buckmaster, E.A., Tarlton, A., Ewing, R.M., Brown, C.M., Lyone, M.F. & Perry, V.H. (1998). An 85-Kb tandem triplication in the slow Wallerian degeneration (Wld^S) mouse. *Proceedings of the National Academy of Sciences of the USA* **95,** 9985-9990.

Coleman, M.P., Mack, T.G.A., Beirowski, B., Reiner, M., Samsam, M., Ferri, A., Mi, W., Emanuelli, M., Wagner, D., Thomson, D., Gillingwater, T., Addicks, K., Magni, G., Kato, A., Martini, R., Perry, V.H. & Ribchester, R.R. (2002). A Ube4b/Nmnat chimeric gene (Wld^S) protects injured axons from Wallerian degeneration and alleviated some neurodegenerative diseases. *FENS Forum 2002,* Session 225-Trauma, **Abstract 225.1**.

Conforti, L., Tarlton A., Mack, T.G.A., Mi, W., Buckmaster E.A., Wagner, D., Perry V.H. & Coleman, M.P. (2000). A Ufd2/D4Cole1e chimeric protein and overexpression of Rbp7 in the slow Wallerian degeneration (Wld^S) mouse. *PNAS* **97,** 11377-11382.

Court, F. & Alvarez, J. (2000). Nerve regeneration is normalised by actinomycin D. *Brain Research* **867,** 1-8.

Courtney.M.J., Lambert.J.J. & Nicolles.D.G. (1990). Interactions between PM depolarisation and glutamate receptor activation in the regulation of cytoplasmic free calcium in cultured cerebellar granule cells. *Journal of Neuroscience* **10,** 3873-3879.

Crawford, T.O., Hsieh, S.T., Schryer, B.L. & Glass, J.D. (1995). Prolonged axonal survival in transected nerves of C57BL/Ola mice is independent of age. *Journal of Neurocytology* **24,** 333-340.

Crick, FH. (1994). The astonishing hypothesis: The scientific search for the soul. New York: Scribner. 317.

Cull-Candy.S.G., Howe.J.R. & Ogden.D.C. (1988). Noise and single channels activated by excitatory amino acids in rat cerebellar granule neurones. *Journal of Physiology* **400,** 189-222.

Datson, N.A., Meijer, L., Steenbergen, P.J., Morsink, M.C., van der Laan, S., Meijer, O.C. & de Kloet, E.R. (2004) Expression profiling in laser-microdissected hippocampal subregions in rat brain reveals large subregion-specific differences in expression. *European Journal of Neuroscience* **20,** 2541-2554.

Deckwerth T.L. & Johnson E.M. (1994). Neurites can remain viable after destruction of the neuronal soma by programmed cell death (Apoptosis). *Developmental Biology* **165,** 63-72.

Descartes, R. (1664). *L'Homme.*

Dijkstra, I.M., Hulshof, S., van der Valk, P., Boddeke, H.W.G.M. & Biber, K. (2004). Cutting edge: activity of human adult microglia in response to CC chemokine ligand 21. *Journal of Immunology* **172,** 2744-2747.

Dityateva. G., Hammond. M., Thiel. C., Ruonala. M.O., Delling. M., Siebenkotten. G., Nix. M. & Dityatev. A. (2003). Rapid efficient electroporation-based gene transfer into primary dissociated neurones. *Journal of Neuroscience Methods* **130,** 65-73

Dormer, P., Spitzer, E. & Moller, W. (2004). EDR is a stress-related survival factor from stroma and other tissues acting on early haematopoietic progenitors (E-Mix). *Cytokine* **27,** 47-57.

Dower, W.J., Miller, J.F. & Ragsdale, C.W. (1998). High efficiency transformation of E.coli by high voltage electroporation. *Nucleic Acids Research* **16,** 6127-45.

Edwards, S.N., Buckmaster, A.E. & Tolkovsky, A.M. (1991). The death programme in cultured sympathetic neurones can be suppressed at the post translational level by nerve growth factor, cyclic AMP and depolarization. *Journal of Neurochemistry* **57,** 2140-2143.

Everett, C,M. & Wood, N.W. (2004). Trinucleotide repeats and neurodegenerative disease. *Brain* **127,** 2385-2405.

Fang, C., Silva, M.B., Coleman, M.P. & Perry, V.H. (2005). The cellular distribution of the Wld^s chimeric protein and its constituent proteins in the CNS. *Neuroscience* **In Press**.

Fernando, F.S., Conforti, L., Tosi, S., Smith, A.D. & Coleman, M.P. (2002). Human homologue of a gene mutated in the slow Wallerian degeneration (C57Bl/Wld^s) mouse. *Gene* **284,** 23-29.

Ferri, A., Sanes, J.R., Coleman, M.P., Cunningham, J.M. & Kato, A.C. (2003). Inhibiting axon degeneration and synapse loss attenuates apoptosis and disease progression in a mouse model of motorneurone disease. *Current Biology* **13,** 669-673.

Fujiki, M., Zhang, Z., Guth, L. & Steward, O. (1996). Genetic influences on cellular reactions to spinal cord injury: activation of macrophages/microglia and astrocytes is delayed in mice carrying a mutation (Wld^s) that causes delayed Wallerian degeneration. *Journal of Comparative Neurology* **371,** 469-484.

Gallo.V., Giovannini.C., Suergiu.R. & Levi.G. (1989). Expression of excitatory amino acid receptors by the cerebellar cells of the type-2 astrocyte cell lineage. *Journal of Neurochemistry* **52,** 1-9.

George, A., Buehl, A. & Sommer, C. (2004). Wallerian degeneration after crush injury of rat sciatic nerve increases endo- and epineurial tumor necrosis factor-alpha protein. *Neuroscience Letters* **372,** 215-219.

Gilbert, W. (1986).The RNA world. *Nature* **319,** 618

Gillingwater, T.H., Haley, J.E., Ribchester, R.R. & Horsburgh, K. (2004) Neuroprotection Following Transient Global Cerebral Ischaemia in Wlds Mutant Mice. *Journal of Cerebral Blood Flow and Metabolism* **24,** 62-66.

Gillingwater, T.H. & Ribchester, R.R. (2001). Compartmental Neurodegeneration and Synaptic Plasticity in the Wld^s Mutant Mouse. *Journal of Physiology* **534,** 627-639.

Gillingwater, T.H. & Ribchester, R.R. (2003). The relationship of neuromuscular synapse elimination to synaptic degeneration and pathology: Insights from Wld^s and other mutant mice. *Journal of Neurocytology* **32,** 863-881.

Gillingwater, T.H., Ingham, C.A., Wright, A.K., Haley, J.E., Wishart, T.M., Arbuthnott, G.W. & Ribchester, R.R. Synaptic protection in the central nervous system of Wld^s mutant mice following cortical ablation. *Submitted.*

Gillingwater, T.H., Thomson, D., Mack, T.G.A., Soffin, E.M., Mattison, R.J., Coleman, M.P. & Ribchester, R.R. (2002). Age-dependent synapse withdrawal at axotomised neuromuscular junctions in Wld^s mutant and Ube4b/Nmnat transgenic mice. *Journal of Physiology* **543.3,** 739-755.

Gillingwater, T.H., Wishart, T.M., Chen, P.E., Haley, J.E., Robertson, K., MacDonald, S.H.F., Middleton, S.E., Wawrowski, K., Shipston, M.J., Melmed, S., Wyllie, D.J.A., Skehel, P.A., Coleman, M.P. & Ribchester. R.R. (2005). The Neuroprotective Wlds

Gene Regulates Expression of PTTG1 and Erythroid Differentiation Regulator 1-Like Gene in Mice and Human Cells. *Human Molecular Genetics* **In Press.**

Gillingwater.T.H. (2001). Degeneration of the neuromuscular synaptic compartment in normal and mutant Wld^s mice. *PhD thesis.* The University of Edinburgh.

Glass, J.D. & Griffin, J.W. (1991). Neurofilament redistribution in transected nerves: evidence for bidirectional transport of neurofilaments. *Journal of Neuroscience* **11,** 3146-3154.

Glass, J.D., Brushart, T.M., George, E.B. & Griffin, J.W. (1993). Prolonged survival of transected nerve fibres in C57BL/Ola mice is an intrinsic characteristic of the axon. *Journal of Neurocytology* **22,** 311-321.

Grey, D.A. (2001). Damage control – a possible non-proteolytic role for ubiquitin in limiting neurodegeneration. *Neuropathology and Applied Neurobiology* **27,** 89-94.

Hershey, A.D. & Chase, M. (1952) independent functions of viral protein and nucleic acid in growth of bacteriophage. *Journal of General Physiology* **36,** 39-56.

Hershko, A. and Ciechanover, A. (1998). The ubiquitin system. *Annual Review of Biochemistry* **67,** 425-479.

Hicke, L. (2001). Protein regulation by monoubiquitin. *Nature Reviews Molecular Cell Biology* **2,** 195-201.

Ikegam, K. & Koike, T. (2003). Non –apoptotic neurite degeneration in apoptotic neuronal death: pivotal role of mitochondrial function in neurites. *Neuroscience* **122,** 617-626.

Iniguez, A. & Alvarez, J. (1999). Isolated axons of Wld^s mice regrow centralward. *Neuroscience letters* **268,** 108-110.

Jesenberger, V. and Jentsch, S. (2002). Deadly encounter: Ubiquitin meets apoptosis. *Nature Reviews Molecular Cell Biology* **3,** 112-121.

Jin. Y., Xu, X.L., Yang, M.C.W., W, F., Ayi, T.C. & Bowcock, A.M. (1997). Cell cycle dependent colocalisation of BARD1 and BRCA1 proteins in discrete nuclear domains. *Proceedings of the National Academy of Science* **94,** 12075-12080.

Kaneko C, Hatakeyama S, Matsumoto M, Yada M, Nakayama K, Nakayama KI. (2003). Characterization of the mouse gene for the U-box-type ubiquitin ligase UFD2a. Biochem. Biophys. Res. Commun. **300,** 297-304.

Kirby, J., Halligan, E., Baptista, M.J., Allen, S., Heath, P.R., Holden, H., Barber, S.C., Loynes, C.A., Allum, C.A.W., Lunec, J. & Shaw, P.J. (2005). Mutant SOD1 alters the motor neuronal transcriptome: implications for familial ALS. *Brain* **128,** 1686-1706.

Kissil, J.L., Cohen, O., Raveh, T. & Kimchi, A. (1999) Structure-function analysis of an evolutionary conserved protein, DAP3, which mediates TNF-alpha- and Fas-induced cell death. *EMBO Journal* **18,** 353-362.

Koegl, M., Hoppe, T., Schlenker, S., Ulrich, H.D., Mayer, T.U. & Jentsch, S. (1999). A novel ubiquitination factor, E4, is involved in multiubiquitin chain assembly. *Cell* **96,** 635-644.

Korhonen, L. & Lindholm, D. (2004) The ubiquitin proteasome system in synaptic and axonal degeneration: a new twist to an old cycle. *Journal of Cell Biology* **165,** 27-30.

Kornberg, A. (1959). The biologic synthesis of deoxyribonucleic acid. *Nobel Lecture.*

Kwok, S. & Higuchi, R. (1989). Avoiding false positives with PCR. *Nature* **339,** 237-238.

Kyrylenko, S., Kyrylenko, O., Suuronen, T. & Salminen, A. (2003). Differentail regulation of the Sir2 histone deacetylase gene family by inhibitors of class I & II histone deacetylases. *Cellular and Molecular Life Sciences* **60,** 1990-1997.

Laird, P.W., Zijderveld, A., Linders, K., Rudnicki, M.A., Jaenisch, R. & Berns, A. (1991). Simplified mammalian DNA isolation procedure. *Nucleic Acids Research* **19,** 4293-4297.

Laribee, R.N., Krogan, N.J., Xiao, T., Shibata, Y., Hughes, T.R., Greenblatt, J.F. & Strahl, B.D. (2005). Bur kinase selectively regulates H3 K4 trimethylation and H2B ubiquitylation through recruitment of the PAF elongation complex. *Current Biology* **In Press**

Laser, H., Conforti, L., Morreale, G., Mack, T.G., Heyer, M., Haley, J.E., Wishart, T.M., Hoppe|, T., Beirowski, B., Haase, G., Celik, A., Adalbert, R., Wagner, D., Grumme, D., Ribchester, R.R., Plomann, M. & Coleman, M.P. Slow Wallerian degeneration protein, Wld^S, alters nuclear distribution of valosin containing protein, ubiquitin and NAD synthesis machinery. *Molecular Biology of the Cell* **In Press**.

Lawson, L.J., Frost, L., Risbridger, S., Fearn, S. & Perry, V.H. (1994). Quantification of the mononuclear phagocyte response to Wallerian degeneration of the optic nerve. *Journal of Neurocytology* **23,** 729-744.

Lin, Y., Randall, W.R. & Schneider, M.F. (2005). Activity dependent and independent nuclear fluxes of HDAC4 mediated by different kinases in adult skeletal muscle. *Journal of Cell Biology* **168,** 887-97.

Liu, T., Rooijen, N.V. & Tracey, D.J. (2000). Depletion of macrophages reduces axonal degeneration and hyperalgesia following nerve injury. *Pain* **86,** 25-32.

Llinás, R.R. (1975). The cortex of the cerebellum. *Scientific American* **232,** 56-71.

Lopukhov, L.V., Ponomareva, A.A. & Yagodian, L.O. (2002). Amyloglucosiadase suppresses interference by glycogen in the quantification of DNA using the Hoechst 3258 Dye. *Biotechniques* **32,** 1250-1256.

Ludwin, S.K. & Bisby, M.A. (1991). Delayed Wallerian degeneration in the central nervous system of Ola mice: an utrastructural study. *Journal of the Neurological Sciences* **109,** 140-147.

Lunn, E.R., Perry, V.H., Brown, M.C., Rosen, H. & Gordon, S. (1989). Absence of wallerain degeneration does not hinder regeneration in peripheral nerve. *European Journal of Neuroscience* **1,** 27-33.

Luo, J., Nikolaev, A.Y., Imai. S.I, Chen, D., Su, F., Shiloh, A., Guarente, L. & Gu, W. (2001). Negative control of p53 by Sir2α promotes cell survival under stress. *Cell* **107,** 137-148.

Lyon, M.F., Ogunkolade, B.W., Brown, M.C., Atherton, D.J. & Perry, V.H. (1993). A gene affecting Wallerian nerve degeneration maps distally on mouse chromosome 4. *Proceedings of the National Academy of Sciences of the USA* **90,** 9717-9720.

MacInnis, B.L. & Campenot, R.B. (2004). Regulation of Wallerian degeneration and nerve growth factor withdrawal-induced pruning of axons of sympathetic neurons by the proteasome and the MEK/Erk pathway. *Molecular and Cellular Neuroscience.* **In Press.**

Mack, T.G.A., Reiner,M., Beirowski, B., Mi, W., Emanuelli, M., Wagner, D., Thomson, D., Gillingwater, T., Court, F., Conforti, L., Fernando, F.S., Tarlton, A., Andressen, C., Addicks, K., Magni, G., Ribchester, R.R., Perry, V.H. & Coleman, M.P. (2001). Wallerain degeneration of injured axons and synapses is delayed by a Ube4b/Nmnat chimeric gene. *Nature Neuroscience* **4,** 1199-1206.

Mendel, Gregor. (1865). Experiments in Plant Hybridization. http://www.mendelweb.org/Mendel.html#sB

Temin, H.M. & Mizutani, S. (1970). RNA-dependent DNA polymerase in virions of Rous sarcoma virus. *Nature* **226,** 1211-1213.

Meselson, M. & Stahl, F.W. (1958). The Replication of DNA in *Escherichia Coli. PNAS* **44,** 671-682.

Mi, W., Conforti, L. & Coleman, M.P. (2002). Genotyping Methods to Detect a Unique Neuroprotective Factor (Wlds) for Axons. *Journal of Neuroscience Research* **113,** 215-218.

Mi, W., Conforti, L. & Coleman, M.P. (2002). The slow Wallerian degeneration mutation (Wld^s): genotyping methods and mutation stability studies. *FENS Forum 2002,* Session 225-Trauma, **Abstract 225.2.**

Mi, W., Glass, J.D. & Coleman, M.P. (2003). Stable inheritance of an 85 Kb triplication in C57BL/Wld^s mice. *Mutation research* **526,** 33-37.

Mi. W, Beirowski. B, Gillingwater. T.H, Adalbert. R, Wagner. D, Grumme. D, Osaka. H, Conforti. L, Arnhold. S, Addicks. K, Wada. K, Ribchester. R.R & Coleman. M.P. (2005) The slow Wallerian degeneration gene, WldS, inhibits axonal spheroid pathology in gracile axonal dystrophy mice. *Brain* **128,** 405-16.

Miledi R, Slater CR. (1968). Electrophysiology and electron-microscopy of rat neuromuscular junctions after nerve degeneration. *Proc R Soc Lond B Biol Sci* **169,** 289-306.

Miledi R, Slater CR. (1970). On the degeneration of rat neuromuscular junctions after nerve section. *Journal of Physiology* **207,** 507-528.

Motta, M.C., Divecha, N., Lemieux, M., Kamel, C., Chen, D., Gu, W., Bultsma, Y., McBurney, M. & Guarente, L. (2004). Mammalian Sirt1 represses forkhead transcription factors. *Cell* **116,** 551-563.

Muratani, M. & Tansey, W.P. (2003). How the ubiquitin proteasome system controls transcription. *Nature Reviews Molecular and Cellular Biology* **4,** 192-201.

Muratani, M., Kung, C., Shokat, K.M. & Tansey, W.P. (2005). The F box potein Dsg1/Mdm30 is a transcriptional coactivator that stimulates Gal4 turnover and cotranscriptional mRNA processing. *Cell* **120,** 887-899.

Parson, S.H., Mackintosh, C.L. & Ribchester, R.R. (1997). Elimination of motor nerve terminals in neonatal mice expressing a gene for slow wallerian degeneration (C57Bl/Wlds). *European Journal of Neuroscience* **9,** 1586-1592.

Perrin, R.J., Woods, W.S., Clayton, D.F & George, J.M. (2000). Interaction of human α-Synuclein and Parkinson's disease variants with phospholipids. *Journal of Biological Chemistry* **275,** 34393-34398.

Perry, V.H., Brown, M.C. & Lunn, E.R. (1990). Very slow retrograde and Wallerian degeneration in the CNS of C57BL/Ola mice. *European Journal of Neuroscience* **3,** 102-105.

Perry, V.H., Brown, M.C. & Tsao, J.W. (1992). The effectiveness of the gene, which slows the rate of Wallerian degeneration in C57Bl/Ola mice, declines with age. *European Journal of Neuroscience* **4,** 1000-1002.

Perry, V.H., Lunn, E.R., Brown M.C., Cahusac S. and Gordon S. (1990). Evidence that the rat of Wallerian degeneration is controlled by a single autosomal dominant gene. *European Journal of Neuroscience* **2,** 408-413.

Peters, I.R., Helps, C.R., Hall, E.J. & Day, M.J. (2004). Real-time RT-PCR: considerations for efficient and sensitive assay design. *Journal of Immunological Methods* **286,** 203– 217.

Qiu-Yue, H., Man-Fu, H., Ohnishi, A., Yamamoto, T. & Murai, Y. (1997). Differential effects of acrylimide on the degeneration and regeneration of myelinated fibres between C57BL/Ola and C57BL/6J mice after crush injury. *J UOEH* **19,** 265-275.

Rafaelli, N., Sorci, L. and Amici, A. (2002). Identification of a novel human nicotinamide mononucleotide adenyltransferase. *Biochemical and Biophysical Research* **297,** 835-840.

Raff, M.C., Whitmore, A.V. & Finn, J.T. (2002). Axonal self-destruction and neurodegeneration. *Science* **296,** 868-871.

Ramer, M.S., French, G.D. & Bisby, M.A. (1997). Wallerain degeneration is required for both neuropathic pain and sympathetic sprouting into the DRG. *Pain* **72,** 71-78.

Revollo, J.R., Grimm, A.A. & Imai, S.I. (2004). The NAD biosynthesis Pathway mediated by nicotanamide phosphoribosyltransferase regulates Sir2 activity in mammalian cells. *The Journal of Biological Chemistry* **49,** 50754-50763.

Ribchester, R.R., Tsao, J.W., Barry, J.A., Asgari-Jirhandeh, N., Perry, V.H. & Brown, M.C. (1995). Persistance of neuromuscular junctions after axotomy in mice with slow Wallerian degeneration (C57BL/Wld^{s}). *European Journal of Neuroscience* **7,** 1641-1650.

Salghetti, S.E., Muratani, M., Wijnen, H., Futcher, B. & Tansey, W.P. (2000). Functional overlap of sequences that activate transcription and signal ubiquitin mediated proteolysis. *Proceedings of the National Academy of Sciences* **97,** 3118-3123.

Samsam M, Mi W, Wessig C, Zielasek J, Toyka K.V., Coleman M.P. & Martini R. (2003). The Wlds mutation delays robust loss of motor and sensory axons in a genetic model for myelin-related axonopathy. *Journal of Neuroscience* **23,** 2833-2839.

Sajadi A., Schneider B.L. & Aebischer, P. (2004). Wlds-mediated protection of dopinergic fibres in an animal model of Parkinson disease. *Current Biology* **14,** 326-330.

Schafer, M., Fruttiger, M., Montag, D., Schachner, M. & Martini, R. (1996). Disruption of the gene for the Myelin-Associated Glycoprotein improves regrowth along myelin in C57BL/Wld^{s} mice. *Neuron* **16,** 1107-1113.

Schroder, R., Watts, G.D., Mehta, S.G., Evert, B.O., Broich, P., Fliessbach, K., Pauls, K., Hans, V.H., Kimonis, V. and Thal, D.R. (2005). Mutant valosine containing protein causes a novel type of frontotemporal dementia. *Annuls of Neurology* **57,** 457-461.

Schweiger M., Hennig K., Lerner F., Niere M., Hirsch-Kauffmann M., Specht T., Weise C., Oei S.L. & Ziegler M. (2001). Characterization of recombinant human nicotinamide mononucleotide adenylyl transferase (NMNAT), a nuclear enzyme essential for NAD synthesis. *FEBS Lett.* **492,** 95-100.

Seigneurin-Berny, D., Verdel, A., Curtet, S., Lemercier, C., Garin, J., Rosseaux, S. & Khochbin, S. (2001). Identification of components of the murine histone deacetylase 6 complex : Link between acetylation and ubiquitin signalling pathways. *Molecular and Cellular Biology* **21,** 8035-8044.

Shamash, S., Reichert, F. & Rotshenker, S. (2002). The cytokine network of wallerian degeneration: tumor necrosis factor-α, interleukin-1α, and interleukin 1β. *Journal of Neuroscience* **22,** 3052-3060.

Shi, B. & Stanfield, B.B. (1996). Differential sprouting in axonal fiber systems in the dentate gyrus following lesions of the perforant path in Wld^s mutant mice. *Brain Research* **740,** 89-101.

Sommer, C. & Schafers, M. (1998). Painful mononeuropathy in C57BL/Wld mice with delayed Wallerain degeneration: differential effects of cytokine production and nerve regeneration on thermal and mechanical hypersensitivity. *Brain research* **784,** 154-162.

Sternsdorf, T., Jensen, K., Reich, B. & Will, H. (1999) The nuclear dot protein Sp100, characterisation of domains necessary for dimerisation, subcellular localisation and modification by small ubiquitin like modifiers. *The Journal of Biochemistry* **274,** 12555-12566.

Stoll, G., Jander, S. & Myers, R.R. (2002). Degeneration and regeneration of the peripheral nervous system: From Augustus Waller's observations to neuroinflammation. *Journal of the Peripheral Nervous system* **7,** 13-27.

Strasbourge *et al.* Mammalian Gene Collection (MGC) Program Team. 2002. Generation and initial analysis of more than 15,000 full-length human and mouse cDNA sequences. *Proc. Natl. Acad. Sci. USA.* **99**, 16899-16903.

Subang, M.C., Bisby, M.A. & Richardson, P.M. (1997). Delay of CNTF decrease following peripheral nerve injury in C57BL/Wld mice. *Journal of Neuroscience Research* **49,** 563-586.

Teare, J.M., Islam, R., Flanagan, R., Gallager, S, Davies, M.G. & Grabau, C. (1997). Measurement of nucleic acid contrations using the DyNA Quant™ and the GeneQuant™. *Biotechniques* **22,**1170-1174.

Büttner, B., Kannicht, C., Schmidt, C., Löster, K., Reutter, W., Lee, H.Y., Nöhring, S. & Horstkorte, R. (2002). Biochemical Engineering of Cell Surface Sialic Acids Stimulates Axonal Growth. The Journal of Neuroscience **22**, 8869-8875.

Tsao, J.W., Brown, M.C., Carden, M.J., McLean, W.G. & Perry, V.H. (1994). Loss of compound action potential: an electrophysiological, biochemical and morphological study of early events in axonal degeneration in the C57BL/Ola mouse. *European Journal of Neuroscience* **6,** 516-524.

Tsao, J.W., George, E.B. & Griffin, J.W. (1999). Temperature modulation reveals three distinct stages of Wallerian degeneration. *The Journal of Neuroscience* **19,** 4718-4726.

Tsao, J.W., Parmananthan, N., parkes, H.G. & Dunn, J.F. (1999). Altered brain metabolism in the C57BL/Wld mouse strain detected by magnetic resonance spectroscopy: association with delayed Wallerian degeneration? *Journal of Neurological Sciences* **168,** 1-12.

Van Vliet. B.J., Sebben. M., Dumuis. A., Gabrion. J., Bockaert. J. & Pin. J.P. (1989). Endogenous amino acid release from cultured cerebellar neuronal cells: Effects of tetanus toxin on glutamate release. *Journal of Neurochemistry* **52,** 1229-1239.

Wang M.S., Fang G, Culver D.G., Davis A.A., Rich M.M. & Glass J.D. (2001). The Wld^S protein protects against axonal degeneration: a model of gene therapy for peripheral neuropathy. *Annules of Neurology* **50,** 773-779.

Wang, J., Zhai, Q., Chen, Y., Lin, E., Gu, W., McBurney, M.W. & He, Z. (2005). A local mechanism mediates NAD dependent protection of axon degeneration. *Journal of Cell Biology* **170,** 349-355.

Wang, M.S., Davis, A.A., Culver, D.G. & Glass, J.D. (2002). Wld^S mice are resistant to paclitaxel (Taxol) neuropathy. *Ann Neurol* **52,** 442-447.

Watson, D.F., Glass, J.D. & Griffin, J.W. (1993). Redistribution of cytoskeletal proteins in mammalian axons disconnected from their cell bodies. *The Journal of Neuroscience* **13,** 4354-4360.

Watts, G.D., Wymer, J., Kovach, M.J., Mehta, S.G., Mumm, S., Darvish, D., Pestronk, A., Whyte, M.P. & Kimonis, V.E. (2004). Inclusion body myopathy associated with Paget diseas of bone and frontotemporal dementia is caused by mutant valosine containing protein. *Nature Genetics* **36,** 377-381.

Wishart, T.M.,Haley, J.E., Gillingwater, T.H., Mack, T.G., Beirowski, B., Coleman, M.P. & Richard R. Ribchester. Mosaic Distribution of Chimerical Neuroprotective Protein Expression in the Nervous System of WldS Mutant Mice and Rats. *Under review.*

Wojcik, C. (2002). VCP-the missing link in protein degradation? *Trends in Cell Biology* **12,** 212.

Wu, Xiaoyang., Li, Hui., Park, J.E. & Chen, D. (2001). SMRTe Inhibits MEF2C Trnscriptional Activation by Targeting HDAC4 and 5 to Nuclear Domains. *The Journal of Biochemistry* **29,** 24177-24185.

Xiao, T., Kao, C.F., Krogan, N.J., Sun, Z.W., Greenblatt, J.F., Osley, M.A. & Strahl, B.D. (2005). Histone H2B ubiquitylation is associated with elongating RNA polymerase II. *Molecular Cell Biology* **25,** 637-651.

Xue, L., Borutaite, V. & Tolkovsky, A.M. (2002). Inhibition of mitochondrial permeability transition and release of cytochrome c by anti-apoptotic nucleoside analogues. *Biochem. Pharmacol.***64,** 441-449.

Xue, L., Fletcher, G.C. & Tolkovsky, A.M. (2001). Mitochondria are selectively eliminated from eukaryotic cells after blockade of caspases during apoptosis. *Current Biology* **11,** 361-365.

Yamanaka, K., Okubo, Y., Suzaki, T, & Ogura, T. (2004). Analysis of the two p97/VCP/Cdc48p proteins of Caenorhabditid elegans and their suppression of polyglutamine induced protein aggregation. *Journal of Structural Biology* **146,** 242-250.

Yeung, F., Hoberg, J.E., Ramsey, C.S., Keller, M.D., Jones, D.R., Frye, R.A. & Mayo, M.W. (2004). Odulation of NF-KB- dependent transcription and cell survival by the SIRT1 deacetylase. *EMBO* **23,** 2369-2380.

Zhai, Q., Wang, J., Kim, A., Liu, Q., Watts, R., Hoopfer, E., Mitchison, T., Luo, L. & He, Z. (2003). Involvement of the ubiquitin-proteasome system in the early stages of Wallerian degeneration. *Neuron* **39,** 217-225.

Zhang, H., Wang, Q., Kajino, K., & Greene, M.I. (2000). VCP, a weak ATPase involved in multiple cellular events, interacts physically with BRCA1 in the nucleus of living cells. *DNA Cell Biol.* **19**, 253-263.

SELECTED ABSTRACTS

Society for Neuroscience meeting, San Diego, October 2004.

Abstract View

NUCLEAR EXPRESSION OF WLD PROTEIN IS REQUIRED FOR AXONAL AND SYNAPTIC PROTECTION IN THE CNS OF WLD^S MICE

J.E.Haley[1]; T.M.Wishart[1]; T.H.Gillingwater[1]; C.A.Ingham[1]; A.K.Wright[1]; G.W.Arbuthnott[1]; R.Adalbert[2]; M.P.Coleman[2]; R.R.Ribchester[1]

1. Neurosci., Edinburgh Univ., Edinburgh, United Kingdom

2. The Babraham Inst., Cambridge, United Kingdom

The Wld^S mouse mutant shows a 10-fold delay in neurodegeneration after peripheral nerve lesions or transient global ischemia (Gillingwater et al., 2004, JCBFM, PMID:14688617). This neuroprotection arises from a spontaneous gene triplication yielding expression of a chimeric gene N70-Ube4b/NMNAT coding for the Wld fusion protein. We used a specific Wld antibody to immunocytochemically map the profile of Wld expression in the brains of Wld^S mice and their transgenic equivalents in mice and rats. Regardless of the promoter driving Wld gene expression, Wld protein staining within the CNS was not uniform with expression in the nucleus of some, but not all, neurons. Furthermore many different patterns of nuclear Wld expression were observed, from intense puncta to fine spots and diffuse staining. We tested the hypothesis that nuclear Wld protein is required for axonal and synaptic protection in the CNS. Cerebellar granule cells, which contain single large nuclear Wld inclusions, had protected neurites in vitro following K^+/serum withdrawal: 4 days after withdrawal only 4% of wild type neurites remained whereas 72% of Wld^S neurites were intact. Most cortical neurons express nuclear Wld and we found a high degree of synaptic preservation in vivo in the cortico-striatal pathway 8 days following removal of the ipsilateral cortex under deep anaesthesia. By contrast, neurons in the hippocampal dentate gyrus appear devoid of nuclear Wld and the mossy fibre axons show no significant protection following axotomy in organotypically-cultured slices. We conclude first, that nuclear Wld protein expression is crucial for the manifestation of the protective phenotype. Second, we have provided the first direct demonstration of synaptic preservation in the CNS of Wld^S mice in vivo.

Support Contributed By: BNA,Wellcome Trust

Citation:J.E. Haley, T.M. Wishart, T.H. Gillingwater, C.A. Ingham, A.K. Wright, G.W. Arbuthnott, R. Adalbert, M.P. Coleman, R.R. Ribchester. NUCLEAR EXPRESSION OF WLD PROTEIN IS REQUIRED FOR AXONAL AND SYNAPTIC PROTECTION IN THE CNS OF WLD^S MICE Program No. 1020.16. *2004 Abstract Viewer/Itinerary Planner.* Washington, DC: Society for Neuroscience,

2004. Online.

Transcriptional regulation of pituitary tumour transforming gene-1 by the neuroprotective WldS gene in mouse cerebellar granule cells and HEK293 cell lines.

Wishart, Thomas M; Gillingwater, Thomas H ; Chen, Phillip E; Haley, Jane E; Middleton, Susan ; Robertson, Kevin ; Wawrowski, Kolja ; Wyllie, David J.A.; Melmed, Shlomo ; Coleman, Michael P; Ribchester, Richard R;

1. Division of Neuroscience, University of Edinburgh, Edinburgh, United Kingdom. 2. ScGTI, University of Edinburgh, Edinburgh, United Kingdom. 3. Burns and Allen Research Institute, Cedars-Sinai Medical Centre, Los Angeles, CA, USA. 4. The Babraham Institute, Babraham, United Kingdom.

WldS mutant mice and their transgenic equivalents show 10-fold slower axonal and synaptic degeneration in response to either peripheral or central nerve lesions, due to overexpression of an Ube4b/Nmnat-1 chimeric protein (Gillingwater & Ribchester, 2001; Mack et al., 2001). The WldS protein forms dense nuclear aggregates, suggesting that the gene exerts its neuroprotective effects indirectly (Gillingwater et al., 2004; Araki et al, 2004). Here we examined the hypothesis that the WldS phenotype is due to transcriptional regulation of other genes. Western analysis and immunostaining of brains isolated from WldS mice killed by cervical dislocation (Home Office Schedule 1) established cerebellar granule cells as a rich source of WldS protein. We therefore extracted cerebellar mRNA from three WldS and three WT control mice and analysed gene expression using Affymetrix microarrays. Changes in the levels of candidate genes were validated by RT-PCR on the same mRNA extracts. As expected, there was a significant increase in Nmnat-1 expression in the WldS cerebellum, but several other genes were more than 5-fold up- or down-regulated, the largest change being a 10-fold downregulation in mRNA for pituitary tumour transforming gene (pttg-1). To test whether downregulation of pttg-1 was caused by WldS expression, we transfected cultures of human embryonic kidney (HEK) 293 cell lines with a fused WldS-EGFP construct, to allow for visual confirmation of protein expression. Semi-quantitative RT-PCR showed gene-dose dependent downregulation of the human PTTG-1 mRNA, 4 days after WldS transfection. Sciatic nerve section under ketamine/xylazine anaesthesia (respectively 100/10 mg/kg, IP) in nine pttg-1 (-/-) null mutant mice showed no evidence of protection of neuromuscular synapses by 48 hours. However, confocal microscopy revealed several intact axon fragments extending over 1mm in length in the distal tibial nerve. We conclude that expression of the WldS gene results in downregulation of the pttg-1 gene. However, the neuroprotective phenotype of WldS mice is not explained by downregulation of only this gene.

We thank the Wellcome Trust for support; and A Thomson, D Thomson and S. Ren for expert technical assistance. Araki, T. et al (2004) Science 305,1010-3. Gillingwater, T.H. et al., (2004) J Cereb Blood Flow Metab. 24,62-66. Gillingwater, T.H. & Ribchester, R.R. (2001) J Physiol. 534,627-639. Mack, T.G. et al (2001) Nat Neurosci. 4,1199-206.

Where applicable, the experiments described here conform with Physiological Society ethical requirements.

Society for Neuroscience meeting, Washington, November 2005.

Abstract View

BIDIRECTIONAL REGULATION OF TRANSCRIPTION BY THE NEUROPROTECTIVE WLDS GENE

T.H.Gillingwater[1]; T.M.Wishart[1]; P.E.Chen[1]; J.E.Haley[1]; K.Robertson[1]; S.Melmed[3]; P.A.Skehel[1]; M.P.Coleman[2]; R.R.Ribchester[1*]

1. Centre for Neuroscience Research, Univ. of Edinburgh, Edinburgh, United Kingdom

2. The Babraham Inst., Babraham, United Kingdom

3. Burns & Allen Institute, Cedars Sinai Med. Ctr., Los Angeles, CA, USA

Axons and synapses are primary pathological targets in many neurodegenerative diseases. The spontaneous WldS mutation blocks degeneration of axons and synapses in mice and offers potential for therapeutic intervention in humans. The mutant gene is a chimera, comprising complete code for the NAD-synthetic enzyme NMNAT-1, and a truncated ubiquitination ligase UBE4B (N70-Ube4b). The WldS protein localises to cell nuclei and its neuroprotective effects on distal axons are therefore indirect. Here we tested the hypothesis that WldS regulates gene expression in vivo and in vitro. Microarray analysis and quantitative PCR measurements of WldS mouse cerebellar mRNA revealed one unrelated gene, pitutitary tumour transforming gene -1 (pttg-1), that was downregulated by a factor of 10 and another, an erythroid differentiation regulating gene homologue (EDR1-like) upregulated by a factor of about 5. Transfection of HEK293 cells with a GFP-tagged full-length construct triggered WldS-dose dependent changes in mRNA expression for these two genes. Downregulation of pttg-1, but not the EDR1-like gene, was partly mimicked by exogenous administration of 1mM NAD to the HEK293 cell culture medium and this effect was blocked by sirtenol. Transfection with separate Nmnat-1 and N70-Ube4b constructs produced selective downregulation of pttg-1 and upregulation of EDR1-like respectively. Sciatic nerve section in six ketamine-xylazine anaesthetised pttg-1 null mutant mice produced no protection of distal axons and neuromuscular junctions when examined 2-6 days later, suggesting pttg-1 downregulation alone does not explain the WldS phenotype. Overall, the data suggest that WldS protein bidirectionally regulates transcription: its separate components linking downregulation of some genes with simultaneous upregulation of others.
Support Contributed By: MRC,Wellcome Trust

Citation:T.H. Gillingwater, T.M. Wishart, P.E. Chen, J.E. Haley, K. Robertson, S. Melmed, P.A. Skehel, M.P. Coleman, R.R. Ribchester. BIDIRECTIONAL REGULATION OF TRANSCRIPTION BY THE NEUROPROTECTIVE WLDS GENE Program No. 434.12. *2005 Abstract Viewer/Itinerary Planner.* Washington, DC: Society for Neuroscience, 2005. Online.

republish any abstract or part of any abstract in any form must be obtained in writing from the SfN office prior to publication